Cell Journal (Yakhteh)

Guide for Authors

Aims and Scope: The "Cell Journal (Yakhteh)**"** is a peer review and quarterly English publication of Royan Institute of Iran. The aim of the journal is to disseminate information through publishing the most recent scientific research studies on exclusively Cellular, Molecular and other related topics. **Cell J**, has been certified by the Ministry of Culture and Islamic Guidance since 1999 and also accredited as a scientific and research journal by HBI (Health and Biomedical Information) Journal Accreditation Commission since 2000 which is an open access journal. T**his journal holds the membership of the Committee on Publication Ethics (COPE).**

1. Types of articles

The articles in the field of Cellular and Molecular can be considered for publications in **Cell J.** These articles are as below:

A. Original articles Original articles are scientific reports of the original research studies. The article consists of English Abstract (structured), Introduction, Materials and Methods, Results, Discussion, Conclusion, Acknowledgements, Author's Contributions, and References **(Up to 40). Sample**

B. Review articles Review articles are the articles written by well experienced authors and those who have excellence in the related fields. The corresponding author of the review article must be one of the authors of at least three published articles appearing in the references. The review article consists of English Abstract (unstructured), Introduction, Conclusion, Author's Contributions, and References **(Up to 70). Sample**

C. Systematic Reviews

Systematic reviews are a type of literature review that collect and critically analyzes multiple research studies or papers. The Systematic reviews consist of English Abstract (unstructured), Introduction, Materials and Methods, Results, Discussion, Conclusion, Acknowledgements, Author's Contributions, and References **(Up to 70). Sample**

D. Short communications Short communications are articles containing new findings. Submissions should be brief reports of ongoing researches. The short communication consists of English Abstract (unstructured), the body of the manuscript (should not hold heading or subheading), Acknowledgements, Author's Contributions, and References **(Up to 30). Sample**

E. Case reports Case reports are short discussions of a case or case series with unique features not previously described which make an important teaching point or scientific observation. They may describe novel techniques or use equipment, or new information on diseases of importance. It consists of English Abstracts (Unstructured), Introduction, Case Report, Discussion, Acknowledgements, Author's Contributions, and References **(Up to 30). Sample**

F. Editorial Editorial should be written by either the editor in chief or the editorial board.

G. Imaging in biology Images in biology should focus on a single case with an interesting illustration such as a photograph, histological specimen or investigation. Color images are welcomed. The text should be brief and informative.

H. Letter to the editors Letter to editors are welcome in response to previously published **Cell J** articles, and may also include interesting cases that do not meet the requirement of being truly exceptional, as well as other brief technical or clinical notes of general interest. **Sample**

I. Debate.

2. Submission Process

It is recommended to see the guidelines for reporting different kinds of manuscripts here. This guide explains how to prepare the manuscript for submission. Before submitting, we suggest authors to familiarize themselves with **Cell J** format and content by reading the journal via the website (www.celljournal.com). The corresponding author ensures that all authors are included in the author list and agree with its order, and they must be aware of the manuscript submission.

A. Author contributions statements

It is essential for authors to include a statement of responsibility in the manuscript that specifies the contribution of every one of them. This participation must include conception and design of the manuscript, data acquisition or data analysis and interpretation, drafting of the manuscript and/or revising it for critically important intellectual content, revision and final approval of the manuscript and statistical analysis, obtaining funding, administrative, technical, or material support, or supervision. Authors who do not meet the above criteria should be acknowledged in the **Acknowledgments section.**

B. Cover letter

Each manuscript should be accompanied by a cover letter, signed by all authors specifying the following statement: "The

manuscript has been seen and approved by all authors and is not under active consideration for publication. It has neither been accepted for publication nor published in another journal fully or partially (except in abstract form). I hereby assign the copyright of the enclosed manuscript to **Cell J.** Corresponding author must confirm the proof of the manuscript before online publishing. Also, is it needed to suggest three peer reviewers in the field of their manuscript.

C. Manuscript preparation

Authors whose first language is not English encouraged to consult a native English speaker in order to confirm his manuscripts to American or British (not a mixture) English usage and grammar. It is necessary to mention that we will check the plagiarism of your manuscript by iThenticate Software. The manuscript should be prepared in accordance with the "International Committee of Medical Journal Editors (ICMJE)". Please send your manuscript in two formats Word and Pdf (including: title, name of all the authors with their degree, abstract, full text, references, tables and figures) and Also send tables and figures separately in the site. The abstract and text pages should have consecutive line numbers in the left margin beginning with the title page and continuing through the last page of the written text. Each abbreviation must be defined in the abstract and text when they are mentioned for the first time. Avoid using abbreviation in the title. Please use the international and standard abbreviations and symbols

It should be added that an essential step toward the integration and linking of scientific information reported in published literature is using standardized nomenclature in all fields of science and medicine. Species names must be italicized (*e.g., Homo sapiens*) and also the full genus and species written out in full, both in the title of the manuscript and at the first mention of an organism in a paper.

It is necessary to mention that genes, mutations, genotypes, and alleles must be indicated in italics. Please use the recommended name by consulting the appropriate genetic nomenclature database, e.g., HUGO for human genes. In another words; if it is a human gene, you must write all the letters in capital and italic (*e.g., OCT4, c-MYC*). If not, only write the first letter in capital and italic (*e.g., Oct4, c-Myc*). **In addition, protein designations are the same as the gene symbol but are not italicized.**

Of note, Cell J will only consider publishing genetic association study papers that are novel and statistically robust. Authors are advised to adhere to the recommendations outlined in the STREGA statement (http://www.strega-statement.org). The following criteria must be met for all submissions:

1. Hardy-Weinberg Equilibrium (HWE) calculations must be carried out and reported along with the P-values if applicable [see Namipashaki et al. 2015 (Cell J, Vol 17, N 2, Pages: 187-192) for a discussion].

2. Linkage disequilibrium (LD) structure between SNPs (if multiple SNPs are reported) must be presented.

3. Appropriate multiple testing correction (if multiple independent SNPs are reported) must be included.

Submissions that fail to meet the above criteria will be rejected before being sent out for review.

Each of the following manuscript components should begin in the following sequence:

Authors' names and order of them must be carefully considered (full name(s), highest awarded academic degree(s), email(s), and institutional affiliation(s) of all the authors in English. Also, you must send mobile number and full postal address of the corresponding author).

Changes to Authorship such as addition, deletion or rearrangement of author names must be made only before the manuscript has been accepted in the case of approving by the journal editor. In this case, the corresponding author must explain the reason of changing and confirm them (which has been signed by all authors of the manuscript). If the manuscript has already been published in an online issue, an erratum is needed.

Title is providing the full title of the research (do not use abbreviations in title).

Running title is providing a maximum of 7 words (no more than 50 characters).

Abstract must include Objective, Materials and Methods, Results, and Conclusion (no more than 300 words).

Keywords, three to five, must be supplied by the authors at the foot of the abstract chosen from the Medical Subject Heading (MeSH). Therefore; they must be specific and relevant to the paper.

The following components should be identified after the abstract:

Introduction: The Introduction should provide a brief background to the subject of the paper, explain the importance of the study, and state a precise study question or purpose.

Materials and Methods: It includes the exact methods or observations of experiments. If an apparatus is used, its manufacturer's name and address should be stipulated in parenthesis. If the method is established, give reference but if the method is new, give enough information so that another author can perform it. If a drug is used, its generic name, dose, and

route of administration must be given. Standard units of measurements and chemical symbols of elements do not need to be defined.

Statistical analysis: Type of study and statistical methods should be mentioned and specified by any general computer program used..

Ethical considerations*:* Please state that informed consent was obtained from all human adult participants and from the parents or legal guardians of minors and include the name of the appropriate institutional review board that approved the project. It is necessary to indicate in the text that the maintenance and care of experimental animals complies with National Institutes of Health guidelines for the humane use of laboratory animals, or those of your Institute or agency.

Clinical trial registration: All of the Clinical Trials performing in Iran must be registered in Iranian Registry of Clinical Trials (www.irct.ir). The clinical trials performed abroad, could be considered for publication if they register in a registration site approved by WHO or www.clinicaltrials.gov. If you are reporting phase II or phase III randomized controlled trials, you must refer to the CONSORT Statement for recommendations to facilitate the complete and transparent reporting of trial findings. Reports that do not conform to the CONSORT guidelines may need to be revised before peer-reviewing.

Results: They must be presented in the form of text, tables, and figures. Take care that the text does not repeat data that are presented in tables and/or figures. Only emphasize and summarize the essential features of the main results. Tables and figures must be numbered consecutively as appeared in the text and should be organized in separate pages at the end of the manuscript while their location should be mentioned in the main text.

Tables and figures: If the result of your manuscript is too short, it is better to use the text instead of tables & figures. Tables should have a short descriptive heading above them and also any footnotes. Figure's legend should contain a brief title for the whole figure and continue with a short explanation of each part and also the symbols used (no more than 100 words). All figures must be prepared based on cell journal's guideline in color (no more than 6 Figures and Tables) and also in GIF or JPEG format.

Of Note: Please put the tables & figures of the result in the results section not any other section of the manuscript.

Supplementary materials would be published on the online version of the journal. This material is important to the understanding and interpretation of the report and should not repeat material within the print article. The amount of supplementary material should be limited. Supplementary material should be original and not previously published and will undergo editorial and peer review with the main manuscript. Also, they must be cited in the manuscript text in parentheses, in a similar way as when citing a figure or a table. Provide a legend for each supplementary material submitted.

Discussion: It should emphasize the present findings and the variations or similarities with other researches done by other researchers. The detailed results should not be repeated in the discussion again. It must emphasize the new and important aspects of the study.

Conclusion: It emphasizes the new and important aspects of the study. All conclusions are justified by the results of the study.

Acknowledgements: This part includes a statement thanking those who contributed substantially with work relevant to the study but does not have authorship criteria. It includes those who provided technical help, writing assistance and name of departments that provided only general support. You must mention financial support in the study. Otherwise; write this sentence "There is no financial support in this study".

Conflict of Interest: Any conflict of interest (financial or otherwise) and sources of financial support must be listed in the Acknowledgements. It includes providers of supplies and services from a commercial organization. Any commercial affiliation must be disclosed, regardless of providing the funding or not.

References: The references must be written based on the Vancouver style. Thus the references are cited numerically in the text and listed in the bibliography by the order of their appearance. The titles of journals must be abbreviated according to the style used in the list of Journals Indexed in PubMed. Write surname and initials of all authors when there are six or less. In the case of seven or more authors, the names of the first six authors followed by "et al." must be listed. You can download Endnote file for Journal references style: endnote file

The reference of information must be based on the following order:

Article:

Surname(s) and first letter of name &middle name(s) of author(s) .Manuscript title. Journal title (abbr).publication date (year); Volume & Issue: Page number.

Example: Manicardi GC, Bianchi PG, Pantano S, Azzoni P, Bizzaro D, Bianchi U, et al. Presence of endogenous nicks in DNA of ejaculated human spermatozoa and its relationship to chromomycin A3 accessibility. Biol Reprod. 1995; 52(4): 864-867.

Book:

Surname(s) and first letter of name & middle name(s) of author(s).Book title. Edition. Publication place: publisher name; publication date (year); Page number.

Example: Edelman CL, Mandle CL. Health promotion throughout the lifespan. 2nd ed. ST Louis: Mosby; 1998; 145-163.

Chapter of book:

Surname(s) and first letter of name & middle name(s) of author(s).Chapter title. In: Surname(s) and first letter of name & middle name(s) of editor(s), editors. Book title. Edition. Publication place: publisher name; publication date (year); Page number.

Example: Phillips SJ, Whisnant JP. Hypertension and stroke. In: Laragh JH, Brenner BM, editors. Hypertension: pathophysiology, diagnosis, and management. 2nd ed. New York: Raven Press; 1995; 465-478.

Abstract book:

Example: Amini rad O.The antioxidant effect of pomegranate juice on sperm parameters and fertility potential in mice. Cell J. 2008;10 Suppl 1:38.

Thesis:

Name of author. Thesis title. Degree. City name. University. Publication date (year).

Example: Eftekhari Yazdi P. Comparison of fragment removal and co-culture with Vero cell monolayers on development of human fragmented embryos. Presented for the Ph.D., Tehran. Tarbiyat Modarres University. 2004.

Internet References

Article:

Example: Jahanshahi A, Mirnajafi-Zadeh J, Javan M, Mohammad-Zadeh M, Rohani M. Effect of low-frequency stimulation on adenosineA1 and A2A receptors gene expression in dentate gyrus of perforant path kindled rats. Cell J. 2008; 10 (2): 87-92. Available from: http://www.celljournal.org. (20 Oct 2008).

Book:

Example: Anderson SC, Poulsen KB. Anderson's electronic atlas of hematology.[CD-ROM]. Philadelphia: Lippincott Williams & Wilkins; 2002.

D. Proofs Proofs are sent by email as PDF files and should be checked and returned within 72 hours of receipt. It is the authors' responsibility to check that all the text and data as contained in the page proofs are correct and suitable for publication. **We are requested to pay particular attention to author's names and affiliations as it is essential that these details be accurate when the article is published.**

E. Pay for publication: Authors do not have to pay any Manuscript Processing Charge or Open Access Publication Fee. **Before publishing author's article, it would be the author's responsibility to pay for the expenses, if the editor feels the level of English used in the manuscript requiresediting.**

F. Ethics of scientific publication: Manuscripts that have been published elsewhere with the same intellectual material will refer to duplicate publication. If authors have used their own previously published work or work that is currently under review, as the basis for a submitted manuscript, they are required to cite the previous work and indicate how their submitted manuscript offers novel contributions beyond those of the previous work. Research and publication misconduct is considered a serious breach of ethics.

The Journal systematically employs iThenticate, plagiarism detection and prevention software designed to ensure the originality of written work before publication. Plagiarism of text from a previously published manuscript by the same or another author is a serious publication offence. Some parts of text may be used, only where the source of the quoted material is clearly acknowledged.

3. General information

A. You can send your manuscript via online submission system which is available on our website. If the manuscript is not prepared according to the format of **Cell J**, it will be returned to authors.

B. The order of article appearance in the Journal is not demonstrating the scientific characters of the authors.

C. Cell J has authority to accept or reject the manuscript.

D. The received manuscript will be evaluated by associate editor. **Cell J** uses a single-blind peer review system and if the manuscript suits the journal criteria, we select the reviewers. If three reviewers pass their judgments on the manuscript, it will

be presented to the editorial board of **Cell J.** If the editorial board has a positive judgment about the manuscript, reviewers' comments will be presented to the corresponding author (the identification of the reviewers will not be revealed). The executive member of journal will contact the corresponding author directly within 3-4 weeks by email. If authors do not receive any reply from journal office after the specified time, they can contact journal office. Finally, executive manager will respond promptly to authors' request.

The Final Checklist

The authors must ensure that before submitting the manuscript for publication, they have to consider the following parts:

1. Title page should contain title, name of the author/coauthors, their academic qualifications, designation & institutions they are affiliated with, mailing address for future correspondence, email address, phone, and fax number.

2. Text of manuscript and References prepared as stated in the "guide for authors" section.

3. Tables and figures should be uploaded separately except in the main manuscript. Figures must be sent in color and also in GIF or JPEG format with 300 dpi resolutions.

4. Cover Letter should be uploaded with signature of all authors.

The Editor-in-Chief: Ahmad Hosseini, Ph.D.

Cell Journal (Yakhteh),

P.O. Box: 16635-148, Iran

Tel/Fax: + 98-21-22510895

Emails: Celljournal@royaninstitute.org

info@celljournal.org

Dr. Saeed Kazemi Ashtiani

IN THE NAME OF GOD

Gone But not Forgotten

In the memory of the late Director of Royan Institute, Founder of Stem Cells Research in Iran and Chairman of ***Cell Journal*** *(Yakhteh)*. May he rest in peace.

PUBLISHED & SPONSORED BY:
Publication of Royan Institute (ACECR)

Indexed in:
1. Thomson Reuters (ISI); *Impact Factor: 2.046*
2. PubMed
3. PubMed Central (PMC)
4. National Library Medicine (NLM)
5. Biosis Preview
6. Index Medicus for the Eastern Mediterranean Region (IMEMR)
7. Regional Information Center for Sciences and Technology (RICeST)
8. Index Copernicus International
9. Cambridge Scientific Abstract (CSA)
10. EMBASE
11. Scopus
12. Cinahl Database
13. Google Scholar
14. Chemical Abstract Service (CAS)
15. Proquest
16. Directory of Open Access Journals (DOAJ)
17. Open Academic Journals Index (OAJI)
18. Directory of Research Journals Indexing (DRJI)
19. Scientific Information Database (SID)
20. Iranmedex
21. Islamic World Science Citation Center (ISC)
22. Magiran
23. Science Library Index

ACECR

Editorial Office Address (Dr. Ahmad Hosseini):
Royan Institute, P.O.Box: 16635-148,
Tehran, Iran
Tel & Fax: (+9821)22510895
Website: www.celljournal.org
Emails: info@celljournal.org
celljournal@royaninstitute.org

Printing Company:
Jurband Ghaemprint Co.
NO. 5, Jalil khoob alley, Niroo Havaei Street,
Tehran, Iran

Cell Journal (Yakhteh), Vol 22, No 2, July-September (Summer) 2020, Serial Number: 86, Pages: 133-252

CONTENTS

Review Article

Original Articles

Review Article

Designing A Transgenic Chicken: Applying New Approaches toward A Promising Bioreactor

Salahadin Bahrami, Ph.D.[1], Amir Amiri-Yekta, Ph.D.[1], Abbas Daneshipour, M.Sc.[1], Seyedeh Hoda Jazayeri, Ph.D.[1], Paul Edward Mozdziak, Ph.D.[2], Mohammad Hossein Sanati, Ph.D.[1, 3*], Hamid Gourabi, Ph.D.[1*]

1. Department of Genetics, Reproductive Biomedicine Research Center, Royan Institute for Reproductive Biomedicine, ACECR, Tehran, Iran
2. Physiology Graduate Program, North Carolina State University, Raleigh, NC, USA
3. Department of Medical Genetics, National Institute of Genetic Engineering and Biotechnology, Tehran, Iran

Corresponding Address: P.O.Box: 16635-148, Department of Genetics, Reproductive Biomedicine Research Center, Royan Institute for Reproductive Biomedicine, ACECR, Tehran, Iran
Emails: m-sanati@nigeb.ac.ir, gourabi@royaninstitute.org

Received: 19/January/2019, Accepted: 15/April/2019

Abstract

Specific developmental characteristics of the chicken make it an attractive model for the generation of transgenic organisms. Chicken possess a strong potential for recombinant protein production and can be used as a powerful bioreactor to produce pharmaceutical and nutritional proteins. Several transgenic chickens have been generated during the last two decades via viral and non-viral transfection. Culturing chicken primordial germ cells (PGCs) and their ability for germline transmission ushered in a new stage in this regard. With the advent of CRISPR/Cas9 system, a new phase of studies for manipulating genomes has begun. It is feasible to integrate a desired gene in a predetermined position of the genome using CRISPR/Cas9 system. In this review, we discuss the new approaches and technologies that can be applied to generate a transgenic chicken with regards to recombinant protein productions.

Keywords: Chickens, CRISPR/Cas9, Ovalbumin, Recombinant Protein, Transgenes

Cell Journal(Yakhteh), Vol 22, No 2, July-September (Summer) 2020, Pages: 133-139

Citation: **Bahrami S, Amiri-Yekta A, Daneshipour A, Jazayeri SH, Mozdziak PE, Sanati MH, Gourabi H. Designing a transgenic chicken: applying new approaches toward a promising bioreactor. Cell J. 2020; 22(2): 133-139. doi: 10.22074/cellj.2020.6738.**

Introduction

The first genetically modified chicken was reported in 1989 (1, 2) and thereafter many other transgenic avian species have been generated, with special attention to chicken and quail (2). These transgenic species possess a great potential for many purposes, including the poultry industry, medicine and drug manufacturing, developmental studies, research and investigation of disease susceptibility and creating biomedical models for different scientific purposes (2-4). Many scientists around the world have focused on exploiting transgenic technology to generate transgenic chicken for a practice known as biopharming, since the chicken egg is used as a preferential bioreactor to produce pharmaceutical and nutritional proteins (5, 6). The most interesting aspect of this new technology is the potential to produce therapeutic recombinant proteins in large quantities. The market demand for some of these recombinant proteins (for example monoclonal antibodies) are high; so a high producing system is required (7).

Overall, transgenic animals and transgenic chicken, in particular, represent a great potential for production of therapeutic recombinant proteins, because they have the ability to produce very complex and active proteins while at the same time providing the appropriate posttranslational modifications (8, 9). An inability to provide the appropriate translational modifications is the most important drawback of bacterial bioreactors (10), the most cost-effective system. Transgenic animals are superior (9) to transgenic plants (11, 12) and insects which have a relatively slow production setup (9). With regard to production cost, a transgenic animal farm is much more cost-effective than building a large-scale manufacturing facility for culturing mammalian cells (13, 14) which Dyck et al. (15) estimates would likely cost over five times more than that needed to produce transgenic animals. The time and expense needed for chicken to reach maturity and begin to produce target compounds is much less than those needed with other farm animals. Although chicken pose the risk of zoonotic diseases, the risk can almost be eliminated by using a closed rearing system and well established specific-pathogen-free (SPF) protocols. For the reasons covered above, chicken seems to be the best farm animal to be used as a transgenic bioreactor (16).

Egg white provides a promising substrate where a protein of interest can be accumulated in large amounts and subsequently be easily harvested for purification. The ovalbumin promoter facilitates localized production of ovalbumin, the main protein in egg white. This promoter can be modified to regulate production of a gene of interest (GOI) in oviduct cells in which the egg white is produced (17). In this short review, we explain the possibility of applying these new technologies in generating transgenic chicken. At the end, we describe a promising new strategy for

generating a transgenic chicken which does not require insertion of an exogenous promoter in the construct.

Methods for introducing the gene construct

Traditionally, DNA microinjection into the pronucleus of a freshly fertilized egg is used as the method of choice in order to introduce the genes in mammalian transgenesis (18, 19). However, microinjection cannot be easily applied to chicken, because there are more than 50000 cells in a freshly-laid fertilized chicken egg (20, 21). For this reason, microinjection can only be used on early stage fertile embryos collected from sacrificed hens (22, 23). Using this method, Love et al. (22) were able to generate a mosaic transgenic rooster carrying the *lacZ* gene. However, the offspring never expressed the protein. Even though microinjection can be successful, it is a slow and inefficient method for creating transgenic chicken. In addition, every time microinjection is performed, a hen must be sacrificed to collect the fertilized eggs (21). Furthermore, even in cases of successfully generated transgenic chicken, the desired protein production may not be achieved due to gene silencing or a positional effect of the gene (7, 24).

An alternative to microinjection is transfection of an exogenous gene done by using non-viral vectors or viral vectors. In most cases using non-viral vectors, the DNA construct is lost after multiple cell divisions, because it is not integrated into the host chromosome (25). Applying viral vectors is the most successful method (7, 21, 26), because the DNA construct naturally integrates into the host chromosomes. In fact, avian retroviral vectors derived from avian retroviruses were used to generate the first genetically modified chicken. The retroviral vectors were injected adjacent to the blastoderm which led to somatic mosaicism in 25% of samples and germinal transmission at rates of 1-11% (27). Since then, multiple scientific groups have applied different viral vectors to create transgenic chickens (1, 21). One drawback of this viral method is that the size of construct these vectors can carry is limited.

Modern retroviral vectors used to create transgenic chicken are replication-defective; the vector construct entails the least possible amount of viral sequence such as long terminal repeat (LTR) and a packaging signal, but not the viral genes essential for packaging gag, pol and env which are removed and replaced by the desired genetic sequences. To produce the virus particle, the vector containing the desired DNA construct is transfected into packaging cells such as HEK293 that produce gag/pol and env proteins. Subsequently, the virus particles are obtained from the culture supernatant. These viral particles can infect host cells and introduce their DNA along with the exogenous construct into the genome. However, in the absence of packaging genes, infection cannot create viral particles in the host cells. Thus, the integrated DNA will remain in the host genome and the transgene will probably have a stable expression (7).

Similar to the other animals, genomes of the avian species are prone to gene silencing (24) which is mainly associated with DNA methylation and it is transmitted to progeny (28). Histone modification and presence of the other chromatin condensing proteins can also cause silencing (7). By changing the timing of viral infection, Kamihira et al. (26) were able to overcome this problem and achieve the desired gene expression. When using viral vectors, the position of gene integration is random. Consequently, there is a strong possibility that transgene may integrate into a location which causes gene silencing. In addition, the gene integration may cause gene disruption in the host. As a result, there is a universal concern about the safety of this method (29).

Primordial germ cells as the main target for transgenesis in chicken

Primordial germ cells (PGCs) are gamete progenitor cells, a population of undifferentiated cells that is separated from all somatic cells during early development. Unlike the PGCs in other species, PGCs in avian and some reptilian species migrate to the genital ridge via blood circulation. In the genital ridge, these PGCs are subjected to a series of complex processes which results in differentiation into functional spermatozoa or ova (30). PGCs have been the focus of researchers around the world and they have been widely used in manipulation of avian embryos (26, 31, 32). A conventional method to generate a transgenic chicken is to inject a high titer of the viral vectors into the subgerminal cavity of the embryos at stage X; so that the virus particles transfect the blastoderm cells along with PGCs (26, 31). In another method, the migrating PGCs are targeted by injecting a vector into the vascular system or directly injecting it into the heart of developing embryos after 50 to 60 hours of incubation (26). In fact, the first chimeric chicken was generated by Tajima et al. (33) by transplanting 100 chicken PGCs into a recipient embryo. Even though direct injection of PGCs successfully generated transgenic chicken, the process proved to be difficult, because it created a mosaic of PGCs in which only a small portion of them were transfected. Consequently, a time-consuming process is required to obtain a transgenic chicken. For this reason, researchers have spent a great deal of time trying to extract and enrich PGCs *in vitro* for subsequent manipulation. These enriched and transfected PGCs can be injected into a recipient embryo at the blastodermal stage or injected intravascularly between stages 13 and 16 thereby allowing them to migrate directly to the genital ridge (30, 31). Chicken PGCs were cultivated *in vitro*, for 4 days, for the first time in 1995 by Chang et al. (34). Kuwana et al. (35), Naito et al. (36) developed a PGC culture using a KAv-1 medium. In 2006, Van de Lavoir et al. (37) successfully cultivated male chicken PGCs

in vitro and maintained the culture for over 100 days. In 2015, Whyte et al. (38) further improved culture conditions and proved that low osmotic pressure (up to 250 mosm/kg) and low calcium concentrations (up to 0.15 mM) were the best conditions for *in vitro* culture of chicken PGCs. This culture condition can maintain PGCs *in vitro* for a long period, so that the DNA manipulations can be achieved easily and transfected cells can be selected and enriched properly.

Surrogate egg shell creates two windows of opportunity to manipulate chicken embryo

Different methods have been employed over the years to access the embryo in order to introduce foreign DNA: shell windowing, *ex vivo* embryo culturing and surrogate egg shell. In shell windowing a narrow window, about 20 mm in diameter, is opened at the blunt end of the egg providing easy access to the embryo, so manipulation can be achieved. Afterward, the window can be sealed with cling-film wrap and thin ovalbumin as a paste (29, 39, 40).

Ex vivo embryo culturing is the external culturing of a chicken embryo in conditions similar to that of the natural environment inside an egg. The method is thoroughly explained by Nakamura (29). In brief, the fertilized chicken egg and the thick surrounding albumin (8-16 ml) layer is collected from a hen and cultured in a sealed cup for one day at 41-42˚C (system I). The cultured embryo is then transferred to a surrogate shell filled with thin ovalbumin and tightly sealed (system II). After three days, the embryo is transferred to a larger, actual host egg with an empty space above the embryo such as a turkey egg shell (system III). This method provides windows of opportunity in which embryo manipulation can be easily performed which makes creating a transgenic chicken more practical.

In surrogate egg shell, the method includes two sequential transfers of the fertilized egg to different shells that correspond with system II and system III of the ex-vivo embryo culturing method (21, 41-43). In brief, the freshly laid fertile egg is transferred to an actual, slightly heavier egg shell (3-4 g), and the shell is filled with thin ovalbumin and sealed tightly with cling-film and ovalbumin paste (system II). After three days, the embryo is transferred to a bigger egg shell (fresh turkey or two yolk egg shell; 35-40 g), and the shell is sealed with cling-film and ovalbumin paste, while an empty space is provided above the embryo to expose the extra-embryonic membrane vascular system to the atmosphere. With this process, the embryo is accessible, but the system I of *ex vivo* embryo culturing process is not necessary, which makes it easier to perform.

Applying CRISPR/Cas9-mediated targeted genome editing to chicken transgenesis

As it was mentioned above, exploiting germ cells such as PGCs provides an opportunity to transfect these cells, select the transfected ones, enrich them and subsequently inject these cells into a recipient embryo to generate transgenic chickens. To render a high and stable expression of a transgene, it is very important to ensure that the gene construct integrates into a position in the host genome that avoids gene silencing. Previously, positional targeting was pursued using homologous recombination vectors entailing homology regions of about 7-8 kb and worked with approximately 30% efficiency (32, 44). The problem with homologous recombination was the low efficiency of obtaining and cloning these long homology regions. Recent methods applying site-specific endonucleases such as Zinc finger nucleases (ZFNs) (45) and transcription activator-like effector nucleases (TALENs) (2, 46) have improved efficiency of the targeting approaches and consequently made them more popular. Despite their high efficiency, these endonucleases have limited use, because the construct design is very difficult and acquiring the desired endonuclease is not feasible in many cases. Moreover, the off-target rates are high (47).

In contrast, a recently emerged system, the clustered regularly interspaced short palindromic repeats (CRISPR)/CRISPR-associated (Cas) system, has rendered a high success rate (80%), with much simpler construct designs (48). In this system, CRISPR-associated protein 9 (Cas9), the DNA endonuclease enzyme, is guided by a 20 bp RNA (gRNA) which pairs with the target DNA site. Other than the gRNA, a short protospacer adjacent motif (PAM) is required to ensure the complete interaction between Cas9 and the target DNA (49, 50). When the target DNA is complementary to the gRNA, Cas9 cleaves the DNA and creates a double-strand break (DSB) which can be repaired by either non-homologous end joining (NHEJ) or homology-directed repair (HDR). NHEJ may lead to small insertions/deletions whereas HDR is used when a template DNA complementary to the break site is present (51, 52) (Fig.1).

Oishi et al. (53) successfully applied CRISPR/Cas9 technology and efficiently (>90%) created mutations in two egg white genes, ovalbumin and ovomucoid, in cultured chicken PGCs which were subsequently injected into recipient chicken embryos. Zuo et al. (54) demonstrated that gene knockouts can be induced in both chicken stem cells and chicken embryos using CRISPR/Cas9 technology. Using the CRISPR/Cas9 system, researchers successfully inhibited the chicken embryonic stem cells differentiation (ESCs) into spermatogonial stem cells (SSCs) by *Stra8* gene knockdown (55). In another study, Dimitrov et al. (32) reported a successful gene editing in chicken PGCs using the CRISPR/Cas9 system and a donor vector for HDR of the DSB. Recently, many scientists have applied this technology to generate gene knock-in in mammalian cells (56-58). With the CRISPR/Cas9 system, it is now possible to introduce a large DNA construct, which can entail a transgene into a specific locus in different cell lines (47, 48, 58, 59).

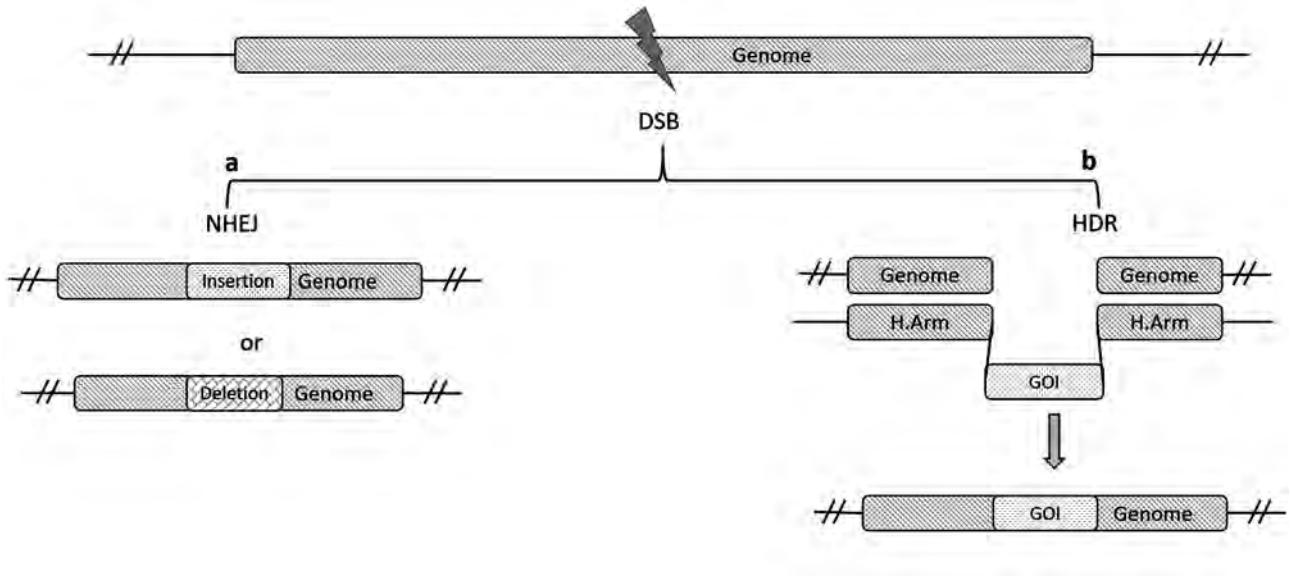

Fig.1: A schematic presentation of the double-strand break (DSB) repair. **a.** Non-homologous end joining (NHEJ) which directly ligates the DSB and can create insertions and deletions and **b.** Homology directed repair (HDR) in which a template DNA complementary to the break site is present.

Tissue-specific ovalbumin promoter: the best candidate for recombinant protein production in chicken

Chicken ovalbumin (OVA), the main protein in egg white, accounts for almost 55% of the total protein and is expressed strictly in oviduct cells. This gene is a well-known promoter with a very high expression ability which has been thoroughly studied as a model for tissue-specific expression (60, 61). Since the ovalbumin gene promoter is a tissue-specific promoter and is thought to have powerful production ability, it has been used to generate transgenic chickens with oviduct-specific production (5, 17, 62, 63). Four DNase I-hypersensitive sites (DHSs) have been identified in the 8.7 kb region between the ovalbumin gene and the Y gene, that is thought to be the regulation elements of the ovalbumin promoter (61, 64). The region is difficult to include entirety in a vector construct, because it is a large DNA sequence. As a result, researchers have investigated the role of DNase I hypersensitive sites, included fragments of the region as the promoter of choice (17, 43, 61), and reported oviduct tissue-specific expression of the transgene. Lillico et al. (62) demonstrated that 2.8 kb of the ovalbumin promoter, which encompasses a steroid-dependent regulatory element (SDRE) and a negative regulatory element (NRE), can strongly drive the transgene expression in oviduct cells. Liu et al. (43) used the same promoter to drive transgene expression inserted in different locations in the chicken genome. Their results showed different levels of expression, all lower than those in the previous study. These studies showed that location of the inserted transgene can significantly affect the expression level thereby emphasizing the importance of the positional effect of the insertion locus. They also indicated the necessity of the larger promoter region to maintain strong tissue-specific protein production, and that there may be other factors close to ovalbumin promoter contributing to its strong and tissue-specific expression.

Applying new approaches

The most effective approach to produce transgenic chicken is to transfect PGCs *in vitro*, select the transfected cells and enrich them. Next, inject the cells into the circulating blood of an embryo or directly into the blastodisc. Using the CRISPR/Cas9 system, it is possible to integrate the DNA construct entailing the transgene into a previously determined position in the genome that ensures availability of the transgene and its favorable expression. As mentioned above, the ovalbumin promoter is one of the most interesting promoters which can regulate gene expression in the oviduct cells and later to the egg white. By using the CRISPR/Cas9 system and providing the homologous arms to induce HDR in the break site, a gene knock-in can be achieved *in vitro* using PGCs as the host cell. In 2015, Rojas-Fernandez et al. (65), successfully integrated a gene construct (firefly luciferase cDNA) downstream of an endogenous promoter (promoter of the TGFβ-responsive gene PAI-1) and demonstrated that the firefly luciferase cDNA expression mimicked that of endogenous PAI-1 expression. Consequently, it is feasible that an exogenous cDNA can be placed downstream of the endogenous ovalbumin promoter. In a recent work conducted by Oishi et al. (66), human interferon beta was inserted into the chicken ovalbumin locus. They created a CRISPR/Cas9-mediated knock-in of *hIFN-β* gene at the ovalbumin start codon located in exon 2 of the ovalbumin gene. The result demonstrated a promising transgene production in the egg white. It is plausible that the exon 1 of ovalbumin gene is a good candidate position to integrate the transgene.

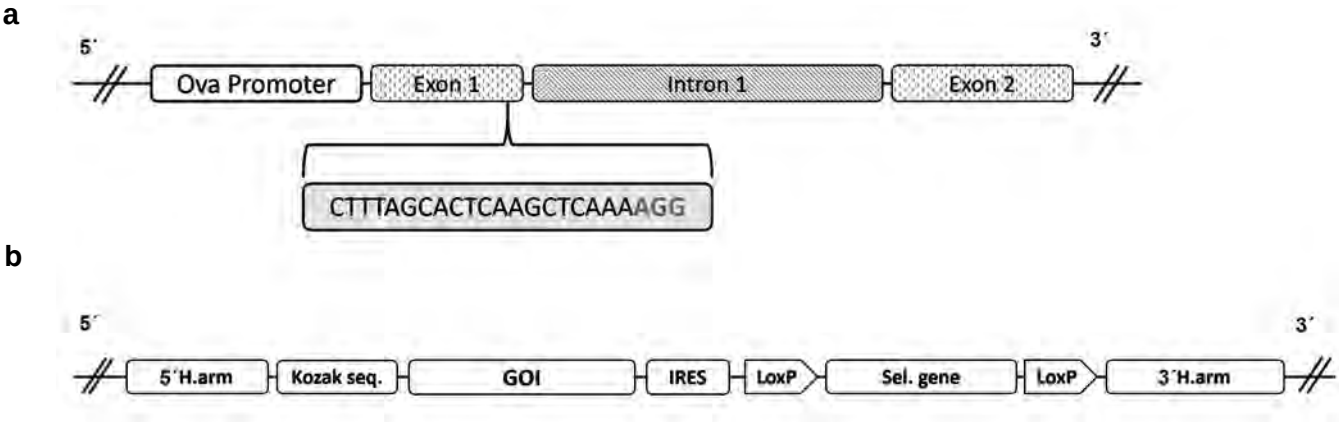

Fig.2: A schematic presentation of the candidate position and required donor vector for targeted integration. **a.** The ovalbumin gene, ova promoter, exons 1 and 2, as well as intron 1 is showed with the location of candidate gRNA and **b.** A schematic presentation of the vector entailing GOI with Kozak sequence and selectable gene flanked by homologous arms complementary to the DNA break site that can be induced by CRISPR.

The ovalbumin gene consists of eight exons and seven introns, and the start codon is located in exon 2. Using E-CRISPR software (67) and CRISPOR online software (68) analysis of the ovalbumin gene reveals a number of potential gRNA sites. The most promising one is CTTTAGCACTCAAGCTCAAAAGG which shows a high target affinity, high efficiency and a low off-target score (Fig.2A). Moreover, this gRNA site is located within the exon 1 which is not part of final ovalbumin cDNA and is not translated, so integrating an exogenous sequence in this location probably would not disrupt the ovalbumin gene and its splicing process. With this gRNA, the Cas9 nuclease will cut the DNA between C and A nucleotides close to the PAM sequence (AGG). The flanking 5′ and 3′ sequences around the break site can be used as homologous arms and add to corresponding terminals of the desired DNA construct (Fig.2B). Finally, adding a Kozak sequence (69) at the 5′ end of gene construct, before the translation start codon, will ensure mRNA translation of the transgene. With this approach of removing promoter from the gene construct, more DNA sequence can be added to the vector (Fig.2A). A reporter gene or a selectable marker gene can be added to the 3′ of the GOI using IRES sequence flanked by two LoxPs which can later be excised from the genome using Cre recombinase (70). Chicken PGCs can be transfected *in vitro* with a CRISPR/Cas9 vector and the DNA construct containing the GOI flanked with homologous arms and relative sequences. Transfected PGCs can be enriched and injected into chicken embryos to produce chickens with transgenic germ cells. Pure transgenic chickens producing the GOI in their egg white can then be achieved by breeding.

Conclusion

Transgenic chicken provides a great opportunity to produce therapeutic proteins in large-scale, in both a timely and cost effective manner. However, developing a practical procedure to generate transgenic chicken proved to be challenging due to specific developmental characteristics of birds. Unlike mammals, a fertilized avian egg cannot be accessed in order to introduce DNA via microinjection, because a freshly laid chicken egg already contains more than 50000 cells. Several alternative methods have been developed and improved over the last decades to produce transgenic chicken, however, few successful cases were reported. Successful culturing of PGCs created a promising opportunity to manipulate these cells *in vitro*. With the advent of CRISPR/Cas9 system, it is now feasible to insert a GOI in a specific location of genome. Establishing a process to create transgenic chicken by inserting a foreign gene in a specific location where the exposure and expression of the gene are ensured, seems more possible than ever. As a result, great progress has already been achieved towards the goal of producing pharmaceutical or nutritional proteins with the creation of transgenic chickens producing a GOI in their egg white.

Acknowledgements

The authors would like to thank colleagues at Royan Institute for Reproductive Biomedicine, Department of Genetics and Genetic Engineering (Tehran, Iran). There is no conflict of interest and no financial support in this study.

Authors' Contributions

S.B., H.G.; Contributed to the main design and coordination required for this work, the main literature review and writings, as well as the bioinformatics analysis. M.H.S., H.G.; Are responsible for overall supervision and contributed mainly to critical revision and approval of the final version. A.A.-Y.; Was responsible for the section related to gene construct and DNA introduction methods, as well as critical revision and feedback. A.D.; Contributed to reviewing and arranging important literatures and participated in preparation of the draft. S.H.J.; Participated in section related to cell culture and primordial germ cell. P.E.M.; Participated in drafting the section related to embryo manipulation and surrogate egg

shell, as well as critical revision of the manuscript. All authors read and approved the final manuscript.

References

1. Salter DW, Crittenden LB. Artificial insertion of a dominant gene for resistance to avian leukosis virus into the germ line of the chicken. Theor Appl Genet. 1989; 77(4): 457-461.
2. Taylor L, Carlson DF, Nandi S, Sherman A, Fahrenkrug SC, McGrew MJ. Efficient TALEN-mediated gene targeting of chicken primordial germ cells. Development. 2017; 144(5): 928-934.
3. Lyall J, Irvine RM, Sherman A, McKinley TJ, Núñez A, Purdie A, et al. Suppression of avian influenza transmission in genetically modified chickens. Science. 2011; 331(6014): 223-226.
4. Lambeth LS, Morris KR, Wise TG, Cummins DM, O'neil TE, Cao Y, et al. Transgenic chickens overexpressing aromatase have high estrogen levels but maintain a predominantly male phenotype. Endocrinology. 2016; 157(1): 83-90.
5. Lillico SG, McGrew MJ, Sherman A, Sang HM. Transgenic chickens as bioreactors for protein-based drugs. Drug Discov Today. 2005; 10(3): 191-196.
6. Ivarie R. Competitive bioreactor hens on the horizon. Trends Biotechnol. 2006; 24(3): 99-101.
7. Nishijima Ki, Iijima S. Transgenic chickens. Deve Growth Differ. 2013; 55(1): 207-216.
8. Houdebine L-M. Production of pharmaceutical proteins by transgenic animals. Comp Immunol Microbiol Infect Dis. 2009; 32(2): 107-121.
9. Wang Y, Zhao S, Bai L, Fan J, Liu E. Expression systems and species used for transgenic animal bioreactors. Biomed Res Int. 2013; 2013: 580463.
10. Swartz JR. Advances in Escherichia coli production of therapeutic proteins. Curr Opin Biotechnol. 2001; 12(2): 195-201.
11. Giddings G, Allison G, Brooks D, Carter A. Transgenic plants as factories for biopharmaceuticals. Nat Biotechnol. 2000; 18(11): 1151-1155.
12. De Muynck B, Navarre C, Boutry M. Production of antibodies in plants: status after twenty years. Plant Biotechnol J. 2010; 8(5): 529-563.
13. Jazayeri SH, Amiri-Yekta A, Gourabi H, Abd Emami B, Halfinezhad Z, Abolghasemi S, et al. Comparative assessment on the expression level of recombinant human follicle-stimulating hormone (FSH) in serum-containing versus protein-free culture media. Mol Biotechnol. 2017; 59(11-12): 490-498.
14. Jazayeri SH, Amiri-Yekta A, Bahrami S, Gourabi H, Sanati MH, Khorramizadeh MR. Vector and cell line engineering technologies toward recombinant protein expression in mammalian cell lines. Appl Biochem Biotechnol. 2018; 185(4): 986-1003.
15. Dyck MK, Lacroix D, Pothier F, Sirard MA. Making recombinant proteins in animals-different systems, different applications. Trends Biotechnol. 2003; 21(9): 394-399.
16. Luginbuhl RE. The commercial production of specific-pathogen-free eggs and chickens: the evolution of an industry. Avian Dis. 2000; 44(3): 632-637.
17. Byun SJ, Kim SW, Kim KW, Kim JS, Hwang IS, Chung HK, et al. Oviduct-specific enhanced green fluorescent protein expression in transgenic chickens. Biosci Biotechnol Biochem. 2011; 75(4): 646-649.
18. Amiri Yekta A, Dalman A, Sanati MH, Fatemi N, Vazirinasab H, Zomorodipour A, et al. Optimization of the electroporation conditions for transfection of human factor IX into the goat fetal fibroblasts. Cell J. 2013; 14(4): 270-275.
19. Amiri Yekta A, Dalman A, Eftekhari-Yazdi P, Sanati MH, Shahverdi AH, Fakheri R, et al. Production of transgenic goats expressing human coagulation factor IX in the mammary glands after nuclear transfer using transfected fetal fibroblast cells. Transgenic Res. 2013; 22(1): 131-142.
20. Spratt NT, Haas H. Morphogenetic movements in the lower surface of the unincubated and early chick blastoderm. J Exp Zool A Ecol Genet Physiol. 1960; 144(2): 139-157.
21. Mozdziak PE, Borwornpinyo S, McCoy DW, Petitte JN. Development of transgenic chickens expressing bacterial beta-galactosidase. Dev Dyn. 2003; 226(3): 439-445.
22. Love J, Gribbin C, Mather C, Sang H. Transgenic birds by DNA microinjection. Biotechnology (N Y). 1994; 12(1): 60-63.
23. Sherman A, Dawson A, Mather C, Gilhooley H, Li Y, Mitchell R, et al. Transpostion of the Drosophila element mariner into the chicken germ line. Nat Biotechnol. 1998; 16(11): 1050-1053.
24. Jähner D, Stuhlmann H, Stewart CL, Harbers K, Löhler J, Simon I, et al. De novo methylation and expression of retroviral genomes during mouse embryogenesis. Nature. 1982; 298(5875): 623-628.
25. Naito M, Sakurai M, Kuwana T. Expression of exogenous DNA in the gonads of chimaeric chicken embryos produced by transfer of primordial germ cells transfected in vitro and subsequent fate of the introduced DNA. J Reprod Fertil. 1998; 113(1): 137-143.
26. Kamihira M, Ono K, Esaka K, Nishijima K, Kigaku R, Komatsu H, et al. High-level expression of single-chain Fv-Fc fusion protein in serum and egg white of genetically manipulated chickens by using a retroviral vector. J Virol. 2005; 79(17): 10864-10874.
27. Salter DW, Smith EJ, Hughes SH, Wright SE, Fadly AM, Witter RL, et al. Gene insertion into the chicken germ line by retroviruses. Poult Sci. 1986; 65(8): 1445-1458.
28. Mizuarai S, Ono K, Yamaguchi K, Nishijima K, Kamihira M, Iijima S. Production of transgenic quails with high frequency of germ-line transmission using VSV-G pseudotyped retroviral vector. Biochem Biophys Res Commun. 2001; 286(3): 456-463.
29. Nakamura Y. Avian Biotechnology. Adv Exp Med Biol. 2017; 1001: 187-214.
30. Tagami T, Miyahara D, Nakamura Y. Avian primordial germ cells. Adv Exp Med Biol. 2017; 1001: 1-18.
31. Motono M, Yamada Y, Hattori Y, Nakagawa R, Nishijima K, Iijima S. Production of transgenic chickens from purified primordial germ cells infected with a lentiviral vector. J Biosci Bioeng. 2010; 109(4): 315-321.
32. Dimitrov L, Pedersen D, Ching KH, Yi H, Collarini EJ, Izquierdo S, et al. Germline gene editing in chickens by efficient CRISPR-mediated homologous recombination in primordial germ cells. PLoS One. 2016; 11(4): e0154303.
33. Tajima A, Naito M, Yasuda Y, Kuwana T. Production of germ line chimera by transfer of primordial germ cells in the domestic chicken (Gallus domesticus). Theriogenology. 1993; 40(3): 509-519.
34. Chang IK, Tajima A, Chikamune T, Ohno T. Proliferation of chick primordial germ cells cultured on stroma cells from the germinal ridge. Cell Biol Int. 1995; 19(2): 143-150.
35. Kuwana T, Hashimoto K, Nakanishi A, Yasuda Y, Tajima A, Naito M. Long-term culture of avian embryonic cells in vitro. Int J Dev Biol. 2003;40(5):1061-1064.
36. Naito M, Harumi T, Kuwana T. Long-term culture of chicken primordial germ cells isolated from embryonic blood and production of germline chimaeric chickens. Anim Reprod Sci. 2015; 153: 50-61.
37. Van de Lavoir MC, Diamond JH, Leighton PA, Mather-Love C, Heyer BS, Bradshaw R, et al. Germline transmission of genetically modified primordial germ cells. Nature. 2006; 441(7094): 766-769.
38. Whyte J, Glover JD, Woodcock M, Brzeszczynska J, Taylor L, Sherman A, et al. FGF, insulin, and SMAD signaling cooperate for avian primordial germ cell self-renewal. Stem Cell Reports. 2015; 5(6): 1171-1182.
39. Nakamura Y, Usui F, Ono T, Takeda K, Nirasawa K, Kagami H, et al. Germline replacement by transfer of primordial germ cells into partially sterilized embryos in the chicken. Biol Reprod. 2010; 83(1): 130-137.
40. Speksnijder G, Ivarie R. A modified method of shell windowing for producing somatic or germline chimeras in fertilized chicken eggs. Poult Sci. 2000; 79(10): 1430-1433.
41. Borwompinyo S, Brake J, Mozdziak PE, Petitte JN. Culture of chicken embryos in surrogate eggshells. Poult Sci. 2005; 84(9): 1477-1482.
42. Mozdziak PE, Hodgson D, Petitte JN. Avian somitic cell chimeras using surrogate eggshell technology. Asian-Australas J Anim Sci. 2008; 21(6): 801-806.
43. Liu T, Wu H, Cao D, Li Q, Zhang Y, Li N, et al. Oviduct-specific expression of human neutrophil defensin 4 in lentivirally generated transgenic chickens. PLoS One. 2015; 10(5): e0127922.
44. Schusser B, Collarini EJ, Yi H, Izquierdo SM, Fesler J, Pedersen D, et al. Immunoglobulin knockout chickens via efficient homologous recombination in primordial germ cells. Proc Natl Acad Sci USA. 2013; 110(50): 20170-20175.
45. Fan B, Huang P, Zheng S, Sun Y, Fang C, Sun Z. Assembly and in vitro functional analysis of zinc finger nuclease specific to the 3′ untranslated region of chicken ovalbumin gene. Anim Biotechnol. 2011; 22(4): 211-222.
46. Park TS, Lee HJ, Kim KH, Kim JS, Han JY. Targeted gene knockout in chickens mediated by TALENs. Proc Natl Acad Sci USA. 2014; 111(35): 12716-12721.
47. Gaj T, Staahl BT, Rodrigues GMC, Limsirichai P, Ekman FK, Doudna JA, et al. Targeted gene knock-in by homology-directed genome

editing using Cas9 ribonucleoprotein and AAV donor delivery. Nucleic Acids Res. 2017; 45(11): e98.
48. Hwang WY, Fu Y, Reyon D, Maeder ML, Tsai SQ, Sander JD, et al. Efficient genome editing in zebrafish using a CRISPR-Cas system. Nat Biotechnol. 2013; 31(3): 227-229.
49. Ran FA, Hsu PD, Wright J, Agarwala V, Scott DA, Zhang F. Genome engineering using the CRISPR-Cas9 system. Nat Protoc. 2013; 8(11): 2281-2308.
50. Crispo M, Mulet AP, Tesson L, Barrera N, Cuadro F, dos Santos-Neto PC, et al. Efficient generation of myostatin knock-out sheep using CRISPR/Cas9 technology and microinjection into zygotes. PLoS One. 2015; 10(8): e0136690.
51. Hsu PD, Lander ES, Zhang F. Development and applications of CRISPR-Cas9 for genome engineering. Cell. 2014; 157(6): 1262-1278.
52. Merkert S, Martin U. Targeted genome engineering using designer nucleases: State of the art and practical guidance for application in human pluripotent stem cells. Stem Cell Res. 2016; 16(2): 377-386.
53. Oishi I, Yoshii K, Miyahara D, Kagami H, Tagami T. Targeted mutagenesis in chicken using CRISPR/Cas9 system. Sci Rep. 2016; 6: 23980.
54. Zuo Q, Wang Y, Chen S, Lian C, Tang B, Wang F, et al. Site-directed genome knockout in chicken cell line and embryos can use CRISPR/Cas gene editing technology. G3 (Bethesda). 2016; 6(6): 1787-1792.
55. Zhang Y, Wang Y, Zuo Q, Li D, Zhang W, Wang F, et al. CRISPR/Cas9 mediated chicken Stra8 gene knockout and inhibition of male germ cell differentiation. PLoS One. 2017; 12(2): e0172207.
56. Byrne SM, Ortiz L, Mali P, Aach J, Church GM. Multi-kilobase homozygous targeted gene replacement in human induced pluripotent stem cells. Nucleic Acids Res. 2014; 43(3): e21.
57. Mali P, Aach J, Stranges PB, Esvelt KM, Moosburner M, Kosuri S, et al. CAS9 transcriptional activators for target specificity screening and paired nickases for cooperative genome engineering. Nat Biotechnol. 2013; 31(9): 833-838.
58. Kherraf Z-E, Conne B, Amiri-Yekta A, Kent MC, Coutton C, Escoffier J, et al. Creation of knock out and knock in mice by CRISPR/Cas9 to validate candidate genes for human male infertility, interest, difficulties and feasibility. Mol Cell Endocrinol. 2018; 468: 70-80.
59. Wang L, Yang L, Guo Y, Du W, Yin Y, Zhang T, et al. Enhancing targeted genomic DNA editing in chicken cells using the CRISPR/Cas9 system. PLoS One. 2017; 12(1): e0169768.
60. Morshed M, Sano S, Nishimiya D, Ando M, Nishijima K, Iijima S. Chicken ovalbumin promoter is demethylated upon expression in the regions specifically involved in estrogen-responsiveness. Biosci Biotechnol Biochem. 2006; 70(6): 1438-1446.
61. Kodama D, Nishimiya D, Nishijima K, Okino Y, Inayoshi Y, Kojima Y, et al. Chicken oviduct-specific expression of transgene by a hybrid ovalbumin enhancer and the Tet expression system. J Biosci Bioeng. 2012; 113(2): 146-153.
62. Lillico SG, Sherman A, McGrew MJ, Robertson CD, Smith J, Haslam C, et al. Oviduct-specific expression of two therapeutic proteins in transgenic hens. Proc Natl Acad Sci USA. 2007; 104(6): 1771-1776.
63. Kwon SC, Choi JW, Jang H-J, Shin SS, Lee SK, Park TS, et al. Production of biofunctional recombinant human interleukin 1 receptor antagonist (rhIL1RN) from transgenic quail egg white. Biol Reprod. 2010; 82(6): 1057-1064.
64. Kaye JS, Pratt-Kaye S, Bellard M, Dretzen G, Bellard F, Chambon P. Steroid hormone dependence of four DNase I-hypersensitive regions located within the 7000-bp 5′-flanking segment of the ovalbumin gene. EMBO J. 1986; 5(2): 277-285.
65. Rojas-Fernandez A, Herhaus L, Macartney T, Lachaud C, Hay RT, Sapkota GP. Rapid generation of endogenously driven transcriptional reporters in cells through CRISPR/Cas9. Sci Rep. 2015; 5: 9811.
66. Oishi I, Yoshii K, Miyahara D, Tagami T. Efficient production of human interferon beta in the white of eggs from ovalbumin gene-targeted hens. Sci Rep. 2018; 8(1): 10203.
67. Heigwer F, Kerr G, Boutros M. E-CRISP: fast CRISPR target site identification. Nat Methods. 2014; 11(2): 122-123.
68. Haeussler M, Schönig K, Eckert H, Eschstruth A, Mianné J, Renaud JB, et al. Evaluation of off-target and on-target scoring algorithms and integration into the guide RNA selection tool CRISPOR. Genome Biol. 2016; 17(1): 148.
69. Kozak M. An analysis of 5'-noncoding sequences from 699 vertebrate messenger RNAs. Nucleic Acids Res. 1987; 15(20): 8125-8148.
70. Badorf M, Edenhofer F, Dries V, Kochanek S, Schiedner G. Efficient in vitro and in vivo excision of floxed sequences with a high-capacity adenoviral vector expressing CRE recombinase. Genesis. 2002; 33(3): 119-124.

Original Article

An Easy and Fast Method for Production of Chinese Hamster Ovary Cell Line Expressing and Secreting Human Recombinant Activin A

Hassan Rassouli, Ph.D.[1, 2*], Ali Sayadmanesh, M.Sc.[3], Siamak Rezaeiani, M.Sc.[3], Zahra Ghezelayagh, M.Sc.[3, 4], Mohammad Reza Gharaati, Ph.D.[3], Yaser Tahamtani, Ph.D.[3, 5*]

1. Department of Molecular Systems Biology, Cell Science Research Center, Royan Institute for Stem Cell Biology and Technology, ACECR, Tehran, Iran
2. Department of Medical Laser, Medical Laser Research Center, Yara Institute, ACECR, Tehran, Iran
3. Department of Stem Cells and Developmental Biology, Cell Science Research Center, Royan Institute for Stem Cell Biology and Technology, ACECR, Tehran, Iran
4. Department of Developmental Biology, University of Science and Culture, Tehran, Iran
5. Interdisciplinary Department for Diabetes, Obesity and Metabolism, Cell Science Research Center, Royan Institute for Stem Cell Biology and Technology, ACECR, Tehran, Iran

Corresponding Addresses: P.O.Box: 16635-148, Department of Molecular Systems Biology, Cell Science Research Center, Royan Institute for Stem Cell Biology and Technology, ACECR, Tehran, Iran
Department of Stem Cells and Developmental Biology, Cell Science Research Center, Royan Institute for Stem Cell Biology and Technology, ACECR, Tehran, Iran
Emails: hassan.rassouli@royaninstitute.org, yasertahamtani@Royaninstitute.org

Received: 2/December/2018, Accepted: 10/February/2019

Abstract

Objective: Growth factors are key elements of embryonic stem cell (ESC) research. Cell line development in eukaryotes is a time-consuming procedure which usually takes 12-18 months. Here, we report an easy and fast method with which production of Chinese hamster ovary (CHO) cells that express and secrete recombinant Activin A, as a major growth factor in endo/mesoderm differentiation of embryonic stem cells is achieved within 3-4 weeks.

Materials and Methods: In this experimental study, we cloned human Activin A into the pDONR/Zeo gateway entry vector using the BP reaction. Activin A was subcloned next into the pLIX_403 and pLenti6.3/TO/V5-DEST destination vectors by the LR reaction. The result was the production of constructs with which 293T cells were finally transfected for virus production. CHO cells were transduced using viral particles to produce a cell line that secretes the His6- Activin A fusion protein.

Results: We developed a quick protocol which saves up to 3-4 weeks of time for producing recombinant proteins in CHO cells. The recombinant cell line produced 90 mg/L of functional Activin A measured in human ESC line Royan H5 (RH5), during *in vitro* differentiation into meso-endoderm and definitive endoderm.

Conclusion: Our results showed no significant differences in functionality between commercial Activin A and the one produced using our novel protocol. This approach can be easily used for producing recombinant proteins in CHO.

Keywords: Activin A, Cell Proliferation, CHO Cells, Embryonic Stem Cells, Recombinant Protein

Cell Journal(Yakhteh), Vol 22, No 2, July-September (Summer) 2020, Pages: 140-148

Citation: Rassouli H, Sayadmanesh A, Rezaeiani S, Ghezelayagh Z, Gharaati MR, Tahamtani Y. An easy and fast method for production of Chinese hamster ovary cell line expressing and secreting human recombinant activin A. Cell J. 2020; 22(2): 140-148. doi: 10.22074/cellj.2020.6580.

Introduction

Growth factors though play important roles in stem cell research, are regarded as one of the most expensive components of culture media. Activin A has a wide range of biological activities in hematopoietic mesoderm induction, reproductive physiology, bone remodeling, and most importantly, in neural cell differentiation (1-4). Activin A plays a critical role in the initial step of stem cells differentiation towards endoderm precursors such as lung cells, hepatocytes and pancreatic progenitors (5-7). Huge progress was made worldwide concerning the differentiation of stem cells towards insulin-secreting beta-like cells. A highly efficient method of endoderm cell production is, therefore, necessary to gain high numbers of pancreatic progenitors and endocrine cells for further clinical applications (8, 9). Activin A, as a growth factor is a homo-dimeric polypeptide (27 kDa molecular weight) which is a member of the transforming growth factor (TGF)-β superfamily (10). The precursor protein has 426 amino acids but after completion of the maturation process, only 116 amino acids Gly311-Ser426 remain. amino acid Cys390 from the two chains attach each other by a disulfide bond to make a homo-dimeric Activin A (11).

The emergence of induced pluripotent stem cells (iPSCs) and trans-differentiation have increased the hope for using recombinant transcription factors associated with cell-penetrating peptides to facilitate the conversion of different cell types toward specific cell types. In this regard, the following differentiation approaches has previously been reported: conversion of human embryonic stem cell (hESC) into cardiomyocyte using ISL1 protein (12), hESC into dopaminergic neurons using recombinant LMX1A factor (13), human fibroblasts into dopaminergic neural progenitor-like cells using recombinant Yamanaka factors (14) and human fibroblasts toward cardiomyocyte-like cells via recombinant Yamanaka factors (15); nevertheless, the growth factors are still key elements in the production of different cell types.

Recombinant growth factors are being commercially produced in both prokaryotes and eukaryotes. The

most popular protein expression systems are bacteria (*E. coli*), yeast (*S. cerevisiae*), insect or mammalian (HEK293 and CHO cells) systems. Factors like: time, amount of needed protein, ease of handling, disulfide bonds formation and type of post-translational modifications (PTM) determine the type of expression system and host used to produce recombinant proteins. Technically, production of recombinant proteins in *E. coli* is simpler and could be done in a significantly shorter period of time (16, 17). Expression of some proteins still needs to be done in eukaryotes because some expressed proteins in *E. coli* are not properly folded and they may require PTM such as glycosylation, lipidation, methylation and acetylation (18), or eukaryotic cells chaperons for correct folding (19) or tertiary/ quaternary structure formation despite its higher costs and longer time period requirement. Also, for protein-protein interaction (PPI) studies, recombinant proteins must be expressed in their original cell so the researchers will have a better understanding of proteins network (20).

CHO cells were derived from a CHO about 61 years ago in Theodore Puck's lab (21) and became the first choice for therapeutic and non-therapeutic recombinant proteins production in eukaryotic cells (22, 23). Nowadays, globally, hundreds of billions of Dollars are annually spent on the production of recombinant proteins in CHO cells (24). This further highlights the importance of producing recombinant proteins in CHO cells. One of the major steps in producing recombinant proteins in eukaryotic cells is the development of stable cell lines which produce sufficient amount of proteins. Typically, this step may take up to 6-12 months (25, 26).

Here, we report the development of a quick protocol which takes 3-4 weeks to develop CHO cell line with acceptable yield. In addition, expression of functional human Activin A was measured by sodium dodecyl sulfate polyacrylamide gel electrophoresis (SDS-PAGE), western blotting, and MTS assay; and hESC differentiation into definitive endoderm was also investigated.

Materials and Methods

Isolation of Activin A cDNA

In this experimental study, according to previously published data (27), 20 day old embryoid bodies (EB) derived from human ESCs express Activin A mRNA. EBs total RNA was isolated using TRIzol (Sigma-Aldrich, USA) according to the manufacturer's protocol. The first strand of cDNA was synthesized using SuperScript III reverse transcriptase (Invitrogen, USA), an oligo dT primer, and 2 µg of purified total RNA. For Activin A amplification, primers were designed to amplify nucleotides 931-1281 (Accession # NM_002192.2) corresponding to Gly311-Ser426 amino acids (Accession # P08476). Generated cDNA was amplified using below-mentioned primers:

AttB1-Ig κ1: 5′-GGG GAC AAG TTT GTA CAA AAA AGC AGG CTG CCG CCA CCA TGG AGA CAG ACA CAC TCC TGC TAT GGG TAC TGC TGC TCT GGG TTC CAG GTT CCA CTG GTG- 3′

Ig κ1-His: 5′- GTT CCA GGT TCC ACT GGT GAC CAT CAC CAC CAC CAT CAT-3′

His-Activin: 5′-CAT CAC CAC CAC CAT CAT GGC TTG GAG TGT GAT GGC-3′

AttB2-activin: 5′-GGG GAC CAC TTT GTA CAA GAA AGC TGG GTC TAT GAG CAC CCA CAC TC-3′

Primers contained Igκ1 signal peptide, 6 His tag, and gateway attachment site B1 (AttB1) and AttB2 sequences used for protein secretion, purification, and quick cloning, respectively. Also, a stop codon was included in the sequence to terminate the translation reaction. For fragment amplification, pfx DNA polymerase (Invitrogen, Carlsbad, CA, USA) and Mastercycler® Gradient PCR (Eppendorf Netheler-Hinz GmbH, Germany) were used. Amplification was done using 3 tandem PCR reactions as follows: The first polymerase chain reaction (PCR) included pre-incubation at 95˚C for 4 minutes; 10 cycles at 95˚C for 30 seconds, 60˚C for 30 seconds, and 68˚C for 40 seconds with His-Activin and AttB2-activin primers; The second PCR was comprised of 10 cycles at 95˚C for 30 seconds, 60˚C for 30 seconds, and 68˚C for 40 seconds with Ig κ1-His and AttB2-activin primers; and the third PCR included 30 cycles at 95˚C for 30 seconds, 60˚C for 30 seconds, and 68˚C for 40 seconds, followed by incubation with AttB1-Ig κ1 and AttB2-activin primers at 68˚C for 8 minutes. PCR products were analyzed by electrophoresis on a 1% agarose gel, stained with ethidium bromide and examined under ultraviolet (UV) light.

Construction of the pENTER/Activin A entry clone

The resultant PCR product was cloned into the pDONR/ Zeo gateway entry vector using the BP clonase according to the supplier's directions (Invitrogen, USA). The recombinant pENTER/Activin A entry clone was transferred into Library Efficiency® DH5α™ Competent Cells (Invitrogen, USA) by the heat shock method as described by the manufacturer. Clones were cultured in Luria-Bertani (LB) broth overnight and plasmid extraction was performed using the AccuPrep® Plasmid Mini Extraction Kit (Bioneer, Korea). Recombinant vectors were examined by PCR using the M13-F and Activin -R primers which generated an amplicon of about 650 bp. DNA sequencing of the inserted segment was done using M13-F: 5′-GTA AAA CGA CGG CCA GT-3′ and R: 5′-AGC GGA TAA CAA TTT CAC ACA GGA-3′primers.

Construction of the pLIX_403/Activin A and pLenti6.3/ TO/V5-DEST/Activin A expression vectors

A pENTER /Activin A entry clone construct with correct direction and sequence was chosen for the LR reaction in which, Activin A was transferred from the entry clone into the pLIX_403 and pLenti6.3/TO/V5-DEST destination vectors according to the manufacturer's instructions (Gateway® Technology, Invitrogen, Carlsbad, CA, USA). Products of LR reaction were transferred into Library Efficiency® DH5α™ Competent Cells (Invitrogen,

Carlsbad, CA, USA) by the heat shock method as described by the manufacturer and recombinant expression vectors were confirmed by PCR. Also, we cloned the GFP and RFP markers in pLenti6.3/TO/V5-DEST and pLIX_403, respectively to test the transduceability of CHO cells as well as vectors' elements proper function.

Viral particle preparation

Viral particle preparation was performed as described previously (28). The 293T cells were seeded in 10-cm cell culture dishes. Once cells reached 70% confluency, they were transfected with Lipofectamine 3000 according to the supplier's manual. Recombinant lentiviral particles were harvested every 24 hours for 2 days, filtered, aliquoted and kept at -80˚C for future uses.

Activin A-secreting cell line establishment

The CHO- DG44 cells were grown in Dulbecco's modified Eagle's medium/F12 (DMEM-F12) medium (Gibco, USA) with 1% fetal bovine serum (FBS, Gibco, USA). Cells were seeded in T25 culture dishes and the frozen viruses were added to culture medium. Addition of viral particles was repeated 24 hours later while exchanging the medium. Cells were kept for another 24 hours and then, replated at a ratio of 3:1 in new T25 dishes for antibiotic selection and stable cell line development. Antibiotics, blasticidin, and puromycin were used for pLenti6.3 TO V5-DEST and pLIX_403, respectively, for 10 days.

Recombinant Activin A expression and secretion

As both pLenti6.3 TO V5-DEST and pLIX_403 are Tet-on vectors, 5-10 µg/ml doxycycline was applied to the culture medium for inducing Activin A expression in generated cell lines. To increase the yield, the temperature was set at 32˚C. Culture medium was refreshed every day and finally collected and stored at -80˚C for protein purification.

Recombinant fusion protein purification

The cell debris was precipitated by centrifugation at 14,000 g for 5 minutes, and the supernatant was used for purification. Recombinant His6-Activin A was purified by the Ni-NTA Fast Start Kit (Qiagen, USA). The column was washed with 10 ml of washing buffer [20 mM Tris-HCl (pH=8.0), 150 mM NaCl and 25 mM imidazole] to remove non-specifically bound proteins. His6-Activin A that remained on the column was eluted using 1 ml elution buffer which contained 250 mM imidazole in 3 separate fractions. In each step, 20 µl sample was preserved for further analysis by SDS-PAGE.

The concentration of the purified protein was determined by the Bradford method. Recombinant Activin A was dissolved in a proper storage buffer, filter-sterilized (0.2 µm), distributed into vials (10 µg per vial), lyophilized, and stored at -80˚C for future functional bioassays. The recombinant Activin A was named "homemade Activin A".

SDS-PAGE and mass spectrometry analysis

Identical volumes of different elution fractions were mixed with 5:1 volume of 5X loading buffer [1 M Tris-HCl (pH=6.8), 10% w/v SDS, 0.05% w/v bromophenol blue, 50% glycerol, and 200 mM β-mercaptoethanol] and heated at 95˚C for 5 minutes before analysis by SDS-PAGE using a 12% (w/v) separating gel followed by staining with 0.1% Coomassie brilliant blue R-250. Bands of interest were excised from the SDS-PAGE gel and samples were analyzed by liquid chromatography coupled with tandem mass spectrometry (LC-MS/MS) at Sydney University.

Western blotting

Western blot analysis was performed as described previously (29). Briefly, proteins were separated by 12% SDS-PAGE electrophoresis at 100 V for 2 hours using a Mini-PROTEAN 3 electrophoresis cell (Bio-Rad, Hercules, CA, USA) then transferred to a polyvinylidene difluoride (PVDF) membrane by wet blotting (Bio-Rad, Hercules, CA, USA). Membranes were blocked for 1 hour using 5% bovine serum albumin (BSA, Sigma- Aldrich, USA), and incubated for 1.5 hours at room temperature (RT) (30) with the following primary antibodies [anti-His6 (provided with Ni-NTA Fast Start Kit (Qiagen, USA) 1:5000]. Membranes were rinsed 3 times (15 minutes each) with Phosphate-buffered saline Tween-20 (PBST, 0.05%) and incubated with the peroxidase-conjugated secondary antibody [anti-mouse (Millipore, 1:6000)], for 1 hour at RT. The blots were visualized using Sigma detection reagents (Sigma- Aldrich, USA) and films were scanned by a densitometer (GS-800, Bio-Rad, USA).

Biological analysis of homemade Activin A by MTS assay

Biological analysis was performed using the method described by Phillips and colleagues (31). For Activin A, examination of dose-dependent inhibition of the proliferation of mouse plasmacytoma cell line (MPC-11) which is routinely employed by companies like Sigma and thermo fisher for testing recombinant Activins, was done. In this assay, rates of inhibition of cell proliferation were assessed using the Cell Titer 96 Non-Radioactive Cell Proliferation MTS Assay Kit (Promega, UK) according to manufacturer's manual. Briefly, after testing the viability of the cell lines, cells were plated in 96-well, flat-bottom plates and allowed to attach for a few hours. Serial dilutions of recombinant homemade Activin A and commercial Activin A from Sigma (0-10 ng/ml) were prepared in 96-well flat-bottom plate in SFM. For the control group, the cells were cultured in the absence of Activin A. Subsequently, the cells were added to the wells of a 96-well plate and incubated for 3 days at 37˚C in a humidified, 5% CO_2 atmosphere. After this period, cells viability was assessed by 3-(4,5-dimethylthiazol-2-yl)-5-(3-carboxymethoxyphenyl)-2-(4-sulfophenyl)-2H-tetrazolium (MTS). In this assay, 20 µl of the MTS reagent was added into each well and cells were incubated

at 37˚C for 3 hours. The absorbance was detected at 490 nm by a microplate reader. All the experiments were repeated three times.

Human embryonic stem cell culture

hESC line RH5 (passage 36) was obtained from the Royan Stem Cell Bank (Royan Institute, Iran) and cultured in ES cell maintenance medium, on Matrigel (Sigma-Aldrich, USA)-coated plates as previously reported (32, 33). ES cell maintenance medium contained DMEM-F12 plus GlutaMAX (Gibco, USA) supplemented with 20% knockout serum replacement (KoSR, Invitrogen, USA), 1% insulin-transferrin-selenium (ITS, Invitrogen, USA), 0.1 mM non-essential amino acids (NEAAs, Invitrogen, USA), 1% penicillin/streptomycin (Invitrogen, USA), 0.1 mM β-mercaptoethanol (Sigma-Aldrich, USA), and 100 ng/ml basic fibroblast growth factor (bFGF, Royan Biotech, Iran). Human ES cells were grown in 5% CO_2 atmosphere with 95% humidity. The medium was changed every other day. For maintenance of the cells, they were passaged every 7 days at a 1:4-1:6 split ratio using collagenase IV (0.5 mg/ml, Invitrogen, USA): dispase (1 mg/ml, Invitrogen, USA) at a ratio of 1:1.

Generation of human embryonic stem cell-derived endoderm

Human ESC-derived definitive endoderm differentiation of stem cell colonies began on day 4 of stem cell culture. In the first step, to achieve the meso-endoderm, the hES medium was changed to RPMI-1640 plus GlutaMAX (Invitrogen, USA) supplemented with 1% penicillin/streptomycin, 0.1 mM NEAAs, 0.5% BSA, 2 μM Chir99021 (Stemgent, USA) and 100 ng/ml Activin A (Sigma-Aldrich, USA) for the control group, or 25, 50,100 and 200 ng/ml homemade Activin A for the 4 experimental groups. After 24 hours, in order to reach the definitive endoderm, Chir99021 was removed and the cells were treated for 48 hours with 50 mM ascorbic acid, 5 ng/ml bFGF and 100 ng/ml Activin A for the control group, or 25, 50,100 and 200 ng/ml homemade Activin A for the experimental groups. Before each differentiation step, cultured cells were washed in Dulbecco's phosphate-buffered saline with calcium and magnesium (DPBS, Gibco, USA). It must be mentioned that all the experimental groups were treated with homemade Activin A lot 111 and 112 batches.

Immunocytostaining analysis

Immunocytofluorescence staining was performed using a previously described method (34). Briefly, cells were fixed with 4% paraformaldehyde (PFA, Sigma-Aldrich, USA) for 20 minutes, permeabilized using 0.1% Triton X-100 for 10 minutes, blocked with 10% secondary antibody host serum in 0.5% BSA for 1 hour at 37˚C, and finally incubated with goat anti-human SOX17 antibody (R&D Systems, USA) diluted 1:200 in 0.5% BSA, at 4˚C overnight. For negative controls, primary antibodies were omitted and a similar staining procedure was followed. Cells were subsequently washed with PBST and incubated with diluted (1:700) donkey anti-goat IgG-Alexa Fluor® 546 antibody (Invitrogen, USA) for 1 hour. Cell nuclei were stained with 4′, 6-diamidino-2-phenylindole (DAPI, Sigma-Aldrich, USA) for 1 minute and afterward observed under a fluorescence microscope (BX51, Olympus, Japan) equipped with Olympus DP72 digital camera for imaging. For each group, six 40X frames were captured and the percentage of positive cells observed in these frames was calculated by ImageJ. The percentage was expressed as mean ± standard deviation (SD).

Results

Cloning of Activin A cDNA and construction of the entry clones and the expression vectors

The 499-bp Activin A /Ig κ1/His tag/AttB1&2 gene was amplified (Fig.1A) from hESC cDNA and subsequently cloned in a pDONR/Zeo gateway entry vector using the BP reaction to produce a pENTER/Activin A entry clone. The recombinant entry clone was transferred into Library Efficiency® DH5α™ Competent Cells and as a result, tens of clones appeared on the next day. Since the gateway cloning method has low false-positive results, all clones were confirmed by PCR analysis and five clones were randomly selected for further analysis (Fig.1B). DNA sequencing results showed that four out of five clones had no mutation; a clone with no mutation was used for further LR reactions with pLIX_403 (Fig.1C) and pLenti6.3 TO V5-DEST (Fig.1D). The pENTER/Activin A entry clone 1 and pLenti6.3/TO/V5-DEST and pLIX_403 destination vectors were separately used for constructing the expression clone using the LR reactions and were transferred into Library Efficiency® DH5α™ Competent Cells. Five clones out of tens of clones were randomly tested by colony PCR for both destination vectors. We observed that all clones were positive for Activin A insertion, indicating that the LR reactions were 100% efficient. For both expression vectors, a similar clone was selected for virus production and cell line establishment.

More than 50% of purified homemade Activin A showed dimer form

The CHO pLIX_403/Activin A (Fig.1C) or pLenti6.3/TO/V5-DEST/Activin A (Fig.1D) stable cell lines were grown in DMEM-F12 medium and induced by addition of 5-10 μg/ml doxycycline. Media were collected every day and expressed fusion proteins were purified by immobilized metal affinity chromatography (IMAC) on a nickel 2^+ column using 25 mM imidazole, which eliminated the majority of contaminating proteins in the flow and through the washing steps. The fusion protein was obtained in the 250 mM imidazole fractions (Fig.1E). The identities of the purified fusion proteins were confirmed by trypsin digest and LC/MS/MS. The MS results indicated that our fusion proteins matched the Activin A protein (Accession No. NP_999193.1; data not shown). Western blotting under non-reduced conditions showed 13 and 26 kD proteins indicating monomer and dimer homemade Activin A, respectively (Fig.1F). This result confirms that at least 50% of the secreted Activin A is in dimer form and are most likely folded correctly.

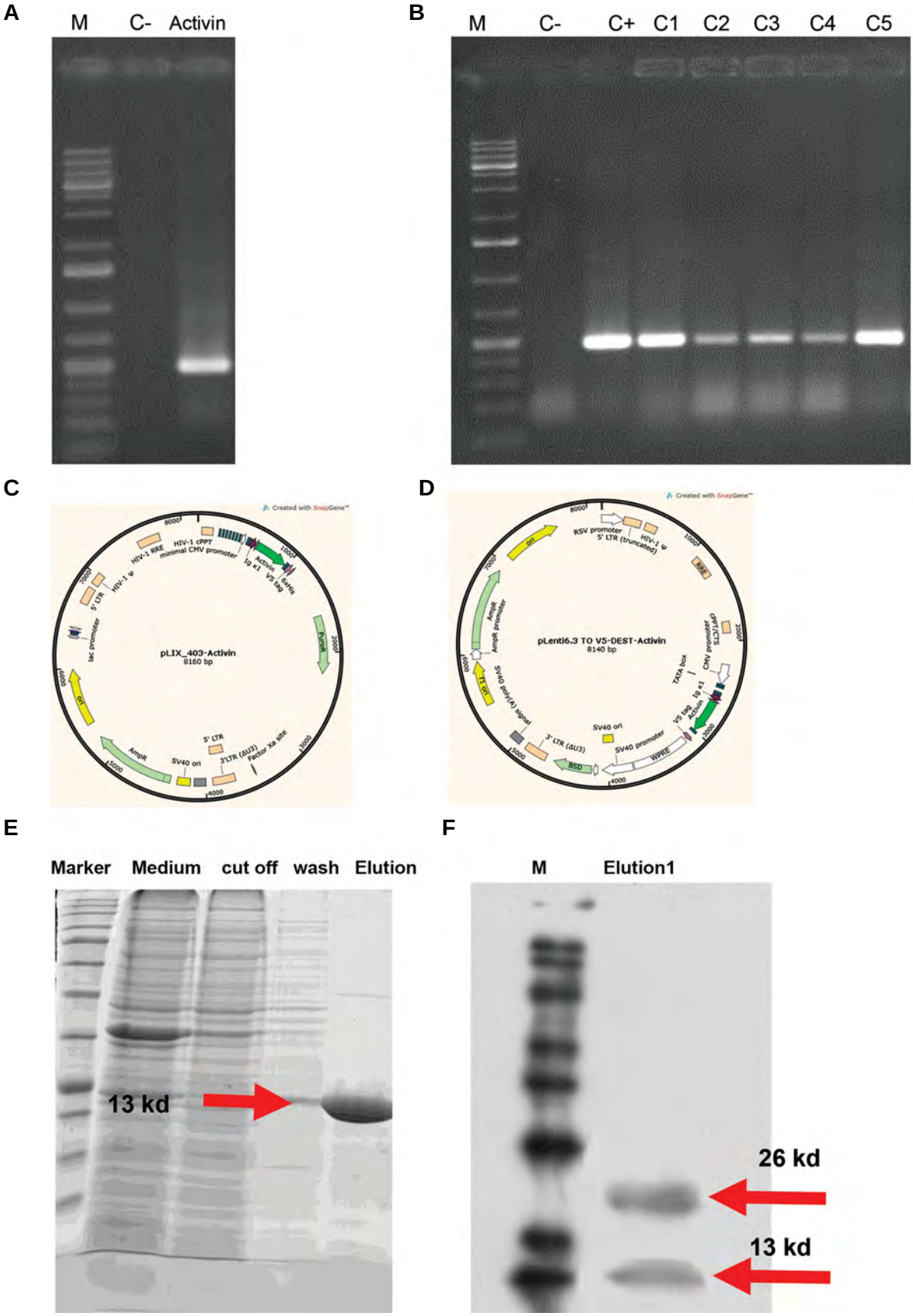

Fig.1: Activin A cloning and expression confirmation. PCR analysis of amplified Activin A, SDS-PAGE analysis and western blotting of produced Activin A. **A.** The expected 499-bp product of Activin A was amplified by PCR using primers that added Ig κ1/His tag/AttB1 to 5´end and AttB2 to 3´end, **B.** Colony PCR products of Activin A for five clones (C1-C5), **C, D.** pLIX_403/Activin & pLenti6.3/TO/V5-DEST/Activin constructs map, **E.** SDS-PAGE analysis of produced Activin A. Recombinant his-tag-Activin A was successfully expressed, secreted and purified. The purified proteins showed the expected size band (13 kD), and **F.** Western blotting of Activin under non-reduced condition. Here, 13 and 26 kD proteins show monomer and dimer forms of Activin, respectively. These results confirm that at least 50% of secreted Activin is in dimer form and possibly folded correctly. M; Size marker, C-; Negative control, C+; Positive control, PCR; Polymerase chain reaction, and SDS-PAGE; Sodium dodecyl sulfate polyacrylamide gel electrophoresis.

pLenti6.3/TO/V5-DEST/GFP and pLIX_403/RFP vectors could express high levels of recombinant protein

As mentioned earlier, pLenti6.3/TO/V5-DEST/GFP and pLIX_403/RFP were used to test the proper function of the vector, viral particle preparation protocol and also, CHO cells transfect ability. Fluorescent microscopy imaging results (Fig.2) showed that both pLenti6.3/TO/V5-DEST/GFP and pLIX_403/RFP expression vectors could express high levels of inserted genes. In addition, both vectors were functional in CHO cells and viral particles produced in 293T cells could transduce CHO cells very efficiently.

Homemade Activin A could inhibit the proliferation of MPC-11 cells

The biological activity of the recombinant Activin A with respect to its ability to dose-dependently inhibit the proliferation of MPC-11 was assessed by MTS assay. The results shown in Figure 3A indicated that Activin A at concentrations up to 20 ng/ml, can inhibit the proliferation of MPC-11 cells in a dose-dependent manner. The activity of homemade Activin A is about 70% of that of the commercial Activin's (Gibco and R&D).

Homemade Activin A-treated human embryonic stem cells expressed high levels of SOX17

To evaluate the efficiency of endoderm induction by homemade Activin A, the expression of definitive endoderm marker, SOX17, was analyzed on differentiation day 4 in human ESCs (RH5 cell line). Immunofluorescent staining showed the expression of SOX17 in both control and treated groups (Fig.3B). The control group treated with commercial Activin A, markedly expressed SOX17 marker (76.3%), while the groups treated with homemade Activin A expressed lower percentages of the endodermal marker. The cells treated with homemade Activin A lot 111 at concentrations of 25, 50, 100 and 200 ng/ml showed 13, 23, 35 and 43% of SOX17 expression, respectively. Cells treated with 25, 50, 100 and 200 ng/ml homemade Activin A lot 112 revealed 30, 37, 20 and 33% of SOX17 expression, respectively.

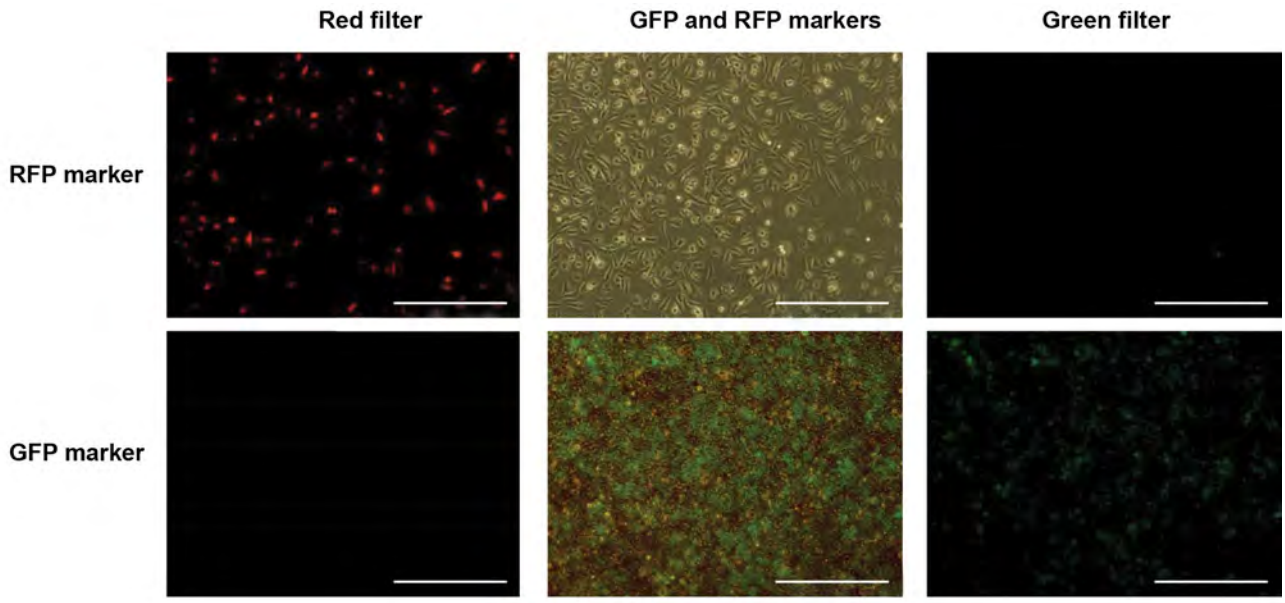

Fig.2: Fluorescent microscopy imaging results confirm that viral particles produced by pLenti6.3/TO/V5-DEST/GFP and pLIX_403/RFP expression vectors, can efficiently transduce CHO cells and express high levels of inserted genes (scale bar: 200 µm).

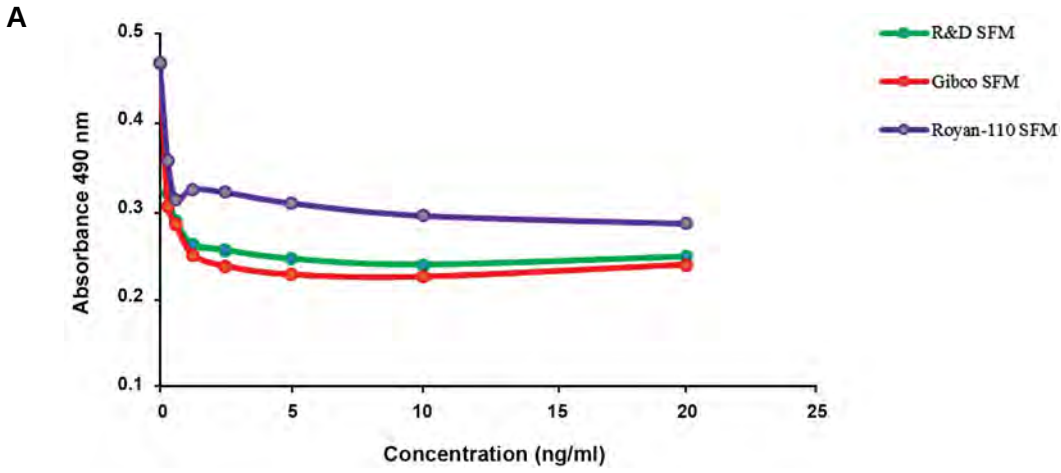

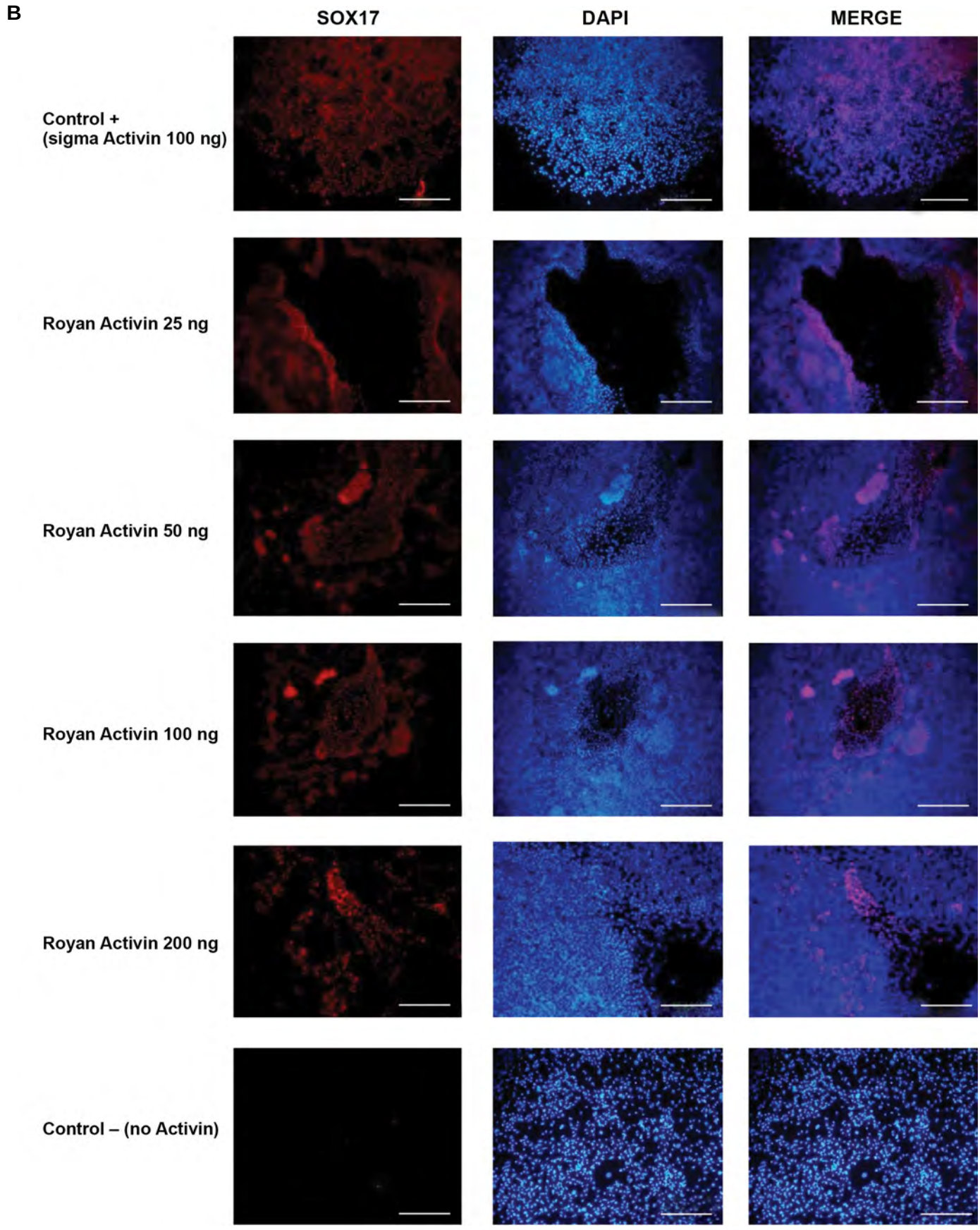

Fig.3: The biological activity of the homemade Activin confirmed it is comparable with commercial Activin's. **A.** Dose-dependent inhibition of MPC-11 proliferation assessed by MTS. The results indicated that Activin A at concentrations up to 20 ng/ml, can inhibit the proliferation of MPC-11 cells in a dose-dependent manner and its activity is about 70% of that of the commercial Activin's (Gibco and R&D) and **B.** Differentiation of human ES cell into definitive endoderm cells. The cells treated with 25, 50, 100 and 200 ng/ml homemade Activin lot 111 showed 13, 23, 35 and 43% SOX17 expression, respectively while cells treated with Activin A from Sigma, expressed 76% SOX17 marker (scale bar: 200 µm).

Discussion

In the present study, we cloned a cDNA encoding human Activin A into the pDNOR/Zeo gateway entry vector using the BP reaction, then, into pLIX_403 and pLenti6.3/TO/V5-DEST destination vectors by using the LR reaction. We used Gateway Technology as it is a rapid, highly-efficient technique and suitable for cloning and sub-cloning of several target genes simultaneously. This technology provides a wide range of destination vectors for different applications. Also any vector could be converted into gateway compatible destination vectors with single step ligation reaction. The pLIX_403 and pLenti6.3/TO/V5-DEST vectors have a strong promoter which allows production of high levels of recombinant proteins under the control of doxycycline and has tight control over the expression induction under desired conditions. We used CHO cells which are the prominent eukaryotic cells used for protein expression. CHO cells glycosylation pattern is highly similar to that observed in humans.

As previously shown by several studies (35), routine and standard approaches take about 12-18 months for cell line development, while our experiment was completed within 3-4 weeks. This allows researchers to test tens of variables to get the optimum conditions and elements needed for best protein expression and possibly industrial applications. The produced recombinant Activin A had correct folding with no inclusion body and its production was markedly cost-effective. We assessed the functionality of homemade Activin A during hES cell line RH5 differentiation into meso-endoderm and definitive endoderm. We also demonstrated that homemade Activin A that was used in this study is of high quality compared with commercial Activin A. This paves the way for cost-effective commercial production of homemade Activin A and substantial reduction in experimental costs especially in the fields of stem cell research and cell therapy.

Conclusion

Our results indicated a little difference in functionality between in-house generated and commercialized Activin A where, this shortcoming could be addressed in future. The availability of large quantities of recombinant Activin A would greatly facilitate mouse and human pluripotent stem cell differentiation cultures.

Acknowledgements

We appreciate the constructive feedback we received from our colleagues at Royan Institute. This study was funded by grants provided by both Royan Institute and the Iranian Council for Stem Cell Technology research. The authors declare no financial or commercial conflicts of interest.

Authors' Contributions

H.R.; Contributed to all experimental work, primers design, construction of genes, viral particle preparation, cell line establishment, protein expression, and purification, SDS-PAGE, and manuscript and figures preparation. A.S., S.R.; Performed biological assay by MTS assay. Z.Gh.; Performed hESCs culture and definitive endoderm cells differentiation. M.R.G., Y.T.; Provided scientific advice throughout the project and preparation of manuscript. All authors approved the final version of this manuscript.

References

1. Ying SY, Zhang Z, Furst B, Batres Y, Huang G, Li G. Activins and activin receptors in cell growth. Proc Soc Exp Biol Med. 1997; 214(2): 114-122.
2. Smith JC, Price BM, Green JB, Weigel D, Herrmann BG. Expression of a Xenopus homolog of Brachyury (T) is an immediate-early response to mesoderm induction. Cell. 1991; 67(1): 79-87.
3. Fathi A, Mirzaei M, Dolatyar B, Sharifitabar M, Bayat M, Shahbazi E, et al. Discovery of novel cell surface markers for purification of embryonic dopamine progenitors for transplantation in parkinson's disease animal models. Mol Cell Proteomics. 2018; 17(9): 1670-1684.
4. Fathi A, Hatami M, Vakilian H, Han CL, Chen YJ, Baharvand H, et al. Quantitative proteomics analysis highlights the role of redox hemostasis and energy metabolism in human embryonic stem cell differentiation to neural cells. Mol Cell Proteomics. 2018; 17(9): 1670-1684.
5. Farzaneh Z, Najarasl M, Abbasalizadeh S, Vosough M, Baharvand H. Developing a cost-effective and scalable production of human hepatic competent endoderm from size-controlled pluripotent stem cell aggregates. Stem Cells Dev. 2018; 27(4): 262-274.
6. Firth AL, Dargitz CT, Qualls SJ, Menon T, Wright R, Singer O, et al. Generation of multiciliated cells in functional airway epithelia from human induced pluripotent stem cells. Proc Natl Acad Sci USA. 2014; 111(17): E1723-E1730.
7. Rezania A, Bruin JE, Arora P, Rubin A, Batushansky I, Asadi A, et al. Reversal of diabetes with insulin-producing cells derived in vitro from human pluripotent stem cells. Nat Biotechnol. 2014; 32(11): 1121-1133.
8. Pagliuca FW, Millman JR, Gürtler M, Segel M, Van Dervort A, Ryu JH, et al. Generation of functional human pancreatic β cells in vitro. Cell. 2014; 159(2): 428-439.
9. Schulz TC, Young HY, Agulnick AD, Babin MJ, Baetge EE, Bang AG, et al. A scalable system for production of functional pancreatic progenitors from human embryonic stem cells. PLoS One. 2012; 7(5): e37004.
10. Xia Y, Schneyer AL. The biology of activin: recent advances in structure, regulation and function. J Endocrinol. 2009; 202(1): 1-12.
11. Stamler R, Keutmann HT, Sidis Y, Kattamuri C, Schneyer A, Thompson TB. The structure of FSTL3.activin A complex. Differential binding of N-terminal domainsinfluences follistatin-type antagonist specificity. J Biol Chem. 2008; 283(47): 32831-32838.
12. Fonoudi H, Yeganeh M, Fattahi F, Ghazizadeh Z, Rassouli H, Alikhani M, et al. ISL1 protein transduction promotes cardiomyocyte differentiation from human embryonic stem cells. PLoS One. 2013; 8(1): e55577.
13. Fathi A, Rasouli H, Yeganeh M, Salekdeh GH, Baharvand HJMb. Efficient differentiation of human embryonic stem cells toward dopaminergic neurons using recombinant LMX1A factor. Mol Biotechnol. 2015; 57(2): 184-194.
14. Mirakhori F, Zeynali B, Rassouli H, Salekdeh GH, Baharvand H. Direct conversion of human fibroblasts into dopaminergic neural progenitor-like cells using TAT-mediated protein transduction of recombinant factors. Biochem Biophys Res Commun. 2015; 459(4): 655-661.
15. Ghazizadeh Z, Rassouli H, Fonoudi H, Alikhani M, Talkhabi M, Darbandi-Azar A, et al. Transient activation of reprogramming transcription factors using protein transduction facilitates conversion of human fibroblasts toward cardiomyocyte-like cells. Mol Biotechnol. 2017; 59(6): 207-220.
16. Rassouli H, Tabe Bordbar MS, Rezaei Larijani M, Pakzad M, Baharvand H, Salekdeh GH. Cloning, expression and functional characterization of in-house prepared human basic fibroblast growth factor. Cell J. 2013; 14(4): 282-291.
17. Rassouli H, Nemati S, Rezaeiani S, Sayadmanesh A, Gharaati MR, Salekdeh GH, et al. Cloning, expression, and functional characterization of in-house prepared human leukemia inhibitory factor.

Cell J. 2013; 15(2): 190-197.
18. Walsh G, Jefferis R. Post-translational modifications in the context of therapeutic proteins. Nat Biotechnol. 2006; 24(10): 1241-1252.
19. Hartl FU. Molecular chaperones in cellular protein folding. Nature. 1996; 381(6583): 571-579.
20. Yousefi M, Hajihoseini V, Jung W, Hosseinpour B, Rassouli H, Lee B, et al. Embryonic stem cell interactomics: the beginning of a long road to biological function. Stem Cell Rev. 2012; 8(4): 1138-1154.
21. Tjio JH, Puck TT. Genetics of somatic mammalian cells. II. Chromosomal constitution of cells in tissue culture. J Exp Med. 1958; 108(2): 259-268.
22. Wurm FM. Production of recombinant protein therapeutics in cultivated mammalian cells. Nat Biotechnol. 2004; 22(11): 1393-1398.
23. Ashall F, Sullivan N, Puck TT. Specificity of the cAMP-induced gene exposure reaction in CHO cells. Proc Natl Acad Sci USA. 1988; 85(11): 3908-3912.
24. Aggarwal RS. What's fueling the biotech engine-2012 to 2013. Nat Biotechnol. 2014; 32(1): 32-39.
25. Sleiman RJ, Gray PP, McCall MN, Codamo J, Sunstrom NA. Accelerated cell line development using two-color fluorescence activated cell sorting to select highly expressing antibody-producing clones. Biotechnol Bioeng. 2008; 99(3): 578-587.
26. Wurm FM. Production of recombinant protein therapeutics in cultivated mammalian cells. Nat Biotechnol. 2004; 22(11): 1393-1398.
27. Fathi A, Hatami M, Hajihosseini V, Fattahi F, Kiani S, Baharvand H, et al. Comprehensive gene expression analysis of human embryonic stem cells during differentiation into neural cells. PLoS One. 2011; 6(7): e22856.
28. Ghasemi-Kasman M, Hajikaram M, Baharvand H, Javan M. MicroRNA-mediated in vitro and in vivo direct conversion of astrocytes to neuroblasts. PLoS One. 2015; 10(6): e0127878.
29. Fathi A, Pakzad M, Taei A, Brink TC, Pirhaji L, Ruiz G, et al. Comparative proteome and transcriptome analyses of embryonic stem cells during embryoid body-based differentiation. Proteomics. 2009; 9(21): 4859-4870.
30. Hotchko M, Robert P. Recent market status and trends of fractionated plasma products. Ann Blood. 2018; 3(2): 1-6.
31. Phillips DJ, Brauman JN, Mason AJ, de Kretser DM, Hedger MP. A sensitive and specific in vitro bioassay for activin using a mouse plasmacytoma cell line, MPC-11. J Endocrinol. 1999; 162(1): 111-116.
32. Fathi A, Rasouli H, Yeganeh M, Salekdeh GH, Baharvand H. Efficient differentiation of human embryonic stem cells toward dopaminergic neurons using recombinant LMX1A factor. Mol Biotechnol. 2015; 57(2): 184-194.
33. Faradonbeh MZ, Gharechahi J, Mollamohammadi S, Pakzad M, Taei A, Rassouli H, et al. An orthogonal comparison of the proteome of human embryonic stem cells with that of human induced pluripotent stem cells of different genetic background. Mol Biosyst. 2012; 8(6): 1833-1840.
34. Tahamtani Y, Azarnia M, Farrokhi A, Sharifi-Zarchi A, Aghdami N, Baharvand H. Treatment of human embryonic stem cells with different combinations of priming and inducing factors toward definitive endoderm. Stem Cells Dev. 2013; 22(9): 1419-1432.
35. Lai T, Yang Y, Ng SK. Advances in mammalian cell line development technologies for recombinant protein production. Pharmaceuticals (Basel). 2013; 6(5): 579-603.

Original Article

Comparison of Epigenetic Modifier Genes in Bovine Adipose Tissue-Derived Stem Cell Based Embryos, as Donors, with *In Vitro* and Parthenogenesis Embryos

Mohammad Salehi, Ph.D.[1, 2], Beheshteh Abouhamzeh, Ph.D.[3*], Ahmad Hosseini, Ph.D.[1], Zohreh Zare, Ph.D.[4], Azizollah Bakhtari, Ph.D.[5]

1. Cellular and Molecular Biology Research Center, Shahid Beheshti University of Medical Sciences, Tehran, Iran
2. Department of Biotechnology, School of Advanced Technologies in Medicine, Shahid Beheshti University of Medical Sciences, Tehran, Iran
3. Department of Anatomical Sciences, Faculty of Medicine, AJA University of Medical Sciences, Tehran, Iran
4. Department of Anatomical Sciences, Faculty of Medicine, Mazandaran University of Medical Sciences, Sari, Iran
5. Department of Reproductive Biology, School of Advanced Medical Sciences and Technologies, Shiraz University of Medical Sciences, Shiraz, Iran

Corresponding Address: P.O.Box: 1411718541, Department of Anatomical Sciences, Faculty of Medicine, AJA University of Medical Sciences, Tehran, Iran
Email: b.abouhamzeh.ba@gmail.com

Received: 14/January/2019, Accepted: 13/March/2019

Abstract

Objective: Regarding that undifferentiated mesenchymal stem cells, as donor cells, require less epigenetic reprogramming, possibility of using bovine adipose tissue-derived stem cells (BASCs) with low level of *DNMTs* and *HDACs* expression was evaluated.

Materials and Methods: In this experimental study, we examined gene expression of epigenetic modifiers including DNA methyltransferases (*DNMT1, DNMT3A* and *DNMT3B*) and histone deacetylases (*HDAC1-3*), as well as protein levels of histone H3 acetylation at lysine 9 (H3K9ac) and POU5F1 (also known as OCT4) at two stages of preimplantation development among *in vitro* fertilization (IVF), parthenogenetic activation (PA) and somatic cell nuclear transfer (SCNT) groups.

Results: The results revealed that developmental competence of IVF embryos was higher than SCNT embryos ($P<0.05$). In the PA and SCNT groups, *DNMT1, HDAC2* and *HDAC3* mRNA were overexpressed ($P<0.05$), and proteins levels of H3K9ac and POU5F1 were reduced at 6-8 cells and blastocyst stages compared to IVF ($P<0.05$). The mRNA expression of *DNMT1* and *HDAC1* and proteins levels of POU5F1 and H3K9ac were significantly different between SCNT and PA groups ($P<0.05$) in both developmental stages (except *HDAC1* in blastocyst stage).

Conclusion: The SCNT embryos derived from BASCs have endured considerable nuclear reprogramming during early embryo development. Comparison of PA and SCNT blastocysts demonstrated that *HDAC1* and *DNMT1* may attribute to developmental competence variability of bovine embryos.

Keywords: DNA Methyltransferases, Histone Deacetylases, Mesenchymal Stem Cells, POU5F1

Cell Journal(Yakhteh), Vol 22, No 2, July-September (Summer) 2020, Pages: 149-157

Citation: Salehi M, Abouhamzeh B, Hosseini A, Zare Z, Bakhtari A. Comparison of epigenetic modifier genes in bovine adipose tissue-derived stem cell based embryos, as donors, with in vitro and parthenogenesis embryos. Cell J. 2020; 22(2): 149-157. doi: 10.22074/cellj.2020.6714.

Introduction

Although several cloned mammals have been created following somatic cell nuclear transfer (SCNT) in a number of animals, less than 5% of them resulted in live birth. One of the reasons for this failure is using differentiated cells as donor cells that are unable to undergo a suitable epigenetic reprogramming, as a necessary point for better developmental competence in the cloned embryos (1).

Abnormal epigenetic marks of DNA and histone, including disruption of imprinted gene expression and high levels of global DNA methylation in the SCNT embryos, are suggested to be the cause of aberrant gene expression during early embryonic development (2). In cloned embryos, global DNA demethylation of CpG sites (except imprinted gene), occurring soon after fertilization, undergoes extensive changes during early embryonic developmental stage (3).

DNA methyltransferase 1 (DNMT1) is responsible for the maintenance of methylation of CpG dinucleotides in the daughter strand of DNA during replication (4). During cleavage-stage, *DNMT1* levels in the nucleus remain low. Nevertheless, DNMT3A and DNMT3B have a pivotal role in de novo methylations which are considerably increased at the 8-16 cells stage in bovine embryos. Unlike bovine IVF-derived embryos, DNA demethylation in the SCNT embryos is not occurred after the 2 cells stage (3). Previous studies have found that using donor cells with low levels of *DNMT1* mRNA for SCNT caused higher developmental competence than those with high levels (5, 6).

Other epigenetic marks of chromatin, including post-translational modification of histone tails by methylation or acetylation, closely associate with DNA methylation (7). Generally, histone marks are subject to dynamic changes during preimplantation development. In the case of histone H3, lysine acetylation occurs at the lysine sites

of 14, 23 18, and 9, in order (8). Acetylation of histone is modulated by histone acetyltransferases (HATs) and deacetylases (HDACs) (9). HDAC also negatively regulates *DNMT1* expression by inhibition of *DNMT1* promoter activity (10).

Studies have shown that Trichostatin A (TSA), a HDAC inhibitor, can improve histone marks in the SCNT embryos derived from various mammalian species. This results in higher developmental competence of the related embryos (2, 11-13). Therefore, it seems necessary to identify normal pattern of histone acetylation to ameliorate potential development of SCNT embryos.

A considerable body of evidences has indicated that success in the SCNT outcome is closely related to the origin of donor cells. As adult stem cells (ASCs), such as mesenchymal stem cells (MSCs), are more differentiated than ESCs, they require additional reprogramming with SCNT (14). Undifferentiated embryonic stem cells (ESCs), as donors, require less epigenetic reprogramming than a differentiated somatic cell, and they show better preimplantation development (15, 16).

Improvement in our understanding of epigenetic reprogramming events will give us insight to the potential of SCNT for various agricultural and biomedical applications. To achieve this goal, bovine adipose derived stem cells (BASCs) were used as donor cells, and dynamic changes of histone H3 acetylation at lysine 9 (H3K9ac) and POU5F1 (also known as OCT4) as well as gene expression of *HDACs* and *DNMTs* were evaluated in two different stages of embryo development in the SCNT, parthenogenetic activation (PA) and *in vitro* fertilization (IVF) derived embryos.

Materials and Methods

All chemicals and reagents were purchased from Sigma Chemical Co. (USA) and Gibco (USA) unless otherwise specified.

Oocyte collection and *in vitro* maturation

In this experimental study, local abattoir-derived bovine ovaries were collected and transported to the laboratory at 27-30˚C. Cumulus-oocytes complexes (COCs) were retrieved from antral follicles (3-8 mm). The COCs with several layers of intact cumulus cells and uniformly granulated cytoplasm were selected and cultured in the groups of 10, at 38.5˚C in 50 µl maturation medium tissue culture medium (TCM)-199 supplemented with 10% fetal bovine serum (FBS), 10 ng/ml epidermal growth factor (EGF), 1 µg/ml 17-β estradiol, 10 µg/ml follicle stimulating hormone (FSH), 10 µg/ml luteinizing hormone (LH) and 24.2 mg/l sodium pyruvate) in a humidified 5% CO_2 for 22-24 hours under mineral oil. Matured oocytes were randomly assigned into three groups, as follows: IVF (n=350), PA (n=443) and SCNT (n=130). All procedures were approved by the Institutional Ethical Committee of the Shahid Beheshti University of Medical Sciences (Tehran, Iran).

Nuclear donor cell preparation

BASCs, obtained from subcutaneous fat of Holstein cows, immediately after slaughter at a commercial abattoir, were used as nuclear donors. Briefly, fat pieces of 1-2 mm were washed twice in phosphate-buffered saline (PBS^-) supplemented with 1% penicillin-streptomycin (P/S), and they were digested by 0.5% collagenase type II in 5% CO_2 at 39˚C for 3 hours in high glucose Dulbecco's modified Eagle medium (DMEM). Isolated cells were cultured at 39˚C, 5% CO_2 in DMEM supplemented with 10% FBS, 1% P/S. In order to evaluate differentiation potential, the isolated cells at passage three were treated with osteogenic or adipogenic media. The adipogenic media consisted of DMEM supplemented with 5% FBS, 1% P/S, 0.5 mM isobutyl methylxanthine (IBMX), 250 nM dexamethasone and 50 µM indomethacin. Osteogenesis was induced using DMEM with 5% FBS, 1% P/S, 50 µg/ml L-ascorbic acid biphosphate, 10-7 M dexamethasone and 10 mM beta-glycerophosphate. After 21 days, the cells were fixed in 4% paraformaldehyde solution and stained with alizarin red and oil red for osteogenic and adipogenic differentiation assessment, respectively.

In vitro fertilization, parthenogenetic activation and somatic cell nuclear transfer

The matured oocytes were used for IVF, PA and SCNT. For IVF, groups of 15-20 oocytes were transferred to 100 µl IVF-TALP (Tyrode's albumin lactate pyruvate) medium containing 114 mM NaCl, 3.2 mM KCl, 0.4 mM $NaHPO_4$, 0.5 mM $MgSO_4$, 25 mM $NaHCO_3$, 2.6 mM $CaCl_2$, 10 mM lactate, 0.25 mM pyruvate, 10 µg/ml P/S, 10 µg/ml heparin and 6 mg/ml bovine serum albumin (BSA). Frozen bull semen was thawed at 37˚C for 30 seconds. The motile spermatozoa were harvested from Percoll gradient (90 and 45% Percoll). Approximately 1×10^6 sperm/ml were added to IVF-TALP medium containing expanded COCs and co-incubated for 16 hours at 38.5˚C in a humidified atmosphere of 5% CO_2. Cumulus cells were removed by 1 mg/ml hyaluronidase and vortexing for 4 minutes. The denuded presumptive zygotes were cultured in CR1 medium supplemented with 10% FBS, 2% essential amino acids (EAAs) and 1% non-essential amino acids (NEAAs) at 38.5˚C in a humidified atmosphere of 5% CO_2, 5% O_2 and 90% N_2.

For PA, cumulus cells were removed from mature MII oocytes using 1 mg/ml hyaluronidase and vortexing for 4 minutes. The denuded oocytes were randomly divided into two groups: PA and SCNT. In the PA group, oocytes were incubated in 5 µM Ionomycin for 5 minutes followed by 4 hours exposure to 2 mM 6DMAP in HTCM medium at 38.5˚C and 5% CO_2 in air. After washing for three times, presumptive parthenotes were cultured in CR1 as described for IVF.

For SCNT, mature denuded oocytes were treated with 0.5 µg/ml demecolcine for 30 minutes and they were placed in the manipulation medium supplemented with 7.5 µg/ml cytochalasin B and subsequently enucleation

was performed using a Nikon TE2000U inverted microscope (Nikon, USA) equipped with Narishige micromanipulators at the room temperature. The polar body and MII chromosomes were removed by an 18 µm (internal diameter) glass pipette. The fifth passage of BASCs with the lowest level of chromatin condensation was used as donor cells for SCNT. A single donor cell was placed into the perivitelline space of each enucleated oocyte through the same hole made previously in the zona pellucida during enucleation. The couplets were electrically fused using two direct current pulses of 150 V/mm for 50 miliseconds in a buffer composed of 0.3 M mannitol, 0.15 mM calcium, 0.15 mM magnesium and 0.01% polyvinyl alcohol (PVA). After one hour, couplets were activated by ionomycin and 6DMAP as described for PA embryos.

For all three groups, cleavage and blastocyst rates were evaluated on day 2 and 8 after insemination or activation, respectively. Seven replicates per group were evaluated. 6-8 cells and blastocysts were collected in order to evaluate *DNMTs* and *HDACs* gene expression using quantitative reverse transcription polymerase chain reaction (qRT-PCR), and perform immunostaining for POU5F1 and H3K9ac.

RNA extraction, cDNA synthesis and quantitative reverse transcription polymerase chain reaction

Embryos at the 6-8 cells (embryonic genome activation) and blastocyst stages of development, in all groups (IVF, PA and SCNT) were removed from CR1 medium and washed in PBS. RNA extraction was performed as previously described (17). Briefly, 30 embryos in three biological replicates (10 embryos for each replicate per group) were transferred into 0.2 ml nuclease-free tubes containing 1.5 µl lysis buffer plus 2 µl poly N and 5 µl nuclease free water. The tubes were placed in a Thermal Cycler (Applied Bio-Rad, USA) at 75˚C for 5 minutes, followed by adding 5 µl RT Buffer (5X), 1 µl RT Enzyme (200 U), 3 µl dNTP (10 mM) and 0.25 µl RNase inhibitor (10 U) to each tube. cDNA synthesis program for each embryo pool (6-8 cells and blastocyst) was as follows: 25˚C for 10 minutes, 37˚C for 15 minutes, 42˚C for 45 minutes and 72˚C for 10 minutes.

In order to evaluate gene expression pattern of *DNMTs* (*DNMT1, DNMT3A* and *DNMT3B*) and *HDACs* (*HDAC1, HDAC2* and *HDAC3*) at two stages of preimplantation development, qRT-PCR was performed in the Rotor Gene Q instrument (Qiagen, Germany). PCR reaction was performed in a final volume of 13 µl consisting of 6.5 µl of 2X SYBR Green master mix (Quanta, USA) and 1 µl mixed primer (10 pmol/µl), and 1 µl cDNA. At least three biological replicates were used for each group. *GAPDH* was used as a reference gene for normalization of the comparisons within the same developmental stage. Relative gene expression was then calculated using the $2^{-\Delta\Delta Ct}$ method (18). The primers used for qRT-PCR are listed in Table 1.

Table 1: Details of primers used for quantitative reverse transcription polymerase chain reaction

Gene	Nucleotide sequences (5′–3′)	Fragment size (bp)	Accession number
DNMT1	F: CGGAACTTCGTCTCCTTC	114	NM_182651.2
	R: CACGCCGTACTGACCAG		
DNMT3A	F: TTACACAGAAGCATATCCAGG	143	NM_001206502.1
	R: GAGGCGGTAGAACTCAAAG		
DNMT3B	F: ATCTTGTGTCGTGTGGGG	140	NM_181813.2
	R: CTCGGAGAACTTGCCATC		
HDAC1	F: AGAGAAGAAAGAAGTCACAGAAG	135	NM_001037444.2
	R: GGATAAAGGTAGGGATTTGG		
HDAC2	F: GGCGGTCGTAGAAATGTG	162	NM_001075146.1
	R: TTCTGATTTGGCTCCTTTG		
HDAC3	F: GATGACCAGAGTTACAAGCAC	193	NM_001206243.1
	R: CCAGTAGAGGGATATTGAAGC		
GAPDH	F: GTCGGAGTGAACGGATTC	176	NM_001034034.2
	R: TTCTCTGCCTTGACTGTGC		

Immunofluorescent staining of embryos

Presence of POU5F1 and H3K9ac was assessed by immunofluorescence staining at two stages of preimplantation development (6-8 cells and blastocyst), as previously described (19). Briefly, embryos were washed in washing buffer (PBS^- containing 0.1% Tween-20 and 1% BSA), and fixed for 20 minutes in 4% paraformaldehyde. After three times washing, the embryos were permeabilized with 0.5% Triton X-100 in washing buffer for 40 minutes and incubated with blocking buffer containing 0.1% Triton X-100 and 10% normal goat serum in washing buffer for 60 minutes. The embryos were then incubated in either rabbit polyclonal anti H3K9ac (1:200; Abcam, UK) or rabbit polyclonal anti OCT4 antibody (1:200, Abcam, UK) in blocking buffer overnight at 4˚C. After several times washing, the embryos were incubated in goat anti-rabbit IgG fluorescein conjugated (1:500, Abcam, UK) for 60 minutes. Following DNA staining by 1 µg/ml 4,6-diamino-2-phenylindole (DAPI), the embryos were mounted on slides, and imaged by fluorescence microscope (Olympus, Japan). Images were quantified by ImageJ software (v. 1.48, National Institute of Mental Health, USA). Briefly, the average gray value was measured by manually outlining the nuclear intensity of blastomeres and corrected based on the mean gray value of five different cytoplasmic areas, as a background.

Statistical analysis

Normality of data was evaluated, and all data was verified for homogeneity of variances by Levene's Test. Data were analyzed by one-way ANOVA as well as duncan's post-hoc test for multiple comparison of groups, using IBM SPSS statistics for windows, version 20.0 (SPSS Inc. Chicago, IL, USA). $P<0.05$ were considered statistically significant.

Results

Nuclear donor cell preparation

Multipotent differentiation potential of BASCs was verified by differentiation into the osteogenic and adipogenic lineages. DNA methyltransferases (*DNMT1*, *DNMT3A* and *DNMT3B*) and histone deacetylases (*HDAC1*, *HDAC2* and *HDAC3*) mRNA expression were evaluated at the third, fifth and seventh passages. The results indicated that *DNMTs* and *HDACs* were significantly downregulated at the fifth passage ($P<0.05$). The highest levels of H3K9ac and POU5F1 were also detected at this passage ($P<0.05$). Regarding the upregulation of stemness and downregulation of chromatin condensation at the fifth passage, the cells at this passage were considered as donor cells for SCNT.

Effect of different *in vitro* embryo production procedures on developmental competence

Nine hundred and twenty-three bovine oocytes in seven replicates were matured and randomly divided into three groups of IVF, PA and SCNT. As shown in Table 2, the rate of embryo cleavage among the three groups was not significantly different. The blastocyst development rate in the IVF and PA groups (39.11 ± 2.36 and 34.41 ± 3.54 for IVF and PA groups, respectively) was significantly higher ($P<0.001$) than SCNT group (14.19 ± 2.43).

Expression of *DNMTs* and *HDACs* in bovine preimplantation embryos derived from IVF, PA and SCNT

Transcript abundance of DNA methyltransferases (*DNMT1*, *DNMT3A* and *DNMT3B*) and histone deacetylases (*HDAC1*, *HDAC2* and *HDAC3*) was evaluated for each group at the 6-8 cells and blastocyst stages. The highest and lowest level of *DNMT1* transcript was found at both stages of 6-8 cell and blastocyst in the respectively SCNT and IVF groups ($P<0.05$, Fig.1A, B).

Although there was no significant difference between these groups for the expression level of *DNMT3A* and *DNMT3B* at the 6-8 cells stage, the expression level was significantly lower in SCNT than IVF group at blastocyst stage. In addition, *DNMT3B* mRNA level was lower in PA group compared to IVF group at blastocyst stage ($P<0.05$, Fig.1B).

Table 2: Effect of three different bovine embryo production on developmental competence

Group	Number of oocytes	Cleavage (% ± SEM)	8-16 cells (% ± SEM)	Blastocyst (% ± SEM)
IVF	350	73.69 ± 2.88	46.72 ± 2.19[a]	39.11 ± 2.36[a]
PA	443	81.09 ± 2.96	47.01 ± 4.49[a]	34.41 ± 3.54[a]
SCNT	130	77.34 ± 4.70	35.67 ± 3.02[b]	14.19 ± 2.43[b]

IVF; *In vitro* fertilization, PA; Parthenogenetic activation, SCNT; Somatic cell nuclear transfer, and [a, b]; Within each column, superscript letters represent statistically significant differences between groups ($P<0.05$).

We found the highest level of *HDAC1* in SCNT embryos at the 6-8 cells stage (P<0.05, Fig.2A), not the blastocyst stage (Fig.2B). In PA and SCNT groups, the expression level of *HDAC2* and *HDAC3* was higher than IVF group at the 6-8 cells and blastocyst stages (P<0.05, Fig.2A, B).

Effect of *in vitro* embryo production on POU5F1 and acetylation of H3K9 in bovine embryos

The fluorescence intensity of H3K9ac and POU5F1 were not significantly different between inner cell mass (ICM) and trophectoderm (TE, data not shown). Thus, ICM and TE blastomers, both were used to evaluate the fluorescence intensity. Figures 3 and 4 reveal the H3K9ac and POU5F1 protein contents in the experimental groups at two different stages of preimplantation development. In the SCNT group, the fluorescence intensity of H3K9ac and POU5F1 were lower than the IVF and PA groups in both the 6-8 cells and blastocyst stages (P<0.05). Additionally, there was statistically significant difference between PA and IVF groups (P<0.05).

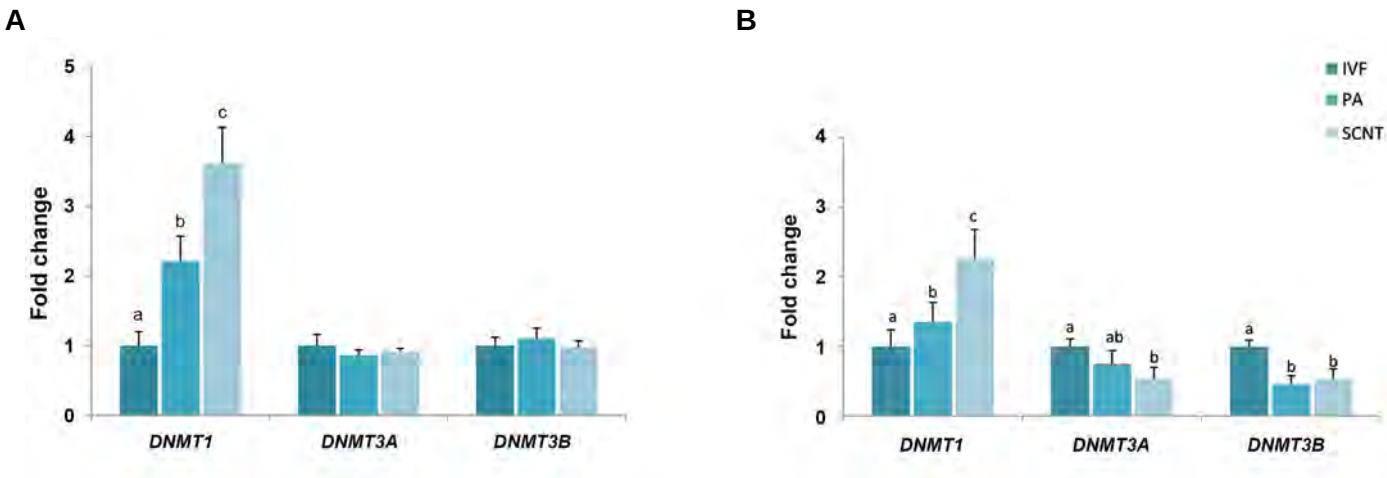

Fig.1: Analysis of DNA methyltransferase gene expression among the three groups. Transcript abundance of *DNMT1*, *DNMT3A* and *DNMT3B* at the **A.** 6-8 cells and **B.** Blastocyst stages in bovine embryos derived from IVF, PA and SCNT. Different superscripts (a, b, c) indicate a significant difference between groups (P<0.05). Data are expressed as mean ± standard error mean (SEM). IVF; *In vitro* fertilization, PA; Parthenogenetic activation, and SCNT; Somatic cell nuclear transfer.

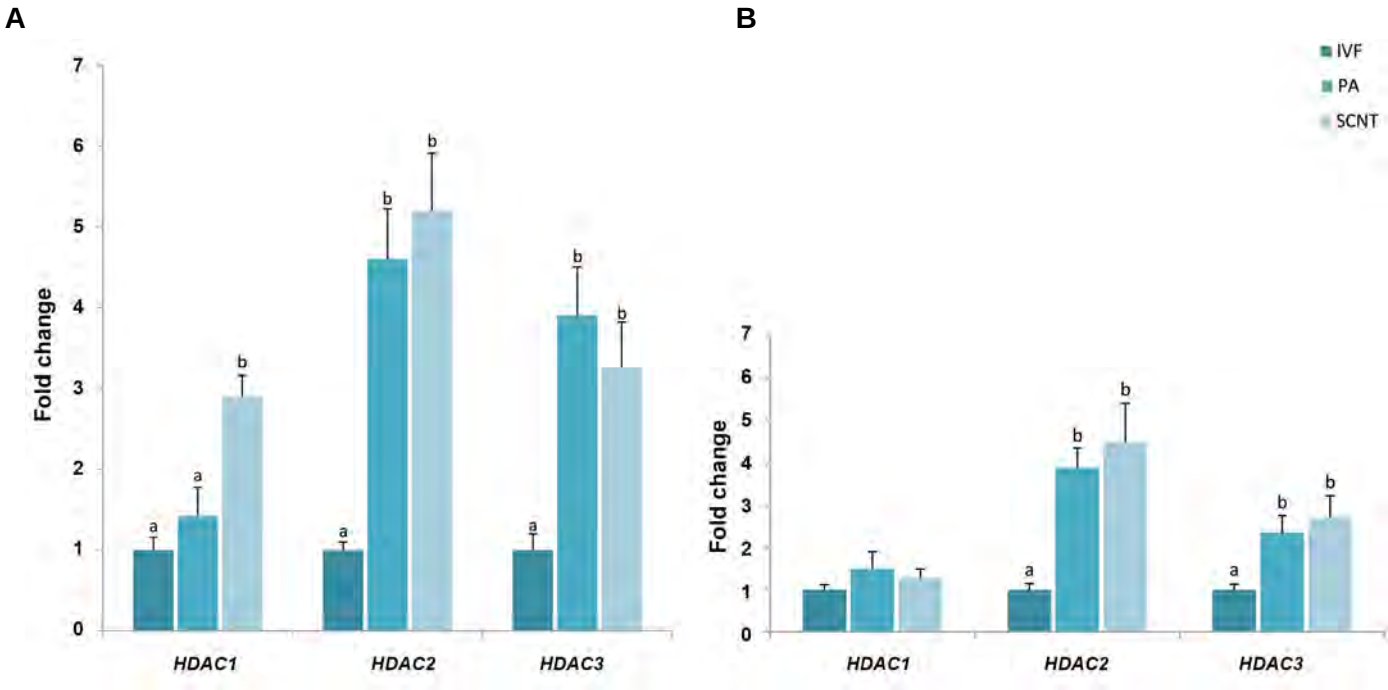

Fig.2: Analysis of histone deacetylase gene expression among the three groups. Transcript abundance of *HDAC1*, *HDAC2* and *HDAC3* at the **A.** 6-8 cells and **B.** Blastocyst stages in bovine embryos derived from IVF, PA and SCNT. Different superscripts (a, b) indicate a significant difference between the groups (P<0.05). Data are expressed as mean ± SEM. IVF; *In vitro* fertilization, PA; Parthenogenetic activation, and SCNT; Somatic cell nuclear transfer.

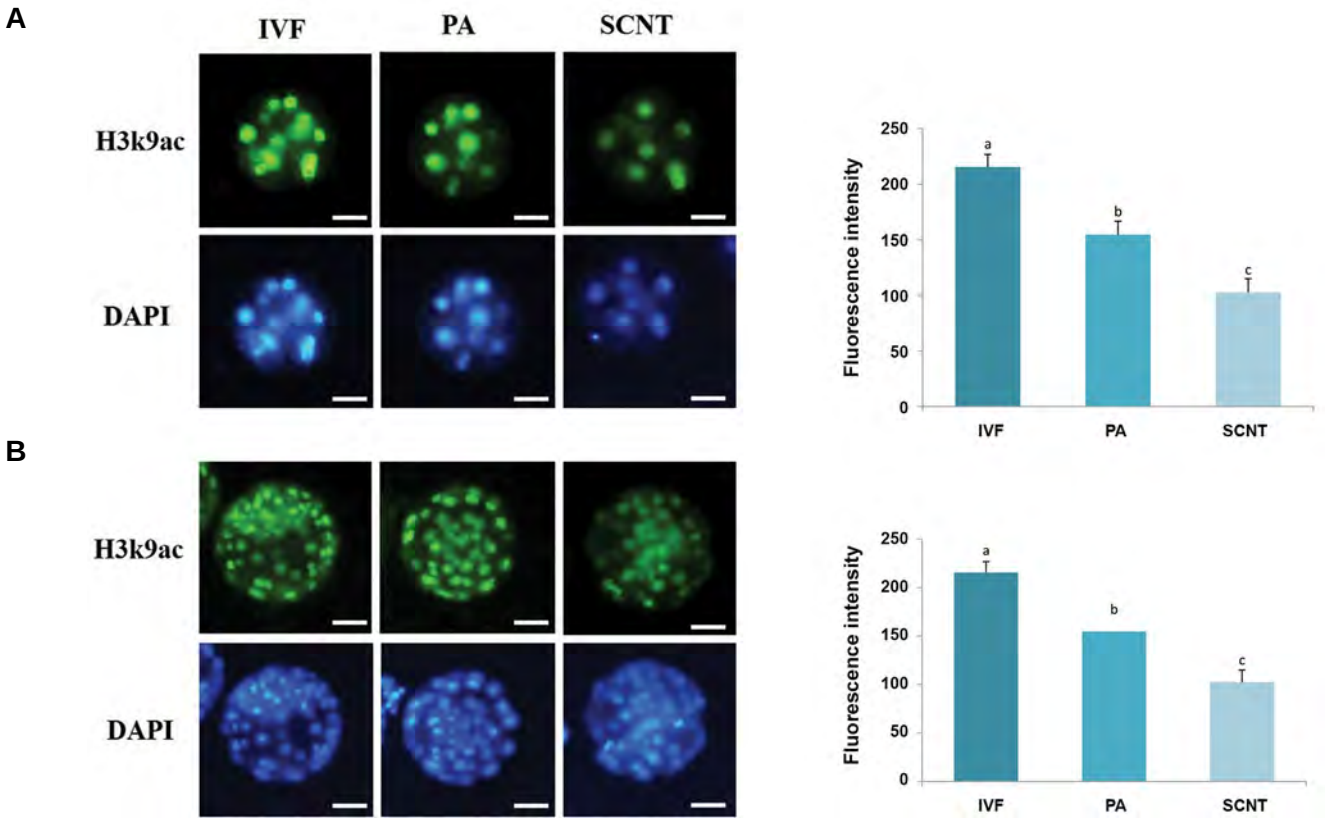

Fig.3: Comparison of H3K9ac fluorescence intensity among the three groups. Immunofluorescent staining of H3K9ac at the **A.** 6-8 cells and **B.** Blastocyst stages in bovine embryos derived from IVF, PA and SCNT. Different superscripts (a, b, c) indicate a significant difference between groups (P<0.05) (scale bar: 50 µm). Data are expressed as mean ± SEM. IVF; *In vitro* fertilization, PA; Parthenogenetic activation, and SCNT; Somatic cell nuclear transfer.

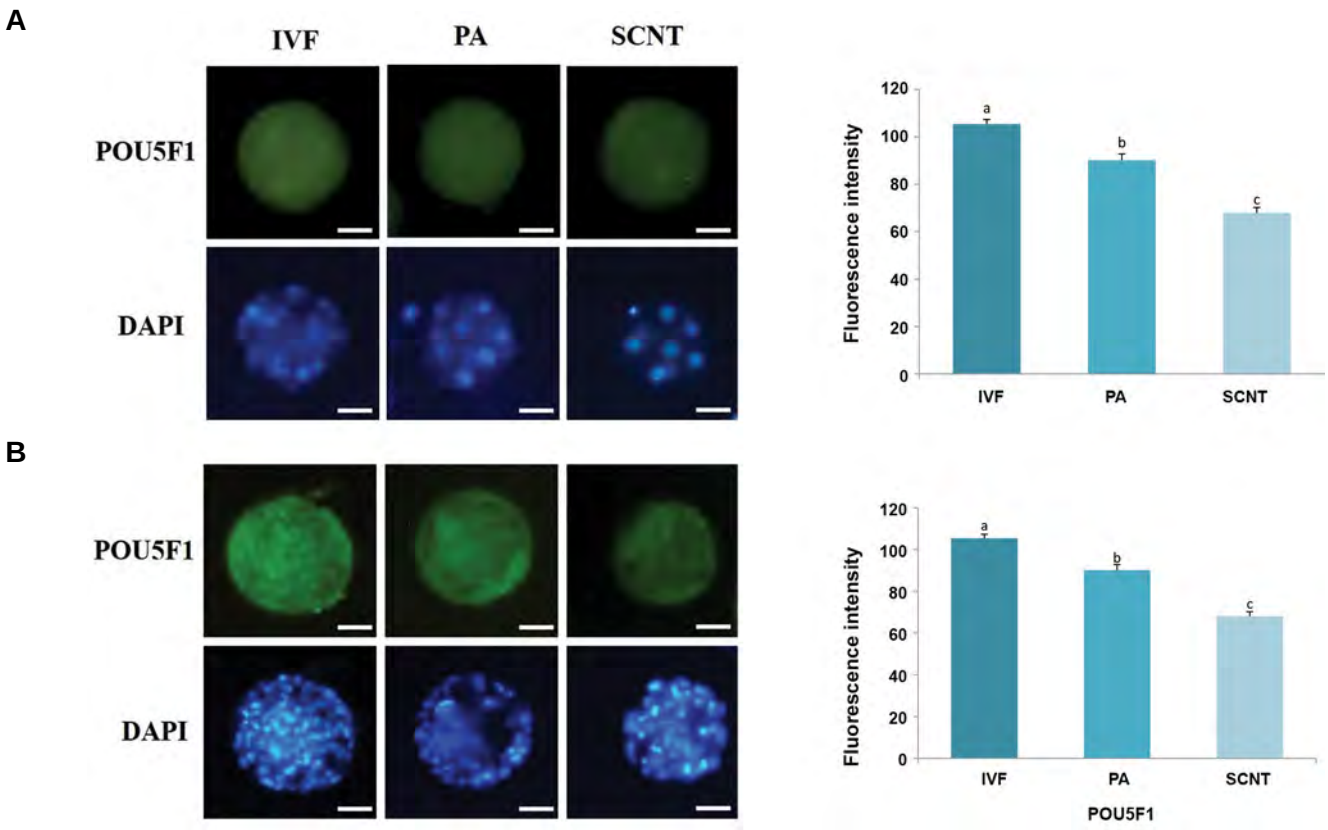

Fig.4: Comparison of POU5F1 fluorescence intensity among the three groups. Immunofluorescent staining of POU5F1 at the **A.** 6-8 cells and **B.** Blastocyst stages in bovine embryos derived from IVF, PA and SCNT. Different superscripts (a, b, c) indicate a significant difference between the groups (P<0.05) (scale bar: 50 µm). Data are expressed as mean ± SEM. IVF; *In vitro* fertilization, PA; Parthenogenetic activation, and SCNT; Somatic cell nuclear transfer.

Discussion

Results of this study showed a reduction in the blastocyst rate of SCNT group with high levels of *DNMT1* and *HDAC2-3* transcript abundance and less fluorescence intensity of H3K9ac and POU5F1 at the 6-8 cells and blastocyst stages in comparison with IVF group. *DNMT3A* and *B* mRNA level was low at blastocyst stage and *HDAC1* was high at the 6-8 cells stage in SCNT group compared to IVF group. Data also indicated an increasing in the level of *DNMT1* and *HDAC2-3* and a reduction in the fluorescence intensity of H3K9ac and POU5F1 in PA embryos at the 6-8 cells and blastocyst stages.

Since the creation of Dolly as the first successful SCNT in sheep, various somatic cells have been used as donors for SCNT (20, 21). Previous studies have demonstrated that the differentiation and methylation state of donor cells can affect efficiency of SCNT process (1, 22). Based on the previous studies, showing that donor cells with low levels of *DNMT1* mRNA as well as inhibition of HDACs could improve developmental competence in the SCNT embryos (2, 5, 6, 11, 13), in the present study, for first time, BASCs were used as donor cell at passage five with the lowest levels of *DNMTs* (*DNMT1*, *DNMT3A* and *DNMT3B*) and *HDACs* (*HDAC1*, *HDAC2* and *HDAC3*) genes.

A considerable body of evidences indicates the incomplete demethylation and early remethylation of cloned embryos derived by SCNT (3, 23). Thus, we conducted this study aiming to investigate whether using a donor cells with low mRNA levels of DNA methyltransferases (*DNMT1*, *DNMT3A* and *DNMT3B*) would modulate epigenetic status of resultant cloned embryos at the 6-8 cells and blastocyst stages. Our findings revealed that at the 6-8 cells embryos, the *DNMT1* mRNA level was more than three-times greater in the SCNT group compared to IVF group. Moreover, embryos derived from PA, which almost were female, showed higher mRNA levels of *DNMT1* compared to IVF group. This pattern of gene expression was also maintained by the blastocyst stage.

De novo methyltransferases were evaluated in the three groups and data showed similar level of expression for both *DNMT3A* and *DNMT3B* mRNA at the 6-8 cells embryos which is consistent with Golding et al. (24) study. At the blastocyst stage, however, *DNMT3A* and *DNMT3B* expressions in the SCNT group were lower than IVF group. This is in contrast with the previous study that did not find any significant difference in the de novo DNA methyltransferases expression among the three groups of IVF, PA and SCNT. In another study performed by Wang et al. (25), *Dnmt3a* expression was found to be lower in bovine SCNT blastocysts compared to IVF, whereas the *Dnmt3b* was higher in the SCNT group versus IVF. These differences between different studies might be related to the epigenetic status, differentiation level of donor cells, and/or *in vitro* culture conditions. Bakhtari and Ross (26) suggested that protection of at least one pronucleus from DNA demethylation may be required for normal preimplantation development. On the other hand, another study reported that treatment of donor cells with 5-aza-20-deoxycytidine (5-aza-dC), a DNA methylation inhibitor, could not ameliorate developmental competence of bovine SCNT embryos (27). In contrast, treatment of early SCNT embryos with TSA, a HDAC inhibitor, showed similar blastocyst rate compared to IVF group (11, 27). Therefore, we proposed that histone reprogramming might be more important than establishment of normal DNA modification in the cloned embryos.

HDACs are commonly expressed in the various tissues and different stages of preimplantation development and they play a pivotal role in the modulation of gene expression (28). In our study, *HDAC1-3* expression levels were compared among IVF, PA and SCNT groups during 6-8 cells and blastocyst stages. The results showed that *HDAC1* mRNA level at the 6-8 cells, but not at the blastocyst stage, was significantly affected by SCNT process. Transcript abundance of both *HDAC2* and *HDAC3* was higher in the PA and SCNT groups at the 6-8 cells and blastocyst stages in comparison with IVF. Beyhan et al. (29) indicated that increasing mRNA level of *HDACs* in the SCNT embryos at the morula stage might be required to promote transcriptional silencing in order to reprogram the somatic cells nuclei. However, in our study, *HDAC1* mRNA level in the SCNT blastocysts is comparable to IVF and PA groups. Ma and Schultz (30) demonstrated that *Hdac1* is the main *Hdac* transcript in the preimplantation of mouse embryos. On the other hand, in our experiment, the PA group which had a normal *HDAC1* expression level showed the same blastocyst formation rate compared to IVF group. Thus, it seems that *HDAC1* is more important than *HDAC2* and *HDAC3* in preimplantation development of bovine embryos. In this study, one reason for the similar level of *HDAC1* expression among these three groups and reduction of blastocyst rate in the SCNT group might be due to undesirable effects of the *HDAC1* transcript overexpression for the normal development up to blastocyst stage. Thus, regulation of *HDAC1* transcription may play an important role in improvement of bovine SCNT embryo developmental competence. It is likely that SCNT blastocysts were rescued from gene suppressing, by HDAC1. Previous study demonstrated that *DNMT1* is associated with histone deacetylase activity and it has a transcriptional repressor domain which can interact with the HDAC1 (31). Suppression of the *DNMT1* expression in the 6-8 cells stage embryos might be due to the upregulated expression of *HDAC1*.

Acetylation of histone tail residues is an important process resulting in chromatin unfolding and allow access to the regulatory transcriptional factors (32). In this study, we assessed the rate of H3K9ac during 6-8 cells and blastocyst stages, using immunofluorescence staining. Our finding showed that the value of acetylated H3K9 in the SCNT group was less than IVF and PA groups. Regarding the impact of HDACs on the acetylation of H3K9 (33), reduction of H3K9ac in the PA and SCNT

groups might be resulted from overexpression of HDACs.

Since *Pou5f1* is the earliest expressed gene to encode a transcription factor in mouse embryos, and it plays a critical role in the self-renewal of undifferentiated embryonic stem cells (34), we evaluated the level of this protein at the 6-8 cells and blastocyst stages. Results showed that in the SCNT group, this level was less than that of the other groups. In addition, a significant difference of *POU5F1* was found between IVF and PA groups which is consistent with the previous study indicating that the *POU5F1* and *DNMT3A* genes were downregulated in the PA (35) and SCNT embryos (29) versus IVF embryos. It has been demonstrated that HDAC1 and HDAC2 as a multiprotein complex are associated with *POU5F1* gene expression (36). Thus, *HDAC1-2* overexpression may result in reduction of POU5F1 expression level in the resultant embryos.

Conclusion

The results of this study demonstrated that i. The rate of blastocyst formation in the cloned bovine SCNT embryos derived from BASCs with low mRNA levels of *DNMT1* and *HDACs* (except *HDAC1* in blastocyst stage), was less than that of the IVF group, ii. Different values of H3K9ac and POU5F1, detected among the groups and over the different developmental stages, may be related to the overexpression of HDACs in the PA and SCNT groups, and iii. Despite various aberrant epigenetic modifications in preimplantation development of both PA and SCNT groups, normal blastocyst rate of the PA compared to SCNT embryos may be related to the improving role of *HDAC1* and *DNMT1* in the developmental competence of bovine embryos.

Acknowledgements

The authors would like to express their gratitude to Cellular and Molecular Biology Research Center, Shahid Beheshti University of Medical Sciences and Department of Anatomical Sciences, AJA University of Medical Sciences, Tehran, Iran for their financial support. There is no conflict of interest in this study.

Authors' Contributions

B.A.; Carried out the oocyte collection and *in vitro* maturation, nuclear donor cell preparation and performed IVF, PA and SCNT. Z.Z.; Carried out gene expression analysis and immunofluorescence staining of embryos. B.A., Z.Z.; Collected the experimental data. A.B., M.S., A.H.; Analyzed and interpreted the data. A.B.; Wrote the first draft of the manuscript. M.S., A.H.; Participated in the design of the study. All authors read and approved the final manuscript.

References

1. Wakayama S, Wakayama T. Improvement of mouse cloning using nuclear transfer-derived embryonic stem cells and/or histone deacetylase inhibitor. Int J Dev Biol. 2010; 54(11-12): 1641-1648.
2. Kishigami S, Mizutani E, Ohta H, Hikichi T, Thuan NV, Wakayama S, et al. Significant improvement of mouse cloning technique by treatment with trichostatin A after somatic nuclear transfer. Biochem Biophys Res Commun. 2006; 340(1): 183-139.
3. Dean W, Santos F, Stojkovic M, Zakhartchenko V, Walter J, Wolf E, et al. Conservation of methylation reprogramming in mammalian development: Aberrant reprogramming in cloned embryos. Proc Nat Acad Sci USA. 2001; 98(24): 13734-13738.
4. Li E. Chromatin modification and epigenetic reprogramming in mammalian development. Nat Rev Genet. 2002; 3(9): 662-673.
5. Giraldo AM, Hylan DA, Ballard CB, Purpera MN, Vaught TD, Lynn JW, et al. Effect of epigenetic modifications of donor somatic cells on the subsequent chromatin remodeling of cloned bovine embryos. Biol Reprod. 2008; 78(5): 832-840.
6. Yamanaka K, Sakatani M, Kubota K, Balboula AZ, Sawai K, Takahashi M. Effects of downregulating DNA methyltransferase 1 transcript by RNA interference on DNA methylation status of the satellite I region and in vitro development of bovine somatic cell nuclear transfer embryos. J Reprod Dev. 2011; 57(3): 393-402.
7. Cantone I, Fisher AG. Epigenetic programming and reprogramming during development. Nat Struct Mol Biol. 2013; 20(3): 282-289.
8. Turner BM. Histone acetylation and control of gene expression. J Cell Sci. 1991; 99(Pt 1): 13-20.
9. Gong F, Miller KM. Mammalian DNA repair: HATs and HDACs make their mark through histone acetylation. Mutat Res. 2013; 750(1-2): 23-30.
10. Kimura H, Nakamura T, Ogawa T, Tanaka S, Shiota K. Transcription of mouse DNA methyltransferase 1 (Dnmt1) is regulated by both E2F-Rb-HDAC-dependent and -independent pathways. Nucleic Acids Res. 2003; 31(12): 3101-3113.
11. Lee MJ, Kim SW, Lee HG, Im GS, Yang BC, Kim NH, et al. Trichostatin A promotes the development of bovine somatic cell nuclear transfer embryos. J Reprod Dev. 2011; 57(1): 34-42.
12. Shi LH, Miao YL, Ouyang YC, Huang JC, Lei ZL, Yang JW, et al. Trichostatin A (TSA) improves the development of rabbit-rabbit intraspecies cloned embryos, but not rabbit-human interspecies cloned embryos. Dev Dyn. 2008; 237(3): 640-648.
13. Zhao J, Ross JW, Hao Y, Spate LD, Walters EM, Samuel MS, et al. Significant improvement in cloning efficiency of an inbred miniature pig by histone deacetylase inhibitor treatment after somatic cell nuclear transfer. Biol Reprod. 2009; 81(3): 525-530.
14. Pan S, Chen W, Liu X, Xiao J, Wang Y, Liu J, et al. Application of a novel population of multipotent stem cells derived from skin fibroblasts as donor cells in bovine SCNT. PLoS One. 2015; 10(1): e0114423.
15. Humpherys D, Eggan K, Akutsu H, Hochedlinger K, Rideout WM, Biniszkiewicz D, et al. Epigenetic instability in ES cells and cloned mice. Science. 2001; 293(5527): 95-97.
16. Rideout WM 3rd, Wakayama T, Wutz A, Eggan K, Jackson-Grusby L, Dausman J, et al. Generation of mice from wild-type and targeted ES cells by nuclear cloning. Nat Genet. 2000; 24(2): 109-110.
17. Zare Z, Abouhamzeh B, Masteri Farahani R, Salehi M, Mohammadi M. Supplementation of L-carnitine during in vitro maturation of mouse oocytes affects expression of genes involved in oocyte and embryo competence: an experimental study. Int J Reprod Biomed (Yazd). 2017; 15(12): 779-786.
18. Bahmanpour S, Bakhtari A, Abouhamzeh B. Protective effect of vitrified-warmed media with clove bud (syzygium aromaticum) extract on mouse oocytes and resultant blastocysts. Cryo Letters. 2018; 39(5): 288-297.
19. Bakhtari A, Rahmani HR, Bonakdar E, Jafarpour F, Asgari V, Hosseini SM, et al. The interfering effects of superovulation and vitrification upon some important epigenetic biomarkers in mouse blastocyst. Cryobiology. 2014; 69(3): 419-427.
20. Cho JK, Lee BC, Park JI, Lim JM, Shin SJ, Kim KY, et al. Development of bovine oocytes reconstructed with different donor somatic cells with or without serum starvation. Theriogenology. 2002; 57(7): 1819-1828.
21. Lee GS, Hyun SH, Kim HS, Kim DY, Lee SH, Lim JM, et al. Improvement of a porcine somatic cell nuclear transfer technique by optimizing donor cell and recipient oocyte preparations. Theriogenology. 2003; 59(9): 1949-1957.
22. Blelloch R, Wang Z, Meissner A, Pollard S, Smith A, Jaenisch R. Reprogramming efficiency following somatic cell nuclear transfer is influenced by the differentiation and methylation state of the donor nucleus. Stem Cells. 2006; 24(9): 2007-2013.
23. Bourc'His D, Le Bourhis D, Patin D, Niveleau A, Comizzoli P, Renard JP, et al. Delayed and incomplete reprogramming of chromosome methylation patterns in bovine cloned embryos. Curr Biol. 2001; 11(19): 1542-1546.

24. Golding MC, Williamson GL, Stroud TK, Westhusin ME, Long CR. Examination of DNA methyltransferase expression in cloned embryos reveals an essential role for Dnmt1 in bovine development. Mol Reprod Dev. 2011; 78(5): 306-317.
25. Wang Y, Su J, Wang L, Xu W, Quan F, Liu J, et al. The effects of 5-aza-2′-deoxycytidine and trichostatin A on gene expression and DNA methylation status in cloned bovine blastocysts. Cell Reprogram. 2011; 13(4): 297-306.
26. Bakhtari A, Ross PJ. DPPA3 prevents cytosine hydroxymethylation of the maternal pronucleus and is required for normal development in bovine embryos. Epigenetics. 2014; 9(9): 1271-1279.
27. Enright BP, Kubota C, Yang X, Tian XC. Epigenetic Characteristics and Development of Embryos Cloned from Donor Cells Treated by Trichostatin A or 5-aza-2′-deoxycytidine1. Biol Reprod. 2003; 69(3): 896-901.
28. McGraw S, Robert C, Massicotte L, Sirard MA. Quantification of histone acetyltransferase and histone deacetylase transcripts during early bovine embryo development. Biol Reprod. 2003; 68(2): 383-389.
29. Beyhan Z, Forsberg EJ, Eilertsen KJ, Kent-First M, First NL. Gene expression in bovine nuclear transfer embryos in relation to donor cell efficiency in producing live offspring. Mol Reprod Dev. 2007; 74(1): 18-27.
30. Ma P, Schultz RM. Histone deacetylase 1 (HDAC1) regulates histone acetylation, development, and gene expression in preimplantation mouse embryos. Dev Biol. 2008; 319(1): 110-120.
31. Fuks F, Burgers WA, Brehm A, Hughes-Davies L, Kouzarides T. DNA methyltransferase Dnmt1 associates with histone deacetylase activity. Nat Genet. 2000; 24(1): 88-91.
32. Kouzarides T. Chromatin modifications and their function. Cell. 2007; 128(4): 693-705.
33. Wang Z, Zang C, Cui K, Schones DE, Barski A, Peng W, et al. Genome-wide mapping of HATs and HDACs reveals distinct functions in active and inactive genes. Cell. 2009; 138(5): 1019-1031.
34. Niwa H, Masui S, Chambers I, Smith AG, Miyazaki J. Phenotypic complementation establishes requirements for specific POU domain and generic transactivation function of Oct-3/4 in embryonic stem cells. Mol Cell Biol. 2002; 22(5): 1526-1536.
35. Gómez E, Gutiérrez-Adán A, Díez C, Bermejo-Alvarez P, Muñoz M, Rodriguez A, et al. Biological differences between in vitro produced bovine embryos and parthenotes. Reproduction. 2009; 137(2): 285-295.
36. Delcuve GP, Khan DH, Davie JR. Roles of histone deacetylases in epigenetic regulation: emerging paradigms from studies with inhibitors. Clin Epigenetics. 2012; 4(1): 5.

Original Article

Hsa-miR-587 Regulates TGFβ/SMAD Signaling and Promotes Cell Cycle Progression

Mahnaz Jahangirimoez, M.Sc.[1#], Abdallah Medlej, M.Sc.[1#], Mahmoud Tavallaie, Ph.D.[2], Bahram Mohammad Soltani, Ph.D.[1*]

1. Department of Molecular Genetics, Faculty of Biological Sciences, Tarbiat Modares University, Tehran, Iran
2. Department of Medical Genetics, Baqiyatallah University of Medical Sciences, Tehran, Iran

#The first two authors equally contributed to this work.

Corresponding Address: P.O.Box: 1411713116, Department of Molecular Genetics, Faculty of Biological Sciences, Tarbiat Modares University, Tehran, Iran
Email: soltanib@modares.ac.ir

Received: 22/October/2018, Accepted: 6/April/2019

Abstract

Objective: Transforming growth factor beta/single mothers against decapentaplegic (TGFβ/SMAD) signaling pathway plays important roles in various biological processes. It acts as a tumor suppressor during the early stages of cancer progression. Discovering the regulators of this pathway provides important options for therapeutic strategies. Here, we searched for candidate microRNAs (miRNAs) that potentially target the critical components of the TGFβ signaling pathway.

Materials and Methods: In the current experimental study, we first predicted miRNAs that target TGFβ components using a bioinformatics software. After that, quantitative real-time polymerase chain reaction (RT-qPCR) was used to detect the expression of miR-587, *TGFBR2, SMAD4, p21, CCND1* and *c-MYC* genes in transfected HEK293T and HCT116 cells. Dual Luciferase assay was performed to analyze the interactions between miRNAs and the target genes. Propidium iodide flow cytometry was used to determine cell cycle progression in HEK293T and HCT116 cells under hsa-miR-587 (miR-587) overexpression circumstances.

Results: Multiple miRNA responsive elements (MREs) were predicted for *miR-587* within the 3'UTRs of the *TGFBR2* and *SMAD4* genes. Overexpression of *miR-587* in HEK293T and HCT116 cells resulted in downregulation of *TGFBR2* and *SMAD4* genes. In addition, a downstream target gene of TGFβ/SMAD signaling, P21, was significantly downregulated in the HCT116 cells overexpressing miR-587. Dual luciferase assay analysis provided evidence that there is a direct interaction between *miR-587* and the 3'UTR sequences of *TGFBR2* and *SMAD4* genes. Moreover, miR-587 overexpression in HEK293T and HCT116 cells resulted in reducing the SubG1 cell populations in both cell lines, as detected by flow cytometry.

Conclusion: Altogether, our data revealed an important role for *miR-587* in regulating TGFβ/SMAD signaling and promoting cell cycle progression. These characteristics suggest that *miR-587* is an important candidate for cancer therapy research.

Keywords: Cancer, Cell Cycle, *miR-587*, TGFβ/SMAD Signaling

Cell Journal(Yakhteh), Vol 22, No 2, July-September (Summer) 2020, Pages: 158-164

Citation: **Jahangirimoez M, Medlej A, Tavallaie M, Mohammad Soltani B. Hsa-miR-587 regulates TGFβ/SMAD signaling and promotes cell cycle progression. Cell J. 2020; 22(2): 158-164. doi: 10.22074/cellj.2020.6483.**

Introduction

Transforming growth factor beta/single mothers against decapentaplegic (TGFβ/SMAD) signaling plays crucial roles in various cellular processes, cell development, and carcinogenesis (1). TGFβ is a member of the superfamily of multifunctional cytokines that binds to the TGFBR1 and TGFBR2 receptor serine/threonine kinases. Binding of TGFβ to TGFBR1 and TGFBR2 leads to direct phosphorylation and activation of receptor-regulated SMAD (R-SMAD) proteins, SMAD2 and SMAD3. Activated R-SMADs form a heteromeric complex with the Co-SMAD protein, SMAD4. Once fully formed, the SMAD complex is translocated into the nucleus, where it associates with other transcriptional regulators to activate or suppress the transcription of specific target genes (2, 3). Although TGFβ signaling is known to induce apoptosis and cell cycle arrest during the early stages of carcinogenesis, it has been also shown to promote cancer progression and metastasis in the advanced stages of cancer (4, 5).

MicroRNAs (miRNAs) are small (18-24 nucleotides) non-coding RNAs that control gene expression post-transcriptionally (6). They are involved in the regulation of several biological processes. miRNAs generally bind to the 3′untranslated region (3′UTR) of their target mRNAs leading to their degradation or translational repression (7). Dysregulation of miRNA expression has been observed in various human tumors (8, 9). Interestingly, miRNAs are implicated in the process of carcinogenesis by acting as either tumor suppressors or oncogenes (10, 11). In addition, miRNAs play important roles in modulating signaling pathways by regulating the expression of their components. Various miRNAs have been reported to control core components of the TGFβ/SMAD signaling pathways (12-16).

Here, we demonstrated that *miR-587* likely has a negative effect on the expression of TGFβ/SMAD signaling components. Bioinformatics analysis showed that *miR-*

587 has multiple recognition sites within the 3'UTRs of two essential components of the TGFβ pathway, the *TGFBR2* and *SMAD4* genes. Overexpressing *miR-587* in HEK293T and HCT116 cells (TGFβ pathway-active cells) resulted in the downregulation of *TGFBR2* and *SMAD4* expression. Furthermore, dual luciferase assay results suggested a direct interaction between *miR-587* and the two target genes. Moreover, overexpression of *miR-587* resulted in reducing the SubG1-phase cellular population of HEK293T and HCT116 cells. The results of the current study suggest *miR-587* as an important regulator of TGFβ signaling pathway.

Materials and Methods

Bioinformatics tools

Prediction of miRNAs that target components of the TGFβ pathway was performed using the Targetscan (17), DIANA MicroT-CDS (18, 19) and miRmap (20) web servers. TargetScan predicts miRNA targets by searching for the presence of sites that match the seed region of each miRNA (17). DIANA MicroT-CDS has the potential to predict miRNA responsive elements (MREs) located in both the 3′-UTRs and coding sequence (CDS) regions (18, 19). miRmap uses thermodynamic, evolutionary, probabilistic, or sequence-based features in its prediction process (20). The phylogenetic conservation of the predicted MREs of miR-587 within the 3′UTRs of its target genes was evaluated using the UCSC genome browser (21).

Plasmid construction

The *miR-587* precursor was polymerase chain reaction (PCR)-amplified using a pair of specific primers (Table 1), and the PCR product was cloned into the multiple cloning site of the pmR-mCherry expression vector (Clontech, USA). The resulting construct was transformed and amplified into the DH5-Alpha *E.coli* bacterial strain and later extracted by mini-prep kit (Qiagen, Germany) and sequenced to verify the absence of any mutations.

Cell culture

HEK293T and HCT116 cells were cultured in Dulbecco's Modified Eagle Medium:Nutrient Mixture F-12 (DMEM/F12) or RPMI media, respectively (Invitrogen, USA), supplemented with 100 U/ml penicillin, 100 µg/ml streptomycin (Sigma, USA), and 10% fetal bovine serum (Invitrogen, USA), and incubated at 37˚C with 5% CO_2. HEK293T and HCT116 cells were obtained from Pasteur Institute (Tehran, Iran).

Transfection

HEK293T or HCT116 cells were seeded in 12-well plates (12×10^4 cells per well). Transfection was performed using Lipofectamine 2000 reagent according to the manufacturer's instructions (Invitrogen, USA).

Table 1: Primers used in the study

Primer	Primer sequence (5′-3′)
Anchored Oligo dT	GCGTCGACTAGTACAACTCAAG GTTCTTCCAGTCACGACGT$_{18}$N
U48	TGACCCCAGGTAACTCTGAGTGTGT
miR-587	GGCGCTTTCCATAGGTGATGAGT
Anchored reverse	GCGTCGACTAGTACAACTCAAG
Pre-*miR-587*	F: TCAGCTCAGACCACATTTCATCA
	R: ATGAGGACAGCCATGAGACAGAT
GAPDH	F: GCCACATCGCTCAGACAC
	R: GGCAACAATATCCACTTTACCAG
CCND1	F: CAGAGTGATCAAGTGTGACCC
	R: CGTCGGTGGGTGTGCAAGC
c-MYC	F: CTCCTACGTTGCGGTCACAC
	R: CGGGTCGCAGATGAAACTCT
SMAD4-3′UTR	F: AAGTAATGGCTCTGGGTTGGG
	R: TCAAACAGCAGAACAAAGATAAGGAA
TGFBR2-3′UTR	F: TTTGGATGGTGGAAGGTCTC
	R: GCAACAGCTATTGGGATGGT
K-RAS-3′UTR	F: GTGAGGGAGATCCGACAATACAGA
	R: GCCGCGCTGCTGCTACCTTTGGGC

RNA extraction, cDNA synthesis and quantitative real-time polymerase chain reaction

Total RNA was extracted using Trizol reagent according to the manufacturer's instructions (Invitrogen, USA). Genomic DNA was removed by DNaseI treatment as the following: DNase I treatment (Takara, Japan) at 37˚C for 30 minutes, followed by heat and EDTA inactivation of the enzyme for 10 minutes. cDNA was synthesized using Prime Script II reverse transcriptase (Takara, Japan) according to the manufacturer's instructions. For miRNA detection, polyA tailing was performed before cDNA synthesis using the E. coli Poly (A) Polymerase kit (NEB, England). Real-time PCR was performed according to standard protocols by StepOne™ system (Applied Biosystems, USA). *GAPDH* and *U48* expression levels were used to normalize the real-time PCR results.

Western blot

Total cellular proteins were extracted from RiboX-precipitated cell extracts according to a recently reported protocol (22). The extracted protein concentrations were

determined using Bradford assay (23). 40 µg of each protein sample were separated by polyacrylamide gel electrophoresis and transferred to a polyvinylidene difluoride (PVDF) membrane. Primary antibodies against cyclin D1 protein (Santa Cruz, USA), β-actin (Santa Cruz, USA) and goat anti-mouse secondary antibody (BIORAD, USA) were diluted according to the manufacturers' instructions. The expression levels of CCND1 protein was normalized against β-actin protein expression.

Luciferase assay

The desired fragments of the 3′UTRs of *TGFBR2* and *SMAD4* genes in addition to a similar-sized fragment of the K-RAS_3′UTR (off target) were cloned downstream of the Renilla luciferase gene of the PSI-CHECK2 plasmid. The resulting constructs were co-transfected with the pmR-mCherry/pre-miRNA or pmR-mCherry vectors in HEK293T cells. 48 hours after transfection, dual luciferase assay was performed using Dual-Glo luciferase assay kit (Promega, USA).

Cell cycle analysis

HEK293T or HCT116 cells transfected with *miR-587* or mock were collected 36 hours after transfection, centrifuged at 1200 rpm for 5 minutes and washed twice with phosphate buffered saline (PBS). Subsequently, cells were fixed in 1 ml of 70% ethanol for at least 30 minutes. For each sample, 500 µl propidium iodide staining solution was added to each sample and incubated for 30 minutes at room temperature. Cell cycle analysis was performed by the FACSCalibur flow cytometer (BD Biosciences, USA).

Statistical analysis

The relative expression of the desired genes was calculated according to the $2^{-\Delta\Delta Ct}$ method. Real-time PCR results were normalized against the endogenous expression of the *U48* or *GAPDH* genes. GraphPad Prism 7 (GraphPad software, USA) was used to perform statistical tests (t test) and graph construction. Results with $P<0.05$ were considered statistically significant. All experiments were performed in triplicates.

Results

Bioinformatics analysis suggests miR-587 as an inhibitor of TGFβ signaling

A set of miRNAs was predicted by the utilized software to target important genes implicated in the TGFβ signaling pathway. For instance, hsa-let-7f-5p and hsa-miR-4458 were predicted to target TGFβR1, hsa-miR-302a-3p, hsa-miR-302d-3p and hsa-miR-587 were predicted to target TGFβR2 and hsa-miR-548g-5p, hsa-miR-4288 and hsa-miR-587 were predicted to target the *SMAD4* gene. To select one of the candidate miRNAs for experimental validation, we focused on the miRNAs that can target more than one gene of the TGFβ signaling components at the same time. In addition, the scores obtained by the software used were taken into consideration and led to the final selection of *miR-587* as a potential candidate. In terms of its possible role, *miR-587* was predicted to potentially target two important genes related to the TGFβ signaling pathway, the *TGFBR2* and *SMAD4* genes (Fig.1A). Our bioinformatics predictions showed that each of the 3′UTRs of the *TGFBR2* and *SMAD4* genes contains more than one MRE for *miR-587*. Additionally, the seed sequence of *miR-587* showed high-scored base pairing with the targets' MREs (Fig.1B).

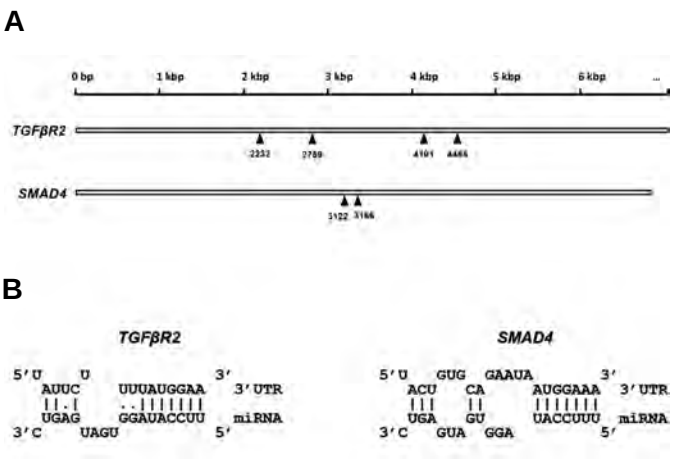

Fig.1: Predicted miRNA responsive elements (MREs) of *miR-587* within the 3′UTRs of *TFFBR2* and *SMAD4* genes. **A.** The positions of *miR-587* binding sites within the 3′UTRs of *TGFBR2* and *SMAD4* transcripts. The numbers indicate the position of the first nucleotide of each MRE with respect to the transcription initiation site and **B.** Schematic representation of the base-pairing status between the *miR-587* seed sequence and the MREs of the target genes. One MRE is presented for each target gene.

Downregulation of *TGFBR2* and *SMAD4* following the overexpression of *miR-587*

In order to validate the prediction results, *miR-587* was overexpressed in HEK293T and HCT116 cells. Overexpression of *miR-587* was performed by transfecting the cells with the pmCherry/pre-*miR-587* construct or empty pmCherry as a control. Significant overexpression of *miR-587* was detected in both cell lines transfected by pre-*miR-587* in comparison to the controls (Fig.2A, B). As a result, RT-qPCR analysis indicated that *TGFBR2* and *SMAD4* expression levels decreased significantly in both cell lines (HEK293T and HCT116) overexpressing *miR-587* compared to the controls (Fig.2C, D). Moreover, the *P21* gene showed a significant downregulation in the HCT116 cells overexpressing *miR-587* compared to the controls, while *CCND1* and *c-MYC* genes showed a significant upregulation in the same samples (Fig.2E). In addition, western blot analysis confirmed these results and showed a significant upregulation of the CCND1 protein level in comparison to the control samples (Fig.2F).

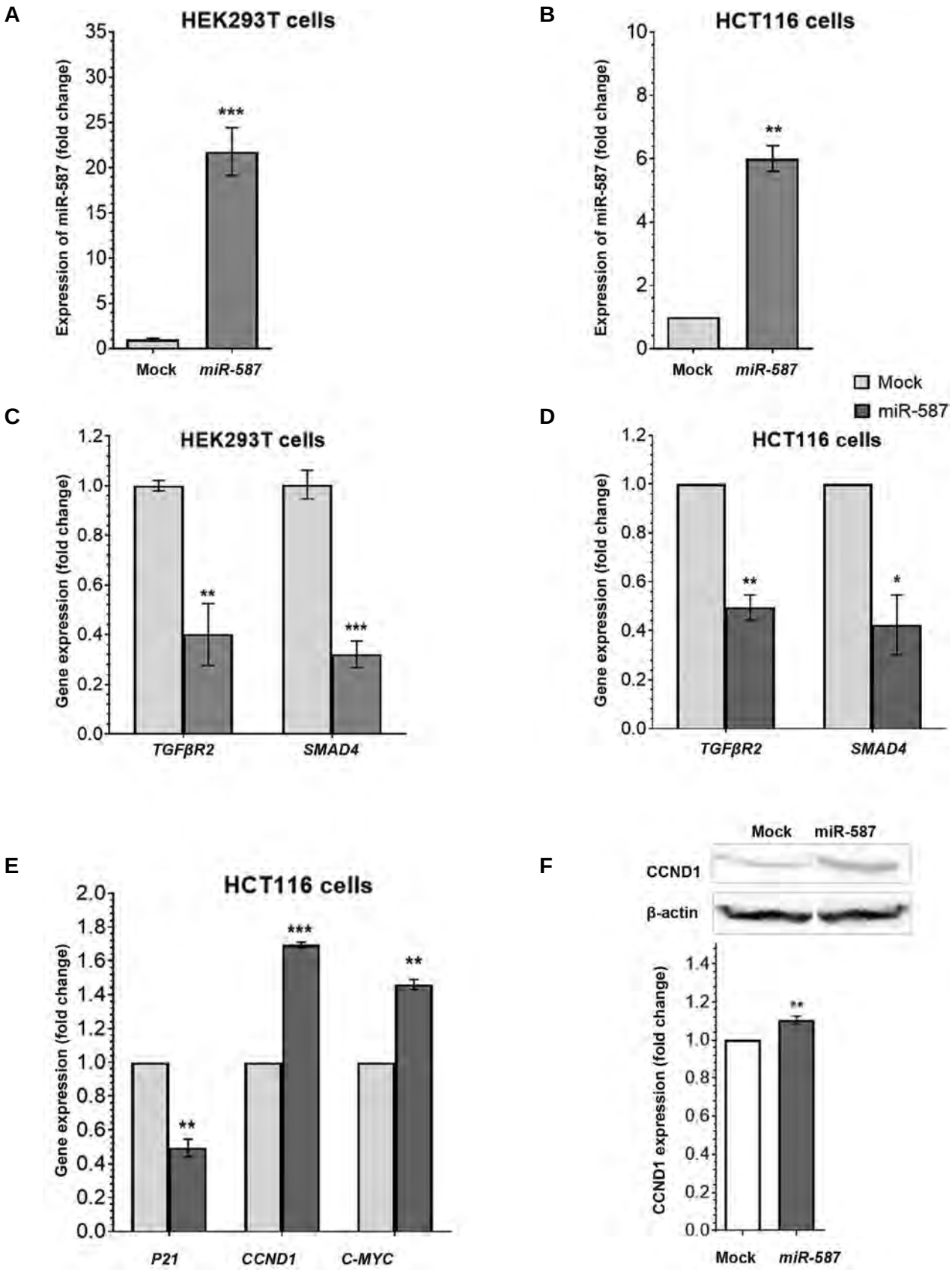

Fig.2: Effect of *miR-587* overexpression on the expression of its predicted target genes. **A, B.** HEK293T and HCT116 cells transfected with the pmCherry/pre-*miR-587* construct or empty pmCherry control. Reverse transcription quantitative polymerase chain reaction (RT-qPCR) analysis indicated more than 25-fold overexpression of *miR-587* in HEK293T cells and ~7-fold in HCT116 cells following the transfection of the pmCherry/pre-*miR-587* construct in comparison to controls (P=0.0002 and 0.0064, respectively), **C, D.** Following the overexpression of *miR-587*, the expression levels of *TGFBR2* and *SMAD4* reduced significantly in both HEK293T and HCT116 cell lines, **E.** Overexpressing of miR-587 in HCT116 cells resulted in the downregulation of *p21* gene expression, and upregulation of *CCND1* and *c-MYC* genes, and **F.** Western blot analysis showed a significant upregulation in the CCND1 protein level in the HCT116 cells overexpressing miR-587 compared to control. RT-qPCR results were normalized according to the endogenous expression of *U48* and *GAPDH* genes. Western blot results were normalized according to the endogenous expression of β-actin protein. *; 0.01<P<0.1, **; P≤0.01 and ***; P≤0.001.

Interaction between *miR-587* and the 3′UTRs of the *TGFBR2* and *SMAD4* genes

In order to examine a direct interaction between *miR-587* and the 3′UTRs of *TGFBR2* and *SMAD4* genes, a dual luciferase assay was performed. HEK293T cells were co-transfected with PSI-CHECK2/TGFBR2_3′UTR, PSI-CHECK2/SMAD4_3′UTR or PSI-CHECK2/K-RAS_3′UTR constructs and pmCherry/pre-*miR-587* or mock. PSI-CHECK2/K-RAS_3′UTR was used as an off-target. Dual luciferase analysis indicated a significant reduction in the luciferase activity of the cells co-transfected with *miR-587* and its target genes 3′UTRs in comparison to the controls (Fig.3). These results suggest a direct interaction between *miR-587* and the 3′UTRs of *TGFBR2* and *SMAD4* genes.

The effects of *miR-587* overexpression on cell cycle progression

We used propidium iodide flow cytometry analysis to investigate the effects of *miR-587* overexpression on HEK293T and HCT116 cell cycle progression. The obtained results showed a significant reduction in the SubG1-phase and G2-phase populations of the HEK293T cells overexpressing *miR-587* compared to the controls (Fig.4A). In addition, a significant increase in the S-phase population of the HEK293T cells compared to the controls was observed (Fig.4). In HCT116 cells, on the other hand, overexpression of *miR-587* resulted in a significant reduction of the SubG1-phase population of the cells, but no significant variations in cells in other cell cycle phases were observed in comparison to the controls (Fig.4B). These results suggest a role for *miR-587* in arresting the progression of the cell cycle.

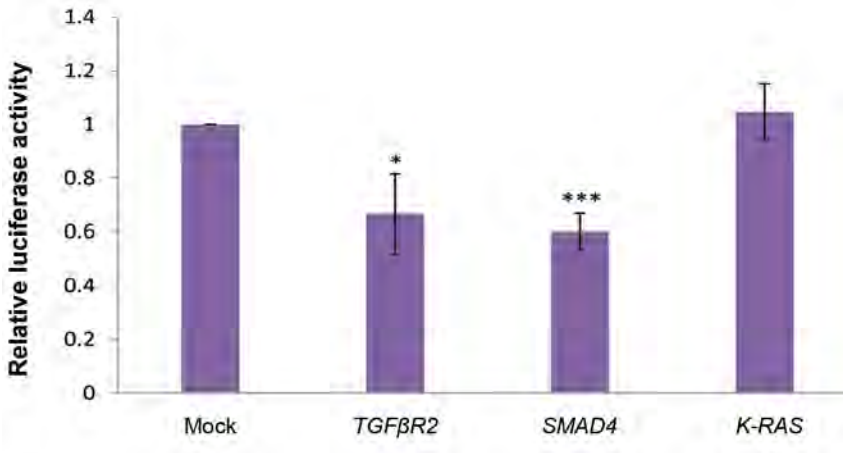

Fig.3: Direct interaction between *miR-587* and the 3′UTRs of *TGFBR2* and *SMAD4*. A significant luciferase activity reduction was detected in the HEK293T cells co-transfected with PSICHECK-2/*TGFBR2*_3′UTR or PSICHECK-2/*SMAD4*_3′UTR (P=0.02 and 0.0007, respectively), and pmCherry/pre-*miR-587* construct, compared to mock or off-target (PSICHECK-2/*K-RAS*_3′UTR) controls. *; P≤0.05 and ***; P≤0.001.

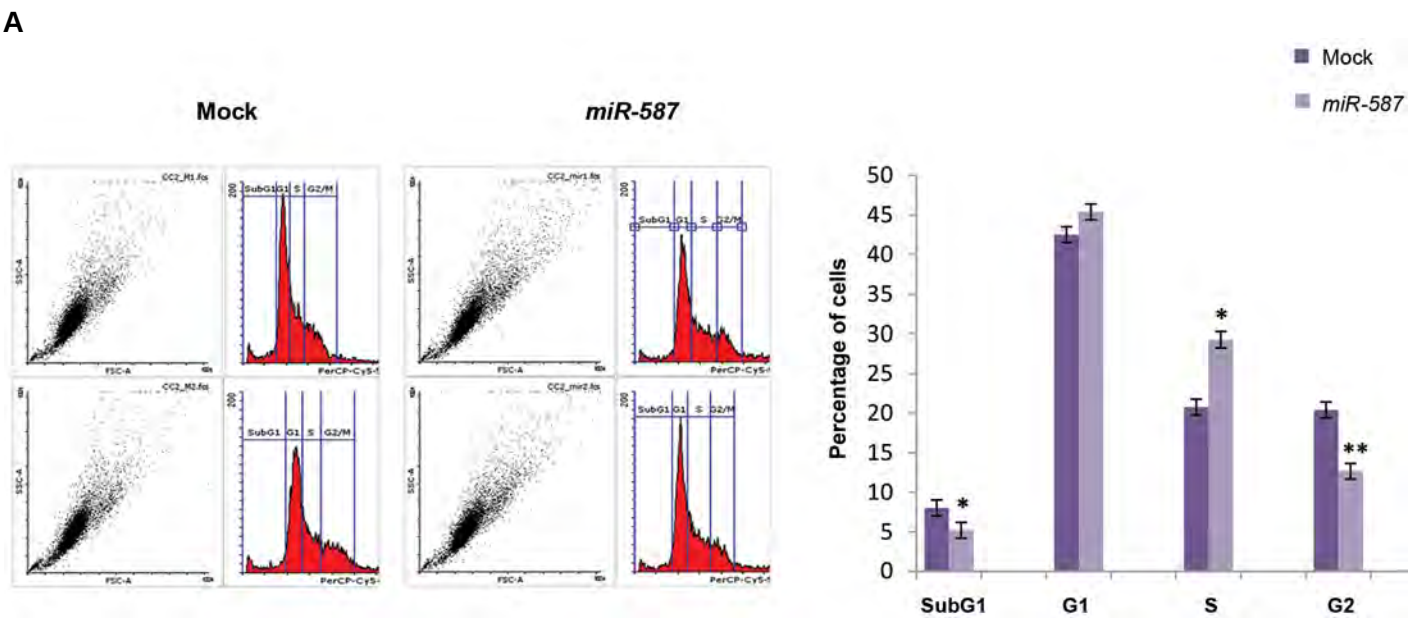

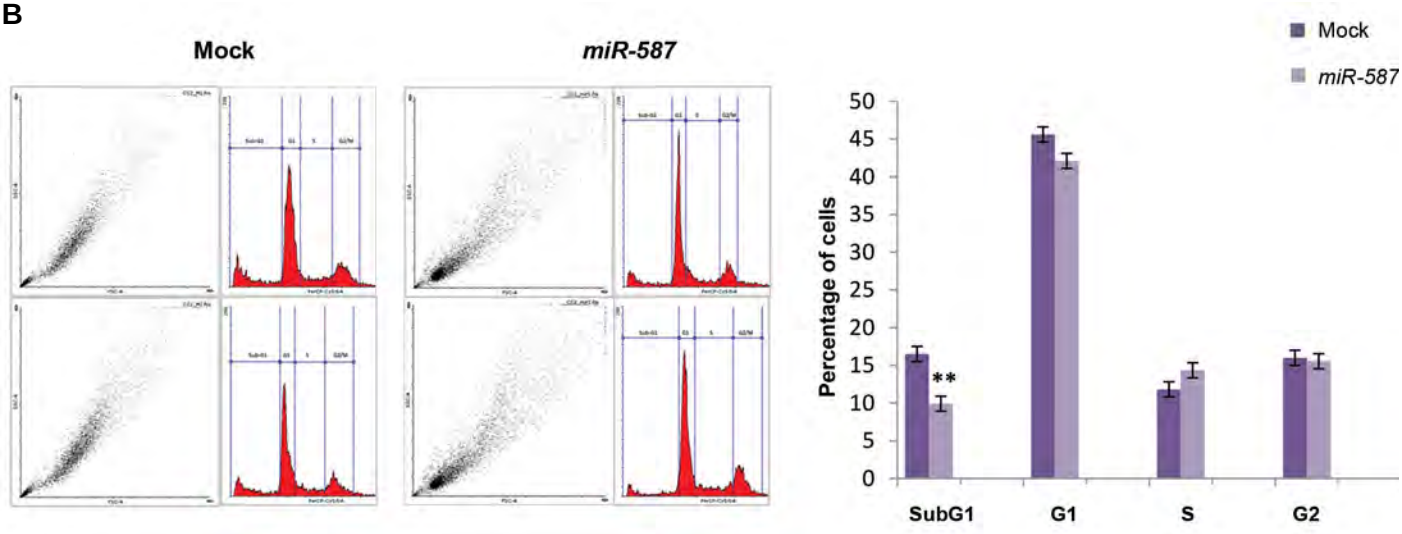

Fig.4: *Hsa-miR-587* overexpression effect on cell cycle status. **A.** Flow cytometry analysis indicated that the overexpression of *miR-587* in HEK293T cells resulted in a significant increase of the S-phase cell population (~1.5-folds, P=0.019), and a significant decrease in the SubG1-phase and G2-phase populations of cells (~1.5-folds, P=0.02 and 0.005, respectively) and **B.** Overexpression of *miR-587* in HCT116 cells resulted in a significant increase of the SubG1-phase cell population (~1.7-folds, P=0.01), but no significant variation was observed in the populations of the other cell cycle phases in comparison to the control. *; P≤0.05 and **; P≤0.01.

Discussion

TGFβ/SMAD signaling pathway represents a complex network that effectively controls fundamental cellular processes. The activation of this pathway causes an arrest in the cell cycle of normal cells and early tumors. Mutational inactivation or dysregulated expression of the TGFβ/SMAD signaling components has been observed in human cancers (4, 24). TGFβ signaling has been shown to play a dual role in the course of cancer progression. It exhibits a tumor suppressive role in the early stages of the carcinogenesis process by inhibiting cell cycle progression and promoting apoptosis (5, 25). However, in the late stages, it exerts tumor-promoting effects by increasing tumor invasiveness and metastasis (4, 5).

Previous studies described TGFβ/SMAD signaling as an important inhibitor of cellular proliferation (26). TGFβ/SMAD signaling downregulates the expression of a set of genes resulting in the inhibition of cell cycle transition from G1 to S phase (27, 28). In the current study, in silico and experimental tools showed that miR-587 targets important components of the TGFβ/SMAD signaling pathway. Moreover, overexpressing *miR-587* in HEK293T cells resulted in increasing the S-phase cell population, and reducing the SubG1-phase population. While in HCT116 cells, overexpressing this miRNA resulted in reducing the SubG1-phase only, without exerting any effect on the other cell cycle phases. This variation may be due to the differences between the two cell line origins, identities and status. However, the common effect exerted on the two cell lines at the SubG1-phase, indicates that miR-587 plays a role in the arrest of the cell cycle at this phase.

The dbDEMC 2.0 database that presents differentially expressed miRNAs in human cancers, has provided important evidence about the expression of *miR-587* in a set of human cancer samples (29). The available expression data showed that *miR-587* expression is upregulated in colon and breast tumors in comparison to normal tissue, and downregulated in high-grade colon tumors in comparison to low-grade tumors (5). These data provide an evidence about the function of this miRNA and its regulatory effects on the TGFβ signaling pathway that is downregulated in early tumor stages and upregulated during the late stages (30).

Conclusion

In the current study, we demonstrated a regulatory role for *miR-587* against TGFβ/SMAD signaling. In addition, our results showed that *miR-587* promotes cell cycle progression.

Acknowledgements

This work was supported by Tarbiat Modares University, and National Institute for Medical Research Development financial aids. We thank all those who provided any type of assistance in conducting this study. The authors declare no conflict of interest.

Authors' Contributions

M.J., A.M.; Performed the experiments and analyzed the results. M.J., A.M., B.M.S.; Wrote the manuscript. B.M.S., M.T.; Designed the experiments. All authors have read and approved the final draft of the manuscript.

References

1. Derynck R, Zhang YE. Smad-dependent and Smad-independent pathways in TGF-beta family signalling. Nature. 2003; 425(6958): 577-584.
2. Hinck AP. Structural studies of the TGF-βs and their receptors -

insights into evolution of the TGF-β superfamily. FEBS Lett. 2012; 586(14): 1860-1870.
3. Zi Z, Chapnick DA, Liu X. Dynamics of TGF-β/Smad signaling. FEBS Lett. 2012; 586(14): 1921-1928.
4. Neuzillet C, Tijeras-Raballand A, Cohen R, Cros J, Faivre S, Raymond E, et al. Targeting the TGFβ pathway for cancer therapy. Pharmacol Ther. 2015; 147: 22-31.
5. Neel JC, Humbert L, Lebrun JJ. The dual role of TGFβ in human cancer: from tumor suppression to cancer metastasis. ISRN Molecular Biology. 2012; 2012: 1-28.
6. Macfarlane LA, Murphy PR. MicroRNA: biogenesis, function and role in cancer. Curr Genomics. 2010; 11(7): 537-561.
7. Bartel DP. MicroRNAs: genomics, biogenesis, mechanism, and function. Cell. 2004; 116(2): 281-297.
8. Lu J, Getz G, Miska EA, Alvarez-Saavedra E, Lamb J, Peck D, et al. MicroRNA expression profiles classify human cancers. Nature. 2005; 435(7043): 834-838.
9. Adams BD, Kasinski AL, Slack FJ. Aberrant regulation and function of MicroRNAs in cancer. Curr Biol. 2014; 24(16): R762-R776.
10. Peng Y, Croce CM. The role of MicroRNAs in human cancer. Signal Transduct Target Ther. 2016; 1: 15004.
11. Palmero EI, de Campos SG, Campos M, de Souza NC, Guerreiro ID, Carvalho AL, et al. Mechanisms and role of microRNA deregulation in cancer onset and progression. Genet Mol Biol. 2011; 34(3): 363-370.
12. Li J, Liang H, Bai M, Ning T, Wang C, Fan Q, et al. miR-135b promotes cancer progression by targeting transforming growth factor beta receptor II (TGFBR2) in colorectal cancer. PLoS One. 2015; 10(6): e0130194.
13. Zhang X, Chang A, Li Y, Gao Y, Wang H, Ma Z, et al. miR-140-5p regulates adipocyte differentiation by targeting transforming growth factor-β signaling. Sci Rep. 2015; 5: 18118.
14. Jafarzadeh M, Mohammad Soltani B, Ekhteraei Tousi S, Behmanesh M. Hsa-miR-497 as a new regulator in TGFβ signaling pathway and cardiac differentiation process. Gene. 2018; 675: 150-156.
15. Ekhteraei-Tousi S, Mohammad-Soltani B, Sadeghizadeh M, Mowla SJ, Parsi S, Soleimani M. Inhibitory effect of hsa-miR-590-5p on cardiosphere-derived stem cells differentiation through downregulation of TGFB signaling. J Cell Biochem. 2015; 116(1): 179-191.
16. Abedini Bakhshmand E, Mohammad Soltani B, Fasihi A, Mowla SJ. Hsa-miR-5582-3P regulatory effect on TGFβ signaling through targeting of TGFβ-R1, TGFβ-R2, SMAD3, and SMAD4 transcripts. J Cell Biochem. 2018; 119(12): 9921-9930.
17. Agarwal V, Bell GW, Nam JW, Bartel DP. Predicting effective microRNA target sites in mammalian mRNAs. Elife. 2015; 4.
18. Paraskevopoulou MD, Georgakilas G, Kostoulas N, Vlachos IS, Vergoulis T, Reczko M, et al. DIANA-microT web server v5.0: service integration into miRNA functional analysis workflows. Nucleic Acids Res. 2013; 41(Web Server issue): W169-W173.
19. Reczko M, Maragkakis M, Alexiou P, Grosse I, Hatzigeorgiou AG. Functional microRNA targets in protein coding sequences. Bioinformatics. 2012; 28(6): 771-776.
20. Vejnar CE, Blum M, Zdobnov EM. miRmap web: comprehensive microRNA target prediction online. Nucleic Acids Res. 2013; 41(Web Server issue): W165-W168.
21. Kent WJ, Sugnet CW, Furey TS, Roskin KM, Pringle TH, Zahler AM, et al. The human genome browser at UCSC. Genome Res. 2002; 12(6): 996-1006.
22. Kopec AM, Rivera PD, Lacagnina MJ, Hanamsagar R, Bilbo SD. Optimized solubilization of TRIzol-precipitated protein permits Western blotting analysis to maximize data available from brain tissue. J Neurosci Methods. 2017; 280: 64-76.
23. Bradford MM. A rapid and sensitive method for the quantitation of microgram quantities of protein utilizing the principle of protein-dye binding. Anal Biochem. 1976; 72: 248-254.
24. Gordon KJ, Blobe GC. Role of transforming growth factor-beta superfamily signaling pathways in human disease. Biochim Biophys Acta. 2008; 1782(4): 197-228.
25. Lin RL, Zhao LJ. Mechanistic basis and clinical relevance of the role of transforming growth factor-β in cancer. Cancer Biol Med. 2015; 12(4): 385-393.
26. Iordanskaia T, Nawshad A. Mechanisms of transforming growth factor β induced cell cycle arrest in palate development. J Cell Physiol. 2011; 226(5): 1415-1424.
27. Chen CR, Kang Y, Siegel PM, Massagué J. E2F4/5 and p107 as Smad cofactors linking the TGFbeta receptor to c-myc repression. Cell. 2002; 110(1): 19-32.
28. Mukherjee P, Winter SL, Alexandrow MG. Cell Cycle arrest by transforming growth factor β1 near G_1/S Is mediated by acute abrogation of prereplication complex activation involving an Rb-MCM interaction. Mol Cell Biol. 2010; 30(3): 845-856.
29. Yang Z, Wu L, Wang A, Tang W, Zhao Y, Zhao H, et al. dbDEMC 2.0: updated database of differentially expressed miRNAs in human cancers. Nucleic Acids Res. 2017; 45(D1): D812-D818.
30. Syed V. TGF-β signaling in cancer. J Cell Biochem. 2016; 117(6): 1279-1287.

Original Article

Evaluation of The Expression Levels of Three Long Non-Coding RNAs in Multiple Sclerosis

Afshin Moradi, M.Sc.[1#], Mahdis Rahimi Naiini, M.Sc.[2, 3#], Nasrin Yazdanpanahi, M.Sc.[4#], Hossein Tabatabaeian, Ph.D.[5, 6#], Fariba Nabatchian, Ph.D.[1*], Masoud Baghi, M.Sc.[7, 8], Mansoureh Azadeh, M.Sc.[3], Kamran Ghaedi, Ph.D.[7, 8*]

1. Department of Medical Laboratory Sciences, Faculty of Allied Medicine, Tehran University of Medical Sciences, Tehran, Iran
2. Department of Biochemistry, Medical School and Kerman Physiology Research Center, Kerman University of Medical Science, Kerman, Iran
3. Zist-fanavari Novin, Biotechnology Institute, Isfahan, Iran
4. Department of Genetics, Falavarjan Branch, Islamic Azad University, Isfahan, Iran
5. Division of Genetics, Department of Biology, Faculty of Sciences, University of Isfahan, Isfahan, Iran
6. Department of Biochemistry, Yong Loo Lin School of Medicine, National University of Singapore, Singapore
7. Department of Biology, School of Sciences, University of Isfahan, Isfahan, Iran
8. Department of Cellular Biotechnology, Cell Science Research Center, Royan Institute for Biotechnology, ACECR, Isfahan, Iran

#The first four authors equally contributed to this work.

**Corresponding Addresses: P.O.Box: 14155-6559, Department of Medical Laboratory Sciences, Faculty of Allied Medicine, Tehran University of Medical Sciences, Tehran, Iran*

P.O. Box: 816513-1378, Department of Cellular Biotechnology, Cell Science Research Center, Royan Institute for Biotechnology, ACECR, Isfahan, Iran

Emails: fnabatchian@yahoo.com, kamranghaedi@royaninstitute.org

Received: 23/November/2018, Accepted: 12/March/2019

Abstract

Objective: Multiple sclerosis (MS) is a chronic disorder involving both inflammatory and neurodegenerative responses. Long non-coding RNAs (lncRNAs) have been had an emerging role as the biomarkers of different disorders, including autoimmune diseases. Previous studies have shown that NR_003531.3 (MEG3a), AC000061.1_201, and AC007182.6 play a role in the pathogenesis of human autoimmune diseases. However, the potential significance of these lncRNAs, as the diagnostic biomarkers of MS, has not been studied yet. We aimed to quantitatively evaluate the expression levels of NR_003531.3, AC000061.1_201, and AC007182.6 in peripheral blood samples of MS patients in comparison with healthy controls.

Materials and Methods: In this case-control study, the blood samples from 20 MS patients and 10 healthy controls were collected. Total RNA was extracted, and the expression levels of three selected lncRNAs were quantitatively measured using the quantitative real time-polymerase chain reaction (qRT-PCR) method.

Results: We detected a significant down-regulation in the expression of NR_003531.3 in MS patients, while no marked changes were observed in the expression of AC000061.1_201 and AC007182.6 in patients compared with controls. Based on the receiver operating characteristic (ROC) curve analysis, NR_003531.3 could discriminate MS patients from healthy subjects effectively. Regarding the prognosis of MS patients, NR_003531.3 is significantly and inversely correlated with the expanded disability status scale (EDSS).

Conclusion: The potential role of NR_003531.3 lncRNA as a diagnostic biomarker to distinguish MS patients is proposed. Prognostically, NR_003531.3 correlates with lower disability rates in MS patients.

Keywords: Autoimmune Disease, Gene Expression Profiling, Long Non-coding RNA, Multiple Sclerosis, Neurodegenerative Disease

Cell Journal(Yakhteh), Vol 22, No 2, July-September (Summer) 2020, Pages: 165-170

Citation: **Moradi A, Rahimi Naiini M, Yazdanpanahi N, Tabatabaeian H, Nabatchian F, Baghi M, Azadeh M, Ghaedi K. Evaluation of the expression levels of three long non-coding RNAs in multiple sclerosis. Cell J. 2020; 22(2): 165-170. doi: 10.22074/cellj.2020.6555.**

Introduction

Multiple sclerosis (MS) is a chronic disorder involving both inflammatory and neurodegenerative responses. The origins of MS have been summarized as the environmental, genetic, and hormonal factors. Dramatic changes in human lifestyle have triggered a pervasive vitamin D deficiency worldwide. This phenomenon has elevated MS incidence (1). Along with vitamin D deficiency, estrogen hormone in females has synergistically worsened the immune tolerance and increased the number of MS cases (2).

Although the precise etiology of MS is still unrevealed, multiple genetic pathways have been identified to participate in the pathogenesis of MS, including HLA-DQB1*0602, HLA-DQA1*0102, HLA-DRB1*1501, and HLA-DRB5*0101 (3), as well as some microRNAs namely, miR-326 and miR-26a (4). MS disease is an inflammatory response with infiltrated activated monocytes, B and T cells into the central nervous system (5). Among them, T helper-17 (Th-17) plays a pivotal role in MS pathogenesis. Th-17 is a $CD4^+$ T helper cell originated from Naïve $CD4^+$ cells upon the

expression and activation of interleukin-23 (IL-23), IL-6 and transforming growth factor-beta (TGF-β) (6-8). Increased level of Th-17 cells has been reported in various human autoimmune diseases including MS (9), systemic lupus erythematosus (10), psoriasis (11), and rheumatoid arthritis (12). Th-17 cells impose their degenerative impact via up-regulating different cytokines such as granulocyte/macrophage colony-stimulating factor (GM-CSF), IL-21, IL-17, and IL 22, which in turn, leads to the tissue injuries.

Several studies have identified numerous potential biomarkers that can predict the MS disease, as well as its progression. Among the applicable biomarkers, long non-coding RNAs (lncRNAs) contribute to the pathogenesis of many disorders such as MS (13). lncRNAs are >200-nucleotide non-coding transcripts expressed ubiquitously from the genome. AC007182.6 has been recently shown to be involved in Th-17 differentiation. This lncRNA is co-expressed with its nearby gene, *BATF*, which has a significant role in determining the naïve cell fate to be differentiated into Th-17 cells (14).

Furthermore, the overexpression of Homo sapiens maternally expressed 3a (MEG3a), also known as NR_003531.3, has been reported in the development of $CD4^+$ T cells in autoimmune diseases. This excessive expression is strongly linked to the lowered percentage of Th-17 cells (15). The fundamental role of another lncRNA, named AC000061.1-201, has been revealed in rheumatoid arthritis. This lncRNA is significantly overexpressed in the peripheral blood mononuclear cells of these patients and tightly associated with the serum level of IL-6 and tumor necrosis factor-alpha (TNF-α) (16). Albeit these lncRNAs have substantial roles in the pathogenesis of autoimmune disorders, mainly through regulating the population of Th-17 cells, no study has been conducted to evaluate their significance in MS disease. Therefore, we aimed to quantitatively study the expression levels of NR_003531.3, AC000061.1-201, and AC007182.6 in the peripheral blood samples of the patients with MS disease. This study may help nominate the lncRNA(s), differentially expressed in MS patients, as prognostic molecules especially in MS subclinical cases.

Material and Methods

Patients and samples

The case-control study was carried out to compare lncRNA expression levels in 20 Iranian relapsing-remitting MS (RRMS) patients who had not taken any kinds of MS drug. The diagnosis of RRMS has been made based on the revised McDonald's criteria (17). The control group comprised of 10 healthy sex-matched volunteers whose neurological disorders were ruled out. Both groups of men and women, with the age range of 10 to 55, who signed the written informed consent, were included in the study. The participants with the history of autoimmune and/or neurological diseases, as well as diabetes mellitus, were excluded from the investigation. The characteristics of RRMS patients are summarized in Figure 1. In this research, 5 ml of peripheral blood was collected from all participants in EDTA-containing tubes.

All procedures performed in studies involving human participants were in accordance with the ethical standards of the Ethics Committee of Tehran University of Medical Sciences, Iran, and with the 1964 Helsinki declaration and its later amendments or comparable ethical standards. All participants signed the informed consents.

RNA extraction

Total RNA was isolated with GeneAll Hybrid-RTM blood RNA extraction kit. The RNA concentration was estimated using Nanodrop Spectrophotometer (ND-1000, ThermoFisher, MA, USA). Purified RNA was stored at -80˚C for further steps.

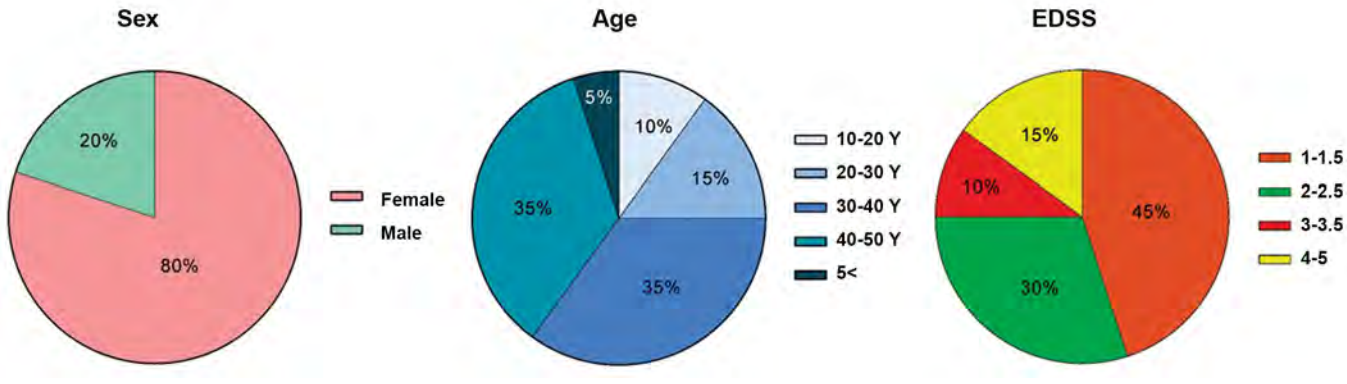

Fig.1: The characteristics of multiple sclerosis (MS) patients. The number of individuals as well as their gender, age, and the Expanded Disability Status Scale (EDSS) scores is illustrated.

cDNA synthesis and quantitative real time-polymerase chain reaction

RNA was treated with DNase I prior to cDNA synthesis. The cDNA was performed using cDNA Synthesis Applied by Universal cDNA Synthesis Kit (ParsGenome, Iran) based on the manufacturer's protocol. The synthesized cDNAs were stored at -20˚C until the polymerase chain reaction (PCR). The Oligo 7 software (Molecular Biology Insights, Inc., CO, USA) was employed for designing the specific primers, which are listed in Table 1. Quantitative real time- polymerase chain reacttion (qRT-PCR) reactions were performed on the ABI PRISM 7500 instrument (Applied Biosystems, USA). All reactions were carried out in triplicate. qRT-PCR data were assessed according to the $2^{-\Delta\Delta CT}$ method (18). The corresponding lncRNA C_t values were normalized against *GAPDH*, as a reference gene.

Table 1: The sequence of the primers

lncRNA	Primer sequence (5´-3´)
NR_003531.3	F: TGGCATAGAGGAGGTGAT
	R: GGAGTGCTGTTGGAGAATA
AC000061.1_201	F: ATGCTGCTATGCTTCCC
	R: GCTTCTGTAGTTCGGTCTT
AC007182.6	F: TGTGTTACTCAGCGTCCTA
	R: CGTATTGAGAGCGTGTGTT

lncRNA; Long non-coding RNA.

Statistical analysis

Statistical analyses were performed by the GraphPad Prism 7 (CA, USA). The Mann-Whitney U test was carried out to analyze the quantitative expression level of lncRNAs between patients and healthy groups. Spearman's rank correlation test was performed to evaluate the possible correlation between the relative expression levels of lncRNAs and the clinical data. The $P<0.05$ were considered statistically significant.

Results

Expression levels of lncRNAs in RRMS patients and controls

The expression levels of three lncRNAs including NR_003531.3, AC000061.1-201, and AC007182.6 were quantitatively assessed using the qRT-PCR method in MS and healthy groups. Statistical analyses showed that there was a significant down-regulation in the expression of NR_003531.3 in RRMS patients, while no significant difference was observed concerning the expression levels of AC000061.1-201 and AC007182.6 in patients as compared to controls (Fig.2).

NR_003531.3 discriminated MS patients from healthy controls

To assess the potential of NR_003531.3, as a diagnostic biomarker for distinguishing the health/ disease status, the expression level of this lncRNA was analyzed by the receiver operating characteristic (ROC) analysis in both groups. The ROC curve analysis indicated that NR_003531.3 could effectively discriminate RRMS patients from healthy individuals with an area under the curve (AUC) of 0.90 (P=0.0019) (Fig.3). This finding may propose the NR_003531.3 as a potential screening tool.

NR_003531.3 expression level is negatively correlated with the expanded disability status scale

In order to explore the prognostic value of NR_003531.3, the correlation between NR_003531.3 and the level of disability caused by MS disease was investigated. To this aim, the expression level of NR_003531.3 was evaluated based on the EDSS scores among 20 RRMS patients. It was demonstrated that there was a significant negative correlation between NR_003531.3 expression levels and the EDSS scores, r=-0.669 (P=0.0013). It implies that the higher expression of NR_003531.3 lncRNA was linked with the lowered disability rate in MS patients (Fig.4).

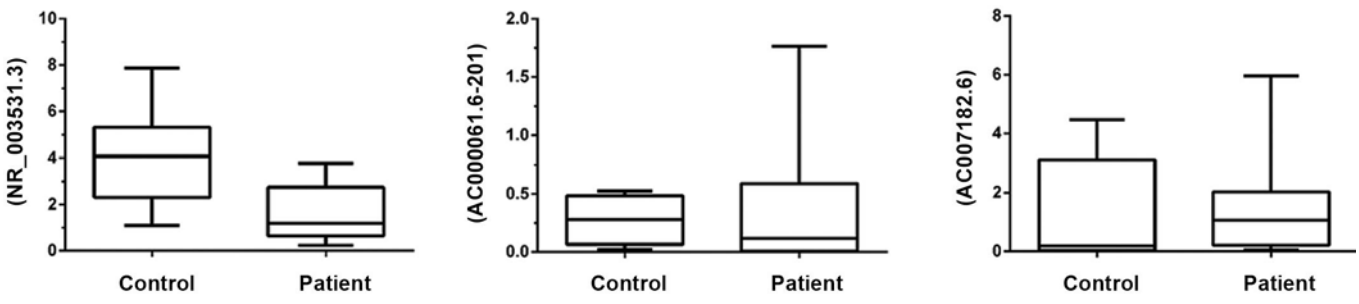

Fig.2: Expression level of NR_003531.3 (***; P=0.0003), AC000061.6-201 (P=0.99), and AC007182.6 (P=0.1619) in multiple sclerosis (MS) and healthy groups. While the previous long non-coding RNA (lncRNAs) had no significant differences, NR-003531.3 expression shows a significant increase in MS patients as compared to healthy controls.

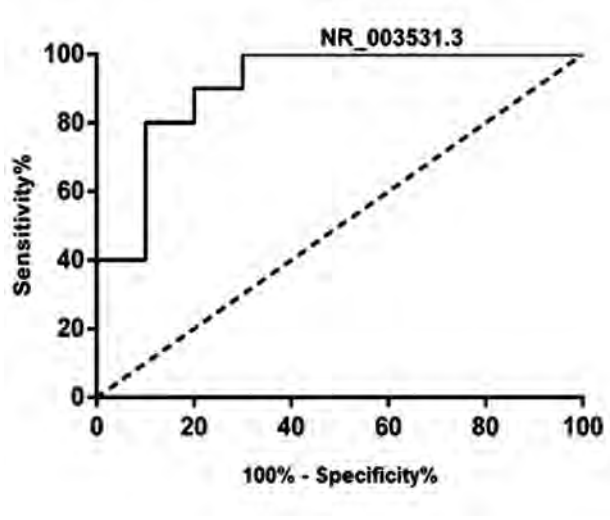

Fig.3: The receiver operating characteristic (ROC) curve of healthy/patients analyzed for the expression level of NR-003531.3. NR-003531.3 is adequately potent to discriminate between healthy subjects and MS patients with the area under the curve (AUC) of 0.91 (P=0.0019).

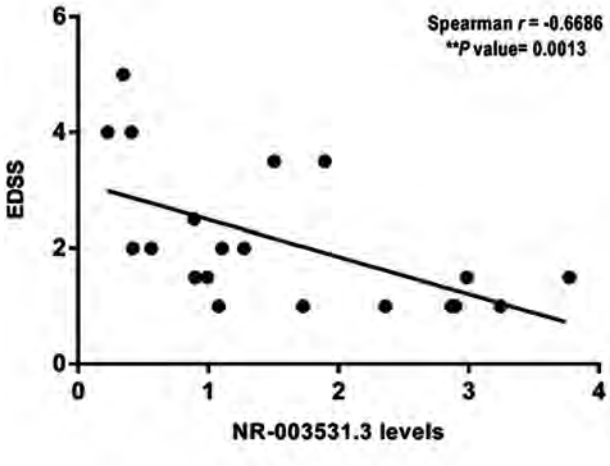

Fig.4: The correlation study. NR_003531.3 is negatively associated with the Expanded Disability Status Scale (EDSS) in multiple sclerosis (MS) patients.

Discussion

Non-coding RNAs have critical indications in a variety of human disorders including cancer (19-21), cardiovascular diseases (22), diabetes (23), and autoimmune diseases (24). LncRNAs are the emerging type of non-coding RNAs, playing crucial roles in the pathogenesis of human autoimmune diseases, especially MS (13). In this study, we screened the expression levels of three lncRNAs with implications in other human autoimmune diseases, in order to understand whether they are differentially expressed in MS versus healthy subjects.

NR_003531.3 is known to inhibit the miR-125a-5p expression in $CD4^+$ T cells which, in turn, results in the lower percentage of Th-17 cells in immune thrombocytopenic purpura (15). More importantly, NR_003531.3 has been reported to be critical as a functional lncRNA, which plays a significant role as a competing endogenous RNA (ceRNA). NR_003531.3, indeed, competes with programmed cell death 4 (PDCD4) mRNA thereby binding to miR-21. The ultimate consequence of this phenomenon is ischemic neuronal death (25). It has been shown that NR_003531.3 is normally expressed in the nucleus accumbens of normal human brain tissue, while it shows a drastic up-regulation in the brain of heroin abusers (26), which may cause a neurodegenerative condition. All these data support the notion that NR_003531.3 might be necessary for the regulation of the pathway, thought to be involved in the modulation of the immune system and central nervous system.

In this study and for the first time, we have demonstrated the expression level of three lncRNAs including NR_003531.3, AC000061.1-201, and AC007182.6 in MS patients. The evaluation of extensive alterations that occur in the expression of lncRNAs during the immune response could result in designing novel diagnostic and therapeutic approaches for MS patients. Based on the analysis, NR_003531.3, but not other lncRNAs, showed a significant down-regulation in RRMS patients. It strongly suggests that NR_003531.3 could decrease the risk of developing MS by reducing the percentage and activity of Th-17 cells.

Additionally, the ROC curve analysis showed that NR_003531.3 is effectively capable and potent to distinguish between RRMS and healthy individuals. These findings suggest that NR_003531.3 might be considered a novel potential biomarker for the diagnosis of MS patients. However, since MS patients are mainly diagnosed by the clinical and imaging findings, the applicability of NR_003531.3 would be useful when its altered expression is assessed in relapse/acute phase of the disease in comparison with the remission stage. This hypothesis can be examined by the determination of the expression level of NR_003531.3 in MS patients when they experience the relapse phase in comparison with those at the remission stage.

The correlation analyses between NR_003531.3 lncRNA expression levels and EDSS scores of MS patients revealed a significant negative correlation between NR_003531.3 levels and the EDSS, denoting that the lower expression of NR_003531.3 is associated with the higher disability rate in MS patients. This finding highlights the prognostic value of NR_003531.3 in MS disease.

As NR_003531.3 has a differential expression in MS patients, as compared to controls, this lncRNA might be participating in the pathogenesis of MS. This hypothesis could be expanded by *in vitro* and *in vivo* studies using NR_003531.3 expression plasmid and/or specific siRNAs. As modulating the percentage of Th-17 cells might be the main function of NR_003531.3, incorporating the quantitative studies to analyze the population of Th-17 cells, downstream of NR_003531.3, could gain an insight on the mechanistic role of this lncRNA in MS disease.

A number of altered lncRNAs in MS have been reported. Based on the microarray analysis in MS patients, Zhang et al. (27) have shown that ENSG00000231898.3, XLOC_009626, and XLOC_010881 underwent up-regulation, while ENSG00000233392.1, ENSG00000259906.1, and lncRNA XLOC_010931 exhibited a lower amount in MS patients. Eftekharian et al. (13) revealed that PVT1 and FAS-AS1 lncRNAs had lower expression as compared with healthy individuals, whereas THRIL had significantly higher expression in RRMS patients. Moreover, a lncRNA PCR array-based study showed the down-regulation of NRON and TUG1 in MS patients (28). Unlike the latter study, TUG1 along with NEAT1 and PANDA has been reported to be overexpressed in MS patients (29), reflecting the significance of validating the results at least for TUG1 lncRNA. Besides, Pahlevan Kakhki et al. (30) indicated that HOTAIR lncRNA underwent up-regulation in MS patients. In contrast to these studies, we have evaluated the diagnostic and prognostic values of lncRNAs that were earlier mentioned.

In brief, we have demonstrated the down-regulation of NR_003531.3 in MS patients. Based on the ROC curve analysis, this lncRNA is capable of discriminating the MS patients effectively. Prognostically, the lower expression of NR_003531.3 is linked with a poorer prognosis in MS disease.

This study lacked sufficient sample size. Therefore, to confirm the results, further studies are required to examine the expression level of NR_003531.3 in a larger population of MS and control groups, as well as a separate group of MS patients to test whether the disease stage (relapse/remission) influence the expression of NR_003531.3. Moreover, animal models of MS could be employed to corroborate the results of our study. As shown in our study that NR_003531.3 is downregulated in MS patients, the overexpressing this lncRNA would affect the onset or the prognosis of MS in murine models.

Conclusion

NR_003531.3 is significantly downregulated in the peripheral blood of MS patients. This lncRNA can discriminate MS patients from healthy controls. These findings propose the potential diagnostic value of NR_003531.3 lncRNA. Moreover, NR_003531.3 is inversely correlated with disability scores of MS patients, suggesting the potential prognostic role of this lncRNA on MS disease course.

Acknowledgements

The authors wish to thank the Vice-Chancellor for Research in Tehran University of Medical Sciences and for supporting this study financially. This manuscript was the results of a research project approved by the Tehran University of Medical Sciences (contract number: 97-02-31-38599). The authors declare no conflict of interests.

Authors' Contributions

F.N., K.G.; Designed and Conceived the experiments and supervised the project. A.M., M.R.N., N.Y.; Conducted the molecular experiments and extensively contributed to the interpretation of the data and conclusion. M.B.; Performed statistical analyses and interpretation of data. M.A.; Collected and prepared the samples for RNA extraction and assisted other experiments. H.T.; Data Collection analysis and manuscript writing. All authors performed editing and approving the final version of the manuscript for the submission. They also participated in the finalization of the manuscript and approved the final draft.

References

1. Pierrot-Deseilligny C, Souberbielle JC. Vitamin D and multiple sclerosis: an update. Mult Scler Relat Disord. 2017; 14: 35-45.
2. Nashold FE, Spach KM, Spanier JA, Hayes CE. Estrogen controls vitamin D3-mediated resistance to experimental autoimmune encephalomyelitis by controlling vitamin D3 metabolism and receptor expression. J Immunol. 2009; 183(6): 3672-36781.
3. Barcellos LF, Oksenberg JR, Begovich AB, Martin ER, Schmidt S, Vittinghoff E, et al. HLA-DR2 dose effect on susceptibility to multiple sclerosis and influence on disease course. Am J Hum Genet. 2003; 72(3): 710-716.
4. Honardoost MA, Kiani-Esfahani A, Ghaedi K, Etemadifar M, Salehi M. miR-326 and miR-26a, two potential markers for diagnosis of relapse and remission phases in patient with relapsing-remitting multiple sclerosis. Gene. 2014; 544(2): 128-133.
5. Mount HT. Multiple sclerosis and other demyelinating diseases. Can Med Assoc J. 1973; 108(11): 1356 passim.
6. Veldhoen M, Hocking RJ, Atkins CJ, Locksley RM, Stockinger B. TGFbeta in the context of an inflammatory cytokine milieu supports de novo differentiation of IL-17-producing T cells. Immunity. 2006; 24(2): 179-189.
7. Harrington LE, Hatton RD, Mangan PR, Turner H, Murphy TL, Murphy KM, et al. Interleukin 17–producing CD4+ effector T cells develop via a lineage distinct from the T helper type 1 and 2 lineages. Nat Immunol. 2005; 6(11): 1123-1132.
8. Lassmann H, Brück W, Lucchinetti C. Heterogeneity of multiple sclerosis pathogenesis: implications for diagnosis and therapy. Trends Mol Med. 2001; 7(3): 115-121.
9. Brucklacher-Waldert V, Stuerner K, Kolster M, Wolthausen J, Tolosa E. Phenotypical and functional characterization of T helper 17 cells in multiple sclerosis. Brain. 2009; 132(Pt 12): 3329-3341.
10. Yang J, Chu Y, Yang X, Gao D, Zhu L, Yang X, et al. Th17 and natural Treg cell population dynamics in systemic lupus erythematosus. Arthritis Rheum. 2009; 60(5): 1472-1483.
11. Fujishima S, Watanabe H, Kawaguchi M, Suzuki T, Matsukura S, Homma T, et al. Involvement of IL-17F via the induction of IL-6 in psoriasis. Arch Dermatol Res. 2010; 302(7): 499-505.
12. Jacobs JP, Wu H-J, Benoist C, Mathis D. IL-17-producing T cells can augment autoantibody-induced arthritis. Proc Natl Acad Sci USA. 2009; 106(51): 21789-21794.
13. Eftekharian MM, Ghafouri-Fard S, Soudyab M, Omrani MD, Rahimi M, Sayad A, et al. Expression analysis of long non-coding RNAs in the blood of multiple sclerosis patients. J Mol Neurosci. 2017; 63(3-4): 333-341.
14. Spurlock CF 3rd, Tossberg JT, Guo Y, Collier SP, Crooke PS 3rd, Aune TM. Expression and functions of long noncoding RNAs during human T helper cell differentiation. Nat Commun. 2015; 6: 6932.
15. Li JQ, Hu SY, Wang ZY, Lin J, Jian S, Dong YC, et al. Long noncoding RNA MEG3 inhibits microRNA-125a-5p expression and induces immune imbalance of Treg/Th17 in immune thrombocytopenic purpura. Biomed Pharmacother. 2016; 83: 905-911.
16. Yuan M, Wang S, Yu L, Qu B, Xu L, Liu L, et al. Long noncoding RNA profiling revealed differentially expressed lncRNAs associated with disease activity in PBMCs from patients with rheumatoid arthritis. PLoS One. 2017; 12(11): e0186795.
17. Polman CH, Reingold SC, Banwell B, Clanet M, Cohen JA, Filippi M, et al. Diagnostic criteria for multiple sclerosis: 2010 revisions to the McDonald criteria. Ann Neurol. 2011; 69(2): 292-302.
18. Sadeghi S, Hojati Z, Tabatabaeian H. Cooverexpression of EpCAM and c-myc genes in malignant breast tumours. J Genet. 2017; 96(1): 109-118.
19. Adami B, Tabatabaeian H, Ghaedi K, Talebi A, Azadeh M, Deh-

dashtian E. miR-146a is deregulated in gastric cancer. J Cancer Res Ther. 2019; 15(1): 108-114.
20. Noormohammad M, Sadeghi S, Tabatabaeian H, Ghaedi K, Talebi A, Azadeh M, et al. Upregulation of miR-222 in both Helicobacter pylori-infected and noninfected gastric cancer patients. J Genet. 2016; 95(4): 991-995.
21. Rouigari M, Dehbashi M, Tabatabaeian H, Ghaedi K, Mohammadynejad P, Azadeh M. Evaluation of the expression level and hormone receptor association of miR-126 in breast cancer. Indian J Clin Biochem. 2018: 1-7.
22. Thum T, Catalucci D, Bauersachs J. MicroRNAs: novel regulators in cardiac development and disease. Cardiovasc Res. 2008; 79(4): 562-570.
23. Leung A, Natarajan R. Long noncoding RNAs in diabetes and diabetic complications. Antioxid Redox Signal. 2018; 29(11): 1064-1073.
24. Soifer HS, Rossi JJ, Sætrom P. MicroRNAs in disease and potential therapeutic applications. Mol Ther. 2007; 15(12): 2070-2079.
25. Yan H, Rao J, Yuan J, Gao L, Huang W, Zhao L, et al. Long noncoding RNA MEG3 functions as a competing endogenous RNA to regulate ischemic neuronal death by targeting miR-21/PDCD4 signaling pathway. Cell Death Dis. 2017; 8(12): 3211.
26. Michelhaugh SK, Lipovich L, Blythe J, Jia H, Kapatos G, Bannon MJ. Mining Affymetrix microarray data for long non-coding RNAs: altered expression in the nucleus accumbens of heroin abusers. J Neurochem. 2011; 116(3): 459-466.
27. Zhang F, Gao C, Ma XF, Peng XL, Zhang RX, Kong DX, et al. Expression profile of long noncoding RNAs in peripheral blood mononuclear cells from multiple sclerosis patients. CNS Neurosci Ther. 2016; 22(4): 298-305.
28. Fenoglio C, Oldoni E, Serpente M, De Riz MA, Arcaro M, D'Anca M, et al. LncRNAs expression profile in peripheral blood mononuclear cells from multiple sclerosis patients. J Neuroimmunol. 2018; 324: 129-135.
29. Dastmalchi R, Ghafouri-Fard S, Omrani MD, Mazdeh M, Sayad A, Taheri M. Dysregulation of long non-coding RNA profile in peripheral blood of multiple sclerosis patients. Mult Scler Relat Disord. 2018; 25: 219-226.
30. Pahlevan Kakhki M, Nikravesh A, Shirvani Farsani Z, Sahraian MA, Behmanesh M. HOTAIR but not ANRIL long non-coding RNA contributes to the pathogenesis of multiple sclerosis. Immunology. 2018; 153(4): 479-487.

Original Article

Investigation of *VASA* Gene and Protein Expression in Neonate and Adult Testicular Germ Cells in Mice *In Vivo* and *In Vitro*

Hossein Azizi, Ph.D.[1*], Mojtaba Ranjbar, Ph.D.[1], Somayeh Rahaiee, Ph.D.[1], Mostafa Govahi, Ph.D.[1], Thomas Skutella, Ph.D.[2]

1. Faculty of Biotechnology, Amol University of Special Modern Technologies, Amol, Iran
2. Institute for Anatomy and Cell Biology, Medical Faculty, University of Heidelberg, Im Neuenheimer Feld, Heidelberg, Germany

Corresponding Address: P.O.Box: 46168-49767, Faculty of Biotechnology, Amol University of Special Modern Technologies, Amol, Iran
Email: h.azizi@ausmt.ac.ir

Received: 16/December/2018, Accepted: 7/April/2019

Abstract

Objective: We aimed to examine the expression levels of the *VASA* gene and protein in testis sections of neonate and adult mice as well as testicular cell cultures.

Materials and Methods: In this experimental study, in order to investigate the expression of this germ cell marker gene in more detail, we analyzed the expression of VASA by immunocytochemistry, immunohistochemistry and fluidigm reverse transcription-polymerase chain reaction (RT-PCR).

Results: The immunohistochemical assays showed that the VASA protein was exclusively expressed in germ cells in the seminiferous tubules of the neonate and adult testis and not in somatic cells. VASA was not detectable in PLZF positive spermatogonial stem cells (SSCs), was weakly expressed in proliferating spermatogonia, and became abundant in spermatocytes and round spermatozoa. Counting VASA-positive cells in the seminiferous tubules of the neonate and adult testis depicted significant higher expression ($P<0.05$) of VASA in the adult testis in comparison to its neonate counterpart. SSC colonies were established *in vitro* after digestion of the testis and characterized by immunocytochemistry for CD90 and stage-specific embryonic antigens 3 (SSEA3). Immunocytochemistry confirmed that in contrast to the not detectable signal *in vivo*, VASA protein was strongly localized in the cytoplasm of both neonate and adult mouse SSCs under *in vitro* conditions. The results of Fluidigm RT-PCR revealed a significant higher expression of the germ cell gene VASA in adult SSCs in comparison to neonate SSCs in cell culture ($P<0.05$).

Conclusion: The VASA protein is, therefore, an extremely specific marker of testicular germ cell differentiation *in vivo* and mostly expressed in the adult testis in spermatocytes and round spermatids. The immunohistochemical signal in spermatogonia is very low. So, PLZF positive SSCs are negative for VASA *in vivo,* while in contrast, once isolated from the testicular niche VASA is also strongly expressed in SSCs under *in vitro* conditions.

Keywords: Germ Cells, Mouse, Spermatogonial Stem Cells, Testis, VASA

Cell Journal(Yakhteh), Vol 22, No 2, July-September (Summer) 2020, Pages: 171-177

Citation: Azizi H, Ranjbar M, Rahaiee S, Govahi M, Skutella T. Investigation of VASA gene and protein expression in neonate and adult testicular germ cells in mice in vivo and in vitro. Cell J. 2020; 22(2): 171-177. doi: 10.22074/cellj.2020.6619.

Introduction

In most animal species germ cells go through two complex stages of development. In the first stage, which takes place throughout early embryogenesis, primordial germ cells are generated and actively migrate to the gonadal anlage, which is supposed to comprise all of the somatic components necessary to establish the mature gonads (1, 2). During the second stage of germline development, the germ cells are provided with appropriate cues from the gonadal somatic environment and recruit one of two separate developmental programs of either oogenesis or spermatogenesis to form sex-specific gametes (1, 3). Spermatogonial stem cells (SSCs) are the unipotent adult stem cells of the testis that participate in spermatogenesis and can proliferate under certain cell culture conditions (4, 5). The amount of undifferentiated Oct4-positive SSCs in the adult mouse testis section is very low (4). In the germline epithelium, SSCs are located directly in the stem cell compartment above the basement membrane of the seminiferous tubules enclosed by Sertoli cells. Patches of Leydig cell islands, blood vessels, and macrophages are localized in the peritubular space. These kinds of somatic cells in combination with the peritubular fibrocytes and intratubular Sertoli cells secrete factors that regulate the self-renewal and differentiation of SSCs (6). In the testicular niche, extrinsic and intrinsic factors regulate the maintenance of SSCs. At least some extrinsic factors, such as glial cell-derived neurotrophic factor (GDNF) (4, 7) and KIT ligand (KITL) (8), are produced and delivered by Sertoli cells. Intrinsic factors-genes essential for regulating the mitotic phase of spermatogenesis - include transcription regulators such as the Zinc finger and the BTB domain containing 16 (ZBTB16/PLZF) (7, 9), ETS variant gene 5 (ETV/ERM) (10), Taf4b (11), Atm (12); Bcl6b (13); Pin1 (14), Pou5f1, Nrg1, Nanog and Gja1 (15) and the GDNF receptor complex Gfra1, RET (16).

The VASA gene has been firstly found to be essential for the development of female germ stem cells (GSCs) in Drosophila (17). In mice with systematic genetic deletions of the VASA gene, males exhibit a reproductive deficiency with a loss of sperm production. The male GSCs die at the zygotene step of meiosis phases, whereas the ovarian function appears to be normal (18). It has been observed that VASA is localized in PGCs in mice from embryonic day 12.5 onwards directly after entering the gonadal anlage (18-20).

In the current study, we have extended our research on the expression of VASA in the neonate and adult testis sections and testicular culture to determine if VASA has the same pattern of expression in testicular germ cells both *in vivo* and *in vitro*.

Materials and Methods

Tissue digestion and culture of testicular cells

In this experimental study, animal experiments were approved by Amol University of Special Modern Technologies Ethical Committee (Ir.ausmt.rec.1398.03.07). Testis cells from 6 day- to 12 week-old mice from the C57BL/6 strain were isolated by a one-step enzymatic digestion solution, which contained collagenase IV (0.5 mg/ml, Sigma Aldrich, USA), DNAse (0.5 mg/ml, Sigma Aldrich, USA) and Dispase (0.5 mg/ml, Sigma Aldrich, USA) in a Hank's Balanced Salt Solution (HBSS) buffer with Ca^{++} and Mg^{++} (PAA, USA) (21). The suspension of digested testis cells was plated in SSCs medium, which contained StemPro-34 medium, 1% N2-supplement (Invitrogen, USA), 6 mg/ml D+ glucose (Sigma Aldrich, USA), 5 µg/ml bovine serum albumine (Sigma Aldrich, USA), 1% L-glutamine (PAA, USA), 0,1% ß-mercaptoethanol (Invitrogen, USA), 1% penicillin/streptomycin (PAA, USA), 1% MEM vitamins (PAA, USA), 1% non-essential amino acids (PAA, USA), 30 ng/ml estradiol (Sigma Aldrich, USA), 60 ng/ml progesterone (Sigma Aldrich, USA), 20 ng/ml epidermal growth factor (EGF, Sigma Aldrich, USA), 10 ng/ml fibroblast growth factor (FGF, Sigma Aldrich, USA), 8 ng/ml GDNF (Sigma Aldrich, USA), 100 U/ml human leukemia inhibitory factor (LIF, Millipore, USA), 1% ES cell qualified FBS, 100 µg/ml ascorbic acid (Sigma Aldrich, USA), 30 µg/ml pyruvic acid (Sigma Aldrich, USA) and 1 µl/ml DL-lactic acid (Sigma Aldrich, USA) at 37˚C and 5% CO_2 (4).

Gene expression analyses on the Fluidigm Biomark system

Measurements of the expression of the gene DEAD (Asp-Glu-Ala-Asp) box polypeptide 4 (DDX4 or VASA) Mm00802445_m1 in the neonate and adult SSCs were analyzed with Dynamic Array chips (Fluidigm). A housekeeping gene glyceraldehyde-3-phosphate dehydrogenase (*GAPDH*) Mm99999915_g1 was used for normalization, in different types of cultured cells. SSCs were picked with a micromanipulator, lysed with a lysis buffer solution containing 9 µl RT-PreAmp Master Mix (5.0 µl Cells Direct 2× Reaction Mix) (Invitrogen, USA), 2.5 µl 0.2× assay pool, 0.2 µl RT/Taq Superscript III (Invitrogen, USA) and 1.3 µl TE buffer. The number of RNA-targeted transcripts was measured using TaqMan PCR assays on the BioMark Real-Time quantitative PCR (qPCR) system. Each sample was analyzed in two technical repeats. The Ct values were examined using GenEx software from MultiD for analysis (4, 5).

Immunocytochemical staining

In this experimental study, samples were fixed with 4% paraformaldehyde (PFA)/phosphate buffered saline (PBS) and permeabilized with 0.1% Triton/PBS solution. Samples were blocked with 1% bovine serum albumin (BSA)/PBS buffer and incubated overnight with the primary antibody against VASA (Abcam, USA), PLZF (Millipore, USA), CD90 (Abcam, USA) and SSEA3 (R&D, USA). This step was followed by incubation with secondary antibodies. We diluted the primary and secondary antibodies at 1: 200. The labeled cells were counterstained with 0.2 µg/ml DAPI (4', 6-diamidino-2-phenylindole) (Sigma, USA). Fluorochrome positive cells were studied with a Zeiss LSM 700 confocal microscope (Zeiss, Germany), and images were acquired with a Zeiss LSM-TPMT camera (Zeiss, Germany) (4, 22).

Tissue processing for immunohistofluorescence staining

Testis tissue samples were selected from neonate and adult male animals, washed twice in PBS buffer, and fixed in 4% PFA. The testis tissue samples were dehydrated and embedded in Paraplast Plus. The tissue samples were then cut with a microtome at a thickness of approximately 10 µm. The tissue sections were mounted on super frost plus slides and kept at room temperature. Before staining, sections were deparaffinized in xylene and rehydrated in a graded ethanol series. Following heat induced epitope retrieval (using a microwave), non-specific binding of antibodies and other detection agents were blocked with 10% serum/0.3% Triton in PBS, and ICC staining continued as described above (4).

Statistical analysis

The experiments were replicated at least three times. The average number of VASA-positive cells in groups were evaluated using the one-way analysis of variance (ANOVA), followed by Tukey's posthoc test. The expression of VASA was compared with non-parametric Mann-Whitney's test. The variation between neonate and adult groups was considered statistically reliable if a value of $P<0.05$ had been acquired. All statistical testes were performed using Statistical Package for the Social Sciences (SPSS) software.

Results

In the first step, we examined the expression of VASA in the neonate (Fig.1A1, A2) and adult testis (Fig.1B1, B2) through immunohistochemistry. Immunohistochemistry with confocal microscopy revealed that the VASA protein was expressed in the seminiferous tubules of both the neonate and adult testis but with different localizations. In the neonate testis, VASA-positive cells were located in the center of the seminiferous tubules, while in the adult testis sections, the cells were distributed through spermatogonia, spermatocytes, and spermatids with the exclusion of SSCs located in the cell layer directly connected to the base membrane of the seminiferous tubule and were also abundant in sperm. The staining of the spermatogonia, directly in contact with the basement membrane, was weak while the PLZF protein was clearly expressed in this region (Fig.1). Counting of VASA-positive cells in the seminiferous tubules of the neonate and adult testis showed that about 8% of the cells in the neonate and 57% of the cells in the adult testis were positive. Therefore, a higher number of VASA-positive cells were observed in the adult testis (Fig.2. $P<0.05$). In the next step, we evaluated the expression level of VASA in neonate and adult SSCs. Analysis of immunocytochemistry images revealed that the generated SSCs were positive for the CD90 and SSEA3 markers (Fig.3). Quantitative PCR analysis using single cells revealed that the expression of VASA mRNA in adult SSCs was significantly higher than in neonate SSCs ($P<0.05$, expression fold change of VASA mRNA analyzed on MEF feeder cells). Following immunocytochemistry, we observed no difference in the expression of VASA at the protein level in neonate and adult SSCs (Fig.4). The characterization of SSCs was conducted as designated in our former study (4).

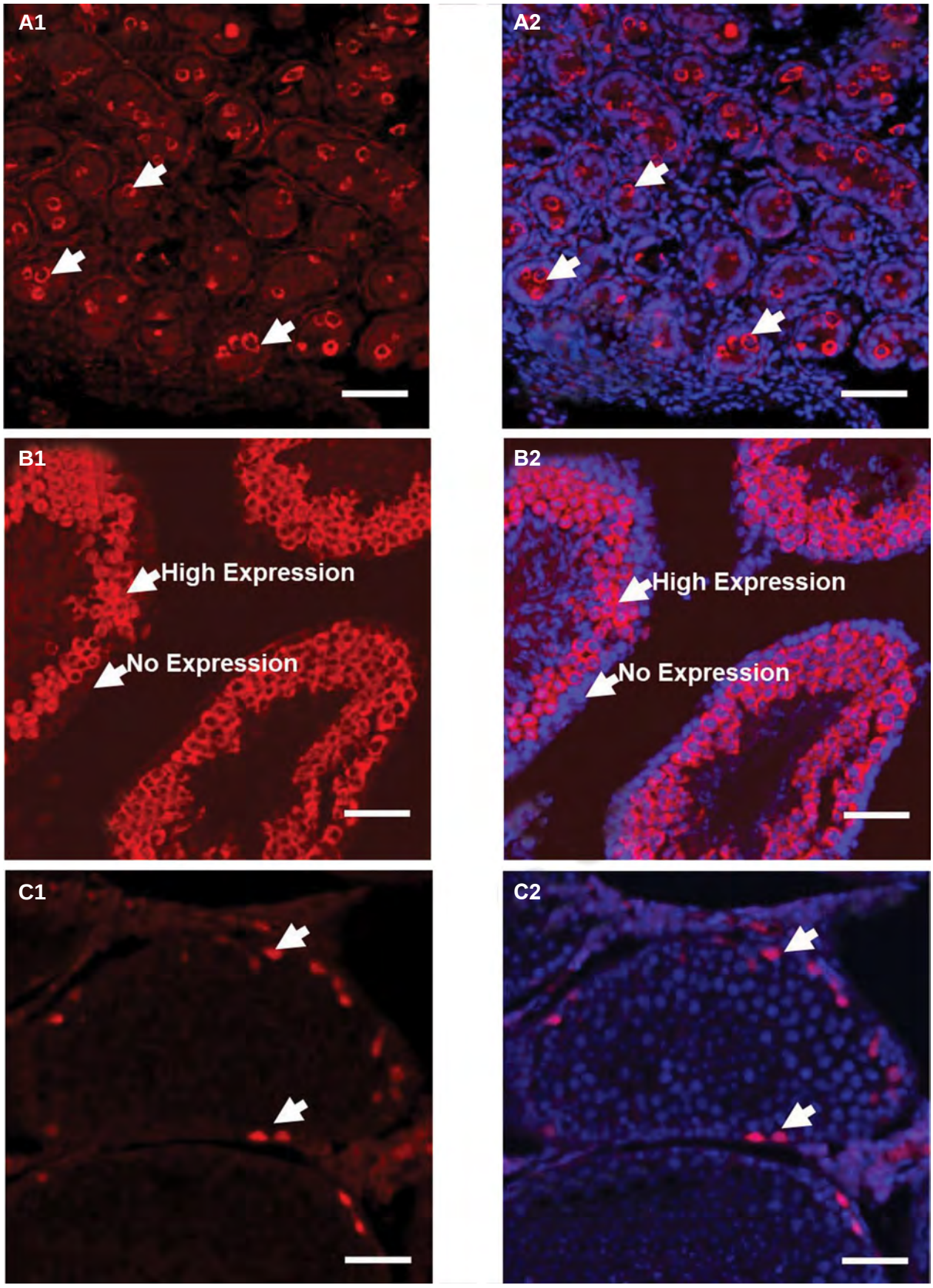

Fig.1: Immunocytochemical characterization in testis sections. **A.** Immunohistochemistry for the expression of VASA in the cross-section of the neonate testis, **A1.** Red fluorescence for VASA, **A2.** Merged image for red fluorescence for VASA and blue fluorescence for DAPI, **B.** Immunohistochemistry for the expression of VASA in the cross-section of the Adult testis, **B1.** Red fluorescence for VASA, **B2.** Merged image for red fluorescence for VASA and blue fluorescence for DAPI, **C.** PLZF protein was expressed in the base compartment of the seminiferous tubules of the testis, **C1.** Red fluorescence for PLZF, and **C2.** Merged image for red fluorescence for PLZF and blue fluorescence for DAPI. The arrows show the expression of related protein in the seminiferous tubule.

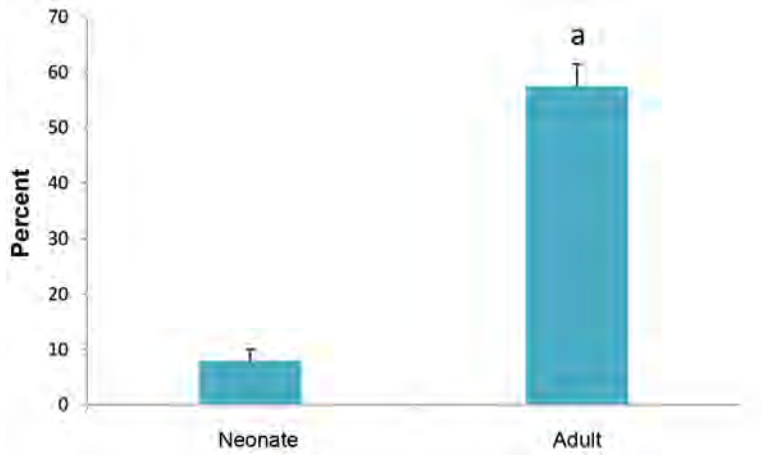

Fig.2: Number of VASA-positive cells in testis sections. Counting of VASA-positive cells in the testis section of the neonate and adult mouse. a; At least P<0.05 versus other groups.

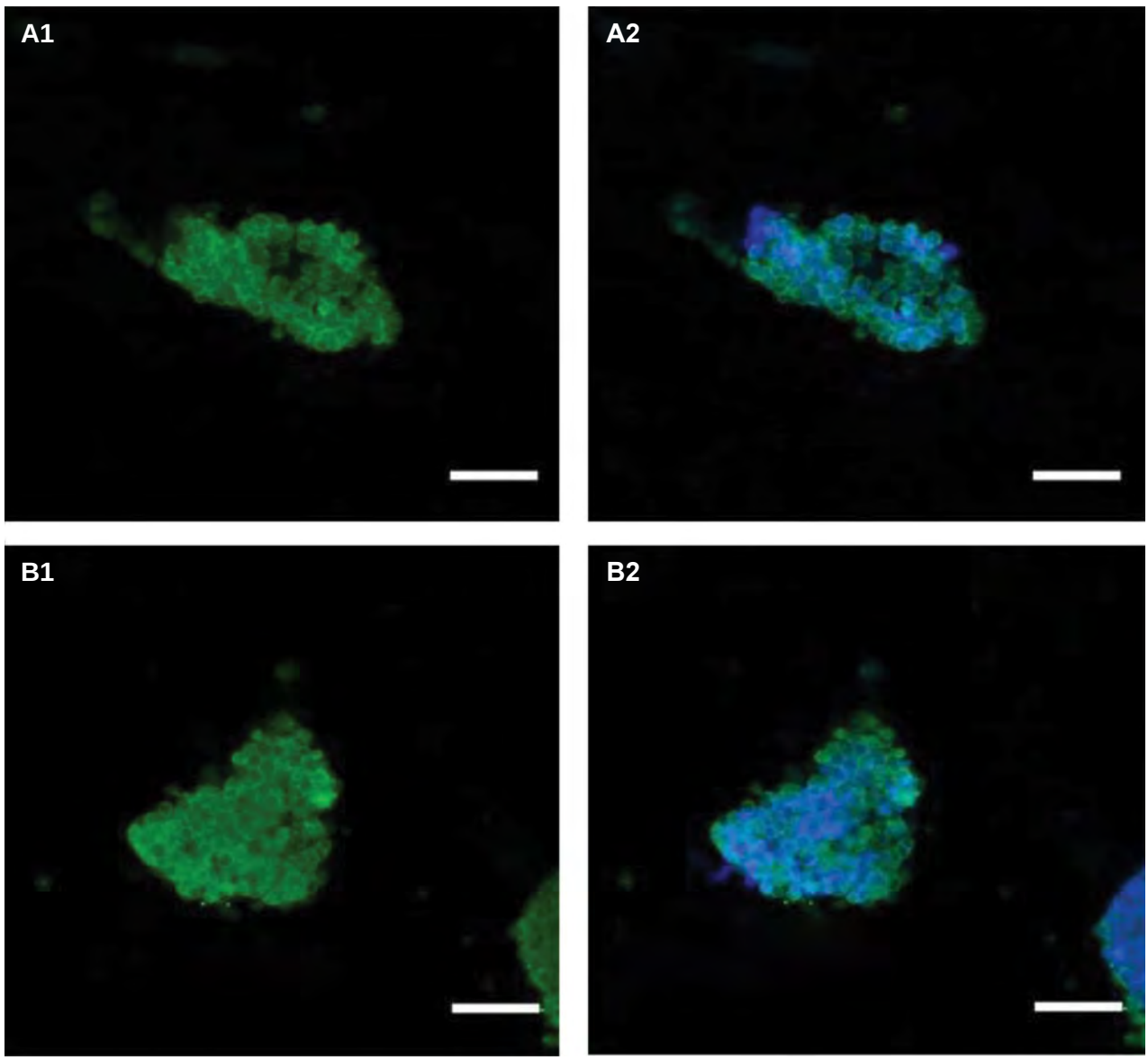

Fig.3: Characterization of spermatogonial stem cells (SSCs). **A.** Immunocytochemistry of generated SSCs with CD90 and **B.** SSEA3 antibodies. **A1.** Green fluorescence for CD90, **A2.** Merged image for green fluorescence for VASA and blue fluorescence for DAPI, **B1.** Green fluorescence for SSEA3, and **B2.** Merged image for green fluorescence for SSEA3 and blue fluorescence for DAPI.

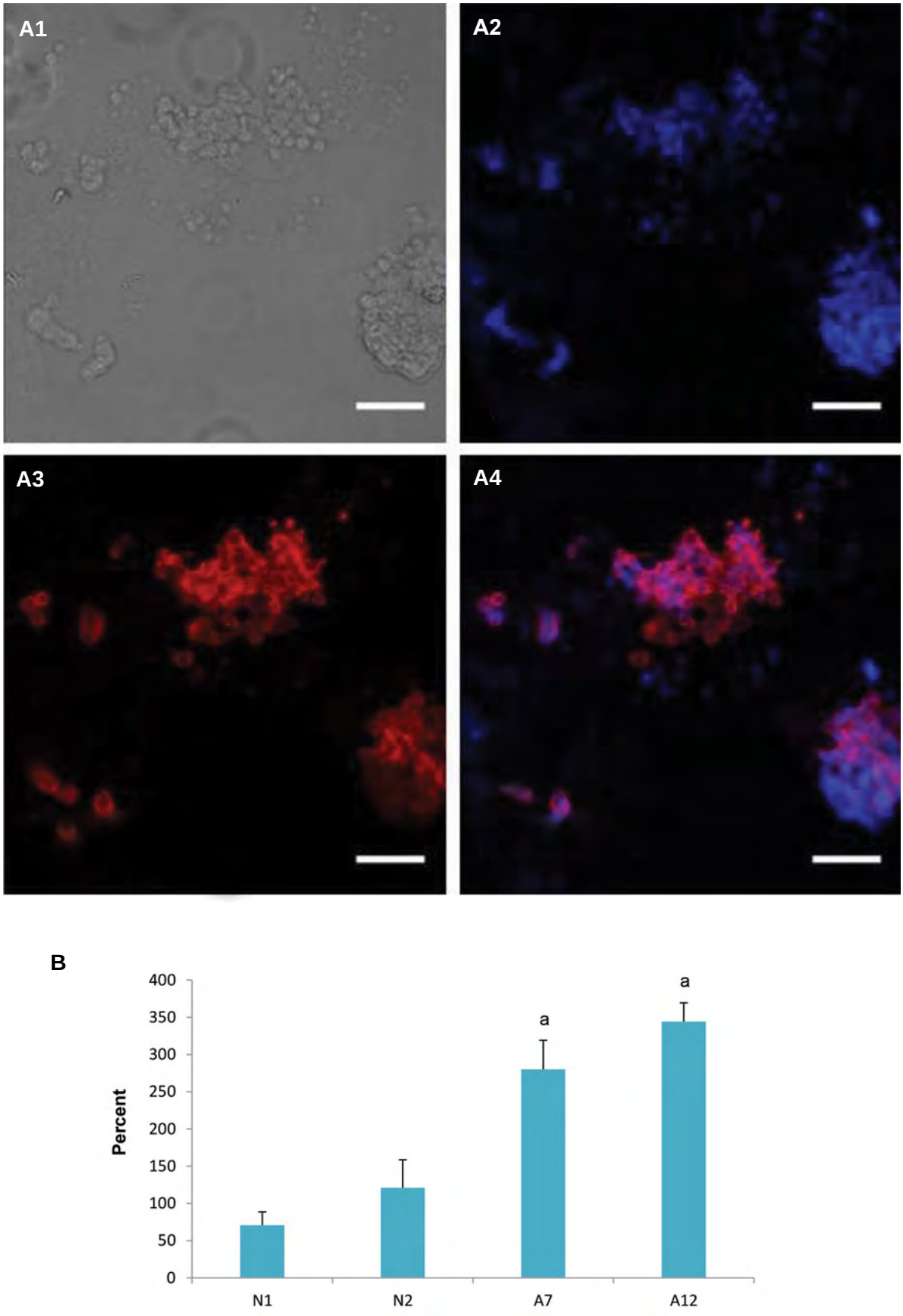

Fig.4: Immunocytochemistry and quantitative polymerase chain reaction (PCR) for spermatogonial stem cells (SSCs). **A.** Immunocytochemistry for generated SSCs using anti-VASA antibody. **A1.** Bright field photo of SSC colony, **A2.** DAPI staining which shows all cells in the plate, **A3.** VASA-positive cells, **A4.** Merge, and **B.** Quantitative PCR analysis for the expression of VASA in the neonate and adult testis. a; At least $P<0.05$ versus other groups.

Discussion

In the seminiferous tubules of the neonate mouse, the expression of VASA was specifically expressed in the center of the testicular cords. It seems that these cells were T1-prospermatogonia. During the first postnatal week, the T1-prospermatogonia relocate to the seminiferous tubules and form T2 prospermatogonia. These cells start to populate the basement membrane and initiate the spermatogenesis pathway throughout post-pubertal life (23). We observed the expression of the VASA protein in spermatocytes located above the spermatogonial cell layer in the seminiferous tubule of the adult mouse testis, and a decrease of VASA protein expression during spermiogenesis. Our study demonstrated that the expression of VASA was evident in the spermatocytes and round spermatids of the adult mouse testis, absent in SCCs and weakly expressed in spermatogonia in neonate and adult mouse testis sections. We also confirmed that the expression of VASA in the adult mouse SSCs was higher than in neonates with Fluidigm RT-PCR.

Our experiment demonstrated that SSCs generated under the stimulation of the growth factors FGF, EGF and GDNF expressed CD90 and SSEA3 (24). We observed that in contrast to the *in vivo* situation, SSCs in culture express higher amounts of VASA. This might be due to histological changes in the stem cell compartment, including feeders and the separation from Sertoli cells. In mice, the preservation and amount of male germ line stem cells *in vitro* could be diminished by somatic Sertoli feeder cells (25). Zebra fish SSCs are also differentiated into functional sperm under the effect of these feeder cells in culture (26). In contrast, some studies have reported of the suitability of Sertoli cell feeder layers for long term *in vitro* culture of SSCs (27, 28). Bovine fetal fibroblasts have been shown to promote maintenance of bovine undifferentiated spermatogonia for at least two months (29). It has also been demonstrated that amniotic epithelial cells retain SSCs, which are capable of self-renewal, in an undifferentiated, proliferative state (30).

It has been reported that bFGF is an efficient growth factor for the *in vitro* proliferation of primordial germ cells (31, 32). Furthermore, it has been shown that bFGF may be an important factor in addition to GDNF and GFR-α1 for inducing SSC replication on Sertoli cell feeders (4, 27). Also, there are recent studies on human testes that imply a critical function of bFGF in SSC proliferation (5, 33). In contrast, Kuijk et al. (34) observed that FGF can impede the successful derivation of porcine SSCs from the neonate pig testis. This is while it has been demonstrated that TGFß1, insulin-like growth factor I and FGF promoted the cell proliferation of goat SSCs (35). Additionally, the growth conditions generally used for mouse SSCs have been shown to be insufficient for the proliferation of human SSCs (36).

Our results are in line with previous studies, suggesting that VASA is a germline marker during spermatogenesis and also in proliferating spermatogonia (19, 37). We observed that VASA expression is not detectable in PLZF-positive SCCs of the mouse testis. Choi et al. (38) demonstrated that SSCs from Oct4 reporter mice cultured under feeder-free conditions expressed the SSC marker genes *Oct4* and *Vasa*, which is in accordance with our observation of VASA-positive SSCs under *in vitro* conditions. Further studies are required to analyze the possible mechanisms involved in the regulation of VASA expression during SSC self-renewal *in vivo* in comparison to *in vitro* and the influence exerted by Sertoli cells.

Conclusion

Our findings indicate that VASA is expressed in both the neonate and adult testis and also in testicular cultures, the rate of expression in the adult testis was higher than in its neonate counterpart. In the future it would be of interest to understand why VASA is not expressed in the PLZF-positive SSCs of the adult mouse testis whereas it is highly expressed in SSCs *in vitro*.

Acknowledgements

This research was financially supported by International Scientific Meeting Office, Ministry of Science, Research and Technology of Islamic Republic of Iran, and the University of Heidelberg, Institute for Anatomy and Cell Biology III, Department of Neuroanatomy, Germany. The authors declare no conflicts of interest in this study.

Authors' Contributions

H.A., T.S.; Participated in study design, data collection and evaluation, drafting and statistical analysis. M.R., S.R., M.G.; Contributed extensively in interpretation of the data and the conclusion. All authors read and approved the final manuscript.

Reference

1. Nikolic A, Volarevic V, Armstrong L, Lako M, Stojkovic M. Primordial Germ cells: current knowledge and perspectives. Stem Cells Int. 2016; 2016: 1741072.
2. Liang S, Liu D, Li X, Wei M, Yu X, Li Q, et al. SOX2 participates in spermatogenesis of Zhikong scallop Chlamys farreri. Sci Rep. 2019; 9(1): 76.
3. Gao JJ, Pan XR, Hu J, Ma L, Wu JM, Shao YL, et al. Pattern of mutation rates in the germline of Drosophila melanogaster males from a large-scale mutation screening experiment. G3 (Bethesda). 2014; 4(8): 1503-1514.
4. Azizi H, Conrad S, Hinz U, Asgari B, Nanus D, Peterziel H, et al. Derivation of pluripotent cells from mouse SSCs seems to be age dependent. Stem Cells Int. 2016; 2016: 8216312.
5. Conrad S, Azizi H, Hatami M, Kubista M, Bonin M, Hennenlotter J, et al. Expression of genes related to germ cell lineage and pluripotency in single cells and colonies of human adult germ stem cells. Stem Cells Int. 2016; 2016: 8582526.
6. Rossi P, Dolci S. Paracrine mechanisms involved in the control of early stages of Mammalian spermatogenesis. Front Endocrinol (Lausanne). 2013; 4: 181.
7. Conrad S, Azizi H, Skutella T. Single-cell expression profiling and proteomics of primordial germ cells, spermatogonial stem cells, adult germ stem cells, and oocytes. Adv Exp Med Biol. 2018; 1083: 77-87.
8. Naughton CK, Jain S, Strickland AM, Gupta A, Milbrandt J. Glial cell-line derived neurotrophic factor-mediated RET signaling regulates spermatogonial stem cell fate. Biol Reprod. 2006; 74(2): 314-321.
9. Buaas FW, Kirsh AL, Sharma M, McLean DJ, Morris JL, Griswold

MD, et al. Plzf is required in adult male germ cells for stem cell self-renewal. Nat Genet. 2004; 36(6): 647-652.
10. Chen C, Ouyang W, Grigura V, Zhou Q, Carnes K, Lim H, et al. ERM is required for transcriptional control of the spermatogonial stem cell niche. Nature. 2005; 436(7053): 1030-1034.
11. Falender AE, Shimada M, Lo YK, Richards JS. TAF4b, a TBP associated factor, is required for oocyte development and function. Dev Biol. 2005; 288(2): 405-419.
12. Takubo K, Ohmura M, Azuma M, Nagamatsu G, Yamada W, Arai F, et al. Stem cell defects in ATM-deficient undifferentiated spermatogonia through DNA damage-induced cell-cycle arrest. Cell Stem Cell. 2008; 2(2): 170-182.
13. Oatley JM, Avarbock MR, Telaranta AI, Fearon DT, Brinster RL. Identifying genes important for spermatogonial stem cell self-renewal and survival. Proc Natl Acad Sci USA. 2006; 103(25): 9524-9529.
14. Lolicato F, Marino R, Paronetto MP, Pellegrini M, Dolci S, Geremia R, et al. Potential role of Nanos3 in maintaining the undifferentiated spermatogonia population. Dev Biol. 2008; 313(2): 725-738.
15. Hamra FK, Chapman KM, Nguyen D, Garbers DL. Identification of neuregulin as a factor required for formation of aligned spermatogonia. J Biol Chem. 2007; 282(1): 721-730.
16. Jijiwa M, Kawai K, Fukihara J, Nakamura A, Hasegawa M, Suzuki C, et al. GDNF-mediated signaling via RET tyrosine 1062 is essential for maintenance of spermatogonial stem cells. Genes Cells. 2008; 13(4): 365-374.
17. Lasko PF, Ashburner M. The product of the Drosophila gene vasa is very similar to eukaryotic initiation factor-4A. Nature. 1988; 335(6191): 611-617.
18. Tanaka SS, Toyooka Y, Akasu R, Katoh-Fukui Y, Nakahara Y, Suzuki R, et al. The mouse homolog of Drosophila Vasa is required for the development of male germ cells. Genes Dev. 2000; 14(7): 841-853.
19. Toyooka Y, Tsunekawa N, Takahashi Y, Matsui Y, Satoh M, Noce T. Expression and intracellular localization of mouse Vasa-homologue protein during germ cell development. Mech Dev. 2000; 93(1-2): 139-149.
20. Fujiwara Y, Komiya T, Kawabata H, Sato M, Fujimoto H, Furusawa M, et al. Isolation of a DEAD-family protein gene that encodes a murine homolog of Drosophila vasa and its specific expression in germ cell lineage. Proc Natl Acad Sci USA. 1994; 91(25): 12258-12262.
21. Azizi H, Skutella T, Shahverdi A. Generation of Mouse spermatogonial stem-cell-colonies in A non-adherent culture. Cell J. 2017; 19(2): 238-249.
22. Bojnordi MN, Azizi H, Skutella T, Movahedin M, Pourabdolhossein F, Shojaei A, et al. Differentiation of spermatogonia stem cells into functional mature neurons characterized with differential gene expression. Mol Neurobiol. 2017; 54(7): 5676-5682.
23. Kluin PM, de Rooij DG. A comparison between the morphology and cell kinetics of gonocytes and adult type undifferentiated spermatogonia in the mouse. Int J Androl. 1981; 4(4): 475-493.
24. Wang JL, Yang S, Tian RH, Zhu ZJ, Guo Y, Yuan QQ, et al. Isolation, culture, and identification of human spermatogonial stem cells. Zhonghua Nan Ke Xue. 2015; 21(3): 208-213.
25. Nagano M, Ryu BY, Brinster CJ, Avarbock MR, Brinster RL. Maintenance of mouse male germ line stem cells in vitro. Biol Reprod. 2003; 68(6): 2207-2214.
26. Kawasaki T, Siegfried KR, Sakai N. Differentiation of zebrafish spermatogonial stem cells to functional sperm in culture. Development. 2016; 143(4): 566-574.
27. Baazm M, Abolhassani F, Abbasi M, Habibi Roudkenar M, Amidi F, Beyer C. An improved protocol for isolation and culturing of mouse spermatogonial stem cells. Cell Reprogram. 2013; 15(4): 329-336.
28. Baazm M, Mashayekhi FJ, Babaie S, Bayat P, Beyer C, Zendedel A. Effects of different Sertoli cell types on the maintenance of adult spermatogonial stem cells in vitro. In Vitro Cell Dev Biol Anim. 2017; 53(8): 752-758.
29. Oatley MJ, Kaucher AV, Yang QE, Waqas MS, Oatley JM. Conditions for long-term culture of cattle undifferentiated spermatogonia. Biol Reprod. 2016; 95(1): 14.
30. Liu T, Guo L, Liu Z, Cheng W. Human amniotic epithelial cells maintain mouse spermatogonial stem cells in an undifferentiated state due to high leukemia inhibitor factor (LIF) expression. In Vitro Cell Dev Biol Anim. 2011; 47(4): 318-326.
31. Matsui Y, Zsebo K, Hogan BL. Derivation of pluripotential embryonic stem cells from murine primordial germ cells in culture. Cell. 1992; 70(5): 841-847.
32. Resnick JL, Bixler LS, Cheng L, Donovan PJ. Long-term proliferation of mouse primordial germ cells in culture. Nature. 1992; 359(6395): 550-551.
33. Koruji M, Shahverdi A, Janan A, Piryaei A, Lakpour MR, Gilani Sedighi MA. Proliferation of small number of human spermatogonial stem cells obtained from azoospermic patients. J Assist Reprod Genet. 2012; 29(9): 957-967.
34. Kuijk EW, Colenbrander B, Roelen BA. The effects of growth factors on in vitro-cultured porcine testicular cells. Reproduction. 2009; 138(4): 721-731.
35. Bahadorani M, Hosseini SM, Abedi P, Abbasi H, Nasr-Esfahani MH. Glial cell line-derived neurotrophic factor in combination with insulin-like growth factor 1 and basic fibroblast growth factor promote in vitro culture of goat spermatogonial stem cells. Growth Factors. 2015; 33(3): 181-191.
36. Medrano JV, Rombaut C, Simon C, Pellicer A, Goossens E. Human spermatogonial stem cells display limited proliferation in vitro under mouse spermatogonial stem cell culture conditions. Fertil Steril. 2016; 106(6): 1539-1549. e8.
37. Noce T, Okamoto-Ito S, Tsunekawa N. Vasa homolog genes in mammalian germ cell development. Cell Struct Funct. 2001; 26(3): 131-136.
38. Choi NY, Park YS, Ryu JS, Lee HJ, Arauzo-Bravo MJ, Ko K, et al. A novel feeder-free culture system for expansion of mouse spermatogonial stem cells. Mol Cells. 2014; 37(6): 473-479.

Original Article

A Comparative Study of *HOTAIR* Expression in Breast Cancer Patient Tissues and Cell Lines

Asghar Arshi, M.Sc.[1], Farzaneh Raeisi, M.Sc.[2, 3], Esmaeil Mahmoudi, M.Sc.[2], Fatemeh Mohajerani, M.Sc.[4], Hamidreza Kabiri, M.Sc.[2], Razieh Fazel, M.Sc.[5], Maedeh Zabihian-Langeroudi, M.Sc.[6], Amela Jusic, Ph.D.[7]*

1. Young Researchers and Elite Club, Najafabad Branch, Islamic Azad University, Najafabad, Iran
2. Young Researchers and Elite Club, Shahrekord Branch, Islamic Azad University, Shahrekord, Iran
3. Department of Medical Physics, School of Medicine, Isfahan University of Medical Sciences, Isfahan, Iran
4. Department of Genetics, Faculty of Modern Medical Science, Islamic Azad University of Medical Sciences of Tehran, Tehran, Iran
5. Student Research Committee, Jahrom University of Medical Sciences, Jahrom, Iran
6. Department of Biology, Tonekabon Branch, Islamic Azad University, Tonekabon, Iran
7. Department of Biology, Faculty of Natural Sciences and Mathematics, University of Tuzla, Tuzla, Bosnia and Herzegovina

Corresponding Address: Department of Biology, Faculty of Natural Sciences and Mathematics, University of Tuzla, Tuzla, Bosnia and Herzegovina
Email: amela.jusic@untz.ba

Received: 21/January/2019, Accepted: 25/February/2019

Abstract

Objective: Recent data suggest that increased levels of the *HOTAIR* long non-coding RNA (lncRNA) are involved in the development of various types of malignancy, including breast cancer. The aim of present study was to investigate *HOTAIR* lncRNA expression profile in breast cancer (BC) patients and cell lines.

Materials and Methods: In this experimental study, expression level of *HOTAIR* lncRNA was evaluated in BC and normal tissues of 15 patients as well as MDA-MB-231, MCF-7 and MCF-10A cell lines, using quantitative reverse-transcription polymerase chain reaction (qRT-PCR). *HOTAIR* lncRNA expression levels were estimated using $2^{-\Delta\Delta Ct}$ method. Further, receiver operating characteristic (ROC) curve analysis was done to evaluate the selected lncRNA diagnostic potential. The Cox's proportional hazards regression model was performed to evaluate the predictive value of this lncRNA level in BC patients.

Results: The results of present study demonstrated no significant difference in the expression of *HOTAIR* lncRNA in MCF7 and MDA-MB-231 cancer cell lines compared to MCF-10A as normal cell line ($P>0.05$). However, we observed a significantly increase in the expression of *HOTAIR* in BC patients compared to normal tissues ($P<0.001$). Significant associations were found between gene expression and tumour size and margin. We found 91.1% sensitivity and 95.7% specificity of circulating *HOTAIR* with an area under the ROC curve of 0.969. The Kaplan-Meier analysis indicated significant correlation between *HOTAIR* expression and overall survival.

Conclusion: This study demonstrated that expression of *HOTAIR* is increased in BC and might be associated with its progression. According to these findings, *HOTAIR* expression could be proposed as biomarkers for BC early diagnosis and prognosis.

Keywords: Breast Cancer, Cell Line, *HOTAIR* lncRNA, Quantitative Reverse-Transcription Polymerase Chain Reaction

Cell Journal(Yakhteh), Vol 22, No 2, July-September (Summer) 2020, Pages: 178-184

Citation: Arshi A, Raeisi F, Mahmoudi E, Mohajerani F, Kabiri H, Fazel R, Zabihian-Langeroudi M, Jusic A. A comparative study of HOTAIR expression in breast cancer patient tissues and cell lines. Cell J. 2020; 22(2): 178-184. doi: 10.22074/cellj.2020.6543.

Introduction

Long non-coding RNAs (lncRNAs) are a diverse and large class of non-coding RNA molecules with more than 200 nucleotides length which are mostly transcribed by RNA polymerase II (RNA pol II) (1). lncRNAs play essential role in regulation of different cellular processes. Recently, lncRNAs are reported as key regulators of gene expression and they can act as oncogenes or tumour suppressor genes. According to their oncogenic potential they may play a critical role in oncogenesis, migration, cell differentiation, angiogenesis, apoptosis and proliferation (2). Furthermore, lncRNAs associate with different cancers and malignant behaviour of cancer cells (3). One of the first described lncRNAs is the Hox (homeobox) transcript antisense intergenic lncRNA (*HOTAIR* lncRNA) and they play important role in development of breast cancer (BC) (4). Current studies suggest that *HOTAIR* lncRNA reprograms chromatin state which can promote cancer metastasis (5). *HOTAIR* coordinates in chromatin modification and through which it affects expression of multiple genes involved in various cellular functions (6). Recent studies indicated an association between circadian rhythm (CR) disruption and increased risk of BC development (7). Interestingly, CR disruption has been associated with decreased telomere length, where short telomere length, itself, is correlated with BC development (8).

HOTAIR expression levels are significantly high in breast tumours, and its measurement is a determinative indicator of primary breast tumours, possibility of metastasis and patient survival (9). The most commonly used cell line in BC research is MDA-MB-231 which provides essential tools for complex biological expression

analysis (10). This cell line is originated from a pleural effusion with a metastatic mammary adenocarcinoma and it is a highly aggressive, used as a model of triple negative BC (TNBC) (11, 12). In the present study, we measured *HOTAIR* lncRNA expression level in BC and normal epithelial tissues, in addition to MCF7 and MDA-MB-231 BC cell lines.

Materials and Methods

Breast cancer and normal tissue sample collections

In this experimental study, BC and normal breast tissues from 15 patients (morphologically confirmed by a pathologist) were collected consecutively between July and November 2015 at Shiraz General Hospital (Shiraz, Iran). These 15 patients were included in the present study, according to the inclusion and exclusion criteria. The inclusion criteria were as follows: i. All patients hospitalized during 2015, those with diagnosis or procedure codes related to breast cancer, and ii. Adult patients (19 years of age or older) with cancer of the breast. The exclusion criteria include: i. History of any other malignancy, ii. History of previous relevant treatment, including chemotherapy, radiotherapy or endocrinotherapy, and iii. People with 18 years of age or younger. In this research, ethical considerations were approved based on the International Campus of Shahrekord University of Medical Sciences, Shahrekord, Iran.

Culture of the cell lines

MDA-MB-231 (ATCC® HTB-26™), MCF-7 (ATCC® HTB22™) and MCF-10A (ATCC® CRL-10317™) cell lines were cultured and maintained in RPMI-1640 medium (Sigma-Aldrich, USA) supplemented with L-Glutamine (Sigma-Aldrich, USA), 10% fetal bovine serum (FBS, Gibco, USA), 100 U/ml penicillin (Sigma-Aldrich, USA) and 100 µg/ml streptomycin (Sigma-Aldrich, USA) in the cell culture incubator at 37˚C, 5% CO_2 and 95% humidity.

RNA extraction and cDNA synthesis

Total RNA was extracted from the tissue samples and cell lines, using the RNX™-Plus solution (SinaClon, Iran) according to the manufacturer's instructions except the additional step of extended treatment with DNaseI for one hour. Purity, concentration and quality of the extracted RNAs were analysed by Thermo Scientific NanoDrop™ 1000 Spectrophotometer (USA) and electrophoresis on 2% agarose gel. For complementary DNA (cDNA) synthesis, 1 µg RNA was added to PrimeScript™-RT reagent kit (TaKaRa, Japan) containing random hexamer priming mix. Concentration of the synthesized cDNA was measured by spectrophotometry.

Quantitative reverse transcription polymerase chain reaction

HOTAIR expression level in BC and normal breast epithelial tissues as well as MDA-MB-231, MCF7 and MCF-10A cell lines was evaluated by quantitative reverse transcription PCR (qRT-PCR) method, using a rotor gene 6000 Corbett detection system (Qiagen, Germany) and SYBR®Premix Ex Taq™ II kit (TaKaRa, Japan), according to the manufacturer's instructions. Thermal cycling amplification was set up according to next protocol: initial activation at 95˚C for 5 minutes followed by 40 cycles at 95˚C for 15 seconds and 65˚C for 1 minute. As control sample nuclease free water was used without adding any template. Melting curve analysis was performed to verify specificity of PCR products. The size and specificity of PCR products were verified by electrophoresis on 2% agarose gel. For qRT-PCR analysis, all samples were normalized to Pumilio RNA Binding Family Member 1 gene (*PUM1*). The qRT-PCR assays were performed in triplicate and the data were presented as the mean ± standard error of mean (SEM). The mean value in each triplicate was used to calculate the relative lncRNA level (ΔCt=Ct mean lncRNAs-Ct mean *PUM1*). Expression fold changes were calculated using $2^{-\Delta\Delta Ct}$ methods.

Statistical analysis

The relationship between expression of *HOTAIR* and clinical pathological parameters was determined using the chi-square test and Fisher's exact test. Receiver operating characteristic (ROC) curves were used to assess diagnostic value of the marker. Area under the curve (AUC) was computed for ROC curve. Overall survivals (OS) were presented by the Kaplan-Meier curves, and the log-rank test was used to determine significance between gene expression levels and patient outcome. Data are shown as the means ± SEM and case (%) or number (%). A P value of 5% (*; $P<0.05$) was considered significant. Statistical analyses were performed by the Graph Pad Prism version 7.00 (Graph Pad Software, USA).

Results

Table 1 summarizes the available patients' demographic and clinical data. All tissue samples at the time of resection were transferred into RNA-later solution (Sigma-Aldrich, USA) and stored at -20˚C for the further RNA extraction. Applicable international, national and institutional guidelines for the care of human were followed. Figure 1A shows relative expression of *HOTAIR* in MDA-MB-231 and MCF-7 cancer cell lines compared to MCF-10A control cell line. There is no significant difference of *HOTAIR* expression in both of MCF-7 and MDA-MB-231 cancer cell lines compared to normal cell line MCF-10A ($P>0.05$). The expression level of *HOTAIR* was significantly increased in BC tissue of patients compared to normal tissues ($P<0.001$, Fig.1B). Correlation between *HOTAIR* expression and the clinical pathological variables of BC cases are shown in Table 2. Significant associations were found between gene expression and tumour size and margin.

Table 1: Characteristics of the cancer specimens used in this study

Variables	Frequency	Valid percent	Cumulative percent
Age (Y)			
≤47	15	65.2	65.2
>47	8	34.8	100
Histologic grade			
Well differentiated	1	6.7	6.7
Moderate differentiated	10	66.7	73.3
Poor differentiated	4	26.7	100
Tumour side			
Left	7	46.7	46.7
Right	8	53.3	100
Prevascular invasion			
Negative	4	26.7	26.7
Positive	10	66.7	93.3
Other	1	6.7	100
Preneural invasion			
Negative	3	20	20
Positive	12	80	100
Lymph-node involvement status			
Free	6	40	40
Involved	9	60	100
Total	15	100	
Staging (TNM, Clinical)			
I	8	53.3	53.3
II	7	46.7	100
Total	15	100	

TNM; Tumour, nodes and metastases.

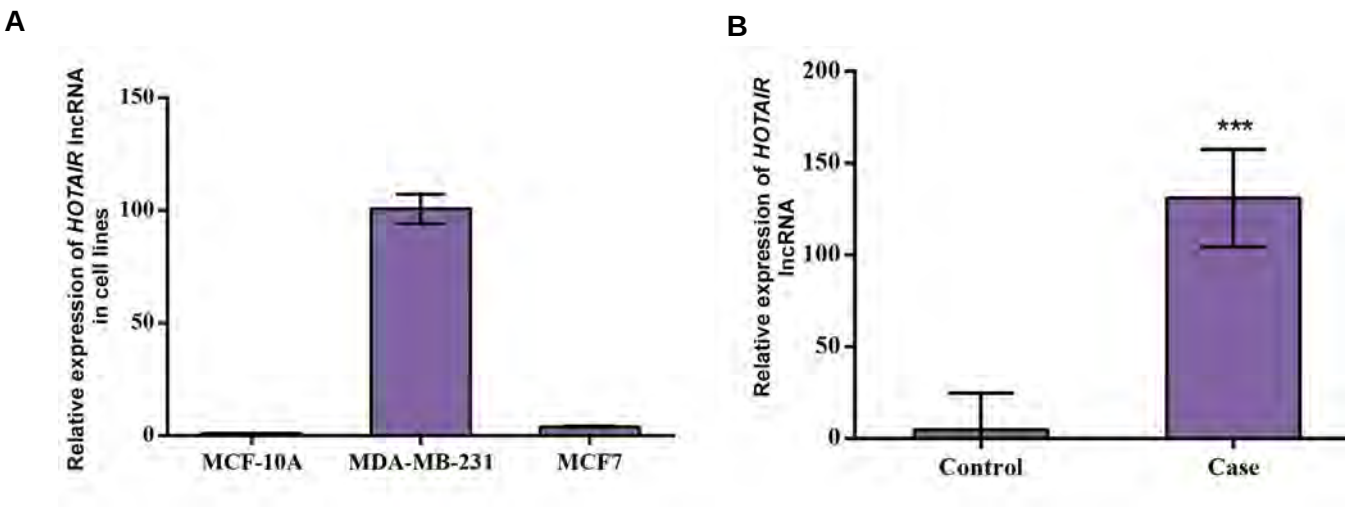

Fig.1: Relative expression of *HOTAIR* in breast cancer cell lines, case and control samples. **A.** MDA-MB-231 and MCF-7 cancer cell lines compared to that in MCF-10A control cells. There is no significant difference in the expression of *HOTAIR* in both of MCF-7 and MDA-MB-231 cancer cell lines compared to normal cell line MCF-10A (P>0.05) and **B.** Breast cancer compared to normal breast tissues. There is a significant increase in the expression level of *HOTAIR* in patients with breast cancer compared to the controls (P<0.001). ***; Significant at the 0.0001 level.

Table 2: Correlation of *HOTAIR* expression level and clinical pathological variables in the breast cancer cases

Variables	Cases (%)	*HOTAIR* lncRNA		P value
		Low	High	
Age (Y), 46.80 ± 2.57 (32-65) (mean ± SE)				0.782
≤47	53.3	26.7	26.7	
>47	46.7	26.7	20	
Tumour grade				0.626
I	6.7	6.7	0	
II	66.7	33.3	33.3	
III	26.7	13.3	13.3	
Nuclear grade				0.394
Low	7.1	7.1	0	
High and intermediate	28.6	21.4	7.1	
High	64.3	28.6	35.7	
Tumour stage				0.232
T1	40	26.7	33.33	
T2	13.3	0	13.3	
T3	40	26.7	13.33	
T4	6.7	0	6.7	
Tumour size (cm)				**0.029**
<2	73.3	26.7	46.7	
≥2	26.7	26.7	0	
Area of invasive component, 4.09 ± 0.13 (0.7-9.5 cm^2) (mean ± SE)				0.464
<4	66.7	40	26.7	
≥4	33.3	13.3	20	
Tumour side				0.447
Right	53.3	33.3	20	
Left	46.7	20	26.7	
Margin				**0.029**
Free	73.3	26.7	46.7	
Involved	26.7	26.7	0	
Prevascular Invasion				0.512
Negative	26.7	13.3	13.3	
Positive	73.3	40	33.3	
Preneural Invasion				0.506
Negative	20	13.3	6.7	
Positive	80	40	40	

Bold values indicate P<0.05.

Diagnostic value of *HOTAIR* in breast cancer

The ROC curve was created and the AUC was computed to determine capability of the *HOTAIR* expression and difference between cancer and control tissues by calculating sensitivity and specificity for possible cut-off point of *HOTAIR*. The ROC analysis distinguished the optimal cut-off value for *HOTAIR*. We found 91.1% sensitivity and 95.7% specificity for circulating *HOTAIR* with an area under the ROC curve of 0.969 (Fig.2A).

Correlation of *HOTAIR* expression with patient survival

In order to assess prognostic value of *HOTAIR* as a BC biomarker, we investigated association of the *HOTAIR* expression levels with survival through Kaplan-Meier analysis. We used the log-rank test in BC patients. The Cox proportional hazards regression model was also used to evaluate predictive value of *HOTAIR* in BC patients. OS was defined as the time between date of surgery and date of death or last follow-up. Clinical pathological factors and OS were then analysed in the high and low level of *HOTAIR* expression groups. Results indicated that low levels of *HOTAIR* have shorter survival time (P>0.048, Table 3, Fig.2B).

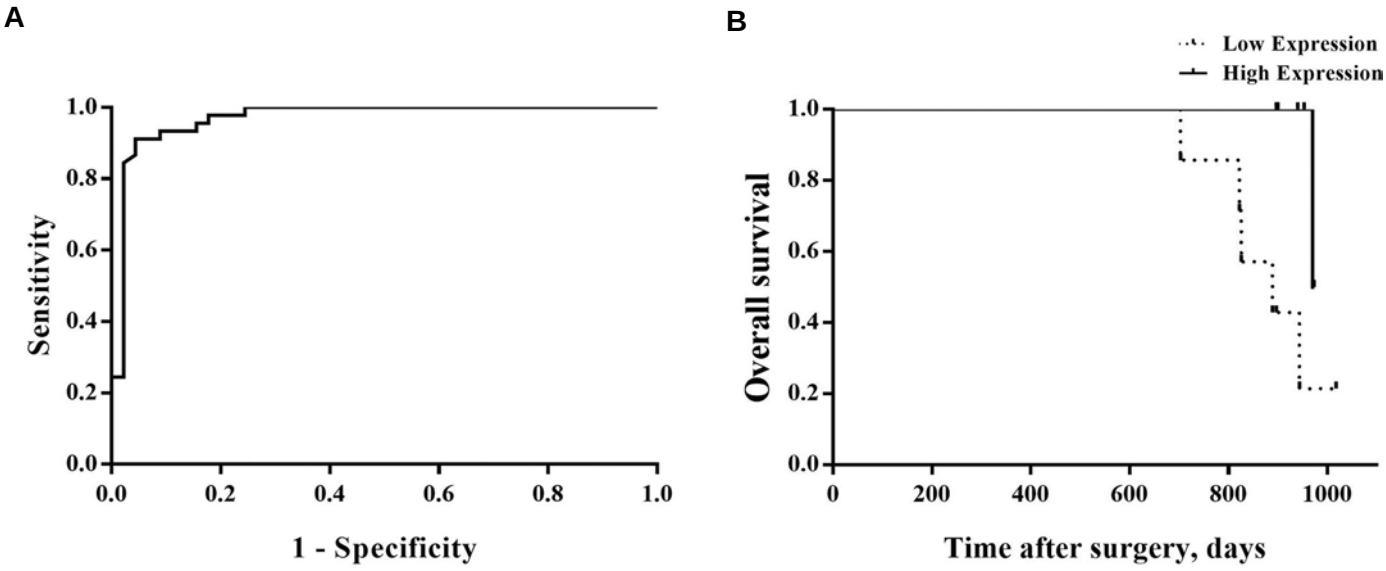

Fig.2: Receiver operating characteristic (ROC) and Kaplan-Meier curves for *HOTAIR* expression. **A.** ROC curve analysis to determine cut-off point for high expression of *HOTAIR*. The area under curve (AUC) was 0.969 (95% CI, 0.933 - 1.005) and **B.** Kaplan-Meier curve for BC patients in high-expression (46.7%) and low-expression (53.3%) groups segregated by the cut-off point. BC patients with a low expression level of *HOTAIR* had a poor prognosis (log-rank test, P=0.048).

Table 3: Log rank test for all patients with breast cancer

Variables	Overall survival		P value
	HR	95% CI	
HOTAIR (low vs. high)	6.423	1.128-32.22	**0.048**
Age (Y), (<47 vs. ≥47)	1.749	0.3501-8.657	0.506
Tumour grade (I-II vs. III)	0.560	0.07296-3.501	0.493
Nuclear grade (Low vs. high and intermediate-high)	1.977	0.1596-40.67	0.517
Tumour stage (T1-T2 vs. T3-T4)	0.5745	0.1041-2.891	0.800
Tumour size (<2 cm vs. ≥2 cm)	0.460	0.04656-2.841	0.347
Area of invasive component (<4 cm^2 vs. ≥4 cm^2)	0.576	0.07625-3.827	0.378
Tumour side (right vs. left)	0.585	0.1185-2.937	0.525
Margin (free vs. involved)	0.507	0.05886-3.166	0.416
Prevascular invasion (negative vs. positive)	1.605	0.3264-8.170	0.566
Preneural invasion (negative vs. positive)	0.336	0.01890-1.809	0.166

HR; Hazard ratio. Bold values indicate P<0.05.

Discussion

A number of different genetic and environmental factors that can increase the likelihood of BC have been identified. Accumulated data suggests that lncRNAs play crucial roles in RNA processing, genomic reprogramming, apoptosis, cell proliferation, cell cycle and chromatin modification (13). *HOTAIR* is recognised as a risk factor of various types of tumourigenesis including BC (14). Overexpression of *HOTAIR* may influence tumour formation and induce invasion, migration and proliferation of BC. According to that, altered expression of *HOTAIR* may induce cell proliferation of BC. In this study we evaluated expression level of *HOTAIR* in BC patients and cell lines. Our result showed that *HOTAIR* was up-regulated in BC tissues, while it was not increased in MCF-7 and MDA-MB-231 cell lines.

Regarding the lncRNA functions, BC is one of the most studied malignancies. In has been demonstrated that *HOTAIR* might have a vital role in this regulation due to the interaction with a wide spectrum of miRNAs (15, 16). Recent studies indicated a significant association of *HOTAIR* overexpression with tumour size, advances and extensive metastasis in BC (16-19). *HOTAIR* might act as a gene expression regulator in the BC related to mutations of *BRCA1*. *HOTAIR* promoter contains several estrogen receptors (ERs), and it has been shown that estradiol regulated *HOTAIR* expression in ER positive BC cells. However, this regulation was abolished in BC cells with inactive ERs, indicating the critical role of these receptors in estradiol-mediated control of *HOTAIR* expression (20). *HOTAIR* and some other lncRNA expression analyses in 164 ER-positive primary BC cases demonstrated that these lncRNAs could be independent prognostic markers (21). Gökmen-Polar et al. (22) indicated that the utility of *HOTAIR* as a prognostic marker in BC is limited to ER-negative cases. Therefore, significant up-regulation of *HOTAIR* obtained from BC tumour samples compared to BC cell lines, in this study, may explain the molecular mechanism causing poor prognosis of this cancer. We found that level of *HOTAIR* expression was not associated with clinical characteristics of BC, while enhanced expression level of *HOTAIR* might associate with tumour size, margins and lower disease relapse. In a research, Lu et al. studied *HOTAIR* expression and methylation of its downstream intergenic CpG islands in 348 samples of primary BC (23). Their results indicated that increased methylation could associate with a worse prognosis in the patient.

According to the results of present study, patients with low level of *HOTAIR* showed shorter survival time. Bhan et al. (20) demonstrated that *HOTAIR* is critical for survival and proliferation of MCF-7 BC cells. Pádua Alves et al. (24) showed that *HOTAIR* in a BC cell line was a critical regulator of genes involved in epithelial to mesenchymal transition. Up-regulation of *HOTAIR* has been described as a useful predictor of survival and progression in several cancer types including pancreatic cancer (25), hepatocellular carcinoma (26) oesophageal cancer (27), gastrointestinal stromal (28), nasopharyngeal carcinoma (29) and colorectal cancer (30).

One major obstruction of this study was limited number of BC and control samples enrolled from the same hospital which might not fully substantiate accuracy of the results.

Conclusion

Taking into consideration that the major problem in early diagnostic and treatment of different types of cancer, including BC, is lack of highly sensitive and specific tumour biomarkers, altered expression levels of *HOTAIR* lncRNA can be a guide for investigation of cancer biomarkers. Thus, our results indicated that *HOTAIR* expression profiling and elucidating its function may be proposed as a useful biomarker for BC diagnosis as well as a therapeutic target in cancer gene therapy. However, further investigations and follow up studies on larger patient samples are required.

Acknowledgements

The authors are grateful to the collaboration and valuable help of Cellular and Molecular Research Centre staff, Shahrekord University of Medial Sciences (Shahrekord, Iran). This research did not receive any specific grant from funding agencies in the public, commercial or not-for-profit sectors. The authors declare they have no conflict of interest.

Authors' Contributions

A.A., F.R., E.M.; Participated in design and evaluation experiments. F.M., H.K.; Responsible for Software, validation and formal analysis. R.F., M.Z.-L.; Responsible for investigation, resources and molecular experiments. A.J., A.A.; Writing-original draft preparation, writing-review and editing and supervision. All the authors read and approved the final manuscript.

References

1. Gibb EA, Brown CJ, Lam WL. The functional role of long non-coding RNA in human carcinomas. Mol Cancer. 2011; 10: 38.
2. Hajjari M, Salavaty A. HOTAIR: an oncogenic long non-coding RNA in different cancers. Cancer Biol Med. 2015; 12(1): 1-9.
3. Kondo Y, Shinjo K, Katsushima K. Long non-coding RNAs as an epigenetic regulator in human cancers. Cancer Sci. 2017; 108(10): 1927-1933.
4. Zhang Y, Zhou Y, Xu T, Tian W, Yang C, Wang X, et al. Clinical Value of long noncoding rna HOTAIR as a novel biomarker in digestive cancers : a meta-analysis. Technol Cancer Res Treat. 2018; 17: 1533034618756783.
5. Kogo R, Shimamamura T, Mimori K, Kawahara K, Imoto S, Sudo T,et al. Long non-coding RNA HOTAIR regulates Polycomb-dependent chromatin modification and is associated with poor prognosis in colorectal cancers. Cancer Res. 2011; 71(20): 6320-6326.
6. Tsai MC, Manor O, Wan Y, Mosammaparast N, Wang JK, Lan F, et al. Long noncoding RNA as modular scaffold of histone modification complexes. Science. 2010; 329(5992): 689-693.
7. Samulin Erdem J, Notø HØ, Skare Ø, Lie JS, Petersen-Øverleir M, Reszka E, et al. Mechanisms of breast cancer risk in shift workers: association of telomere shortening with the duration and intensity of night work. Cancer Med. 2017; 6(8): 1988-1997.
8. Samulin Erdem J, Skare Ø, Petersen-Øverleir M, Notø HØ, Lie JS,

Reszka E, et al. Mechanisms of Breast Cancer in Shift Workers: DNA Methylation in Five Core Circadian Genes in Nurses Working Night Shifts. J Cancer. 2017; 8(15): 2876-2884.
9. Kong X, Liu W, Kong Y. Roles and expression profiles of long non-coding RNAs in triple-negative breast cancers. J Cell Mol Med. 2018; 22(1): 390-394.
10. Shi Y, Ye P, Long X. Differential expression profiles of the transcriptome in breast cancer cell lines revealed by next generation sequencing. Cell Physiol Biochem. 2017; 44(2): 804-816.
11. Zhou Y, Wang C, Liu X, Wu C, Yin H. Long non-coding RNA HOTAIR enhances radioresistance in MDA-MB231 breast cancer cells. Oncol Lett. 2017; 13(3): 1143-1148.
12. Wang Q, Gao S, Li H, Lv M, Lu C. Long noncoding RNAs (lncRNAs) in triple negative breast cancer. J Cell Physiol. 2017; 232(12): 3226-3233.
13. Ding W, Ren J, Ren H, Wang D4. Long noncoding RNA HOTAIR modulates MiR-206-mediated Bcl-w signaling to facilitate cell proliferation in breast cancer. Sci Rep. 2017; 7(1): 17261.
14. Zhao W, Geng D, Li S, Chen Z, Sun M. LcnRNA HOTAIR influences cell growth, migration, invasion, and apoptosis via the miR-20a-5p/HMGA2 axis in breast cancer. Cancer Med. 2018; 7(3): 842-855.
15. Yu Y, Lv F, Liang D, Yang Q, Zhang B, Lin H, et al. HOTAIR may regulate proliferation, apoptosis, migration and invasion of MCF-7 cells through regulating the P53/Akt/JNK signaling pathway. Biomed Pharmacother. 2017; 90: 555-561.
16. Nagini S. Breast cancer: current molecular therapeutic targets and new players. Anticancer Agents Med Chem. 2017; 17(2): 152-163.
17. Qiu JJ, Wang Y, Ding JX, Jin HY, Yang G, Hua KQ. The long noncoding RNA HOTAIR promotes the proliferation of serous ovarian cancer cells through the regulation of cell cycle arrest and apoptosis. Exp Cell Res. 2015; 333(2): 238-248.
18. Yoon JH, Abdelmohsen K, Kim J, Yang X, Martindale JL, Tominaga-Yamanaka K, et al. Scaffold function of long non-coding RNA HOTAIR in protein ubiquitination. Nat Commun. 2013; 4: 2939.
19. Chiyomaru T, Fukuhara S, Saini S, Majid S, Deng G, Shahryari V, et al. Long non-coding RNA HOTAIR is targeted and regulated by MIR-141 in human cancer cells. J Biol Chem. 2014; 289(18): 12550-12565.
20. Bhan A, Hussain I, Ansari KI, Kasiri S, Bashyal A, Mandal SS. Antisense transcript long noncoding RNA (lncRNA) HOTAIR is transcriptionally induced by estradiol. J Mol Biol. 2013; 425(19): 3707-3722.
21. Sørensen KP, Thomassen M, Tan Q, Bak M, Cold S, Burton M, et al. Long non-coding RNA expression profiles predict metastasis in lymph node-negative breast cancer independently of traditional prognostic markers. Breast Cancer Res. 2015; 17: 55.
22. Gökmen-Polar Y, Vladislav IT, Neelamraju Y, Janga SC, Badve S. Prognostic impact of HOTAIR expression is restricted to ER-negative breast cancers. Sci Rep. 2015; 5: 8765.
23. Lu L, Zhu G, Zhang C, Deng Q, Katsaros D, Mayne ST, et al. Association of large noncoding RNA HOTAIR expression and its downstream intergenic CpG island methylation with survival in breast cancer. Breast Cancer Res Treat. 2012; 136(3): 875-883.
24. Pádua Alves C, Fonseca AS, Muys BR, de Barros E Lima Bueno R, Bürger MC, de Souza JE, et al. Brief report: The lincRNA Hotair is required for epithelial-to-mesenchymal transition and stemness maintenance of cancer cell lines. Stem Cells. 2013; 31(12): 2827-2832.
25. Chen FJ, Sun M, Li SQ, Wu QQ, Ji L, Liu ZL, et al. Upregulation of the long non-coding RNA HOTAIR promotes esophageal squamous cell carcinoma metastasis and poor prognosis. Mol Carcinog. 2013; 52(11): 908-915.
26. Nie Y, Liu X, Qu S, Song E, Zou H, Gong C. Long non-coding RNA HOTAIR is an independent prognostic marker for nasopharyngeal carcinoma progression and survival. Cancer Sci. 2013; 104(4): 458-464.
27. Ishibashi M, Kogo R, Shibata K, Sawada G, Takahashi Y, Kurashige J, et al. Clinical significance of the expression of long non-coding RNA HOTAIR in primary hepatocellular carcinoma. Oncol Rep. 2013; 29(3): 946-950.
28. Kim K, Jutooru I, Chadalapaka G, Johnson G, Frank J, Burghardt R, et al. HOTAIR is a negative prognostic factor and exhibits pro-oncogenic activity in pancreatic cancer. Oncogene. 2013; 32(13): 1616-1625.
29. Tano K, Akimitsu N. Long non-coding RNAs in cancer progression. Front Genet. 2012; 3: 219.
30. Xu ZY, Yu QM, Du YA, Yang LT, Dong RZ, Huang L, et al. Knockdown of long non-coding RNA HOTAIR suppresses tumor invasion and reverses epithelial-mesenchymal transition in gastric cancer. Int J Biol Sci. 2013; 9(6): 587-597.

Original Article

The Dilemma of *TP53* Codon 72 Polymorphism (rs1042522) and Breast Cancer Risk: A Case-Control Study and Meta-Analysis in The Iranian Population

Fahimeh Afzaljavan, Ph.D.[1, 2#], Negin Chaeichi Tehrani, B.Sc.[1#], Mahdi Rivandi, D.V.M.[1, 2#], Saeed Zarif Ghasemian, B.Sc.[2, 3], Elham Vahednia, M.Sc.[1], Reza Khayami, B.Sc.[4], Mohammad Abavisani, B.Sc.[2], Alireza Pasdar, M.D., Ph.D.[1, 5*]

1. Department of Modern Sciences and Technologies, Faculty of Medicine, Mashhad University of Medical Science, Mashhad, Iran
2. Student Research Committee, Faculty of Medicine, Mashhad University of Medical Sciences, Mashhad, Iran
3. Department of Radiology Technology, Faculty of Paramedical Sciences, Mashhad University of Medical Sciences, Mashhad, Iran
4. Department of Medical Genetics, Faculty of Medicine, Mashhad University of Medical Science, Mashhad, Iran
5. Division of Applied Medicine, Medical School, University of Aberdeen, Foresterhill, Aberdeen, AB25 2ZD, UK

#The first three authors equally contributed to this work.

Corresponding Address: P.O.Box: 917794-8564, Department of Modern Sciences and Technologies, Faculty of Medicine, Mashhad University of Medical Science, Mashhad, Iran
Email: pasdara@mums.ac.ir

Received: 14/October/2018, Accepted: 9/March/2019

Abstract

Objective: Mutations of *TP53* as a tumor suppressor gene are frequently observed in different types of cancer. A codon 72 polymorphism located on exon 4 with two alleles encoding either Proline (CCC) or Arginine (CGC) has been indicated as a common variation in association with cancers. Controversial results have been reported regarding the association of allelic polymorphism of codon 72 of *TP53* gene and breast cancer risk in Iranian patients. Therefore, a case-control study was designed. A meta-analysis was also carried out to provide evidence of association between this variation and breast cancer in Iran, based on all available published data.

Materials and Methods: In this case-control study, blood sample of 622 participants, including 308 breast cancer cases and 314 controls were collected. Genotyping for rs1042522 was conducted by Allele Specific polymerase chain reaction (AS-PCR). In order to set a meta-analysis study, PubMed, Scopus and ISI Web of Knowledge and Persian databases were searched to explore relevant studies, published up to September 2018, containing information on *TP53* polymorphism and the risk of breast cancer in Iran. Statistical analysis was performed using SPSS 16.0 and MetaGenyo.

Results: All retrieved available data as well as the results of our current study were consisted of 1965 breast cancer cases and 1999 healthy controls. No significant difference was observed in allele frequencies between groups (P=0.90) in our study. The cumulative results did not also show any association between rs1042522 and breast cancer risk on the dominant (P=0.61) and recessive (P=0.89) models.

Conclusion: These findings cannot support contribution of rs1042522 polymorphism to breast cancer risk in an Iranian population. Future larger studies may help confirm this finding with a greater power.

Keywords: Breast Cancer, Genetic Variation, Polymorphism, *TP53*

Cell Journal(Yakhteh), Vol 22, No 2, July-September (Summer) 2020, Pages: 185-192

Citation: **Afzaljavan F, Chaeichi Tehrani N, Rivandi M, Zarif Ghasemian S, Vahednia E, Khayami R, Abavisani M, Pasdar A. The dilemma of TP53 codon 72 polymorphism (rs1042522) and breast cancer risk: a case-control study and meta-analysis in the Iranian population. Cell J. 2020; 22(2): 185-192. doi: 10.22074/cellj.2020.6458.**

Introduction

Breast malignancy is among the major types of cancer and the universal cause of cancer death in women. The incidence of breast cancer in western populations is significantly higher than other populations. However, 50% of new cases and approximately 60% of deaths caused by breast cancer occur in developing countries (1). Breast cancer is one of the most commonest cancers affecting Iranian women, though the epidemiology of breast cancer in Iran has not yet been fully investigated (2).

Based on epidemiological studies, a number of factors have been identified associating with increased risk of breast malignancies. These factors are not necessarily causes of breast cancer and they can be subcategorized in both genetic and environmental factors, increasing liability of the breast cancer. Association studies, whereby the relations of certain markers with the disease are investigated prominently in case-control designs, are of crucial importance to dissect the genetic basis of common multifactorial disorders, such as breast cancer. Based on this, several candidate genes have been analyzed so far in case-control studies.

One of the highest involved genetic factors in the risk of breast cancer is the tumor suppressor gene, *TP53*. The corresponding protein, P53, has a role in cell cycle regulation including cell growth and division, apoptosis, DNA repair and the maintenance of genome stability and its mutations have been commonly observed in different types of cancer (3, 4). Dysfunction of the P53 signaling pathway is an important hallmark of different malignancies

(5). Numerous single nucleotide polymorphisms (SNPs), somatic and germ line mutations are located at the *TP53* locus. Polymorphisms in this gene may affect the susceptibility to cancer development in the way of varying the normal functions of P53. Since many of these variations have been found in intronic loci, they cannot affect the biology of cancer. However, they may be used as markers in dissecting genetic basis of multifactorial diseases. Previously, limited numbers of *TP53* polymorphisms have been studied in relation with biochemical and biological functions and in association with cancer risk. The *TP53* codon 72 polymorphism (C/G) has been located at the exon 4 of this gene and encodes Proline (CCC) or Arginine (CGC). Association of this polymorphism with susceptibility to several forms of cancer has been identified (6). According to research on different populations, genotype frequencies have been found to largely differ with ethnicity changes (7). The difference in the primary structure of P53 protein results in different biochemical functions. The potential role of Arg variant in the induction of apoptosis pathway has been confirmed in a previous research (8). Furthermore, "Pro" variant can block cell cycle pathway progression toward the repair of DNA damage (9).

Association of the *TP53* codon 72 polymorphism and susceptibility to breast cancer has been considered in several regions of Iran. These case-control studies did not indicate consistent results, likely due to the small sample sizes with limited power. A meta-analysis along with combining the different results and small data, can achieve a reasonable level of significance and an increase in power of results. In the present study, we examined association of rs1042522 and breast cancer susceptibility in the North-East of Iran and a meta-analysis was performed to quantitatively assess effect of the *TP53* codon 72 polymorphism on risk of breast cancer in Iran.

Materials and Methods

Population study

In this case-control study, 308 breast cancer cases and 314 healthy controls with no sign of breast cancer or history of malignant breast disease participated in this association study. The important demographics and histopathological data were obtained from a questionnaire. The Ethics Committee of the Mashhad University of Medical Science approved this study (ethical approval number: IR.MUMS.fm.REC.1394.472) and all of the participants signed the written informed consent.

DNA extraction and genotyping analysis

The salting out method was used to extract DNA from peripheral blood samples. Genotyping was performed using Allele specific polymerase chain reaction (AS-PCR) methods (10). We used primers from the previous study (11) and the sequence of four primers (synthesis by metabion international AG, Germany) was shown as follows:
Arginine-based (G) allele:
F: 5′-TCCCCCTTGCCGTCCCAA-3′
R: 5′-CTGGTGCAGGGGCCACGC-3′
Proline-based (C) allele:
F: 5′-GCCAGAGGCTGCTCCCCC-3′
R: 5′-CGTGCAAGTCACAGACTT-3′

PCR was done in a final volume of 10 µl reaction for each allele containing: Taq DNA Polymerase 2x Master Mix RED (Ampliqon, Denmark), 1 µl genomic DNA (200-300 ng), 1 µl of each primer (10 µM, Metabion International AG, Germany) and adequate DNase free water (Sinaclon, Iran). Amplification temperature stages were performed for 5 minutes at 95˚C and then 35 cycles including 30 seconds at 94˚C, 30 seconds at 63˚C, 30 seconds at 72˚C, followed by 7 minutes at 72˚C in a Veriti 96 well PCR Thermal Cycler (Thermo Fisher Scientific).

Identification of studies for meta-analysis

The original publications, reporting association between *TP53* codon 72 polymorphism and breast cancer risk before September 2018, were gathered by searching Scopus, PubMed and ISI Web of Knowledge databases. The Persian articles and conference abstracts were also explored by searching SID, Iranmedex, Magiran, Medlib and Google. The references of retrieved articles were also investigated to discover other related studies. The terms of "TP53" and "genetic variant", "genetic variation" or "polymorphism" and "breast cancer", "breast carcinoma", "breast tumour" or "breast tumor" and "Iran" or "Iranian" were used to search for the articles of interest. Case-control studies were selected for the analysis.

Data extraction

A meta-analysis was designed according to PRISMA guidelines (12). Features of the selected studies were independently extracted by two authors. For each eligible study, first author, date of publication, number of cases and controls, study population (region), frequency of all genotypes for two groups, allele incidence and Hardy-Weinberg equilibrium (HWE) in control groups were extracted or calculated and ultimately the results were reviewed by the third investigator.

Statistical analysis

Chi-square test and logistic regression models were performed to find association between histopathological or demographic criteria and genotypes of rs1042522.

In the meta-analysis study, frequency of two alleles was calculated for the case and control groups in each experiment. HWE test using the X^2 statistic was evaluated by analysis of the genotype frequencies in the controls. Association was measured initially using both random-effect and fixed-effect models. However, since the random-effect method proposes heterogeneity, this method was considered as the main approach. The strength of association between TP53 codon 72 polymorphism and risk of breast cancer was measured by odds ratios (ORs) with 95% confidence intervals (CIs).

The risk for the genotypes GC and CC was compared to the GG homozygote, as the wild-type genotype. Furthermore, according to the dominant and recessive models, the risk of Arg-carriers (GC+GG) versus CC genotype and Pro-carriers (CC+GC) versus GG genotype were evaluated, respectively.

Heterogeneity was evaluated by the Q-test and I^2 index. Probability of publication bias was checked by the funnel plot and Egger's test for all genetic models. Random effects model was used to analyze the data.

Meta-analysis was carried out using MetaGenyo [Pfizer-University of Granada-Junta de Andalucía Centre for Genomics and Oncological Research (GENYO), Spain] (13). All other statistical analyses were carried out using SPSS version 16.0 (SPSS Inc., USA). A P value of less than 0.05 was considered statistically significant.

Results

Characteristics of the population study

A total of 308 breast cancer women, out of 622 samples, and 314 healthy controls were enrolled in this study. The average age of case and control groups were 47.80 ± 10.90 and 44.15 ± 12.07 years, respectively, with a significant difference between the groups (P<0.001). Furthermore, menopausal status was considered as peri- and pre-menopausal, compared to post-menopausal individuals. The control group was younger than cases, and therefore most of the patients typically belonged to the post-menopausal group. The difference between groups was significant (P<0.001).

Body mass index (BMI), as a continuous and categorical variable, was compared between these groups. Mean BMI was higher in the patient cases than in controls and a significant difference was observed (P<0.001). Moreover, by categorizing patients, it was distinguished that a large number of cases were included in BMI ≥25 category.

The history of lactation (P<0.01), history of other cancers (P<0.001) and family history of cancer (P<0.001) were also significantly different between patients and healthy controls. Table 1 shows the most important demographic characteristics of the case and control groups.

Association between rs1042522 and the risk of breast cancer in the Northeast of Iran

Genotypic distribution of the rs1042522 in our study conforms HWE (P>0.05). The C allele (Pro) frequency, as the minor allele was 24% in the cases, compared to 23.7% in the controls. According to this data, no association was found between case and control groups for allele frequency (P=0.90). The most frequent genotype for rs1042522 was GG (Arg/Arg) in both case (60.7%) and control (60.2%) groups. Genotype frequency did not show any significant difference between these two groups (P>0.05). Moreover, dominant and recessive models did not indicate any association with the risk of breast cancer. Results have been shown in Table 2.

Adjustment for confounding factors including age, BMI, history of cancer, family history of cancer and history of lactation did not change the results.

Meta-analysis

133 articles were identified from different databases by two authors, individually. After matching the data, discrepancies were reanalyzed by the third author. 42 articles were similar between databases. Therefore, 91 articles were assessed for eligibility. 73 studies were not related to the subject. Furthermore, two records were not designed as the case-control study. After excluding duplicated, unrelated and improperly designed papers, 16 case-control studies, concerning the association between *TP53* codon 72 polymorphism and breast cancer, were included in the meta-analysis. The selection process has been demonstrated in Figure 1.

Table 1: Results of the association analysis of demographic characteristics between breast cancer cases and healthy group

Characteristics	Cases n (%)	Controls n (%)	P value
Age (Y)			
≤40	74 (25.8)	138 (44.4)	
>40	213 (74.2)	173 (55.6)	<0.001
Mean	47.80 ± 10.90	44.15 ± 12.07	<0.001
Menopausal status			
Peri and premenopausal	86 (45.3)	217 (78.9)	
Postmenopausal	104 (54.7)	58 (21.1)	<0.001
Body mass index (kg/m^2)			
<25	80 (31.2)	154 (51.2)	
≥25	176 (68.8)	147 (48.8)	<0.001
Mean	27.59 ± 5.06	25.20 ± 4.12	<0.001
Abortion			
Yes	172 (67.5)	151 (65.1)	
No	83 (32.5)	81 (34.9)	0.63
History of lactation			
Yes	246 (91.4)	223 (97.4)	
No	23 (8.6)	6 (2.6)	<0.01
Family history of cancer			
Yes	172 (60.8)	229 (73.9)	
No	111 (39.2)	81 (26.1)	<0.001
History of other cancer			
Yes	20 (7.2)	3 (1.0)	
No	259 (92.8)	301 (99.0)	<0.001

Data are presented as mean ± SD or n (%).

Table 2: Distribution of the genotypes and allele frequency of rs1042522 polymorphism in breast cancer cases and controls

Genetic analysis model	Number of case (%)	Number of control (%)	P value	OR (95% CI)
Genotypes				
GG	187 (60.7)	189 (60.2)	Reference	
GC	94 (30.5)	101 (32.2)	0.73	0.94 (0.67-1.33)
CC	27 (8.8)	24 (7.6)	0.67	1.38 (0.63-2.04)
Dominant				
GG+GC	281 (91.2)	290 (92.4)	Reference	
CC	27 (8.8)	24 (7.6)	0.61	0.86 (0.48-1.53)
Recessive				
GG	187 (60.7)	189 (60.2)	Reference	
GC+CC	121 (39.3)	125 (39.8)	0.89	0.98 (0.71-1.35)
Allele				
G	468 (76.0)	479 (76.3)	Reference	
C	148 (24.0)	149 (23.7)	0.90	1.02 (0.78-1.32)

OR; Odd ratio and CI; Confidence interval.

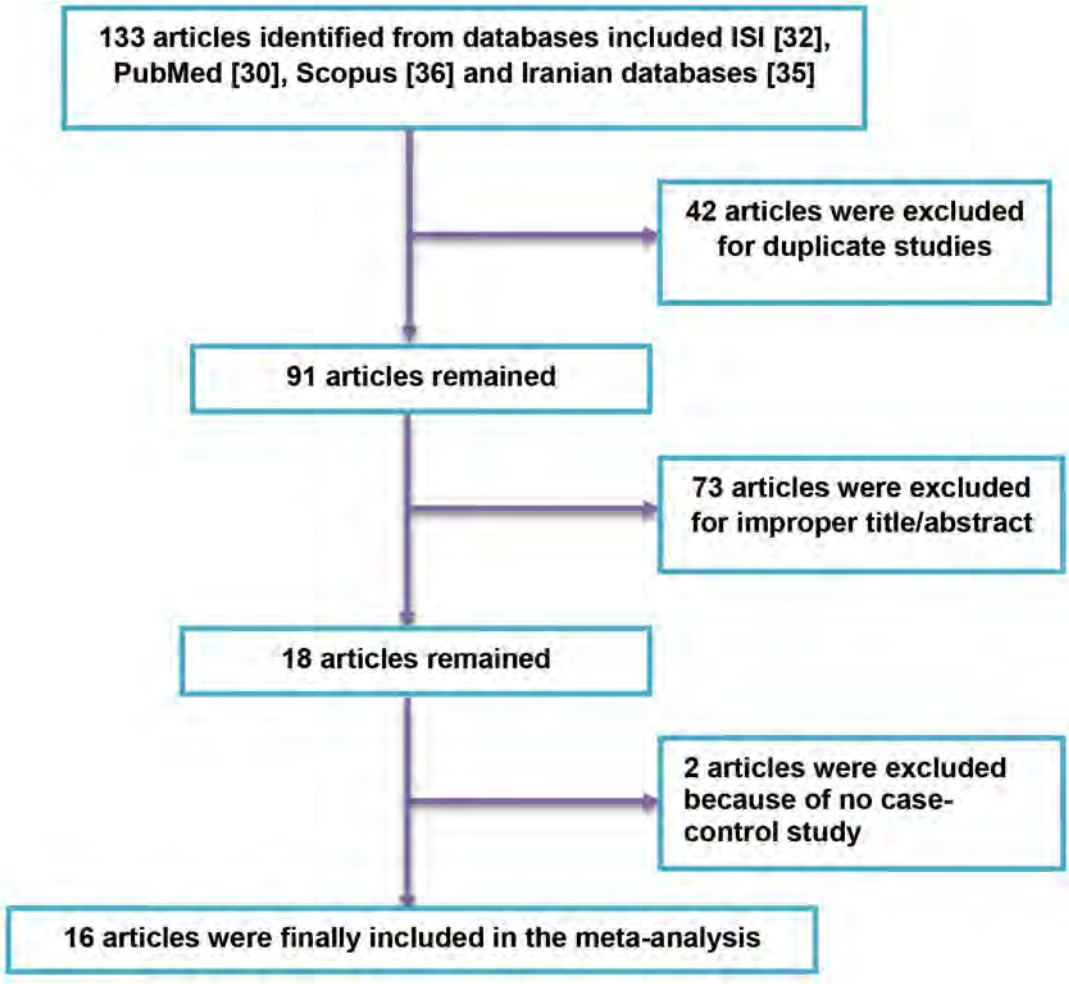

Fig.1: Flowchart of the search strategy and selection of studies. After searching in main databases, with removing 117 studies due to duplication, improper subjects and no case-control design, 16 articles remanied to be included in the mata-analysis.

Data extraction

Overall the data included 1965 breast cancer subjects and 1999 healthy people. Diversity in the sample size, ranged from 42 to 314 individuals, was found between studies. Moreover, genotyping methods were different between projects. Nine studies used the AS-PCR method and seven studies were performed by the PCR-restriction fragment length polymorphism (PCR-RFLP) method. Although the main source of DNA template was blood in many studies, one study had been performed on normal and cancerous tissues and five projects had used tissue samples for patient's genotyping and blood samples for healthy groups.

Frequency of the 72 Pro allele varied in the control participants, from 30 to 60%, depending on the geographical region. Apart from the four studies, HWE was confirmed for frequency of *TP53* codon 72 genotypes in the control group. The results have been shown in Table 3.

Pooled allele frequencies did not significantly differ between Iranian patients and healthy controls. Results confirmed a lack of association between the *TP53* codon 72 and susceptibility to breast cancer in all genetics models. This finding did not vary after removing studies with no HWE data.

Publication bias was evaluated by the analysis of Begg's funnel plots and Egger's test for all genetic models. All plots indicated some evidence of publication bias, however, this finding was not significant (P>0.05, plots have not been shown). According to the P value of heterogeneity, we found high incidence of heterogeneity between the studies in different genetic models (P< 0.01). Results have been shown in Table 4.

Table 3: Extracted data from the selected studies

Study	Year	Region	Type of samples		Method	Sample size		Genotype frequency						p HWE	Allele frequency (%)			
								Cases			Controls				Cases		Controls	
			Cases	Controls		Cases	Controls	A/A	A/P	P/P	A/A	A/P	P/P		G	C	G	C
Faghani et al. (14)	2007	Isfahan	Tissue	Blood	AS-PCR	51	51	44	6	1	22	27	2	0.19	92.1	7.8	69.6	30.4
Khadang et al. (15)	2007	Shiraz	Blood	Blood	AS-PCR	221	205	83	109	29	75	90	40	0.39	62.2	37.8	58.5	41.5
Faghani et al. (16)	2008	Isfahan	Tissue	Blood	AS-PCR	96	96	68	21	7	35	44	17	0.88	81.7	18.2	59.4	40.6
Kazemi et al. (17)	2009	North of Iran	Tissue	Blood	AS-PCR	42	60	6	30	6	12	45	0	0	50	50	39.5	60.5
Doosti et al. (18)	2011	Isfahan	Blood	Blood	PCR-RFLP	135	140	52	70	13	36	82	22	0.09	64.4	35.6	55	45
Hossein Pour Feizi et al. (19)	2012	Tabriz	Blood	Blood	AS-PCR	126	99	56	44	26	30	50	19	0.97	61.9	38.1	55.6	44.4
Golmohammadi and Namazi (20)	2013	Sabzevar	Blood	Blood	AS-PCR	80	80	29	49	2	15	51	14	0.04	66.8	33.2	50.6	49.4
Rouhi Boroujeni et al. (21)	2013	Isfahan	Blood	Blood	PCR-RFLP	135	150	27	102	6	36	93	21	0.01	57.8	42.2	55	45
Behfarjam et al. (22)	2013	Mahabad	Blood	Blood	PCR-RFLP	25	30	9	14	2	9	17	4	0.66	64	36	58.3	42.7
Sheikhpour and Taghipour Zahir (23)	2014	Yazd	Blood	Blood	AS-PCR	104	104	51	31	22	22	54	28	0.91	63.9	36.1	47.1	52.9
Saadatian et al. (24)	2014	Tabriz	Blood	Blood	PCR-RFLP	100	100	22	48	30	13	63	24	0.02	46	54	44.5	55.5
Gohari-Lasaki et al. (25)	2015	Tabriz	Blood	Blood	PCR-RFLP	100	100	31	48	21	31	57	12	0.18	55	45	59.5	40.5
Ahangar Oskouee et al. (26)	2015	Tabriz	Tissue	Tissue	PCR-RFLP	65	65	21	40	4	48	13	4	0.11	63.1	36.9	83.8	16.2
Rajabi Firoozabadi et al. (27)	2016	Yazd	Blood	Blood	AS-PCR	90	83	10	45	35	21	37	25	0.62	36.1	63.9	47.5	52.5
Moradinasab et al. (28)	2017	Bushehr	Blood	Blood	PCR-RFLP	144	162	46	68	30	50	90	22	0.18	55.6	44.4	58.6	41.4
Pouladi et al. (29)	2018	Tabriz	Tissue	Blood	AS-PCR	143	160	63	54	26	54	74	32	0.77	62.9	37.1	56.8	43.2
Our study	2018	Northeast of Iran	Blood	Blood	AS-PCR	308	314	187	94	27	189	101	24	0.14	76	24	76.2	23.8
Total (17 studies)						1965	1999	805	873	287	698	988	310	0.43	63.4	36.6	59.7	40.3

AS-PCR; Allele specific polymerase chain reaction, RFLP; Restriction fragment length polymorphism, and HWE; Hardy-Weinberg.

Table 4: Analysis of the association between TP53 codon 72 polymorphism and breast cancer risk in different genetic models, the test of heterogeneity and publication bias

Model	Test of association		Test of heterogeneity			Publication bias
	OR (95% CI)	P value	Model	P value	I^2	P value (Egger's test)
Allele contrast (G vs. C)	1.18 (0.96-1.47)	0.13	Random	<0.001	0.80	0.63
Recessive model (GG vs. GC+CC)	1.34 (0.95-1.89)	0.10	Random	<0.001	0.83	0.73
Dominant model (GG+GC vs. CC)	1.15 (0.84-1.56)	0.38	Random	<0.01	0.58	0.51
Over dominant (GC vs. GG + CC)	0.79 (0.58-1.06)	0.12	Random	<0.001	0.79	0.50
Pairwise 1 (GG vs. CC)	1.38 (0.93-2.04)	0.11	Random	<0.001	0.67	0.83
Pairwise 2 (GG vs. GC)	1.36 (0.95-1.95)	0.10	Random	<0.001	0.82	0.66
Pairwise 3 (GC vs. CC)	1.00 (0.72-1.36)	0.97	Random	<0.01	0.55	0.63

OR; Odd ratio and CI; Confidence interval.

Discussion

The mortality rate in comparison with the rate of breast cancer is higher in developing rather than developed countries, due to the early detection of diseases using genetic biomarkers in the latter countries. SNPs are a good example of these biomarkers. The *TP53* codon 72 polymorphism (rs1042522) has been reported to have an association with the susceptibility to cancer in the different populations. Due to the lack of association studies with sufficient sample sizes and strong conclusions to assess correlation between rs1042522 and risk of breast cancer development, we conducted the case-control study on 622 breast cancer patients and controls in the northeast of Iran.

A previous meta-analysis study without any ethnicity restriction showed association of *TP53* codon 72 polymorphism with breast cancer risk in the recessive model. This study only confirmed a significant difference in the allelic model of an Asian population (14). However, involvement of other risk factors in this association was suggested. Genetic background and ethnicity are amongst those influential factors that may change association status. Since several case-control studies have reported different results about the association between rs1042522 and breast cancer risk in Iran, the need for a comprehensive analysis was warranted. In order to elucidate this inconsistent conclusion, a meta-analysis was performed to examine the association between *TP53* codon 72 polymorphism and breast cancer risk in Iran, by reviewing all published studies with conflicting results. The final analysis included a total of 1965 breast cancer patients and 1999 healthy individuals, as the control group, to evaluate the existence or absence of any association.

Our pooled data from 17 case-control studies, meeting the inclusion criteria, confirmed lack of association between risk of breast cancer and *TP53* codon 72 polymorphism in Iran. The heterogeneity amongst the studies has been pointed out in the analysis. Ethnicity, minor allele frequency, sample size, genotyping methods, source of DNA and disease phenotypes may be regarded as the source of such heterogeneity. However, we acknowledge that we focused on studies considering germline variants as risk factors, there are some studies which may have investigated the somatic variants to provide a catalogue of tumoral genetic variations (15, 16).

Our results indicated that pooled control samples followed HWE. Four studies failed to show HWE, however, when they were excluded from the analysis, the overall results were not significantly changed (data has been shown in the Table S1) (See Supplementary Online Information at www.celljournal.org).

Pooled allele frequencies were 0.60 and 0.63 for G in the control and case groups, respectively. According to NCBI and OMIM data, C allele is the ancestral allele coding Proline. Allele frequency of C is higher than G in the general population, however, population based studies indicate high heterogeneity related to the C and G allele frequencies. According to some online databases, the frequencies vary between 0.9 for C and 0.1 for G in Oceania and inversely 0.2 and 0.8 for C and G respectively in Europe, suggesting a powerful ethnic influence (17). In our study, minor allele was C allele in the pooled data with a frequency of 0.37 and 0.40 in the respectively controls and cases.

The results did not show a significant difference between allele frequencies in patients and healthy subjects (P in multiplicative model ≤ 0.12). This finding was also seen in recessive and dominant models. Statistical evidence from other meta-analysis studies have indicated this polymorphism may have a potential effect on breast (14) and ovarian cancer risks (18) in the pooled data as well as a subgroup of Asian and Caucasian populations. On the other hand, in another previously conducted meta-analysis (with no ethnicity preference) no association between *TP53* codon 72 polymorphism with breast cancer (19) and cervical cancer (20) risks was reported.

The pooled data indicated that allele frequency difference

between cases and controls was about 3%. Therefore, it is proposed to evaluate the association between *TP53* codon 72 polymorphism and risk of breast cancer with a power of 80%; in other words 4129 individuals is proposed for each group in future studies. In our study the overall power was calculated as 50% which may not support the evidence of this association. Designing proper studies with adequate sample sizes will provide more valuable evidence for this association.

Conclusion

Our results showed that *TP53* codon 72 polymorphism may not influence the overall risk of breast cancer in an Iranian population. By that means, there is no association between *TP53* codon 72 polymorphism and breast cancer risk in the Iranian population of this meta-analysis. Several included studies had limited sample size and they were underpowered. To assess this association more precisely, well-designed case-control studies with adequate sample sizes are still necessary.

Molecular classification, as well as evaluating the effect of other polymorphisms and environmental factors, such as alcohol consumption and tobacco smoke, should also be considered. Characteristics of different individuals, including premenopausal or postmenopausal status, metabolic index, family history, epistasis and clinical course are also important.

Acknowledgements

The authors would like to thank all participants in this research. We would also like to thank Mashhad University of Medical Sciences and Omid Hospital (Mashhad, Iran) for their support to the project. This work was financially supported by Mashhad University of Medical Sciences under Grant No. 930891. No potential conflict of interest was reported by the authors.

Authors' Contribution

A.P., F.A., S.Z.G.; Contributed in designing of the work. F.A., N.C.T., M.R., R.K., S.Z.G.; Contributed in data collection. F.A., N.C.T., M.R., R.K., M.A.; Contributed in the laboratory work. F.A., E.V., A.P.; Contributed in data analysis and interpretation. F.A., E.V.; Contributed in drafting the manuscript. F.A., A.P.; Contributed in the critical revision of the manuscript. All authors helped edit and approve the final version of this manuscript for submission. They also participated in the finalization of manuscript and approved the final draft.

References

1. Forouzanfar MH, Foreman KJ, Delossantos AM, Lozano R, Lopez AD, Murray CJ, et al. Breast and cervical cancer in 187 countries between 1980 and 2010: a systematic analysis. Lancet. 2011; 378(9801): 1461-1484.
2. Montazeri A, Vahdaninia M, Harirchi I, Harirchi AM, Sajadian A, Khaleghi F, et al. Breast cancer in Iran: need for greater women awareness of warning signs and effective screening methods. Asia Pac Fam Med. 2008; 7(1): 6.
3. Green DR, Kroemer G. Cytoplasmic functions of the tumour suppressor p53. Nature. 2009; 458(7242): 1127-1130.
4. Muller PA, Vousden KH. p53 mutations in cancer. Nat Cell Biol. 2013; 15(1): 2-8.
5. Vogelstein B, Lane D, Levine AJ. Surfing the p53 network. Nature. 2000; 408(6810): 307-310.
6. Whibley C, Pharoah PD, Hollstein M. p53 polymorphisms: cancer implications. Nat Rev Cancer. 2009; 9(2): 95-107.
7. Sjalander A, Birgander R, Saha N, Beckman L, Beckman G. p53 polymorphisms and haplotypes show distinct differences between major ethnic groups. Hum Hered. 1996; 46(1): 41-48.
8. Dumont P, Leu JI, Della Pietra AC 3rd, George DL, Murphy M. The codon 72 polymorphic variants of p53 have markedly different apoptotic potential. Nat Genet. 2003; 33(3): 357-365.
9. Siddique M, Sabapathy K. Trp53-dependent DNA-repair is affected by the codon 72 polymorphism. Oncogene. 2006; 25(25): 3489-3500.
10. Suguna S, Nandal DH, Kamble S, Bharatha A, Kunkulol R. Genimic DNA isolation from human whole blood samples by non enzymatic salting out method. International Journal of Pharmacy and Pharmaceutical Sciences. 2014; 6(6): 198-199.
11. Storey A, Thomas M, Kalita A, Harwood C, Gardiol D, Mantovani F, et al. Role of a p53 polymorphism in the development of human papillomavirus-associated cancer. Nature. 1998; 393(6682): 229-234.
12. PRISMA: University of OXFORD; 2015. Available from: http://www.prisma-statement.org/.
13. Martorell-Marugan J, Toro-Dominguez D, Alarcon-Riquelme ME, Carmona-Saez P. MetaGenyo: A web tool for meta-analysis of genetic association studies. BMC Bioinformatics. 2017; 18(1): 563.
14. Faghani M, Nikbahkt M, Salehi M, Rabbani M, Talebi A, Soleimani B, et al. Study of p53 polymorphism at codon 72 in patients of breast cancer in Isfahan. Journal of Isfahan Medical School. 2007; 25(84): 26-33.
15. Khadang B, Fattahi MJ, Talei A, Dehaghani AS, Ghaderi A. Polymorphism of TP53 codon 72 showed no association with breast cancer in Iranian women. Cancer Genet Cytogenet. 2007; 173(1): 38-42.
16. Faghani M, Nasiri E, Bahadori MH, Mohammad Ghasemi F. Genetic predisposing of p53 codon 72 on developing of breast cancer in postmenopausal women in Isfahan. Journal of Guilan University of Medical Sciences. 2008; 17(67): 94-100.
17. Kazemi M, Salehi Z, Chakosari RJ. TP53 codon 72 polymorphism and breast cancer in northern Iran. Oncol Res. 2009; 18(1): 25-30.
18. Doosti A, Ghasemi Dehkordi P, Davoudi N. A p53 codon 72 polymorphism associated with breast cancer in Iranian patients. Afr J Pharm Pharmacol. 2011; 5(10): 1278-1281.
19. Hossein Pour Feizi MA, Ravanbakhsh R, Pourahmad R, Pouladi N, Azarfam P, Montazeri V. Association of p53 Arg/Pro polymorphism at codon 72 with Risk of breast cancer in East Azerbaijani women. J Babol Univ Med Sci. 2012; 14(2): 31-38.
20. Golmohammadi R, Namazi MJ. The role of p53 codon 72 genotype in ductal breast carcinoma. Feyz. 2013; 17(4): 387-393.
21. Rouhi Boroujeni H, Karimi M, Moshkelani S, Parsaei P. Association of the p53 codon 72 polymorphism with breast cancer in central part of Iran. Afr J Pharm Pharmacol. 2013; 7(7): 356-359.
22. Behfarjam F, Rostamzadeh J, Faegh J. Study of TP53 codon 72 & 282 polymorphisms and ABCC1 promoter polymorphism (G-1666A) in archived breast cancer samples mahabadian women by PCR-RFLP and PCR-SSCP. 8th International Breast Cancer Congress; 2013; Tehran, Iran. Tehran, Iran; Shahid Beheshti University of Medical Sciences; 2013.
23. Sheikhpour R, Taghipour Zahir Sh. Analysis of P53 codon 72 polymorphism and protoein level in breast cancer patients in Yazd. Iranian Journal of Breast Diseases. 2014; 7(3): 1-10.
24. Saadatian Z, Gharesouran J, Ghojazadeh M, Ghohari-Lasaki S, Tarkesh-Esfahani N, Mohaddes Ardebili SM. Association of rs1219648 in FGFR2 and rs1042522 in TP53 with premenopausal breast cancer in an Iranian Azeri population. Asian Pac J Cancer Prev. 2014; 15(18): 7955-7958.
25. Gohari-Lasaki S, Gharesouran J, Ghojazadeh M, Montazeri V, Mohaddes Ardebili SM. Lack of influence of TP53 Arg72Pro and 16bp duplication polymorphisms on risk of breast cancer in Iran. Asian Pac J Cancer Prev. 2015; 16(7): 2971-2974.
26. Ahangar Oskouee M, Shahmahmoudi S, Nategh R, Esmaeili HA, Safaeyan F, Zareinghalame Moghaddam M. Three common TP53 polymorphisms and the risk of breast cancer among groups of iranian women. . Arch Breast Cancer. 2015; 2(4): 114-119.
27. Rajabi Firoozabadi S, Shiryazdi SM, Keshavarz F, Nazari T, Ghasemi N. Frequency of p53 gene codon 72 polymorphisms in wom-

en with breast cancer in Iran. IJML. 2016; 3(2): 86-91.
28. Moradinasab M, Ostovar A, Nabipour I, Eghbali SS, Vahdat K, Ghaderi A, et al. TP53 codon 72 genetic polymorphism, rs1042522, Modifies the association between tobacco smoking and breast cancer risk. Iran Red Crescent Med J. 2017; 19(10): e58027.
29. Pouladi N, Dehghan R, Hosseinpour Feizi M, Dastmalchi N. Association of P53 (+16ins-Arg) haplotype with the increased susceptibility to breast cancer in Iranian-Azeri women. Journal of Kerman University of Medical Sciences. 2018; 25(1): 9-17.
30. Gonçalves ML, Borja SM, Cordeiro JA, Saddi VA, Ayres FM, Vilanova-Costa CA, et al. Association of the TP53 codon 72 polymorphism and breast cancer risk: a meta-analysis. Springerplus. 2014; 3: 749.
31. ALFRED: Yale University; 2019, updated 2002. Available from: http://alfred.med.yale.edu/alfred/SiteTable1A_working.asp?siteuid=SI018437X.
32. Zhang Z, Fu G, Wang M, Tong N, Wang S, Zhang Z. P53 codon 72 polymorphism and ovarian cancer risk: a meta-analysis. Journal of Nanjing Medical University. 2008; 22(5): 279-285.
33. Hou J, Jiang Y, Tang W, Jia S. p53 codon 72 polymorphism and breast cancer risk: a meta-analysis. Exp Ther Med. 2013; 5(5): 1397-1402.
34. Klug SJ, Ressing M, Koenig J, Abba MC, Agorastos T, Brenna SM, et al. TP53 codon 72 polymorphism and cervical cancer: a pooled analysis of individual data from 49 studies. Lancet Oncol. 2009; 10(8): 772-784.

Original Article

Arsenic Trioxide and Thalidomide Combination Induces Autophagy Along with Apoptosis in Acute Myeloid Cell Lines

Mahnaz Mohammadi Kian, M.Sc.[1, 2], Atousa Haghi, M.Sc.[1, 3], Mahdieh Salami, M.Sc.[1, 2], Bahram Chahardouli, Ph.D.[1, 2], Shahrbanoo Rostami, Ph.D.[1, 2], Kianoosh Malekzadeh, Ph.D.[4], Hosein Kamranzadeh Foumani, M.D.[1, 2], Saeed Mohammadi, Ph.D.[1, 2*], Mohsen Nikbakht, Ph.D.[1, 2*]

1. Hematology, Oncology and Stem Cell Transplantation Research Center, Tehran University of Medical Sciences, Tehran, Iran
2. Hematologic Malignancies Research Center, Tehran University of Medical Sciences, Tehran, Iran
3. Young Researchers and Elite Club, Pharmaceutical Sciences Branch, Islamic Azad University, Tehran, Iran
4. Molecular Medicine Research Center (MMRC), Hormozgan University of Medical Science (HUMS), Bandar Abbass, Iran

Corresponding Address: P.O.Box: 1411713131, Hematology, Oncology and Stem Cell Transplantation Research Center, Tehran University of Medical Sciences, Tehran, Iran
Emails: m-nikbakht@sina.tums.ac.ir, smohammadi@sina.tums.ac.ir

Received: 18/October/2018, Accepted: 20/February/2019

Abstract

Objective: Autophagy and apoptosis play key roles in cancer survival and pathogenesis and are governed by specific genes which have a dual role in both cell death and survival. Arsenic trioxide (ATO) and thalidomide (THAL) are used for treatment of many types of hematologic malignancies. ATO prevents the proliferation of cells and induces apoptosis in some cancer cells. Moreover, THAL has immunomodulatory and antiangiogenic effects in malignant cells. The aim of present study was to examine the effects of ATO and THAL on U937 and KG-1 cells, and evaluation of mRNA expression level of VEGFs genes, PI3K genes and some of autophagy genes.

Materials and Methods: In this *in vitro* experimental study, U937 and KG-1 cells were treated by ATO (0.4-5 μM) and THAL (5-100 μM) for 24, 48 and 72 hours. Cell viability was measured by MTT assay. The apoptosis rate and cell cycle arrest were evaluated by flow cytometry (Annexin/PI) and cell cycle flow cytometry analysis, respectively. The effect of ATO/THAL on mRNAs expression was evaluated by real-time polymerase chain reaction (PCR).

Results: ATO/THAL combination enhanced cell apoptosis in a dose-dependent manner. Also, ATO/THAL induced SubG1/G1 phase arrest. mRNA expression levels of *VEGFC* (contrary to other *VEGFs* isoform), *PI3K, AKT, mTOR, MEK1, PTEN, IL6, LC3* and *P62* genes were upregulated in acute myeloid leukemia (AML) cells following treatment with ATO/THAL.

Conclusion: Combined treatment with ATO and THAL can inhibit proliferation and invasion of AML cells by down-regulating *ULK1* and *BECLIN1* and up-regulating *PTEN* and *IL6,* and this effect was more marked than the effects of ATO and THAL alone.

Keywords: Acute Myeloid Leukemia, Arsenic Trioxide, Thalidomide

Cell Journal(Yakhteh), Vol 22, No 2, July-September (Summer) 2020, Pages: 193-202

Citation: **Mohammadi Kian M, Haghi A, Salami M, Chahardouli B, Rostami Sh, Malekzadeh K, Kamranzadeh Foumani H, Mohammadi S, Nikbakht M. Arsenic trioxide and thalidomide combination induces autophagy along with apoptosis in acute myeloid cell lines. Cell J. 2020; 22(2): 193-202. doi: 10.22074/cellj.2020.6469.**

Introduction

Acute myeloid leukemia (AML) is a heterogeneous group of malignancies that is caused by uncontrolled proliferation of neoplastic cells in the bone marrow (1, 2). Approximately 50% of patients ultimately experience relapse after chemotherapy because of the presence of subsets of malignant cells that are not completely removed by treatment regimens (3). Various mechanisms are involved in development of cancers, including alterations in the expression of molecules which impair apoptosis and autophagy (4-6). The PI3K/Akt/ mTOR signalling loop is one of the most important pathways that is deregulated in many human cancers threatening survival of normal cells (6, 7). Hyper activation of the PI3K/Akt/mTOR signalling pathway is an unusual feature of AML patients (7, 8). Phosphatase and tensin homolog (*PTEN*) can negatively regulate the activity of PI3K pathway (9). *PTEN* is a critical negative regulator of PI3K signalling. Raf-MEK1/2-ERK1/2 pathway transmits responses to growth factors and cytokines. Ras/Raf-1/ERK1/2 and PI3K/Akt/mTOR signaling pathways are important regulators of *PTEN* that determines the cellular outcomes of its activation (10). In addition to genes which are involved in apoptosis, autophagy genes play key roles in pathogenesis of cancer. *mTOR* is a central regulator of autophagy with two separate complexes namely, *mTORC1* and *mTORC2*. *mTORC1* and *PI3K* are negative regulators of autophagy (11) (Fig.1). When autophagy process is initiated, *PI3K* binds to its core units, *BECLIN1* and simplify the usage of autophagy related 5-7-12 (*ATG5-7-12)* on the membranes (phagophores) to form autophagosomes (12).

Arsenic trioxide (ATO) targets various cellular functions through multiple molecular factors (13-15). ATO has numerous biological effects such as apoptotic and anti-proliferative activities (16). Thalidomide (THAL) has immunological effects and anti-angiogenesis effects on tumour growth and progression (17, 18). It was shown that THAL as a *VEGF* inhibitor, in combination with ATO has a synergistic impact on the inhibition of cell proliferation and promotion of apoptosis in AML cell line (19). Hence, the aim of this study was to explore the effect of a combination of ATO and THAL on apoptosis and expression levels of *VEGF* isoforms, *VEGFR1&2, PI3K, AKT, mTOR, PTEN, IL6, STAT3, B-RAF, RAF1, MEK1*, and *B-CL2* and some autophagy genes such as *BECLIN1, LC3-II, ULK1*, and *ATG5-7-12* in leukemic cell lines.

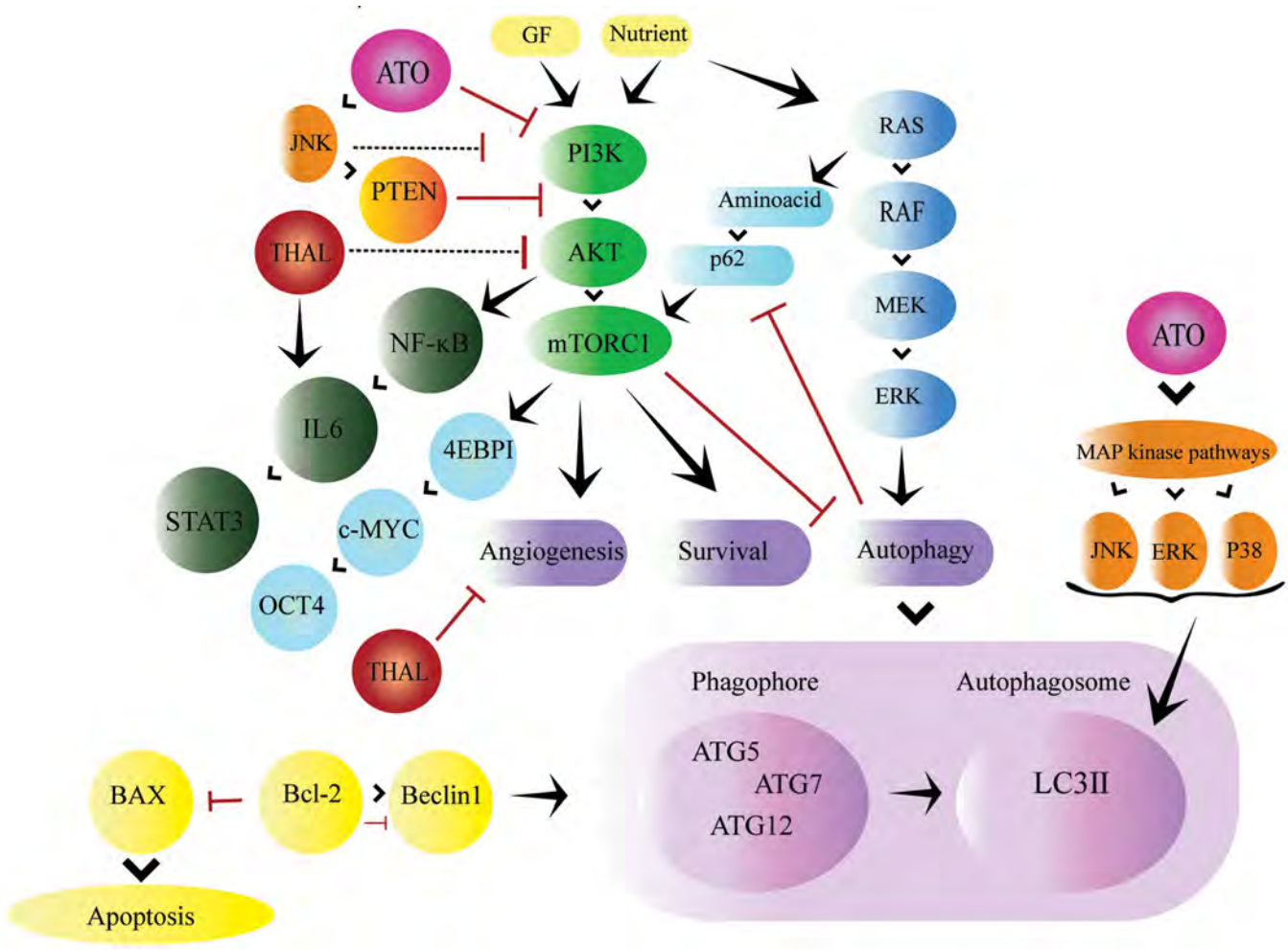

Fig.1: Overview of the PI3K/AKT/mTOR pathway in AML. The PI3K/AKT/mTOR pathway and other pathways related to AML, Inducing autophagy by inhibiting the *mTOR* pathway. Diagram shows that ATO promotes apoptotic mechanisms. Left, PI3K/Akt/NF-κB pathway permanently activated in the absence of ATO. Right, ATO by inducing *JNK* activation, can inhibit the PI3K/Akt/NF-κB signalling pathway. THAL has anti-angiogenesis effects on tumour growth and progression. THAL inhibits *IL6*. ATO/THAL by inhibition of *mTORC1* induces dephosphorylation of *ULK1* and subsequent *ULK1*-mediated phosphorylation of *ATG13*, *FIP200* and *ULK1* itself, inducing autophagosome synthesis. Release of *BCL-2* suppresses *BECLIN1* that induces autophagy through disruption of the *BCL-2/BCL- XL-BECLIN1* interaction. In case of existence of sufficient nutrients, *BECLIN1* binds to *BCL-2* or *BCL-XL*, and loses its ability to initiate autophagy. AML; Acute myeloid leukemia, ATO; Arsenic trioxide, and THAL; Thalidomide.

Material and Methods

Reagents

For this *in vitro* experimental study, THAL was purchased from Santa Cruz Company (Texas) and As_2O_3 (ATO) was obtained from Sina Darou Company (Iran).5- diphenyltetrazolium bromide (MTT) dye, Annexin V-FITC apoptosis detection kit, dimethyl sulfoxide (DMSO) and diethyl pyro carbonate (DEPC) treated water were purchased from Sigma-Aldrich Company (St. Louis, MO). RPMI 1640 medium and fetal bovine serum (FBS) were obtained from Gibco (Carlsbad, CA). cDNA synthesis kit and SYBR Premix Ex Taq™ were bought from Takara Biotechnology Co (Otsu, Japan).

Cell lines and cell culture

KG-1 and U937 were purchased from Pasteur Institute (Iran). U937 cells were cultured in RPMI 1640 medium which was supplemented with 10% FBS, 100 µg/mL penicillin and 100 µg/mL streptomycin. KG-1 cells were cultured in RPMI 1640 medium which was supplemented with 20% FBS, 100 µg/mL penicillin and 100 µg/ml streptomycin. Then, cells were incubated at 37˚C in a humidified atmosphere containing 5% CO_2. THAL was dissolved in DMSO, then dissolved in sterile double-distilled water. As_2O_3 was dissolved in distilled water. Each experiment was performed three time in triplicate.

Analysis of cell viability by MTT assay

KG-1 and U-937 cells (5×10^3 cells per well) were incubated in the absence or presence of THAL and ATO, in a final volume of 400 µl. After 24, 48 and 72 hours, 100 µl MTT reagent (5 mg/ml MTT in RPMI) was added to each well and incubated for 3 hours. Then, 100 µl DMSO was added to dissolve formazan precipitates. Then, in a 96-well plate (SPL, Life

Sciences, Pocheon, Korea), 100 µl of cell lysate were plated in triplicate, and the absorbance was read at 570 nm using an ELISA plate reader (Micro plate Reader; Bio Rad).

Analysis of cell apoptosis and cell viability by flow cytometry

KG-1 and U937 cells were seeded at the density of 3×10^5 cells per well in 12-well culture plates then were treated with selective doses, 1.618 µM and 1 µM concentration of ATO respectively in KG-1 and U937 and also 60 µM and 80 µM concentration of THAL in both cell lines. After 48 hours, cells were harvested and treated with Annexin/PI. AnnexinV staining was quantified by FACS Calibur Flow Cytometer analysis (BD-Biosciences, San Jose, CA, USA). Apoptosis (Annexin V+/PI− is early apoptosis and Annexin V+/PI+ is late apoptosis) and necrosis (Annexin V−/PI+) were investigated in this step.

Cell cycle analysis

KG-1 and U937 cells were seeded at the density of 3×105 cells per well in 12-well culture plates then were treated with selective doses, 1.618 µM and 1 µM concentration of ATO respectively in KG-1 and U937 and also 60 µM and 80 µM concentration of THAL in both cell lines. After that, cells fixed in 70% in ethanol and treated with PI. Cells were assessed by BD flow cytometer instrument and results were analyzed by Flowjow software. The apoptotic cells could predict from hypo-diploid sub G1/G1 DNA content.

Quantitative real-time polymerase chain reaction

KG-1 and U937 cells were seeded at the density of 5×10^5 cells per well in 6-well culture plates then were treated with selective doses, 1.618 µM and 1 µM concentration of ATO respectively in KG-1 and U937 cell lines and 80 µM and 60 µM concentration of THAL respectively in KG-1 and U937 cell lines. After that, total RNA was extracted by TriPure Isolation Reagent (Roche applied science, Germany) according to the manufacturer's instructions. The quality and quantity of total RNA was assessed spectrophotometrically by using Nano Drop ND-1000 (NanoDrop Technologies, Wilmington, DE), and stored at -80˚C. Complementary DNA (cDNA) was manufactured using RNA and cDNA synthesis kit. Real-time RT-PCR analysis was done using a light cycler instrument (Roche Diagnostic, Manheim, Germany) and SYBR Premix Ex Taq. A final volume of 20 µl including 2 µl of a 2-fold diluted cDNA, 10 pmol of primers mixture (0.5 µl of forward and reverse primers), 10 µl of SYBER, and 7 µl of distilled water, was used. PCR reaction included 3 main steps namely, denaturation, annealing and extension. Initial denaturation was done at 94˚C for 5 minutes. After that, denaturation was done at 94˚C for 30 second. In this step, double strands of DNA were separated into two single strands. In the annealing step, the temperature was lowered to enable the DNA primers attach to the template DNA at 50-56˚C for 45 seconds. During the extension, as the final step, the heat was increased to 72˚C to enable the new DNA to be made by a special Taq DNA polymerase enzyme for 1 minute per kb. At the end of PCR reaction, there was final extension at 72˚C for 5 minutes. Data were normalized against *HPRT* expression in each sample. Relative gene expression data were analyzed by $2^{-\Delta\Delta Ct}$ method. Sequences of primers are listed in TableS1 (See Supplementary Online Information at www.celljournal.org).

Statistical analysis

All experiments were repeated independently at least three times in triplicate, and the data are presented as mean ± SE. The results were compared using standard one-way analysis of variance (ANOVA). The diagrams were generated by GraphPad Prism 6.01 software. Significance was defined as *P<0.05, **P<0.01, and ***P<0.001.

Results

ATO and THAL inhibit cell proliferation

In KG1 and U937 cell lines, cytotoxic effect of ATO (0.4-5 µM) and THAL (5-100 µM) was investigated. Growth inhibitory effects of these concentrations of ATO/THAL were assessed by MTT for 24, 48 and 72 hours (Fig.2). Based on the results, half maximal inhibitory concentration (IC_{50}) values for ATO were 1 µM for U937 cells and 1.618 µM for KG-1 cells; IC_{50} values for THAL were 60 µM for U937 cells and 80 µM for KG-1 cells. The results showed that ATO and THAL had a significant cytotoxic effect on both cell lines in dose- and time-dependent manners. To investigate the synergistic activity of ATO and THAL (80 µM THAL/1.618 µM ATO for KG-1 and 60 µM THAL/1 µM ATO for U937), the viability of treated cells were assessed 24 and 48 and 72 hours post-treatments. Results obtained for 48 and 72 hours treatments were not significantly different. The combination therapy showed a significant effect on U937 and KG-1 cells.

Induction of apoptosis by ATO/THAL

We performed flow cytometry assay to investigate apoptotic effects of these compounds on AML cell lines. As seen in Figure 3, we observed an increase in the number of early and late apoptotic cells (Annexin+/PI-,+) and minimum percentage of necrosis (Annexin-/PI+) in treated cells as compared with control in both cell lines. Moreover, significant increases (61% in KG-1 and 88% in U937) in the number of apoptotic cells were seen in cells treated with a combination of ATO and THAL.

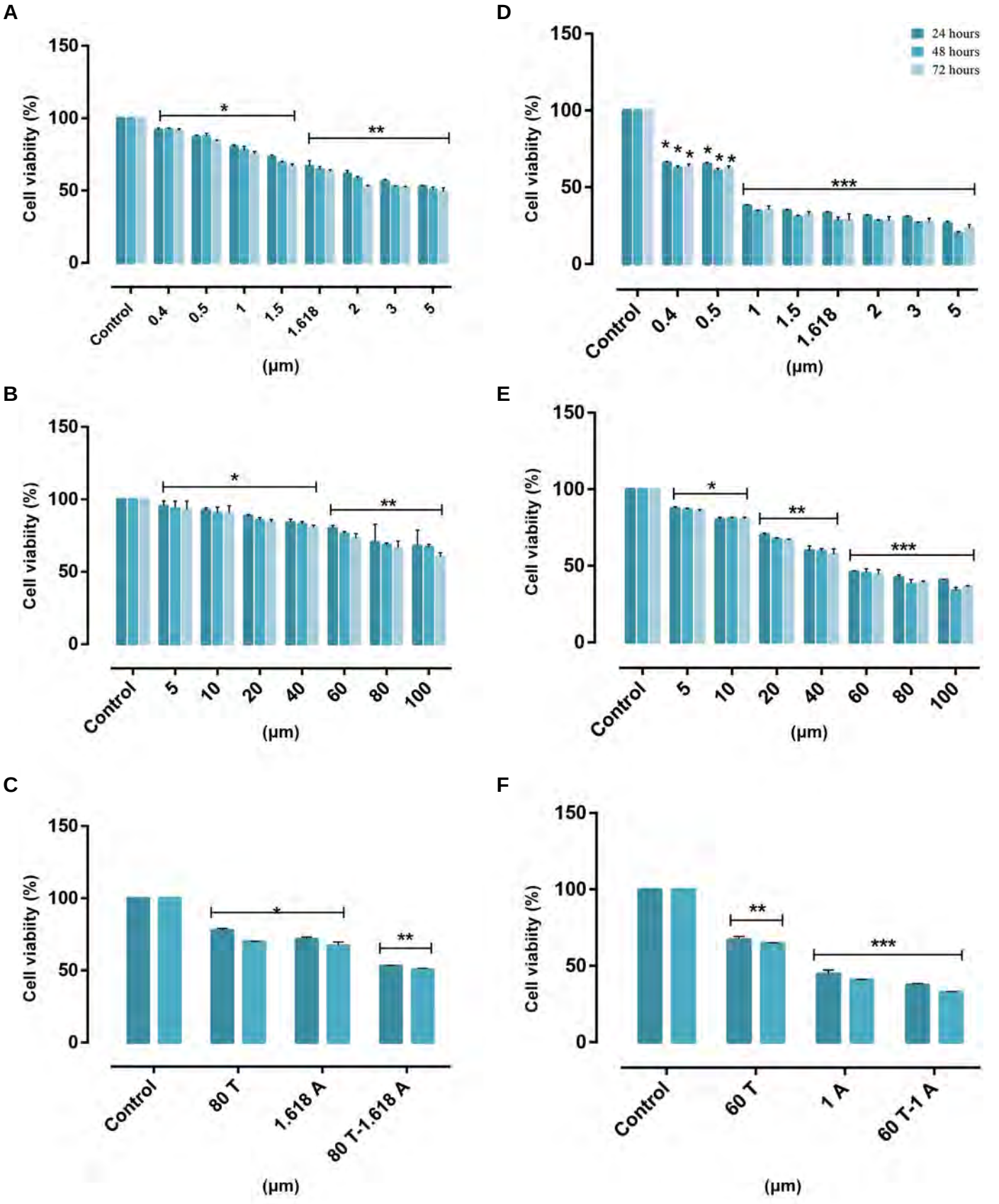

Fig.2: Cell viability in KG-1 and U937. Effects of ATO and THAL on cell viability in KG-1 and U937 cell lines. The anti-proliferative effects of ATO (0.4-5 µM), THAL (5-100 µM) and their combinations in both cell lines were assessed by MTT assay after 24, 48 and 72 hours of treatment. Results obtained following 48 and 72 hours treatment were not significantly different. **A.** Effect of ATO on KG-1 cells, **B.** Effect of THAL on KG-1 cells, **C.** Effect of ATO/THAL on KG-1 cells, **D.** Effect of ATO on U937 cells, **E.** Effect of THAL on U937 cells, and **F.** Effect of ATO/THAL on U937 cells. After detection of suitable doses for ATO (1.618 µM) and THAL (80 µM) for KG-1 and ATO (1 µM) and THAL (60 µM) for U937, effect of a combination of ATO and THAL was evaluated. Data are expressed as mean ± S.E of three independent experiments. Statistical significance was defined at *; P<0.05, **; P<0.01, and ***; P<0.001 compared to corresponding control. ATO; Arsenic trioxide and THAL; Thalidomide.

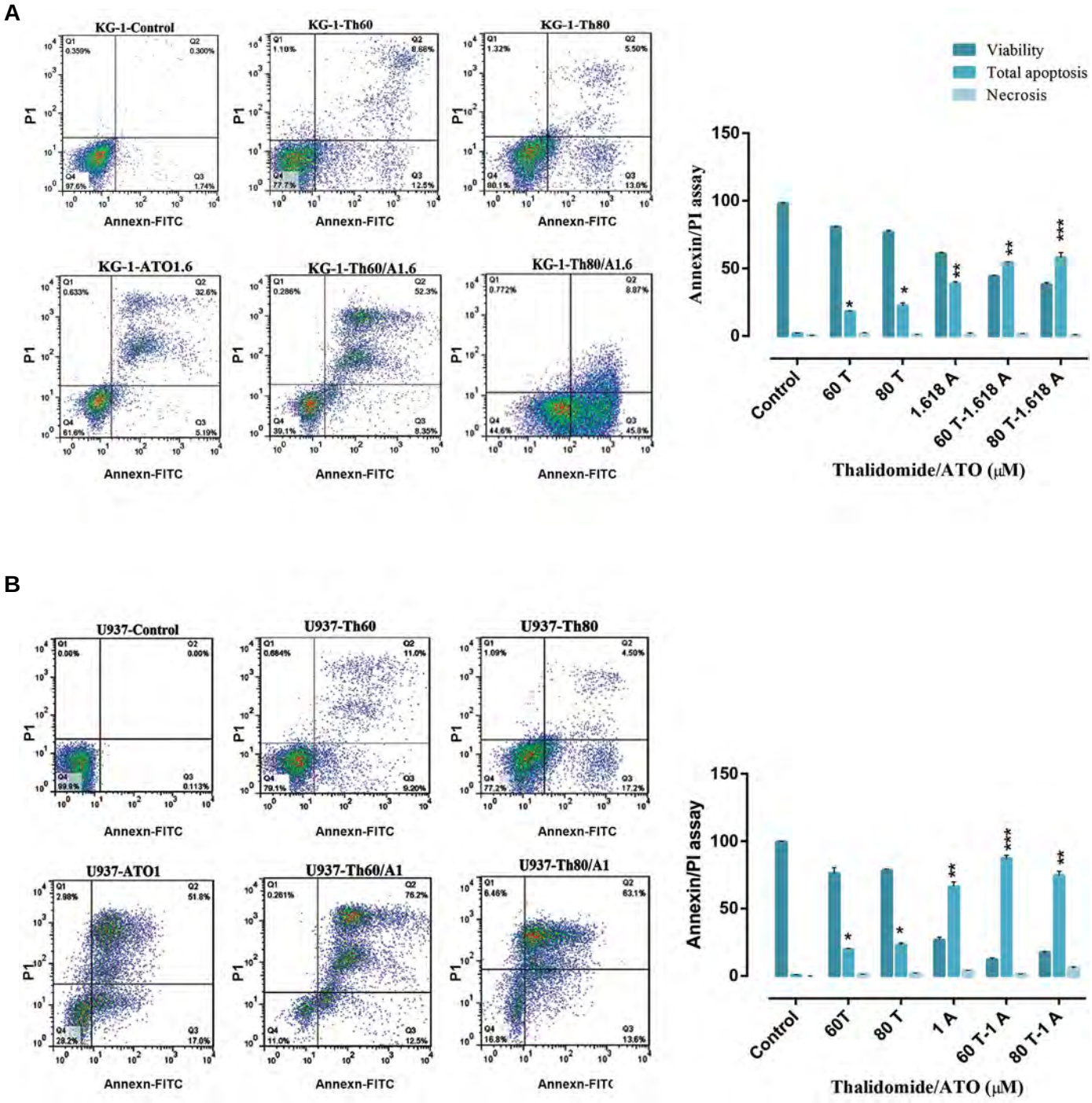

Fig.3: Flow cytometry analysis. **A.** Analysis of flow cytometry in KG-1 cells and **B.** Analysis of flow cytometry in U937 cells. KG-1 cells treated with ATO (1.618 μM) and THAL (80 μM) and their combination. U937 cells treated with ATO (1 μM) and THAL (60 μM) and their combination. Flow cytometry graphs contain the lower left quadrant that shows live cells and the upper left quadrant shows necrotic cells, the lower right shows early apoptotic cells and the upper right shows late apoptotic cells. Data are expressed as mean ± S.E of three independent experiments. Statistical significance was defined at *; P<0.05, **; P<0.01, and ***; P<0.001 compared to corresponding control. ATO; Arsenic trioxide and THAL; Thalidomide.

ATO/THAL induces SubG1/G1 arrest in AML cells

Cell cycle flow cytometry analysis was applied for cells treated with ATO and THAL to study ATO/THAL effects with respect to inducing cell cycle arrest Figure 4. Significant increases in the percentage of cells at SubG1/G1 were observed in a dose-dependent manner in KG-1 and U937 cells. Meanwhile, percentage of cells at G2 phase was reduced in all treated cells. Accordingly, it seems that ATO/THAL induced SubG1/G1 arrest in both cell lines (5.71-21.51% for KG-1 cell and 5.05-36.87% for U937 cell).

Real-time polymerase chain reaction

We analyzed expression levels of VEGF isoforms and receptors of *VEGF* (*VEGFR12* &), *PI3K*, *AKT*, *mTOR*, *PTEN*, *IL6*, *STAT3*, *MEK1*, *B-RAF*, *RAF1*, *BCL-2*, *BECLIN1*, *ULK1*, *LC3-II*, *ATG5*, *ATG7*, *ATG12*, *OCT4*, and *P62* by real-time PCR (Fig.5).

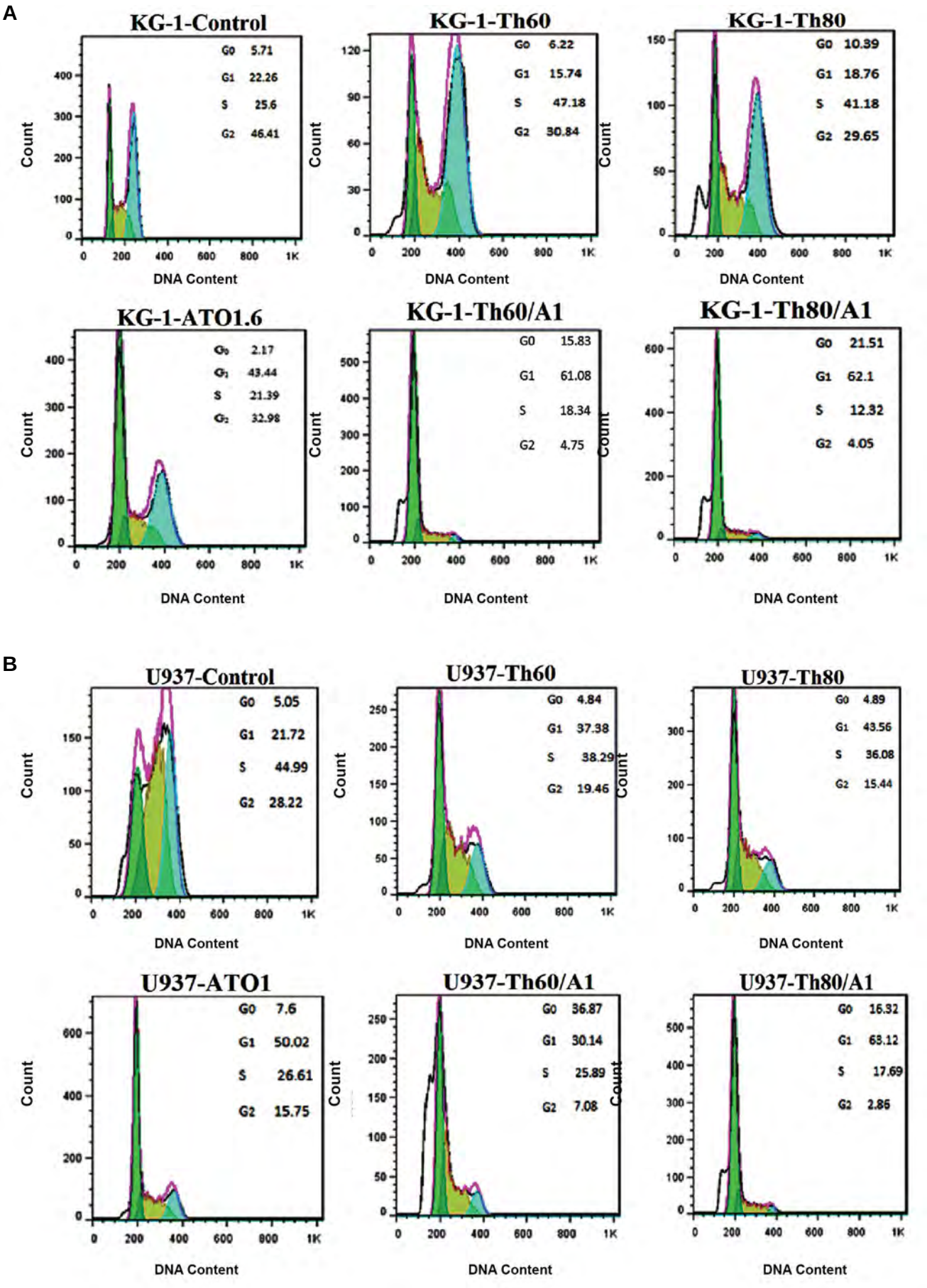

Fig.4: Cell cycle flow cytometry analysis of leukemia cells. **A.** KG-1 cell cycle flow cytometry and **B.** U937 cell cycle flow cytometry. Cells exposed to different concentrations of ATO and THAL for 48 hours, reduced number of cells at G2 phase and increased amount of cells at G1 phase. Data are expressed as mean ± S.E. of three independent experiments. ATO; Arsenic trioxide, and THAL; Thalidomide.

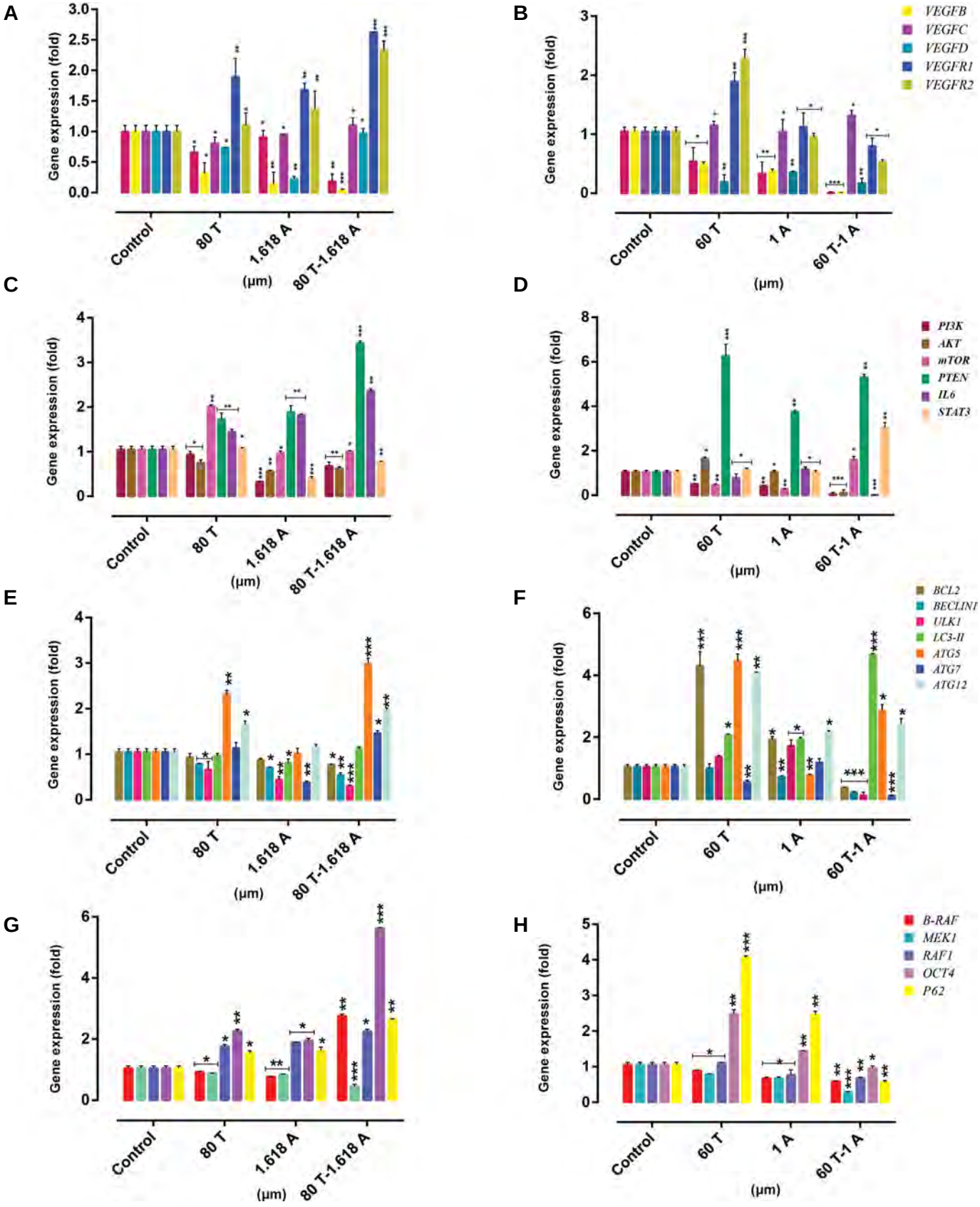

Fig.5: Examination of gene expression. The effects of ATO and THAL on the mRNA level of indicated genes in U937 cells. **A.** Effect of ATO and THAL on the expression level of *VEGF* genes in KG-1 cells. **B.** Effect of ATO and THAL on the expression level of *VEGF* genes in U937 cells, **C.** Effect of ATO and THAL on the expression level of genes that contribute to PI3K/AKT/mTOR pathway in KG-1 cells, **D.** Effect of ATO and THAL on the expression level of genes that contribute to PI3K/AKT/mTOR pathway in U937 cells, **E.** Effect of ATO and THAL on the expression level of autophagy genes in KG-1 cells, **F.** Effect of ATO and THAL on the expression level of autophagy genes in U937 cells, **G.** Effect of ATO and THAL on the expression level of *BRAF/MEK/RAF1/OCT4/P62* genes in KG-1 cells, and **H.** Effect of ATO and THAL on the expression level of *BRAF/MEK/RAF1/OCT4/P62* genes in U937 cells. For normalization of expression levels, *HPRT* was used. Values are given as mean ± S.E. of three independent experiments. Statistical significance was defined at *; P<0.05, **; P<0.01 and ***; P<0.001 compared to corresponding control. ATO; Arsenic trioxide and THAL; Thalidomide.

U937 cells were treated ATO (1 μM), THAL (60 μM) and their combination for 48 hours. We observed that the expression level of *VEGFA* and *VEGFB* significantly decreased and also the expression of VEGF*D* slightly decreased as compare with *VEGFA/B* when treated with each compound alone or their combination. But expression of *VEGFC* increased when cells were treated with each compound alone or with the combination of both; *VEGFR1* and *VEGFR2* expression increased when cells were treated with each compound alone but decreased when treated with the combination.

The expression level of *PI3K* and downstream genes were also investigated. We observed that the expression of *PI3K* and *IL6* decreased when treated with each compound alone or with the combination of both but *AKT* increased when treated with each compound alone and decreased with the combination of both compounds and *mTOR* expression contrary to *AKT*, decreased when treated with each compound alone and increased with the combination of both compounds and *STAT3* gene expression increased with the combination of both compounds. The expression of *PTEN* as a tumor suppressor, significantly increased after treatment with the combination of both compounds. We observed that the expression of *B-RAF* and *RAF-1* decreased following treatment with selective doses (ATO 1 μM and THAL 60 μM for U937) and their combination (ATO 1 μM /THAL 60 μM). Moreover, in this pathway, the expression of *MEK1* significantly decreased following treatment with the combination of both compounds. Furthermore, the expression of *BCL-2* increased when treated with each compound alone, while significantly decreased following treatment with the combination of both compounds. With respect to autophagy-related genes, we observed that the expression of *ULK1* and *BECLIN1* decreased after treatment while the expression of *LC3-II* increased following treatment. Furthermore, the expression of *ATG5* and *ATG12* increased following treatment with THAL, decreased following treatment with ATO and slightly increased following treatment with the combination of these compounds while the expression of *ATG7* significantly decreased following treatment with the combination of these compounds.

KG-1 cells were treated with ATO (1.618 μM), THAL (80 μM) and also their combination for 48h. Our data indicated that the expression of *VEGFA* and *VEGFB* significantly decreased but *VEGF-C* and *VEGF-D* slightly increased while the expression of *VEGFR1* and *VEGFR2* significantly increased following treatment with each compound alone and their combination. Also the expression of *PI3K* and *AKT* in KG-1 cells decreased and *mTOR* slightly increased after treatment with cited doses. The expression of *PTEN* as a tumor suppressor significantly increased after treatment with each compound alone and their combination. In addition, *IL6* expression increased with each compound alone and their combination in KG-1 cells. The expression of *STAT3* slightly increased after treatment with the combination of the two compounds.

Expression level of *B-RAF* and *RAF1* increased when treated with each compound alone but *MEK1* decreased. Furthermore, the expression of *BCL-2* slightly decreased. In addition, the expression of *BECLIN1* and *ULK1* as autophagy activator, decreased by each compound alone in KG-1 cells while the expression of *LC3-II* (a marker of the presence of completed autophagosomes) increased. Furthermore, the expression of *ATG5, ATG7,* and *ATG12* increased in combination of two compounds.

Discussion

The best known regulator of angiogenesis is *VEGF*, which regulates endothelial proliferation, permeability, and survival (20). Most important member of the *VEGF* family is *VEGFA* (21). In our previous study, we demonstrated that ATO/THAL downregulates the expression of *VEGFA* and *VEGFB* in KG-1 cell line and downregulates the expression of *VEGFA , VEGFB* and *VEGFD* in U937 cell line (19).

Kruse et al. (22) reported that THAL inhibits angiogenesis by suppression of basic fibroblast growth factor (*bFGF*) and *VEGF* genes. Keifer et al. (23) reported THAL also inhibits *NF-κB,* a critical regulator of inflammatory processes. Gockel et al. (24) illustrated that THAL induces apoptosis by inhibition of *PI3K-AKT*. In this research, we found that a combination of ATO/THAL significantly reduces the viability of U937 and KG-1 cells while increases cell apoptosis. ATO with anti-leukemic activity in AML cell lines, enhanced the antitumor activity of THAL in both U937 and KG-1 cell population when used in combination.

ATO is used for treatment of many types of hematologic malignancies (25-27). In this study, we observed that cytotoxicity of ATO and induction of apoptosis in both U937 and KG-1 cell lines follow a dose and time-dependent pattern. Our results indicated that ATO can influence cell proliferation and cell death pathway. In 2010, Redondo-Muñoz et al. (28) and Goussetis and Platanias (29) in two studies reported that ATO induces cell apoptosis in chronic lymphocytic leukemia (CLL) that involved upregulation of *PTEN* and inhibition of the PI3K/Akt/NF-κB as a survival pathway Goussetis and Platanias (29) also stated that ATO induces upregulation of *PTEN* but downregulation of X-linked inhibitor of apoptosis protein *(XIAP)*. Nayak et al. (30) reported that ATO in combination with ATRA leads to decreased activation of *AKT*. Our results showed that ATO inhibits *PI3K/AKT/mTOR* but upregulates *PTEN* gene expression.

Previous study reported that different *MAPK* cascades are activated during treatment of cells with ATO, including *P38, MAP* (31), *JNK* (32), and *ERK* (33). Nayak et al. (30) showed that ATO can promote *MAPK* pathways as components of a stress response. We studied *B-RAF/MEK1/RAF1* of *MAPK* signalling for investigating the effect of ATO on this pathway, specially the potential synergistic effects of THAL and ATO on these three central kinases. Goussetis et al reported that ATO can

activate autophagy in a leukemic cell population through induction of autophagy process by activation of the *MAPK* pathway (34). We observed that *B-RAF, MEK 1* and *RAF1* expression was increased by ATO and THAL and their combination in KG-1 cell line. In addition, the expression level of *MEK1,* and *RAF1* decreased following treatment of U937 cell line with a combination of the compounds.

ATO prevents cell proliferation and induces apoptosis in some cancer cells. Recently, some reports showed the effects of ATO on autophagy (35-37). ATO is a powerful inducer of autophagy in acute leukemia cells. ATO by inhibition of *mTOR,* can induce autophagy. Moreover, activation of *MAPK* pathway by ATO can induce autophagy pathway. Verma et al. (31) showed that ATO also induces autophagy in APL cells. Autophagy is mainly controlled by *mTOR* (11). The *mTOR* acts as a suppressor of autophagy in response to nutrient and growth-factor accessibility. Karantza-Wadsworth et al. (38) and Boya et al. (39) showed that autophagy can increase apoptosis in cancer cells. Kruse et al. (22) illustrated that ATO up regulates *LC3-II* in KT1 cells. Chiu et al. (40) reported that ATO treatment increases the expression of LC3-II, p62, Beclin 1, Atg5, and Atg5-12 proteins.

In the present study, we investigated the expression of *Beclin1, LC3-II, ULK1* and *ATG5-7-12* as autophagy activators. Expression level of *BECLIN1* and *ULK1* decreased in U937 cell line whereas the expression of *LC3-II* increased following treatment with a combination of the compounds.

One of the important gene associated with apoptosis is *BCL-2,* which is a suppressor of programmed cell death. The expression of *BCL-2* declined following ATO treatment in U118-MG cells (40). Our results showed that the level of *BCL-2* gene decreases following treatment with a combination of ATO and THAL.

Conclusion

This study demonstrated that ATO in combination with THAL promotes apoptotic mechanisms and by inhibition of PI3K/Akt/mTOR signalling pathway, promotes autophagy in AML cells. These findings implied that ATO/THAL may be used as a novel therapeutic agent for inhibition of AML cells.

Acknowledgements

The study was financially supported by the Hematology, Oncology and Stem Cell Transplantation Research Center, Tehran University of Medical Sciences (HORCSCT). There is no conflict of interest associated with this study.

Authors' Contributions

M.M.K., M.N., S.M.; Contributed to wrote the manuscript, all experimental work, data, statistical analysis, and interpretation of data. M.N., S.M.; Contributed to conception and design. A.H., M.S., B.C., Sh.R., K.M., H.K.F.; Contributed to perform the research and assisting in experimental work. Drafted the manuscript, revising by M.N. and S.M. All authors read and approved the final manuscript.

References

1. Estey E, Döhner H. Acute myeloid leukaemia. Lancet. 2006; 368(9550): 1894-1907.
2. Mohammadi S, Ghaffari SH, Shaiegan M, Nikogoftar Zarif M, Nikbakht M, Alimoghaddam K, et al. Curcumin Veto the effects of osteopontin (OPN) Specific inhibitor on leukemic stem cell colony forming potential via promotion of OPN overexpression. Int J Hematol Oncol Stem Cell Res. 2016; 10(3): 120-129.
3. Walter RB, Kantarjian HM, Huang X, Pierce SA, Sun Z, Gundacker HM, et al. Effect of complete remission and responses less than complete remission on survival in acute myeloid leukemia: a combined Eastern Cooperative Oncology Group, Southwest Oncology Group, and M. D. Anderson Cancer Center Study. J Clin Oncol. 2010; 28(10): 1766-1771.
4. Mohammadi S, Zahedpanah M, Ghaffari SH, Shaiegan M, Nikbakht M, Nikugoftar M. Osteopontin plays a unique role in resistance of CD34+/CD123+ human leukemia cell lines KG1a to parthenolide. Life Sci. 2017; 189: 89-95.
5. Yuan TL, Cantley LC. PI3K pathway alterations in cancer: variations on a theme. Oncogene. 2008; 27(41): 5497-5510.
6. Mohammadi S, Ghaffari SH, Shaiegan M, Zarif MN, Nikbakht M, Akbari Birgani S, et al. Acquired expression of osteopontin selectively promotes enrichment of leukemia stem cells through AKT/mTOR/PTEN/beta-catenin pathways in AML cells. Life Sci. 2016; 152: 190-198.
7. Zahed Panah M, Nikbakht M, Sajjadi SM, Rostami S, Norooznezhad AH, Kamranzadeh Fumani H, et al. Anti-apoptotic effects of osteopontin via the up-regulation of AKT/mTOR/beta-catenin loop in acute myeloid leukemia cells. Int J Hematol Oncol Stem Cell Res. 2017; 11(2): 148-157.
8. Martelli AM, Tazzari PL, Evangelisti C, Chiarini F, Blalock WL, Billi AM, et al. Targeting the phosphatidylinositol 3-kinase/Akt/mammalian target of rapamycin module for acute myelogenous leukemia therapy: from bench to bedside. Curr Med Chem. 2007; 14(19): 2009-2023.
9. Keniry M, Parsons R. The role of PTEN signaling perturbations in cancer and in targeted therapy. Oncogene. 2008; 27(41): 5477-5485.
10. Niault TS, Baccarini M. Targets of Raf in tumorigenesis. Carcinogenesis. 2010; 31(7): 1165-1174.
11. Klionsky DJ. Autophagy: from phenomenology to molecular understanding in less than a decade. Nat Rev Mol Cell Biol. 2007; 8(11): 931-937.
12. Klionsky DJ. The molecular machinery of autophagy: unanswered questions. J Cell Sci. 2005; 118(Pt 1): 7-18.
13. Emadi A, Gore SD. Arsenic trioxide-an old drug rediscovered. Blood Rev. 2010; 24(4-5): 191-199.
14. Rodriguez-Ariza A, Lopez-Pedrera C, Aranda E, Barbarroja N. VEGF targeted therapy in acute myeloid leukemia. Crit Rev Oncol Hematol. 2011; 80(2): 241-256.
15. Haghi A, Mohammadi S, Heshmati M, Ghavamzadeh A, Nikbakht M. Anti-vascular endothelial growth factor effects of sorafenib and arsenic trioxide in acute myeloid leukemia cell lines. Asian Pac J Cancer Prev. 2017; 18(6): 1655-1661.
16. Miller WH Jr, Schipper HM, Lee JS, Singer J, Waxman S. Mechanisms of action of arsenic trioxide. Cancer Res. 2002; 62(14): 3893-3903.
17. Salemi M, Ghavamzadeh A, Nikbakht M. Anti-Vascular endothelial growth factor targeting by curcumin and thalidomide in acute myeloid leukemia cells. Asian Pac J Cancer Prev. 2017; 18(11): 3055-3061.
18. Barnhill RL, Doll NJ, Millikan LE, Hastings RC. Studies on the anti-inflammatory properties of thalidomide: effects on polymorphonuclear leukocytes and monocytes. J Am Acad Dermatol. 1984; 11(5 Pt 1): 814-819.
19. Mohammadi Kian M, Mohammadi S, Tavallaei M, Chahardouli B, Rostami S, Zahedpanah M, et al. Inhibitory effects of arsenic trioxide and thalidomide on angiogenesis and vascular endothelial growth factor expression in leukemia cells. Asian Pac J Cancer Prev. 2018; 19(4): 1127-1134.
20. Hicklin DJ, Ellis LM. Role of the vascular endothelial growth factor pathway in tumor growth and angiogenesis. J Clin Oncol. 2005;

23(5): 1011-1027.
21. Keyt BA, Berleau LT, Nguyen HV, Chen H, Heinsohn H, Vandlen R, et al. The carboxyl-terminal domain (111-165) of vascular endothelial growth factor is critical for its mitogenic potency. J Biol Chem. 1996; 271(13): 7788-7795.
22. Kruse FE, Joussen AM, Rohrschneider K, Becker MD, Völcker HE. Thalidomide inhibits corneal angiogenesis induced by vascular endothelial growth factor. Graefes Arch Clin Exp Ophthalmol. 1998; 236(6): 461-466.
23. Keifer JA, Guttridge DC, Ashburner BP, Baldwin AS Jr. Inhibition of NF-kappa B activity by thalidomide through suppression of IkappaB kinase activity. J Biol Chem. 2001; 276(25): 22382-22387.
24. Gockel HR, Lügering A, Heidemann J, Schmidt M, Domschke W, Kucharzik T, et al. Thalidomide induces apoptosis in human monocytes by using a cytochrome c-dependent pathway. J Immunol. 2004; 172(8): 5103-5109.
25. Berenson JR, Boccia R, Siegel D, Bozdech M, Bessudo A, Stadtmauer E, et al. Efficacy and safety of melphalan, arsenic trioxide and ascorbic acid combination therapy in patients with relapsed or refractory multiple myeloma: a prospective, multicentre, phase II, single-arm study. Br J Haematol. 2006; 135(2): 174-183.
26. Wang Z-Y, Chen Z. Acute promyelocytic leukemia: from highly fatal to highly curable. Blood. 2008; 111(5): 2505-2515.
27. Zheng WL, Zhang GS, Xu YX, Shen JK, Dai CW, Pei MF. Arsenic trioxide, thalidomide and retinoid acid combination therapy in higher risk myelodysplastic syndrome patients. Leuk Res. 2008; 32(2): 251-254.
28. Redondo-Muñoz J, Escobar-Díaz E, del Cerro MH, Pandiella A, Terol MJ, García-Marco JA, et al. Induction of B-chronic lymphocytic leukemia cell apoptosis by arsenic trioxide involves suppression of the phosphoinositide 3-kinase/Akt survival pathway via c-jun-NH2 terminal kinase activation and PTEN upregulation. Clin Cancer Res. 2010; 16(17): 4382-4391.
29. Goussetis DJ, Platanias LC. Arsenic trioxide and the phosphoinositide 3-kinase/akt pathway in chronic lymphocytic leukemia. Clin Cancer Res. 2010; 16(17): 4311-4312.
30. Nayak S, Shen M, Bunaciu RP, Bloom SE, Varner JD, Yen A. Arsenic trioxide cooperates with all trans retinoic acid to enhance mitogen-activated protein kinase activation and differentiation in PML-RARalpha negative human myeloblastic leukemia cells. Leuk Lymphoma. 2010; 51(9): 1734-1747.
31. Verma A, Mohindru M, Deb DK, Sassano A, Kambhampati S, Ravandi F, et al. Activation of Rac1 and the p38 mitogen-activated protein kinase pathway in response to arsenic trioxide. J Biol Chem. 2002; 277(47): 44988-44995.
32. Davison K, Mann KK, Waxman S, Miller WH Jr. JNK activation is a mediator of arsenic trioxide-induced apoptosis in acute promyelocytic leukemia cells. Blood. 2004; 103(9): 3496-3502.
33. Tanaka-Kagawa T, Hanioka N, Yoshida H, Jinno H, Ando M. Arsenite and arsenate activate extracellular signal-regulated kinases 1/2 by an epidermal growth factor receptor-mediated pathway in normal human keratinocytes. Br J Dermatol. 2003; 149(6): 1116-1127.
34. Goussetis DJ, Gounaris E, Platanias LC. BCR-ABL1-induced leukemogenesis and autophagic targeting by arsenic trioxide. Autophagy. 2013; 9(1): 93-94.
35. Kanzawa T, Kondo Y, Ito H, Kondo S, Germano I. Induction of autophagic cell death in malignant glioma cells by arsenic trioxide. Cancer Res. 2003; 63(9): 2103-2108.
36. Qian W, Liu J, Jin J, Ni W, Xu W. Arsenic trioxide induces not only apoptosis but also autophagic cell death in leukemia cell lines via up-regulation of Beclin-1. Leuk Res. 2007; 31(3): 329-339.
37. Goussetis DJ, Altman JK, Glaser H, McNeer JL, Tallman MS, Platanias LC. Autophagy is a critical mechanism for the induction of the antileukemic effects of arsenic trioxide. J Biol Chem. 2010; 285(39): 29989-29997.
38. Karantza-Wadsworth V, Patel S, Kravchuk O, Chen G, Mathew R, Jin S, et al. Autophagy mitigates metabolic stress and genome damage in mammary tumorigenesis. Genes Dev. 2007; 21(13): 1621-1635.
39. Boya P, González-Polo RA, Casares N, Perfettini JL, Dessen P, Larochette N, et al. Inhibition of macroautophagy triggers apoptosis. Mol Cell Biol. 2005; 25(3): 1025-1040.
40. Chiu HW, Ho YS, Wang YJ. Arsenic trioxide induces autophagy and apoptosis in human glioma cells in vitro and in vivo through downregulation of survivin. J Mol Med (Berl). 2011; 89(9): 927-941.

Original Article

In Utero Exposure to Gestational Diabetes Alters DNA Methylation and Gene Expression of *CDKN2A/B* in Langerhans Islets of Rat Offspring

Zahra Nazari, Ph.D.[1], Alireza Shahryari, M.Sc.[2], Soraya Ghafari, M.Sc.[3], Mohammad Nabiuni, Ph.D.[4], Mohammad Jafar Golalipour, Ph.D.[3]*

1. Department of Biology, Faculty of Sciences, Golestan University, Gorgan, Iran
2. Stem Cell Research Center, Faculty of Medicine, Golestan University of Medical Sciences, Gorgan, Iran
3. Congenital Malformations Research Center, Golestan University of Medical Sciences, Gorgan, Iran
4. Department of Cell and Molecular Biology, Faculty of Biological Sciences, Kharazmi University, Tehran, Iran

**Corresponding Address: P.O.Box: 49175-1141, Congenital Malformations Research Center, Golestan University of Medical Sciences, Gorgan, Iran*
Email: dr.golalipour@goums.ac.ir

Received: 2/January/2019, Accepted: 9/March/2019

Abstract

Objective: DNA methylation, a major epigenetic reprogramming mechanism, contributes to the increased prevalence of type 2 diabetes mellitus (T2DM). Based on genome-wide association studies, polymorphisms in *CDKN2A/B* are associated with T2DM. Our previous studies showed that gestational diabetes mellitus (GDM) causes apoptosis in β-cells, leading to a reduction in their number in pancreatic tissue of GDM-exposed adult rat offspring. The aim of this study was to examine the impact of intrauterine exposure to GDM on DNA methylation, mRNA transcription, as well as protein expression of these factors in the pancreatic islets of Wistar rat offspring. Our hypothesis was that the morphological changes seen in our previous study might have been caused by aberrant methylation and expression of *CDKN2A/B*.

Materials and Methods: In this experimental study, we delineated DNA methylation patterns, mRNA transcription and protein expression level of *CDKN2A/B* in the pancreatic islets of 15-week-old rat offspring of streptozotocin-induced GDM dams. We performed bisulfite sequencing to determine the DNA methylation patterns of CpGs in candidate promoter regions of *CDKN2A/B.* Furthermore, we compared the levels of mRNA transcripts as well as the cell cycle inhibitory proteins P15 and P16 in two groups by qPCR and western blotting, respectively.

Results: Our results demonstrated that hypomethylation of CpG sites in the vicinity of *CDKN2A* and *CDKN2B* genes is positively related to increased levels of *CDKN2A/B* mRNA and protein in islets of Langerhans in the GDM offspring. The average percentage of CDKN2A promoter methylation was significantly lower in GDM group compared to the controls (P<0.01).

Conclusion: We postulate that GDM is likely to exert its adverse effects on pancreatic β-cells of offspring through hypomethylation of the *CDKN2A/B* promoter. Abnormal methylation of these genes may have a link with β-cell dysfunction and diabetes. These data potentially lead to a novel approach to the treatment of T2DM.

Keywords: DNA Methylation, Gestational Diabetes, Islets of Langerhans

Cell Journal(Yakhteh), Vol 22, No 2, July-September (Summer) 2020, Pages: 203-211

Citation: Nazari Z, Shahryari A, Ghafari S, Nabiuni M, Golalipour MJ. In utero exposure to gestational diabetes alters DNA methylation and gene expression of CDKN2A/B in langerhans islets of rat offspring. Cell J. 2020; 22(2): 203-211. doi: 10.22074/cellj.2020.6699.

Introduction

Gestational diabetes mellitus (GDM) is generally defined as hyperglycemia that is first recognized during pregnancy. GDM affects up to one in seven pregnancies worldwide (1). It is often associated with further pregnancy complications like preeclampsia or preterm delivery. Additionally, about 50% of the female patients suffering from GDM are likely to develop overt diabetes (2). In Addition to having adverse consequences for mothers, GDM is also associated with a high vulnerability to facing short-term detrimental after-effects such as macrosomia, neonatal hypoglycemia and neonatal cardiac dysfunction, as well as long-term difficulties including lifelong obesity and type 2 diabetes mellitus (T2DM) in the offspring (3-5). It has been demonstrated that animal offspring of diabetic mothers overtly develop diabetes later in life (6-8). A study carried out in the US has shown that 47.2% of diabetic cases among younger people could be attributed to diabetes or obesity of their mothers during her pregnancy (9). In animal models of GDM, a decline in insulin secretion as well as β-cell impairment has been observed in mature offspring (6, 7). Our group previously investigated the effect of GDM on morphological and histological features of pancreas in adult rat offspring. We demonstrated that GDM causes a significant reduction in β-cell mass, islet number and islet diameter in adult rat offspring (8). Our previous data also revealed that in rats, offspring of GDM mothers have more apoptotic β-cells compared to the controls (10).

Currently, little is known about how GDM-exposure contributes to the susceptibility to diabetes development in the offspring. Many research studies link the cell cycle regulators like cyclin-dependent kinase 4 (*Cdk4*) and retinoblastoma protein (*pRB*) to the risk of developing diabetes. *CDK4-pRB-E2F1* pathway has direct effects

on proliferation and insulin secretory capacity of β-cells (10-13). In our previous study on the offspring of GDM rats, we showed that GDM downregulates CDK4-pRB-E2F1 pathway in Langerhans islets (14). Proteins of the INK4 family, like *CDKN2A* and *CDKN2B* (encoding the cell cycle inhibitory proteins $p16^{INK4b}$ and $p15^{INK4a}$, respectively), can negatively regulate the activity of Cdk4 and subsequently block cell cycle progression. This indicates that upregulation of *CDKN2A/CDKN2B* genes may restrict the *CDK4-pRB-E2F1* pathway as well as β-cell proliferation. Other studies have identified novel T2DM susceptibility loci within the *CDKN2A/B* gene regions (chromosome 9p21 in humans and chromosome 5q32 in rats) (15, 16).

Current studies link DNA methylation with both type 1 and type 2 diabetes, at least partially through changes in the β-cell proliferation (17-20). Recent works have however shifted the focus to the effects of intrauterine exposure to hyperglycemia on DNA methylation of genes important in β-cell proliferation and function, which can increase the risk of diabetes in the offspring (21, 22).

In the same line as our previous studies on the effects of GDM on histological, morphological and molecular aspects of pancreas in the offspring (8, 9, 12), in the present study we evaluated the impact of streptozotocin (STZ)-induced GDM on DNA methylation and gene expression of *CDKN2A/B* in pancreatic islets of adult offspring in Wistar rats. We postulated that intrauterine hyperglycemic environment affects the β-cells of the offspring by the loss of *CDKN2A/B* methylation. We performed targeted-bisulfite sequencing to evaluate the CpG islands methylation levels in the regulatory regions of *CDKN2A* and *CDKN2B* in the pancreatic islets of the offspring. In addition, mRNA expression of *CDKN2A/B* and protein levels of p15 and p16 (proteins encoded by *CDKN2B* and *CDKN2A*, respectively) were analyzed by qPCR and western blotting.

Materials and Methods

Animals

This research was an experimental study, in which a total of 40 female and 15 male Wistar rats with an average age of 10-12 weeks were utilized. The animals were obtained from Golestan University of Medical Sciences, Gorgan, Iran. All animal procedures presented in this study adhered to the guidelines proposed by the Institutional Animal Care and Use Committee at Golestan University of Medical Sciences, Gorgan, Iran (code: IR.GOUMS.REC.1394.247).

Induction of experimental gestational diabetes mellitus

As many as 14 female rats were independently paired with a male rat for the purpose of breeding. Following copulation, observation of vaginal plaques was considered as the day zero of gestation. Then, they were equally randomized into control and GDM group. Animals in the GDM group received a single dose of STZ solution through intraperitoneal injection (40 mg/kg bw prepared freshly in citrate buffer, 0.1 mol/L) on day zero of gestation, while the control group received a similar volume of citrate buffer only. We administrated STZ on day zero of gestation because its administration before pregnancy has adverse effects on mating behavior. On the other hand, STZ has a half-life of about five minutes, so it is unlikely that exposure to STZ on day zero affects the earliest stages of embryogenesis. 72 hours after STZ administration, tail incision method was used to measure fasting blood glucose level using a glucometer (ACCU-CHEK Glucometer, Roche Diagnostics). Rats with high serum glucose levels in the range of 120-250 mg/dl were chosen and considered as diabetic models (23). Following spontaneous delivery, pups were allowed to mature for 15 weeks. As for investigation of the effect of GDM during embryonic period (not the effect of breastfeeding by diabetic mothers) on pancreas development, all control and offspring of gestational diabetes (OGD) infants were milked by normal mothers. OGD and control groups were sacrificed and their pancreatic tissues were collected and processed for isolation of islets of Langerhans.

Islets of Langerhans isolation

Collagenase digestion technique was used for isolating pancreatic islets from the control and OGD groups (24). In summary, cannula was inserted into the common bile duct. Digestion solution, containing 2.0 ml of 0.2 mg/ liberase TL or liberase Thermolysin Low (Roche, USA) and 10 pg/ml DNase (Takara, Japan) in serum-free Roswell Park Memorial Institute1640 medium (RPMI 1640 medium, Invitrogen, Germany), was injected into the cannula. Pancreas were placed in a 1.5 ml microtube and incubated at 37˚C for 15 minutes. The tubes were later filled with 10 ml of RPMI 1640 containing 10% fetal bovine serum (FBS, Invitrogen, Germany) serum and were kept on ice for 5 minutes to allow for enzyme deactivation. Following a phase of centrifugation at 800 RPM for 2 minutes, the islets of Langerhans were isolated through centrifugation on a Ficoll gradient (Sigma-Aldrich, USA). The islets were then gathered from the histopaque/media interface and passed through a 100-µm cell strainer (BD Falcon). Finally, the pancreatic islets were rinsed and stored at -80˚C until further extractions. The above procedure was repeated for each animal.

RNA, DNA and protein extractions from islets of langerhans

By applying the total RNA purification kit (Jena Bioscience, Germany), total RNA was elicited from the pancreatic islets. All islets from 5 rats were pooled to create a uniform sample for different extractions. DNA was isolated using the NucleoSpin Tissue XS kit (MN, Germany). Both DNA/RNA quantity and purity were calculated by NanoDrop ND-1000 spectrophotometer,

while RNA integrity was backed up by showing the intact 28s and 18s bands on gel electrophoresis using 1% agarose gels. Furthermore, total protein from pancreatic islets of the control and GDM offspring were obtained using a total protein extraction kit as specified by the manufacturer's directions (Merck Millipore, Germany). The Pierce BCA protein assay kit (Thermo Fisher Scientific) was used to measure protein concentration from total cell lysates.

Bisulfite-specific polymerase chain reaction and Sanger sequencing

Using the Zymo EZ DNA Methylation Gold Kit (Zymo Research, USA), bisulfite treatment was added to 500 ng of genomic DNA, as instructed by the manufacturer. Primers for detecting the methylation pattern of the *CDKN2A* and *CDKN2B* promoters, which are listed in Table 1, were designed by Bisulfite Primer Seeker (Zymo Research, USA) software. Eighteen CpG sites, located between -161 and +281 bp of the CDKN2A promoter and 39 CpG sites, located between -109 and +285 bp of the *CDKN2B* promoter were investigated with specific primers. Amplification of bisulfite converted DNA was performed using EpiTaq HS kit (for bisulfite-treated DNA, Takara, Japan). The thermal cycling phases included a preparatory denaturation at 98˚C lasting for 10 seconds as well as a two-step amplification program of 35 cycles at 55˚C and 72˚C each for 30 seconds. Bisulfite-amplified PCR products were refined by taking advantage of a AccuPrep PCR Purification Kit (Bioneer) and were later directly sequenced using an automatic sequencer (ABI PRISM-77). We derived two DNA sequence per animal for a total of n=6 sequenced samples for OGD and controls. The aligned reads and levels of methylation in both OGD and control groups were visualized using the pairwise sequence alignment online software (https://www.ebi.ac.uk/Tools/psa/).

Quantitative polymerase chain reaction

Islets of Langerhans RNA samples were reverse-transcribed using prime script RT reagent kit (Takara, Japan). Primers for respective genes were designed using the PerlPrimer software (Bio-Rad, USA) and synthesized by the Metabion Company (http://www.metabion.com). The oligonucleotide sequences of primers utilized for qPCR are presented in Table 1. The quantitative polymerase chain reaction (qPCR) was carried out in the Applied Biosystems 7300 Real-Time PCR System (Life Technologies, USA) with the SYBR-Green PCR Master Mix kit (Takara, Japan). We used beta-actin as the housekeeping gene and cDNA from offspring islets of the control group as calibrator. The expression level for each sample was measured using the cycle threshold (Ct) value while relative mRNA expression was calculated using the $2^{-\Delta\Delta Ct}$ formula. All real-time PCR experiments were conducted in triplicates.

Western blot analysis

An immunoblot assay was evaluated for the effect of GDM on p15 and p16 protein expression in the pancreatic islets of the offspring. In short, 35 μg of the total proteins from each control and OGD groups were run on 10% polyacrylamide gels and transferred to nitrocellulose membranes sheets using a transblot system (Bio-Rad, USA). Western blot analysis was performed using the p15 (Sigma, USA) and p16 (Proteintech, Japan) primary antibodies. Monoclonal GAPDH antibody was used as a loading control (Santa Cruz Biotechnology, Japan). Immune-blot assay kit (Bio-Rad, USA) was used to visualize the protein bands. After scanning of the blots, they were quantified using Quantity One Software (BioRad, USA).

Table 1: Bisulfite sequencing polymerase chain reaction (PCR) and qPCR primer name, sequences, product size and number of CpGs

Gene	Primer sequence (5′-3′)	Product size (bp)	Number of CPGs
CDKN2A (Genomic)	F: GGGGTGTGGAATTAGGTTAGGAGTAAAATGTG	342	18
	R: TTCACTCTTCTTAAACAAAAATTATCTCACTAC		
CDKN2B (Genomic)	F: TTTATTATAGTTGTTGGGTTTTTAGAGAGGAG	394	39
	R: ATTTTTACCCTTACAAAAAACAAAACCTACCTCCC		
CDKN2A (mRNA)	F: CTCTGCAGATAGACTAGCCA	127	-
	R: CATCATCACCTGTATCGGG		
CDKN2B (mRNA)	F: AGATCCCAACGCCGTCAAC	184	-
	R: CAGCACCATTAGCGTGTCCAG		
β-actin (mRNA)	F: AAGATCAAGATCATTGCTCCTC	169	-
	R: CTCAGTAACAGTCCGCCT		

Data analysis

For qPCR, bisulfite sequencing and western blot analysis in the 15-week-old offspring, 6 females and 6 males from 6 litters, were studied for each group. Also, we used 6 blood samples of each control and diabetic pregnant rat to measure its fasting blood glucose level. Statistical analyses of all data were performed using the SPSS 18.0 statistical analysis software (SPSS Inc., Chicago, IL, USA) and data were expressed as the mean ± standard deviation (SD). One-way ANOVA was used to determine significant differences in all the parameters (blood glucose level, mRNA expression, DNA methylation and protein level) between the control and OGD groups. For promotor methylation data analysis, we compared the average methylation of CpGs in the control and OGD groups. Significance was determined at $P<0.05$.

Results

Blood glucose level

A significant increase was observed in the fasting blood glucose levels of STZ-induced GDM rats (Fig.1). Seventy-two hours after STZ injection, nearly 70% of dams developed hyperglycemia ($P<0.001$).

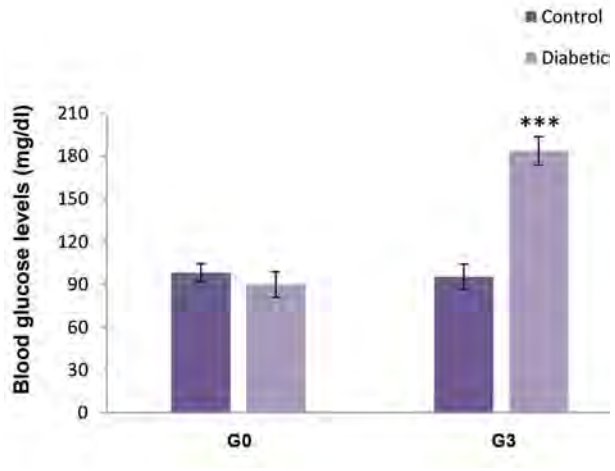

Fig.1: Blood glucose concentrations in diabetic and control pregnant rats. G0; Day 0 of gestation and G3; Day 3 of gestation. All values are presented as means ± SEM. ***; $P<0.001$, n=12.

Bisulfite DNA sequencing

Bisulfite DNA sequencing was employed to identify the methylation levels of the CpGs in the CDKN2A and CDKN2B promoters. Six OGD and six control DNA samples were amplified with a 342 bp fragment in CDKN2A promoter, which comprised of 18 CpG sites and a 394 bp fragment in the CDKN2B promoter, containing 39 CpG sites.

Sequencing data confirmed methylation in CpG islands of the control and OGD samples, while the overall methylation patterns were distinct. Our data revealed that more CpG islets were methylated in the samples derived from controls than the ones acquired from OGDs. We found that the CDKN2A promoter (nucleotides -161 to +181 bp) (Fig.2A) was more methylated in the control samples (40.7%) than in the OGDs (7.3%) and the differences between them were significant ($P<0.01$) (Fig.2B, C). Also, bisulfite sequencing of the 394bp region of the CDKN2B promoter (nucleotides -109 to +285 bp) (Fig.3A) in OGD samples, determined the hypomethylation of CpG islands in this region. As shown in Figures 3B and C, the average DNA methylation in the control and OGD samples were 14.5% and 6%, respectively; thought this difference was not significant. Figure 4 demonstrates a section of bisulfite genomic sequencing chromatography for CDKN2A and CDKN2B. The sequenced region and methylation pattern for CDKN2A and CDKN2B are depict in Figure 2A, B and Figure 3A, B respectively. Interestingly, the control samples shared some common methylation sites (CpG8 for CDKN2A and CpG9 for CDKN2B) while these CpGs were all unmethylated in our OGD samples (Fig.2B, Fig.3B).

Analysis of mRNA expression

After bisulfite sequencing analysis of *CDKN2A/B* genes, we inspected the correlation between DNA methylation and mRNA levels in the pancreatic islets of the control and GDM offspring. *CDKN2A* and *CDKN2B* mRNA expression was detected in both groups, but their expression was significantly upregulated in the OGD samples, which was correlated with hypomethylation in the promoter region of these genes. The strongest correlation between *CDKN2A* mRNA levels and the methylation levels of the CpG islets was detected at -161 to +181 region. Our result suggested that the levels of *CDKN2A* methylation were significantly higher in OGD samples compared to the controls ($P<0.01$, Fig.5A, B). Furthermore, *CDKN2B* mRNA levels were higher in the OGD group compared to the controls; although the difference was not statistically significant (Fig.5A, B).

Western blot analysis results

Western blotting of Langerhans islets protein samples from OGD and control groups, identified two slim bands at 15 and 16kDa for P15 (CDKN2B) and P16 (CDKN2A) proteins, respectively. Both proteins showed an increased band intensity in the OGD samples (Fig.5C-E), which correlates with and confirms our results observed in the real-time PCR analysis. Quantitative analysis of western blotting bands showed that gestational diabetes causes a significant increase in the expression level of P16 protein in the islets of offspring ($P<0.05$, Fig.5,C-E).

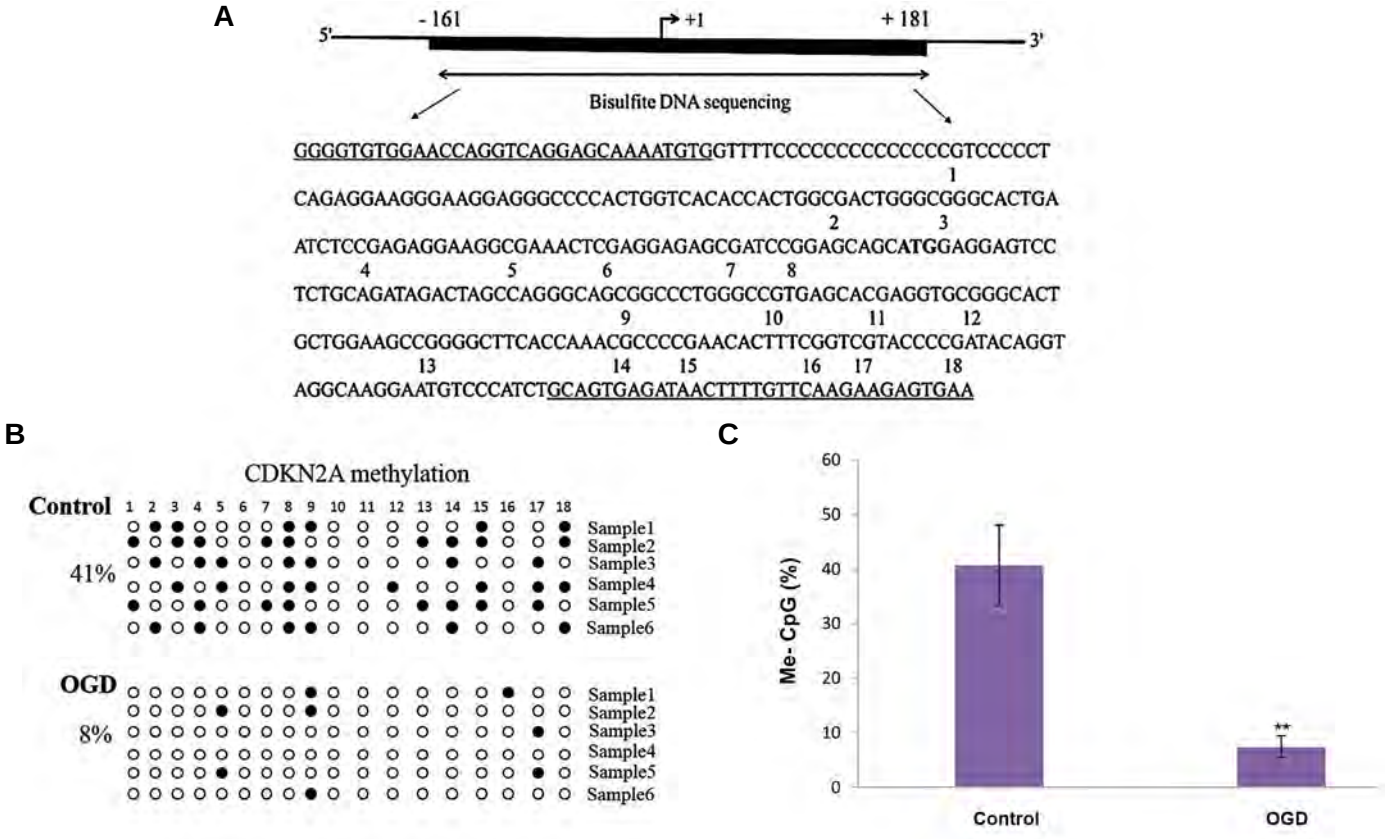

Fig.2: Bisulfite DNA sequencing of the CpGs in the *CDKN2A* promoter. **A.** Diagrammatic illustration of the *CDKN2A* promoter-associated CpG islands, which cover the region from -161 to +181 (the translation initiation site ATG as +1). The region analyzed by bisulfite sequencing polymerase chain reaction (PCR) is depicted. This region covers 342 bp and consists of 18 CpG, **B.** Methylation patterns of the *CDKN2A* CpG island in six control and six OGD samples (each line represents an independent sample). Methylated and unmethylated CpG sites are represented as solid and open circles, respectively, and **C.** Statistical analysis of methylation in the two groups. Data are presented as mean ± SD. **; P<0.01, compared with the controls.

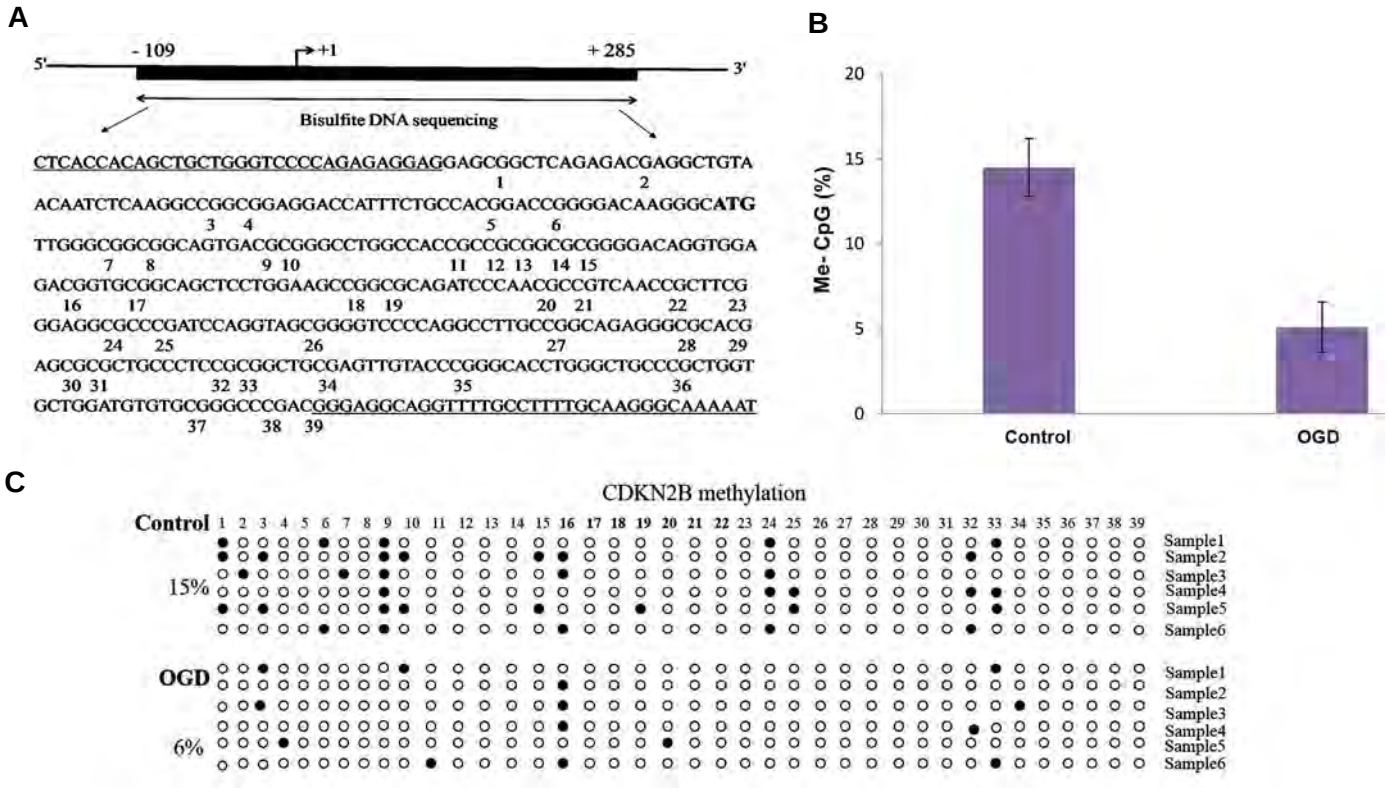

Fig.3: The CpG island in the *CDKN2B* promoter showed by bisulfite sequencing. **A.** Illustrative sketch of the CDKN2B promoter, which covers the region from -109 to +285. The region analyzed by bisulfite sequencing polymerase chain reaction (PCR) is depicted. This region covers 394 bp and includs 39 CpG dinucleotides, **B.** Methylation patterns of the *CDKN2B* CpG island in six control and six OGD samples. Each circle represents a single CpGs (closed and open circles show methylated and unmethylated regions, respectively), and **C.** Statistical analysis of methylation in the two groups. Data are presented as mean ± SD, P=0.064.

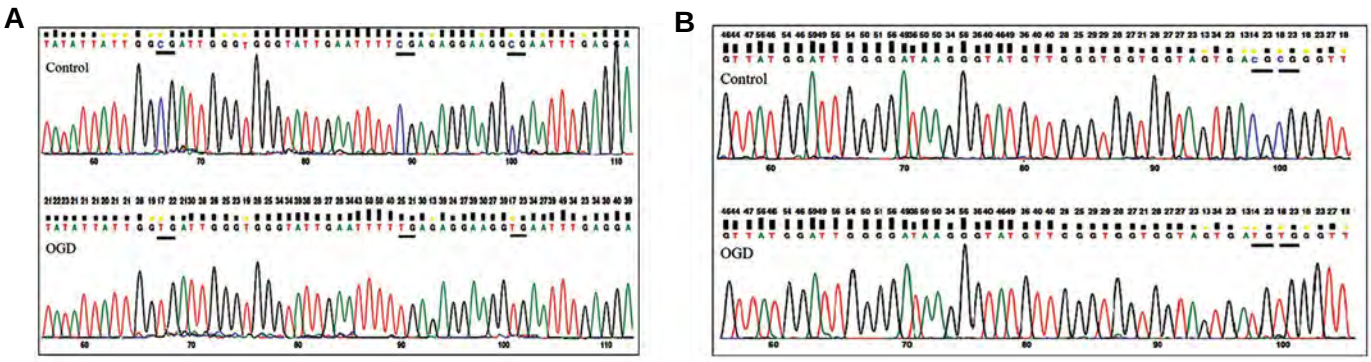

Fig.4: The same sections of the sequencing trace for **A.** *CDKN2A* and **B.** *CDKN2B* in the control and offspring of gestational diabetes (OGD) samples are presented. Underline sections indicate methylated-CpG cytosines (blue) in the control samples that are not converted and the same CpG cytosines in the OGD samples that are unmethylated and converted to thymines (red). CpG2, CpG4 and CpG5 for *CDKN2A* and CpG9 and CpG10 for *CDKN2B* are methylated in the control samples while they are unmethylated in OGDs.

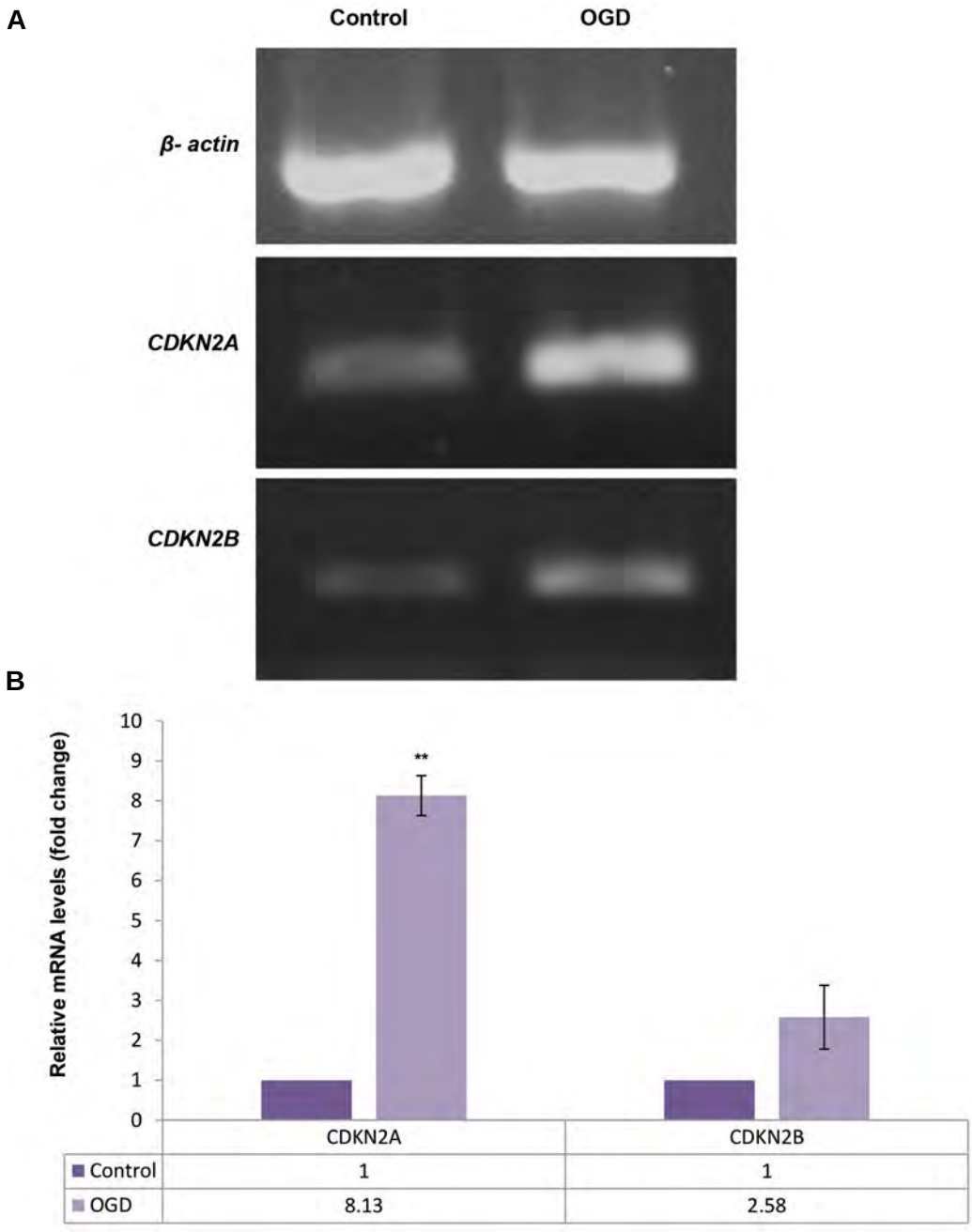

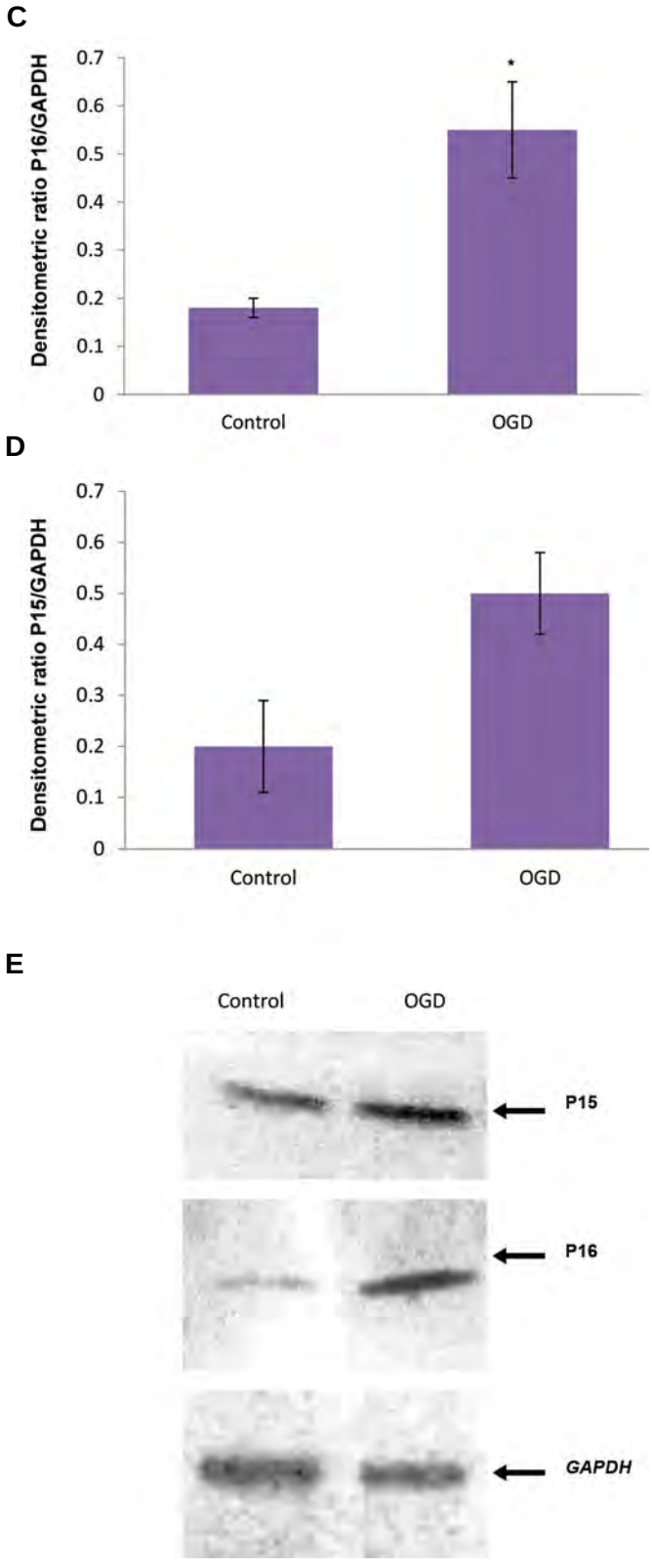

Fig.5: Real-time polymerase chain reaction (PCR) and western blotting analysis of CDKN2A/B in the pancreatic islets of the control and offspring of gestational diabetes (OGD) rats. *CDKN2A/B* mRNAs were determined by quantitive PCR (qPCR). **A.** Reverse transcription polymerase chain reaction (RT-PCR) analysis for the mRNA expression of *CDKN2A/B*, **B.** Real-time PCR analysis for the mRNA level of *CDKN2A/B* in control and OGD samples, **C, D.** Densitometric quantification of western blotting bands for P15 and P16 proteins in the two groups, and **E.** Nitrocellulose blot of sodium dodecyl sulfate polyacrylamide gel electrophoresis SDS-PAGE gel developed with immune-blot assay kit, column 1, control group; column 2, OGD group. *GAPDH* was used as the housekeeping gene. Data are presented as means ± SD, and the experiments were repeated independently three times. *; P<0.05 and **; P<0.01.

Discussion

In the present study, we have analyzed DNA methylation levels of the *CDKN2A/B* genes in pancreatic islets of OGD rats. Data indicated that decreased DNA methylation levels at CpG sites in the *CDKN2A* and *CDKN2B* gene promoter in pancreatic islets of the rat offspring were associated with maternal hyperglycemia. Furthermore, p15 and p16 mRNA and protein levels in the OGD samples increased as compared to the control group, which is probably due to promoter hypomethylation of these genes.

Various animal studies suggest that following gestational diabetes, the offspring exhibit systemic insulin resistance as well as elevated circulating insulin and glucose compared to the offspring of normal dams (6-8). Recently, our team investigated the effects of GDM on some histological aspects of the pancreas in adult rats' offspring (8, 9). Gomori staining showed that β-cell number, islet number and islet diameter is significantly reduced in the offspring of diabetic mothers (8). Also, a separate study by our group indicated that the number of apoptotic β-cells grows in OGDs. In addition, we observed that adult offspring rats mainly developed mild hyperglycemia (9). Strong evidence exists that maternal hyperglycaemia increases the risk of insulin resistance, obesity, and type 2 diabetes in young adult offspring. Although much of the molecular pathways, through which GDM mediates its effects remain unknown. It has been revealed that poor early development of insulin-producing β-cells causes type 2 diabetes later in life (3-7). Considerable attention is being devoted to the potential role of epigenetic modifications including DNA methylation in mediating the influence of environment on both type 1 and type 2 diabetes (25). It has been suggested that DNA methylation changes the expression of genes associated with various aspects of glucose metabolism and in particular glucose intolerance, β-cell proliferation and β-cell dysfunction, which result in diabetes mellitus (26). This gives rise to the speculation that maternal hyperglycemia may change the normal DNA methylation pattern of cell cycle inhibitory genes *CDKN2A* and *CDKN2B* in pancreatic islets of rat offspring. In the current paper, we demonstrated that possible links exist between fetal exposure to maternal GDM and DNA methylation of *CDKN2A/B* promoter in pancreatic islets.

The significance of maintaining appropriate β-cell growth for glucose homeostasis is evident (12). Recently, much effort has been directed to understanding the molecular mechanisms regulating β-cell proliferation. Previous research studies indicated that *CDK4-pRB-E2F1* pathway directly regulates β-cells proliferation (13). Furthermore, this pathway controls the expression of Kir6.2, a key factor involved in the regulation of insulin secretion (11, 13). Previous studies implicate CDK4 as a major regulator of pancreatic β-cells proliferation. An example is the study by Annicotte et al. (27), in which they found that clearance of glucose subsided in mice treated with a CDK4 inhibitor. In our recent study on a rat model, it was observed that GDM can significantly

downregulate the *CDK4-pRB-E2F1* pathway in Langerhans islets of the offspring. *Our results* were thus consistent with earlier *studies mentioned above,* suggesting that there exists a link between CDK4 and the risk of diabetes (14). We hypothesized that inhibition of CDK4 kinase activity and subsequently inhibition of *CDK4-pRB-E2F1* pathway in GDM offspring may be caused by demethylation of *CDKN2A* and *CDKN2B* as CDK4 inhibitors. We therefore decided to study the association between GDM and DNA methylation of *CDKN2A/B* in pancreatic islets of rat offspring. Our findings demonstrated that CDKN2A promoters (-161 to +281 bp) were hypomethylated in the OGD samples. Furthermore, there was a correlation between the increase in CDKN2A expression (in both mRNA and protein levels) and the promoter hypomethylation status. The difference in the average methylation levels for CDKN2A was significant between the control and the OGD samples. On the other hand, some common methylation sites have seen in the control samples (CpG8 for *CDKN2A* and CpG9 for *CDKN2B*).

Such findings indicate that the differential methylation levels of these two CpG sites may be related to poor proliferative capacity of pancreatic β-cells. Human studies have validated the connection between the variants in *CDKN2A/B* and type 2 diabetes (28, 29). In line with previous studies, our data associates CDKN2A/B with the risk of diabetes in the offspring of mothers with gestational diabetes. Nonetheless, the procedure, through which the *CDKN2A/B* locus affects diabetes risk is yet to be discovered.

Conclusion

The present research study provided for the first time, evidence that intrauterine exposure to hyperglycemia causes hypomethylation of *CDKN2A* and *CDKN2B* in pancreatic islets derived from the offspring of GDM rats. This differential methylation was most notable in CpG8 and CPG9 for *CDKN2A* and *CDKN2B*, respectively. These results suggest that a loss of methylation and overexpression of these cell cycle inhibitory genes possibly increase the susceptibility of type 2 diabetes through an inhibited *cyclin D1-CDK4* complex formation, leading to a decreased β-cell mass and mild hyperglycemia in the GDM-exposed offspring. Meanwhile, further investigations and larger-sclae studies are needed to completely investigate the molecular process of inducing diabetes in the offspring by GDM.

Acknowledgements

This study was supported by a grant from Golestan University of Medical Science (Grant number: 237936). The authors wish to thank Mrs. Naemeh Javid for her technical support. There is no conflict of interest in this study.

Authors' Contributions

Z.N.; Performed all experimental work, data collection and evaluation, drafting of the manuscript, and as well as statistical analysis. M.J.G., M.N.; Participated in study design and data interpretation. A.Sh., S.Gh.; Contributed to primer design and also experimental works including western blotting. All authors assisted with editing and approving of the final version of the manuscript prior to its submission. The authors have no conflict of interest to declare.

References

1. Johns EC, Denison FC, Norman JE, Reynolds RM. Gestational diabetes mellitus: mechanisms, treatment, and complications. Trends Endocrinol Metab. 2018; 29(11): 743-754.
2. Agarwal MM, Dhatt GS, Othman Y. Gestational diabetes mellitus prevalence: effect of the laboratory analytical variation. Diabetes Res Clin Pract. 2015; 109(3): 493-499.
3. Ma RC, Chan JC, Tam WH, Hanson MA, Gluckman PD. Gestational diabetes, maternal obesity, and the NCD burden. Clin Obstet Gynecol. 2013; 56(3): 633-641.
4. Tutino GE, Tam WH, Yang X, Chan JC, Lao TT, Ma RC. Diabetes and pregnancy: perspectives from Asia. Diabet Med. 2014; 31(3): 302-318.
5. Bell R, Glinianaia SV, Tennant PW, Bilous RW, Rankin J. Periconception hyperglycaemia and nephropathy are associated with risk of congenital anomaly in women with pre-existing diabetes: a population-based cohort study. Diabetologia. 2012 (Ahead of print).
6. Pinney ES. Metabolic disorders and developmental origins of health and disease. J Dev Orig Health Dis. 2016: 267-289.
7. Ma RC, Tutino GE, Lillycrop KA, Hanson MA, Tam WH5. Maternal diabetes, gestational diabetes and the role of epigenetics in their long term effects on offspring. Prog Biophys Mol Biol. 2015; 118(1-2): 55-68.
8. Moharerri A, Ghafari S, Golalipour MJ. Gestational diabetes reduces pancreatic beta cells in rat offspring. Int J Morphol. 2016; 34(4): 1386-1391.
9. Aceti A, Santhakumaran S, Logan KM, Philipps LH, Prior E, Gale C, et al. The diabetic pregnancy and offspring blood pressure in childhood: a systematic review and meta-analysis. Diabetologia. 2012; 55(11): 3114-3127.
10. Nazari Z, Nabiuni M, Ghaffari S, Saeidi M, Shahriyari A, Golalipour MJ. Gestational Diabetes induces pancreatic beta-cells apoptosis in adult rat offspring. Int J Morphol. 2017; 35(1): 16-20.
11. Nicolay BN, Dyson NJ. The multiple connections between pRB and cell metabolism. Curr Opin Cell Biol. 2013; 25(6): 735-740.
12. Wang P, Fiaschi-Taesch NM, Vasavada RC, Scott DK, García-Ocaña A, Stewart AF. Diabetes mellitus--advances and challenges in human β-cell proliferation. Nat Rev Endocrinol. 2015; 11(4): 201-212.
13. Faja, L, Blanchet E, Annicotte JS. CDK4, pRB and E2F1: connected to insulin. Cell Div. 2010; 5(1): 6.
14. Nazari Z, Nabiuni M, Saeidi M, Golalipour MJ. Gestational diabetes leads to down-regulation of CDK4-pRB- E2F1 pathway genes in pancreatic islets of rat offspring. Iran J Basic Med Sci. 2017; 20(2): 150-154.
15. VinuÉ Á, MartÍnez-HervÁs S, Herrero-Cervera A, SÁnchez-GarcÍa V, AndrÉs-Blasco I, Piqueras L, et al. Changes in CDKN2A/2B expression associate with T-cell phenotype modulation in atherosclerosis and type 2 diabetes mellitus. Transl Res. 2019; 203: 31-48.
16. Hannou SA, Wouters K, Paumelle R, Staels B. Functional genomics of the CDKN2A/B locus in cardiovascular and metabolic disease: what have we learned from GWASs? Trends Endocrinol Metab. 2015; 26(4): 176-184.
17. Nilsson E, Jansson PA, Perfilyev A, Volkov P, Pedersen M, Svensson MK, et al. Altered DNA Methylation and differential expression of genes influencing metabolism and inflammation in adipose tissue from subjects with type 2 diabetes. Diabetes. 2014. 63(9): 2962-2976.
18. Sommese L, Benincasa G, Lanza M, Sorriento A, Schiano C, Lucchese R, et al. Novel epigenetic-sensitive clinical challenges both in type 1 and type 2 diabetes. J Diabetes Complications. 2018; 32(11): 1076-1084.
19. Dayeh TA, Olsson AH, Volkov P, Almgren P, Rönn T, Ling C. Identification of CpG-SNPs associated with type 2 diabetes and differential DNA methylation in human pancreatic islets. Diabetologia. 2013; 56(5): 1036-1046.

20. Dayeh T, Volkov P, Salö S, Hall E, Nilsson E, Olsson AH, et al. Genome-wide DNA methylation analysis of human pancreatic islets from type 2 diabetic and non-diabetic donors identifies candidate genes that influence insulin secretion. PLoS Genet. 2014; 10(3): 41-60.
21. Zhu Z, Chen X, Xiao Y, Wen J, Chen J, Wang K, et al. Gestational diabetes mellitus alters DNA methylation profiles in pancreas of the offspring mice. J Diabetes Complications. 2019; 33(1): 15-22.
22. Ma RC, Tutino GE, Lillycrop KA, Hanson MA, Tam WH. Maternal diabetes, gestational diabetes and the role of epigenetics in their long term effects on offspring. Prog Biophys Mol Biol. 2015; 118(1-2): 55-68.
23. Pasek RC, Gannon M. Advancements and challenges in generating accurate animal models of gestational diabetes mellitus. Am J Physiol Endocrinol Metab. 2013; 305(11): 1327-1338.
24. Carter JD, Dula SB, Corbin KL, Wu R, Nunemaker CS. A practical guide to rodent islet isolation and assessment. Biol Proced Online. 2009; 11: 3-13.
25. Bansal A, Pinney SE. DNA methylation and its role in the pathogenesis of diabetes. Pediatr Diabetes. 2017; 18(3): 167-177.
26. Yokoi N. Epigenetic dysregulation in pancreatic islets and pathogenesis of type 2 diabetes. J Diabetes Investig. 2017 (Ahead of print).
27. Annicotte JS, Blanchet E, Chavey C, Iankova I, Costes S, Assou S, et al. The CDK4-pRB-E2F1 pathway controls insulin secretion. Nat Cell Biol. 2009; 11(8): 1017-1023.
28. Attia HRM, Kamel SA, Ibrahim MH, Farouk HA, Rahman AHA, Sayed GH, et al. Open-array analysis of genetic variants in Egyptian patients with type 2 diabetes and obesity. Egypt J Med Hum Genet. 2017; 18(4): 341-348.
29. Peng F, Hu D, Gu Ch, Lid X, Li Y, Jia N. The relationship between five widely-evaluated variants in CDKN2A/B and CDKAL1 genes and the risk of type 2 diabetes: A meta-analysis. Gene. 2013; 531 (2): 435-443.

Original Article

Platelets Apoptosis and Clearance in The Presence of Sodium Octanoate during Storage of Platelet Concentrate at 4˚C

Vahid Baghdadi, Ph.D., Fatemeh Yari, Ph.D.*, Mahin Nikougoftar, Ph.D., Mohammad Hessam Rafiee, Ph.D.

Blood Transfusion Research Center, High Institute for Research and Education in Transfusion Medicine, Tehran, Iran

Corresponding Address: P.O.Box: 14665-1157, Blood Transfusion Research Center, High Institute for Research and Education in Transfusion Medicine, Tehran, Iran
Email: f.yari@ibto.ir

Received: 2/January/2019, Accepted: 16/March/2019

Abstract

Objective: Platelet (PLT) storage at 4˚C has several benefits, however, it is accompanied by increased clearance of PLTs after transfusion. In this study, we evaluated the potential of sodium octanoate (SO) for reducing apoptosis and clearance rate of PLTs after long-term storage in cold.

Materials and Methods: In this experimental study, PLT concentrates (PCs) were stored for 5 days under the following three conditions: 20-24˚C, 4˚C, and 4˚C in the presence of SO. To measure the viability of PLTs, the water-soluble tetrazolium salt (WST-1) assay was performed. Phosphatidylserine (PS) exposure was determined on PLTs using flow cytometry technique. The amount of human active caspase-3 was determined in PLTs using an enzyme-linked immunosorbent assay. Additionally, the amount of PLT ingestion or clearance was determined by using HepG2 cell line.

Results: The viability was higher in the SO-treated PLTs compared to the other groups. The level of PS exposure on PLTs was lower in the SO-treated PLTs compared to the other groups. The amount of active caspase-3 increased in all groups during 5-day storage. The highest increase in the amount of caspase-3 levels was observed at cold temperature. However, PLTs kept at 4˚C in the presence of SO had a lower amount of active caspase-3 compared to PLTs kept at 4˚C. The amount of PLTs removal by HepG2 cells was increased for 4˚C-kept PLTs but it was lower for PLTs kept at 4˚C in the presence of SO but, the differences were not significant (P>0.05).

Conclusion: SO could partially moderate the effects of cold temperature on apoptosis and viability of platelets. It also decreases the ingestion rate of long-time refrigerated PLTs *in vitro*. Further studies using higher numbers of samples are required to demonstrate the effect of SO on reducing the clearance rate of PLTs.

Keywords: Cold Temperature, HepG2, Octanoic Acid, Platelet

Cell Journal(Yakhteh), Vol 22, No 2, July-September (Summer) 2020, Pages: 212-217

Citation: **Baghdadi V, Yari F, Nikougoftar M, Rafiee MH. Platelets apoptosis and clearance in the presence of sodium octanoate during storage of platelet concentrate at 4˚C. Cell J. 2020; 22(2): 212-217. doi: 10.22074/cellj.2020.6697.**

Introduction

Platelets (PLTs) are anuclear cell fragments that act primarily as homeostasis regulators, and they play a role in angiogenesis and innate immunity (1-3). Transfusion of PLT concentrate (PC) is accompanied by a high prevalence of anaphylactic and febrile reactions compared with fresh frozen plasma (FFP) and red blood cells (4). Storage of PC at room temperature leads to PLT storage lesion, which includes a series of harmful changes that negatively affect PLT function (5).

PCs are typically stored at 20-24˚C with continuous agitation. Storage temperature conditions limit PLTs storage time to 5-7 days due to increased risk of bacterial contamination (6). It was shown that from every 1,000 to 5,000 units of PC, a single unit is infected with bacteria (7). Due to insufficiencies in PCs supplies, an alternative strategy is needed. Over the years, researchers have provided alternative methods for increasing the half-life of PLTs, including the use of additive solutions like PLT additive solution (PAS), storage in cold, lyophilization, etc. Although PLT storage in cold can have several benefits, including reducing the rate of bacterial growth and increasing hemostatic activity, PLT storage in cold was obsolete in the 1970s due to increases in their clearance rates. Several *in vitro* studies since 1970 showed that maintaining PLTs at 4˚C results in better functional and metabolic responses, such as aggregation, adhesion to the subendothelium and minimum lactate formation. PLTs stored at 4˚C had a better function compared to PLTs kept at room temperature; by employing the former, the bleeding time reduced in patients with thrombocytopenia, volunteers receiving aspirin, and in patients with aplastic thrombocytopenia (8, 9).

Short-term maintenance of PLTs in cold causes clustering and exposure of β-N-acetylglucosamine residues that make them detectable by liver macrophages (10). In comparison, PLTs stored in cold for a long time have a severe increase in galactose exposure, specifically on glycoprotein Ibα (GPIbα). Galactose is a ligand for asialoglycoprotein receptors (ASGPRs), and ASGPRs mediate hepatocytes-induced clearance (11).

Studies have shown that some substances such as trehalose, significantly reduce PLT phagocytosis after transfusion, improve the activity of PLTs and retain the response of cold-stored PLTs to agonists *in vitro*; this could be related to the prevention and inhibition of PLTs' apoptosis in cold (12). It has been indicated that activation of caspases leads to rapid removal of PLTs from the circulation (13). Active caspase-3 induces apoptosis by

cleaving the vital proteins of the cell (14). According to the previous studies, the amount of caspase-3 is increased during PLT storage at room temperature (15-18). Additionally, storage in cold increases the amount of caspases in the PLTs (12).

To overcome the problems that platelets encounter in the cold, this study was conducted. We evaluated the potential of sodium octanoate (SO) as a substance which is known as a protein stabilizer against heat. Octanoic acid is a saturated medium-chain fatty acid with an 8-carbon backbone. This substance is present at a concentration of 0.2 μM in serum (19). SO was used for providing infusible PLT membranes (IPMs), as a protein stabilizer against 20-hour heating at 60˚C used for deactivation of viruses. An increase in IPM binding to von willebrand factor (vWF) was observed at an optimum concentration of SO (20). It was shown that 800-1200 μM of octanoic acid has long-term negative effects on embryonic and fetal growth in a mouse model; however, it has no harmful effects on the growth of the embryo at ≤400 μM concentrations (19). Also, it was found that medium-chain fatty acids do not have a toxic effect on humans and animals (21). In this study, we aimed to use SO for reducing the problems related to cold storage of PLTs. For this purpose, we kept the PCs under the following conditions: 20-22˚C with agitation, 4˚C and 4˚C in the presence of SO without agitation. Subsequently, we analyzed the quality of PLTs during 5-day storage in terms of apoptosis rate and the clearance level, by using a cell line originated from human hepatocytes.

Materials and Methods

Preparation of platelet concentrates

This experimental study was approved by the Ethics College's Bioethics Committee (IR. TMI.REC.1396.004). Twelve PC bags with citrate phosphate dextrose adenine anticoagulant solution (CPDA1) (Macopharma, France) were prepared from Iranian Blood Transfusion Organization (IBTO). PLT-rich plasma (PRP) method was used for the preparation of PCs.

Prior to SO addition to the bags, all the parameters of the study were evaluated on day 1. After evaluating the parameters, PCs were divided into three equal volumes (A, B, and C) using a digital balance (Sartorius, Germany) and a Terumo Sterile Connecting Device (TSCD - II, Terumo Tubing welder, Japan). SO was added to one of the bags and the bag was transferred to a 4˚C refrigerator, the second bag was also kept under the same condition and the third bag was stored at 20-24˚C in a shaker-incubator and agitated. It should be noted that PLTs were stored at 4˚C without agitation because according to a previous study, agitation does not improve the quality of PLTs stored at cold in comparison with PLTs stored at cold without agitation (22).

Determination of the effective concentration of sodium octanoate

SO (Merck, Germany, Grade; Ph Eur, NF) with the chemical formula (CH_3 $(CH_2)_6COONa$) was used. Different concentrations of SO (100, 200, 400, and 800 μM) were examined. The PLT bags were placed at 4˚C without agitation or at 22˚C with agitation for 5 days. PLT count, mean PLT volume and phosphatidylserine (PS) were examined on the storage days using an automated hematology analyzer (Sysmex XT-2000i, Kobe, Japan) (data not shown).

Evaluation of the viability and metabolic activity of platelets using WST-1 assay

To measure the mitochondrial activity of PLTs, we used the WST-1 cell proliferation assay kit (WST-1, Cayman, USA). In this method, tetrazolium salt is changed to formazan in viable cells by cellular mitochondrial dehydrogenases. Here, PLTs were diluted with phosphate buffered saline (PBS) and 10×10^6 PLTs (100 μl) were added into each well. Then, 10 μl of WST-1 blend solution was added to each well and the plate was incubated for 4 hours at 37˚C in a CO_2 incubator. The absorbance of the wells was measured using a microplate reader at 450 nm.

Evaluation of phosphatidylserine exposure

The levels of PS exposure were determined on the surface of PLTs using Annexin V-FITC assay kit (Biolegend, US)and flow cytometry technique. In summary, a PLT count of 1.5×10^6 cells was incubated in 300 μl of annexin V binding buffer. Then, 5 μl of FITC-labeled annexin V was added and the tubes were incubated at room temperature for 20 minutes. Samples were analyzed by flow cytometry technique using the CyFlow® Space (Partec, Germany).

Human active caspase-3 evaluation

Human active Caspase-3 level was determined using an enzyme-linked immunosorbent assay kit (Invitrogen, US) with the sensitivity of 1.25 ng/ml. At first, we prepared a cell extraction buffer according to the manufacturer's instructions. For preparation of the cells, we collected 5×10^8 PLTs by centrifugation, and then we washed PLTs three times with PBS. We added the cell extraction buffer to the pellet and incubated them for 15 minutes. After centrifugation at 4000 g for 10 minutes, the supernatant was collected in a clean tube. ELISA assay was done according to the kit instructions. After completing the reactions, the optical density of the wells was read at 450 nm. Finally, the concentration of unknown samples and controls was determined using the plotted standard curve.

Preparation of mepacrine-labeled platelets

Mepacrine is a polyphenol mixture which has an emission wavelength within the range of FITC (Fluorescein). Based on the PLT count on the first day, 5×10^7 cells were treated with 30 μl of phosphate buffered saline (PBS) and 20 μl of 20 mg/mL mepacrine and incubated for 30 minutes at ambient temperature in the dark. Afterward, cells were washed with PBS buffer three times by centrifugation at 1200 g for 15 minutes. Finally, PLTs were exposed to HepG2 cells.

Ingestion of PLTs by HepG2 cells *in vitro*

Initially, cells of the human hepatocellular cancer cell line (HepG2) were cultured in DMEM-F12 supplemented with 10% fetal bovine serum (FBS). After the growth of the adherent cells, they were starved for 30 minutes in serum-free medium. Then, mepacrine-labeled PLTs (5×10^7) were added to each well and incubated at 37˚C for 30 minutes. After the incubation time, the wells were washed three times with PBS. Subsequently, HepG2 cells were detached from the culture plates by treatment with trypsin at 37˚C for 10 minutes. The ingestion of mepacrine-labeled PLTs by HepG2 cells was evaluated by flow cytometry technique. Unbound PLTs were separated from HepG2 cells by their forward and scatter characteristics. HepG2 cells containing the ingested PLTs were identified by their green fluorescence and the HepG2 cells having the adherent but not containing PLTs were identified by labeling with PE-anti-CD42b.

Statistical analysis

SPSS v.22.0 (IBM Corporation, US) software was used to analyze and process the data. For evaluation of the effects of each treatment at different time points, we used two-way repeated measure ANOVA with two within-subject factors (3 paired group×3 times).

Results

The effective concentration of sodium octanoate

Due to the positive effects of SO on the evaluated factors of PLTs, the optimum concentration of 200 µM was selected. Among the parameters of study, at this concentration of SO, the counts of PLTs was higher, and the PS exposure was lower on the third and fifth days of storage in comparison to other concentrations. Additionally, based on WST-1 assay, higher viability of PLTs was observed at this concentration of SO (data not shown).

Cell viability (WST-1) assay

The metabolic activity and survival rate of PLTs were decreased during 5-day storage. The lowest survival rate was detected for 22˚C-stored PLTs. The metabolic activity of PLTs was well-maintained in PLTs treated with SO (4˚C) in comparison to those that were only kept at 4˚C, but the differences were not statistically significant between the groups. The mean ± SD values for WST-1 [optical density 450 (OD_{450} nm)] were as follows: on day 1 of storage 0.522 ± 0.97, on day 3 (4˚C) 0.421 ± 0.56, on day 3 (4˚C+SO) 0.493 ± 0.73, on day 3 (22˚C) 0.274 ± 0.60, on day 5 (4˚C) 0.358 ± 0.55, on day 5 (4˚C+SO) 0.412 ± 0.56, and on day 5 (22˚C) 0.226 ± 0.67.

The exposure level of phosphatidylserine

During the storage time, the exposure of PS increased in all groups. The exposure level of PS was significantly lower in the presence of SO (4˚C) on day 5 in comparison to other groups (P<0.05). The decrease in the PS exposure level was not significantly different among the groups on the third day of storage. Nevertheless, the differences in PS exposure between the PLTs kept at 22˚C and other groups were significant (P<0.05, Table 1, Fig.1).

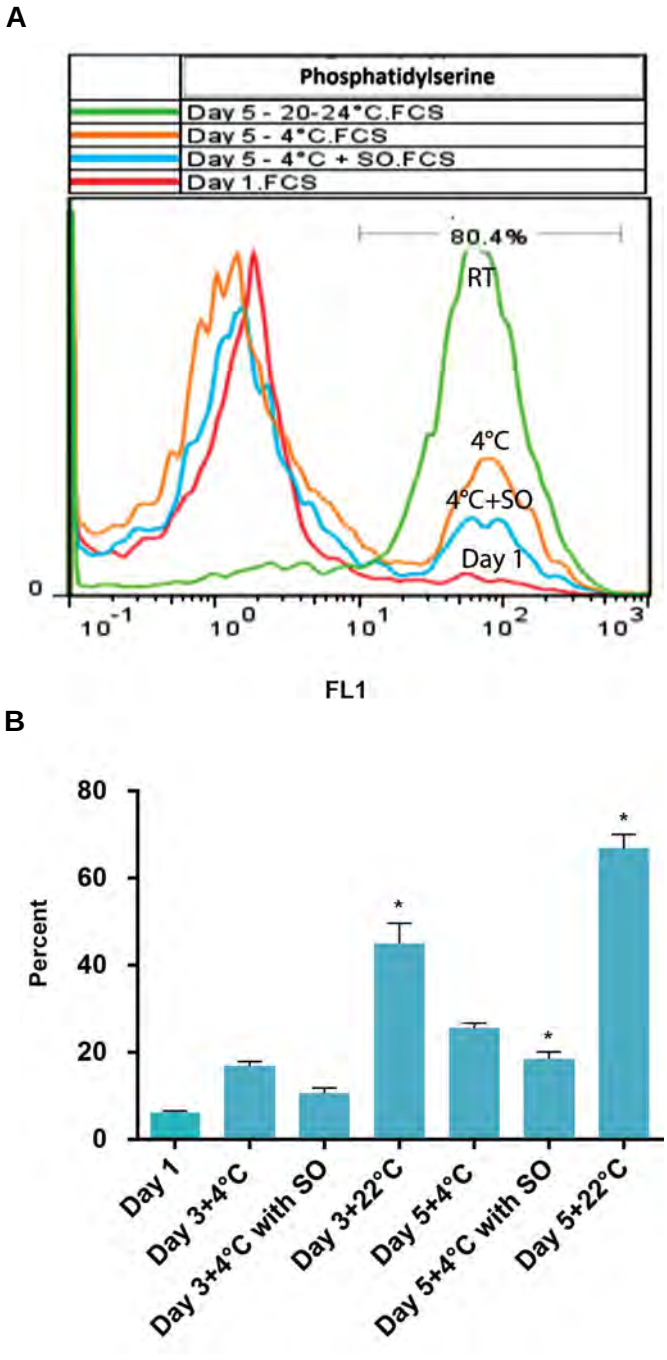

Fig.1: The level of phosphatidylserine (PS) exposure on platelets. **A.** Flow cytometry plot. PS exposure on the fifth day of storage in three groups of platelets kept at 22˚C, 4˚C and 4˚C in the presence of sodium octanoate (SO). This figure shows higher levels of PS on platelets stored at 22˚C (P<0.05). SO caused lower PS exposure on platelets at 4˚C (P<0.05) and **B.** PS exposure levels on platelets on different days of storage in three groups of study. The lowest exposure of PS was seen in SO-treated platelets and the highest exposure was seen in platelets stored at 22˚C. *; P<0.05.

Table 1: The mean and standard deviation for the study variables including phosphatidylserine, human active caspase-3 and the ingestion levels by HepG2 cells during storage days (days 1, 3 and 5) in three groups of study; platelets stored at 4˚C, 4˚C with sodium octanoate (SO) and 22˚C

Study variables n=12	Day 1	Day 3 (4˚C)	Day 3 (4˚C+SO)	Day 3 (22˚C)	Day 5 (4˚C)	Day 5 (4˚C+SO)	Day 5 (22˚C)
Phosphatidylserine (%)	6.2 ± 1.21	16.8 ± 3.7	10.57 ± 4.44	44.88 ± 16.44	25.42 ± 4.4	18.51 ± 5.59	66.77 ± 11.39
Human active caspase-3 (ng/ml)	0.647 ± 0.211	1.326 ± 0.503	1.292 ± 0.436	1.050 ± 0.418	1.485 ± 0.366	1.306 ± 0.424	1.152 ± 0.307
Hep G2 ingestion (%)	17.28 ± 2.644	28.65 ± 5.545	27.88 ± 5.458	20.24 ± 4.416	37.9 ± 2.851	30.98 ± 3.338	25.555 ± 3.161

Data are presented as mean ± SD.

Human active caspase-3 levels in platelets

The level of human active caspase-3 was increased in platelets during storage in all groups (Fig.2). But, a higher increase was observed in cold-stored PLTs. Although the presence of SO was accompanied by a lower increase in active caspase-3 levels in 4˚C-kept PLTs (Fig.2, Table 1), there was no significant difference in active caspase-3 levels between PLTs stored at 4˚C in the presence and absence of SO (P>0.05).

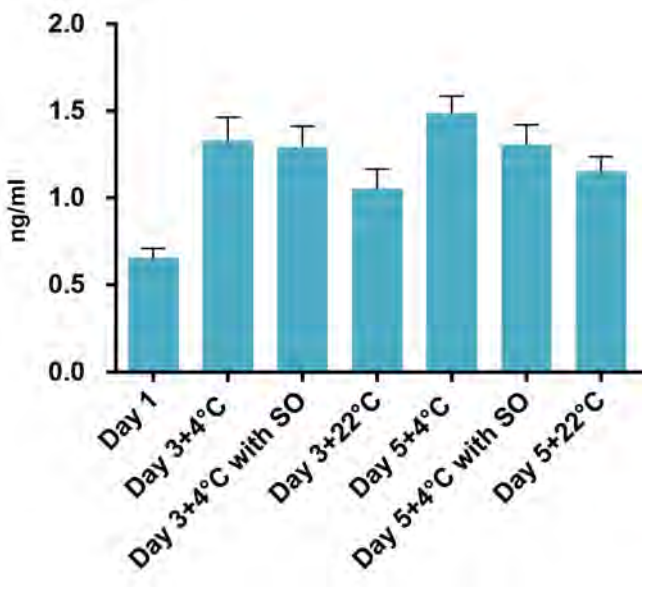

Fig.2: Effect of the temperature and sodium octanoate (SO) presence on the active caspase-3 levels in platelets during storage. Higher levels of active caspase-3 were observed in 4˚C- kept platelets but the presence of SO could decrease the amount of the enzyme although the difference was not significant. Lower amount of active caspase-3 was observed in platelets kept at room temperature compared to 4˚C- kept platelets.

Ingestion of the refrigerated platelets by HepG2 cells

Storage of PLTs at 4˚C caused an increase in the ingestion rate of PLTs by HepG2 cells in comparison with 22˚C-kept PLTs during 5-day storage (P<0.05). SO caused a lower clearance rate for 4˚C-kept platelets by HepG2 cells compared to 4˚C-kept platelets in the absence of SO (Table 1, Fig.3) but the differences were not significant (P>0.05).

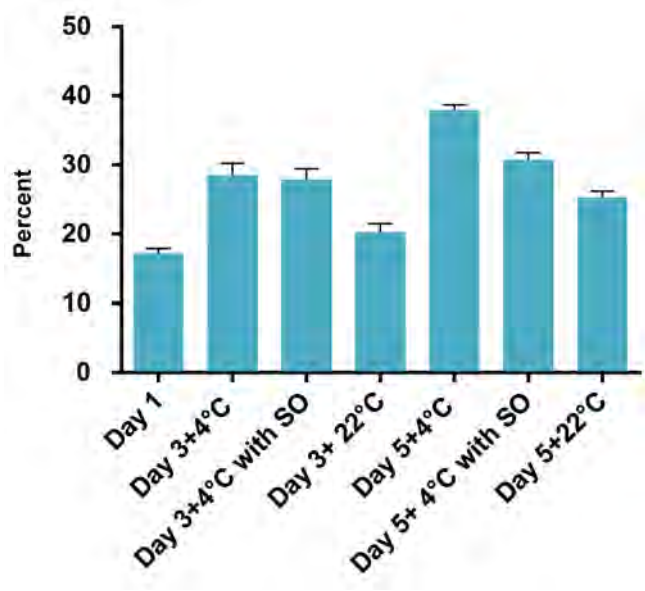

Fig.3: Effect of sodium octanoate (SO) on the ingestion of platelets by HepG2 cells during storage in different groups of study (22˚C, 4˚C and 4˚C+SO). As it can be seen, the ingestion rate of platelets was increased in cold. The presence of SO could decrease the clearance level although the difference was not significant. The lowest ingestion rate was observed for platelets kept at room temperature.

Discussion

One of the strategies to reduce the complications of room temperature storage of PLTs is the maintenance of PLTs at cold temperatures. The main problem with keeping PCs in cold is the rapid removal of PLTs after transfusion due to the changes in the PLTs membrane (8). In this study, we evaluated the potential of SO to reduce the problems related to the cold storage of PLTs. For this purpose, we kept PCs for 5 days under the following three conditions: 20-22˚C, 4˚C temperature and 4˚C+SO.

In this study, the viability was reduced in all groups and the lowest level of viability was observed in PLTs stored at room temperature. It is of note that the highest level of viability was observed in PLTs treated with SO. The results of this study indicated that SO has positive effects on the survival rate of PLTs during storage at 4˚C. Our results were consistent with those reported by some other researches that showed a reduction in the survival rate of PLTs during storage due to the production of lactate and

reduction of pH (23, 24).

It should be noted that this substance has not been used for protection against cold before, but it was used for protection against heat for example for stabilizing the infusible PLT membrane (20). We found that SO could reduce the levels of PS exposure and caspase-3 levels in 4˚C-stored PLTs. The ingestion rates of PLTs by HepG2 cells were also reduced in the presence of SO during storage at 4˚C. Additionally, the SO group had higher PLT count at 4˚C compared to other groups but the differences were not statistically significant. Furthermore, SO also led to improvement in PLTs survival .

Exposure of PS on the surface of PLTs is an important indicator of apoptosis. The results of our study showed that the level of PS exposure in SO-treated PLTs was lower than other groups during storage. Dasgupta et al. (24) showed that PS exposure on PLTs has a direct correlation with the activation of PLTs and the occurrence of apoptosis. Like the study of them, decreases in the exposure of PS in the SO-treated group in our study, may show the anti-apoptotic potential of this substance.

Consistent with previous studies (15-18), our study showed an increase in the amount of caspase-3 in all groups of PLTs during 5-day storage. The highest increase in caspase-3 levels in PLTs was observed at 4˚C, which may indicate the effect of cold temperature on the activation of caspase-3. In SO-treated PCs, the lower amount of caspase-3 was not significantly different from those of other groups. Our results were in line with the findings of Liu and co-workers who stated that storage in cold increases the amount of caspases in PLTs (12). Furthermore, our results were correlated with the study of Wang and co-workers who stated that the mechanism underlying the effect of medium-chain fatty acids (like octanoic acid) involves inhibition of the activities of caspase-3 and -9 in human liver cells (25).

Long-term storage of PLTs in cold leads to an increase in galactose residues on PLTs. Studies have shown that hepatocytes use the Ashwell-Morell receptor to remove these PLTs after transfusion (11). We investigated the simultaneous effect of SO and cold temperature-storage on the removal of PLTs by HepG2 cells. Studies have shown that HepG2 cells are able to remove PLTs in the culture medium and removal rate was increased after long-time storage of PLTs in cold. It has been shown that HepG2 cells do not express αMβ2 receptors. For this reason, they are not able to remove PLTs when they are stored in the cold for a short time. However, using the asialoglycoprotein receptors, HepG2 cells are capable of removing PLTs after long-time storage (26-28). Based on the results of this study, the rate of PLTs removal by HepG2 cells was increased in all groups during storage. However, the lowest increase in PLT removal was related to the 22˚C-kept PLTs, which was consistent with the findings of previous studies and was predictable. Similar to the results of previous studies, in this study, we observed an increase in PLTs removal rate during 5-day storage in cold by HepG2 cells. Despite the lower rate of PLTs' removal by HepG2 cells in the presence of SO in comparison to 4˚C group, the differences were not significant.

Conclusion

SO could partially moderate the effects of cold temperature on apoptosis and viability of platelets. It also decreases the ingestion rate of long-time refrigerated PLTs *in vitro*. Further studies using higher numbers of samples are required to confirm the effect of SO on reducing the clearance rate of PLTs.

Acknowledgments

This manuscript presents the results of a Ph.D. thesis of Vahid Baghdadi financially supported by Blood Transfusion Research Center, High Institute for Research and Education in Transfusion Medicine, Iranian Blood Transfusion Organization, Tehran. None of the authors have any conflicts of interest to declare.

Authors' Contributions

V.B.; Performed all the experimental works and the statistical analysis. M.N., M.H.R.; Were the scientific advisors of the project and did the critical revision of the manuscript. F.Y.; Was the designer of the project, also contributed in the analysis and interpretation of the results. All authors read and approved the final manuscript.

References

1. Rubak P, Nissen PH, Kristensen SD, Hvas AM. Investigation of platelet function and platelet disorders using flow cytometry. Platelets. 2016; 27(1): 66-74.
2. Nishimura S, Nagasaki M, Kunishima S, Sawaguchi A, Sakata A, Sakaguchi H, et al. IL-1α induces thrombopoiesis through megakaryocyte rupture in response to acute platelet needs. J Cell Biol. 2015; 209(3): 453-466.
3. Yaftian M, Yari F, Ghasemzadeh M, Fallah Azad V, Haghighi M. Induction of apoptosis in cancer cells of pre-B ALL patients after exposure to platelets, platelet-derived microparticles and soluble CD40 ligand. Cell J. 2018; 20(1): 120-126.
4. Sarkodee-Adoo CB, Kendall JM, Sridhara R, Lee EJ, Schiffer CA. The relationship between the duration of platelet storage and the development of transfusion reactions. Transfusion. 1998; 38(3): 229-235.
5. Wood B, Padula MP, Marks DC, Johnson L. Refrigerated storage of platelets initiate's changes in platelet surface marker expression and localization of intracellular proteins. Transfusion. 2016; 56(10): 2548-2559.
6. Capocelli KE, Dumont LJ. Novel platelet storage conditions: additive solutions, gas, and cold. Curr Opin Hematol. 2014; 21(6): 491-496.
7. Salunkhe V, van der Meer PF, de Korte D, Seghatchian J, Gutiérrez L. Development of blood transfusion product pathogen reduction treatments: a review of methods, current applications and demands. Transfus Apher Sci. 2015; 52(1): 19-34.
8. Reddoch KM, Pidcoke HF, Montgomery RK, Fedyk CG, Aden JK, Ramasubramanian AK, et al. Hemostatic function of apheresis platelets stored at 4˚C and 22˚C. Shock. Shock. 2014; 41 Suppl 1: 54-61.
9. Stubbs JR, Tran SA, Emery RL, Hammel SA, Haugen AL, Zielinski MD, et al. Cold platelets for trauma-associated bleeding: regulatory approval, accreditation approval, and practice implementation-just the "tip of the iceberg". Transfusion. 2017; 57(12): 2836-2844.
10. Hoffmeister KM, Josefsson EC, Isaac NA, Clausen H, Hartwig JH, Stossel TP. Glycosylation restores survival of chilled blood platelets. Science. 2003; 301(5639): 1531-1534.

11. Rumjantseva V, Grewal PK, Wandall HH, Josefsson EC, Sørensen AL, Larson G, et al. Dual roles for hepatic lectin receptors in the clearance of chilled platelets. Nat Med. 2009; 15(11): 1273-1280.
12. Liu Q, Xu L, Jiao SX, Wang TX, Song Y, Wen ZK. Trehalose inhibited the phagocytosis of refrigerated platelets in vitro via preventing apoptosis. Transfusion. 2009; 49(10): 2158-2166.
13. Pleines I, Lebois M, Gangatirkar P, Au AE, Lane RM, Henley KJ, et al. Intrinsic apoptosis circumvents the functional decline of circulating platelets but does not cause the storage lesion. Blood. 2018; 132(2): 197-209.
14. Kiraz Y, Adan A, Kartal Yandim M, Baran Y. Major apoptotic mechanisms and genes involved in apoptosis. Tumour Biol. 2016; 37(7): 8471-8486.
15. Bertino AM, Qi XQ, Li J, Xia Y, Kuter DJ. Apoptotic markers are increased in platelets stored at 37 degrees C. Transfusion. 2003; 43(7): 857-866.
16. Perrotta PL, Perrotta CL, Snyder EL. Apoptotic activity in stored human platelets. Transfusion. 2003; 43(4): 526-535.
17. Marini I, Aurich K, Jouni R, Nowak-Harnau S, Hartwich O, Greinacher A, et al. Cold storage of platelets in additive solution:The impact of residual plasma in apheresis platelet concentrates. Haematologica. 2019; 104(1): 207-214.
18. Shiri R, Yari F, Ahmadinejad M, Vaeli S, Tabatabaei MR. The caspase-3 inhibitor (peptide Z-DEVD-FMK) affects the survival and function of platelets in platelet concentrate during storage. Blood Res. 2014; 49(1): 49-53.
19. Fredrickson J, Krisher R, Morbeck DE. The impact of the protein stabilizer octanoic acid on embryonic development and fetal growth in a murine model. J Assist Reprod Genet. 2015; 32(10): 1517-1524.
20. Ahmadzadeh N, Yari F, Amirizadeh N, Khorramizadeh MR. Production and characterization of liquid-stored and lyophilized reconstituted human infusible platelet membranes. Int J Lab Hematol. 2011; 33(6): 586-592.
21. Christensen E, Hagve TA, Grønn M, Christophersen BO. β-oxidation of medium chain (C8C14) fatty acids studied in isolated liver cells. Biochim Biophys Acta. 1989; 1004(2): 187-195.
22. NasrEldin E. Effect of cold storage on platelets quality stored in small containers: Implications for pediatric transfusion. Pediatric Hematology Oncology Journal. 2017; 2(2): 29-34.
23. Deyhim MR, Mesbah-Namin SA, Yari F, Taghikhani M, Amirizadeh N. L-carnitine effectively improves the metabolism and quality of platelet concentrates during storage. Ann Hematol. 2015; 94(4):671-80.
24. Dasgupta SK, Argaiz ER, Mercado JE, Maul HO, Garza J, Enriquez AB, et al. Platelet senescence and phosphatidylserine exposure. Transfusion. 2010; 50(10): 2167-2175.
25. Wang B, Li L, Fu J, Yu P, Gong D, Zeng C, Zeng Z. Effects of long-chain and medium-chain fatty acids on apoptosis and oxidative stress in human liver cells with steatosis. J Food Sci. 2016; 81(3): H794-H800.
26. Hoffmeister KM, Felbinger TW, Falet H, Denis CV, Bergmeier W, Mayadas TN, et al. The clearance mechanism of chilled blood platelets. Cell. 2003; 112(1): 87-97.
27. Quach ME, Chen W, Li R. Mechanisms of platelet clearance and translation to improve platelet storage. Blood. 2018; 131(14): 1512-1521.
28. Li Y, Fu J, Ling Y, Yago T, McDaniel JM, Song J, et al. Sialylation on O-glycans protects platelets from clearance by liver Kupffer cells. Proc Natl Acad Sci USA. 2017; 114(31): 8360-8365.

Original Article

Blood Particle Separation Using Dielectrophoresis in A Novel Microchannel: A Numerical Study

Omid Zahedi Siani, M.Sc.[1], Mahdi Sojoodi, Ph.D.[2]*, Mohammad Zabetian Targhi, Ph.D.[1]*, Mansoureh Movahedin, Ph.D.[3]

1. Faculty of Mechanical Engineering, Tarbiat Modares University, Tehran, Iran
2. Faculty of Electrical and Computer Engineering, Tarbiat Modares University, Tehran, Iran
3. Faculty of Medical Sciences, Tarbiat Modares University, Tehran, Iran

Corresponding Addresses: P.O.Box: 14115-111, Faculty of Electrical and Computer Engineering, Tarbiat Modares University, Tehran, Iran
P.O.Box: 14115-111, Faculty of Mechanical Engineering, Tarbiat Modares University, Tehran, Iran
Emails: sojoodi@modares.ac.ir, zabetian@modares.ac.ir

Received: 16/September/2018, Accepted: 6/April/2019

Abstract

Objective: We present a four-branch model of the dielectrophoresis (DEP) method that takes into consideration the inherent properties of particles, including size, electrical conductivity, and permittivity coefficient. By using this model, bioparticles can be continuously separated by the application of only a one-stage separation process.

Materials and Methods: In this numerical study, we based the separation process on the differences in the particle sizes. We used the various negative DEP forces on the particles caused by the electrodes to separate them with a high efficiency. The particle separator could separate blood cells because of their different sizes.

Results: Blood cells greater than 12 µm were guided to a special branch, which improved separation efficiency because it prevented the deposition of particles in other branches. The designed device had the capability to separate blood cells with diameters of 2.0 µm, 6.2 µm, 10.0 µm, and greater than 12.0 µm. The applied voltage to the electrodes was 50 V with a frequency of 100 kHz.

Conclusion: The proposed device is a simple, efficient DEP-based continuous cell separator. This capability makes it ideal for use in various biomedical applications, including cell therapy and cell separation, and results in a throughput increment of microfluidics devices.

Keywords: Biomedical Applications, Blood Cells, Microfluidics

Cell Journal(Yakhteh), Vol 22, No 2, July-September (Summer) 2020, Pages: 218-226

Citation: **Zahedi Siani O, Sojoodi M, Zabetian Targhi M, Movahedin M. Blood particle separation using dielectrophoresis in a novel microchannel: a numerical Study. Cell J. 2020; 22(2): 218-226. doi: 10.22074/cellj.2020.6386.**

Introduction

The field of microfluidics, microfabrication, and research on miniaturized fluidic systems has been developed by 4 main factors: genesis microanalytical methods, microelectronics industry, an expansion of genomic sciences in the 1980s, and development of microfluidic systems for use in biological and chemical weapons in the 1990s (1). For the first time, researchers used microfluidics in the lab-on-a-chip (LOC) devices at the beginning of the 1990s (2). LOC has the capability to run various functions such as microparticle separation and sorting, cell culture, and analysis. An important application of LOC microfluidic devices is the analysis of blood cell components for subsequent applications. Microfluidic devices are used in the chemical industry, to separate micron size objects, mineral processing, biological researches, and diagnostics processes (3). Studies of diagnostics processes have focused on separation of dead cells from living cells and cancer cells from healthy cells.

The mechanical properties and connections among cell structures are important factors for sorting and separation of certain cells from other cells. It has been proven that some diseases such as malaria and gastrointestinal tumours change the mechanical deformability of the cell. Thus, cells can be separated by the use of mechanical properties such as elastic modulus and cell size (4). For example, normal red blood cells pass through blood capillaries; however, those cells infected by malaria parasites cannot circulate in the bloodstream because they are approximately 50 times harder than healthy blood cells, which leads to blocking of the capillaries (5). Similarly, epithelial cancer cells have different physical properties compared with healthy cells.

Cell separation techniques that use microfluidics can be divided into 3 categories: passive, active, and combined. Examples of passive techniques applied for cell or microparticle separation include pinched flow fractionation (6), inertia and dean flow fractionation (7), micro vortex manipulation (8), deterministic lateral displacement (9), hydrodynamic filtration (10), and micro-hydrocyclone (11). Examples of active techniques include dielectrophoresis (DEP) (12), and magnetic (13), optical (14), and acoustic techniques (15). In general, active methods use an external force field in their performance while passive methods do not use the external force field. The structure of devices that use passive techniques are simpler than active techniques, but the throughput of active techniques is more. The devices that use passive techniques are usually massive.

Table S1 (See Supplementary Online Information at www.celljournal.org) compares some of the cell sorting and isolation methods. Both electrical and acoustic methods have advantages of strong controllability, high efficiency, ease of operation, slight damage, and low cost when compared to other methods. These methods are suitable for the separation and sorting of bioparticles. In this research, we have attempted to manipulate human blood cells using the DEP method.

In the early 20th century, researchers first discussed the DEP phenomenon. In 1951, Pohl (16) studied the separation of solid particles from a polymer solution that resulted from polarization forces produced by the activation of an inhomogeneous electric field, which they named "dielectrophoresis". With the development of micromachining technologies and microelectromechanical systems at the beginning of the 1990s, researchers integrated electrochemical functions into chips, which enabled manipulation of cells, microparticles, and nanoparticles (2). Kim et al. (17) positioned 2 sets of electrodes at different angles for dielectrophoretic cell separation. They tagged target cells with DEP tags (polystyrene beads) and conducted the buffer and sample to the microchannels. In this way, they used a multi-target DEP activated cell sorter (MT-DACS) chip to separate tagged bacterial cells from non-target cells with a high purity. In 2011, Piacentini et al. (18) proposed focusing the particles on one side of the main microchannel using a buffer solution. Platelets were separated from red and white blood cells based on their size difference using a single-stage separation with a nonuniform electric field generated by 'liquid electrodes'. This resulted in a purity of 98.8%. In 2013, Li et al. (19) converted the electric field generated by a DC power supply to a local nonuniform electric field in an S-shaped curved microchannel by using both a microchannel curvature and obstacles. In this method, 10 and 15 polystyrene particle suspensions diluted by deionized water were injected into the inlet microchannel, and resulted in a successful, efficient particle separation. By the end of 2014, Lewpiriyawong and Yang (20) aligned 5 polydimethylsiloxane (PDMS) insulating blocks along one side of a main microchannel to induce a nonuniform electric field. Then, the buffer solution and samples that comprised one type of fluorescent particle and 2 types of nonfluorescent particles were injected into the microchannel inputs. Cell mixtures of 3 sizes (2 μm, 5 μm, and 10 μm) were separated at a separation efficiency of 99%. In 2016, Ye et al. (21) developed a device that applied the DEP method to separate samples, including the 3 μm, 10 μm, and 25 μm polystyrene microparticles. The multiple particles were separated continuously using a pair of acupuncture needle electrodes embedded in a PDMS as a hurdle in the microchannel, which resulted in more than 90% separation purity. In 2018, Kale et al. (22) presented a DEP-based device that manipulated latex beads with a diameter of 5 μm. The performance of the latex beads was evaluated as a function of the applied voltage.

After an investigation of the presented previous works, we have developed a relatively simple and efficient model. This model is based on the insulator-based DEP method, where the electric field gradient is produced by the applied alternating electric current to the electrodes. The induced force generated by the gradient electric field results in separation of particles with different sizes. For this purpose, the applied alternating voltages to electrodes are approximately 50 V and -50 V. As a result of the hydrodynamic pressure difference between the input and output zones of the main microchannel, the fluid flows in the microchannel and the fluid driving force is applied to the cells. The DEP forces depend on the size of cells. Both the DEP forces and fluid driving force are simultaneously applied to the cells, which causes them to separate. Therefore, by taking into consideration cell size, the cells are moved into the different branches in the downstream main microchannel.

This work has major advantages compared with previous works. In prior works, the multi-branch model of the DEP method was used to separate the latex particles and other test particles, and the separation of blood cells using this method is offered. In the current study, we have used the simple, efficient electrode structure to separate blood cells based on their size. In the current work, separation of the platelets from the white blood cells (large lymphocytes and neutrophils) and red blood cells is a continuous, one-step process done by the AC-DEP technique, in contrast to multiple steps used in most of the previous works. Previous studies have used a maximum of 3 branches for the multi-branch model of the DEP method to separate the blood cells. However, if these models could lead to deposition of the blood cells with sizes greater than 12 μm. Offering a four-branch model of the DEP method, resulting in the capability of the proposed design to separate the blood cells with sizes greater than 12 μm using the fourth branch. This could improve separation efficiency and prevent deposition of the particles in the other branches. In the present research, we considered both large lymphocytes and neutrophils to separate the white blood cells from the other blood cells. The neutrophils are the most common white blood cell type, and lymphocytes are the second most common in most mammals (23). The most recent studies have only separated one type of white blood cell from the other blood cells. With regards to the various sizes of white blood cells, it seemed necessary to take both types of white blood cells into consideration for a more accurate separation.

Materials and Methods

Dielectrophoretic force exerted on spherical particles

In this numerical study, we considered a variable electric potential with an angular frequency, ω, to produce an alternating electric field (AC). The alternating electrical potential is defined as:

$$\emptyset(x,t)=\mathrm{Re}[\overline{\emptyset}(x)e^{j\omega t}] \quad [1]$$

Where: Re[] is the real part of the complex variable (∅), ω is the angular frequency, t represents time, j is defined as: $j \equiv \sqrt{(-1)}$, x is the position vector, and the symbol $\overline{\emptyset}$ represents the potential phasor, regarding the relationship between electric potential and field, that is (24):

$$\overline{E} = -\nabla \overline{\emptyset} \quad [2]$$

The alternating electric field is obtained:

$$E(x,t) = Re[\overline{E}(x) e^{j\omega t}] \quad [3]$$

In [3], $\overline{E}$ is the electric field phasor. The time-averaged DEP force on the spherical particles in an alternating electric field is calculated as below (24, 25):

$$\langle F_{DEP} \rangle = 2\pi\varepsilon_m Re[f_{cm}] R^3 \nabla E_{rms}^2 \quad [4]$$

Where:‹› indicates the time-averaged DEP force, E_{rms} represents the root-mean-square magnitude of the alternating electric field, ε_m is the electric permeability coefficient of the medium, and f_{cm} is the Clausius-Mossotti factor, which is defined as follows (24, 25):

$$f_{cm}(\tilde{\varepsilon}_m, \tilde{\varepsilon}_p) = (\tilde{\varepsilon}_p - \tilde{\varepsilon}_m)/(\tilde{\varepsilon}_p + 2\tilde{\varepsilon}_m) \quad [5]$$

Where: p indicates the particle, m represents the suspending medium, and $\tilde{\varepsilon}$ is the complex permittivity, which is defined as (24):

$$\tilde{\varepsilon} = \varepsilon - j(\sigma/\omega) \quad [6]$$

Where: σ is electrical conductivities and ω is angular frequency. According to the dielectrophoretic force formula, the following points are notable in the numerical study of particle separation: i. The dielectrophoretic force is a nonlinear function because it is proportional to the square of the electric field, ii. The dielectrophoretic force is proportional to the cube of the particle radius (F_{DEP} has the potential to separate the particles from each other based on the difference in volume), and iii. The dielectrophoretic force is proportional to f_{cm}, and the Clausius-Mossotti factor is proportional to $\tilde{\varepsilon}_p$ and $\tilde{\varepsilon}_m$. Therefore, F_{DEP} can distinguish particles and cells based on their complex permittivity.

Inserting equation [6] into [5], results in:

$$f_{cm} = ((\varepsilon_p - \varepsilon_m) + j/\omega(\sigma_p - \sigma_m))/((\varepsilon_p + 2\varepsilon_m) + j/\omega(\sigma_p + 2\sigma_m)) \quad [7]$$

Which indicates that in the high angular frequency limit, the Clausius-Mossotti factor depends on the dielectric permittivity of the suspending medium and the particle as:

$$\lim_{(\omega \to \infty)} f_{cm} = (\varepsilon_p - \varepsilon_m)/(\varepsilon_p + 2\varepsilon_m) \quad [8]$$

In contrast, in the low angular frequency limit, the Clausius-Mossotti factor depends on electrical conductivities of both the particle and the liquid medium:

$$\lim_{(\omega \to 0)} f_{cm} = (\sigma_p - \sigma_m)/(\sigma_p + 2\sigma_m) \quad [9]$$

Dielectrophoretic force on the spherical shell

The dielectrophoretic force is used in different methods according to the literature. In a report by Li et al. (26), patterning micro-electrodes is within the microchannel by using photolithography, namely, a metal-electrode based DEP (eDEP). Consequently, metal electrodes are fabricated. In this method, it is necessary to apply the AC voltage to the electrodes because separation requires the electric field gradient. The main disadvantages of this method are the complexity of manufacturing and the chemical reactions of the electrodes. To tackle this problem, an alternative method is suggested, insulator-based DEP (iDEP), where the direct voltage is used to create the electric field gradient. iDEP applies methods to create obstacles in the microchannel and uses curvature in the microchannel. Straight microchannels with electrode obstacles have some limitations such as the effect of excessive shear stress applied on the particles, joule heating effect, and creation of local nonuniform electric fields. If the insulating curved microchannels are used (i.e., circular, serpentine, spiral etc.), the limitations are relatively less. It should be noted that, in the alternative method, the applied voltage to the electrodes is direct and greater than the first method (19).

The eDEP-based separation methods have many applications in the fields of chemical and biochemical processes, such as separation and sorting of fine particles (i.e., proteins, carbon-nanotubes, viruses). iDEP-based sorting methods are proper for separation of bioparticles such as bacteria, RNA, and DNA (27). The structure of biological particles is more complex compared with solid homogeneous spherical particles. Therefore, the nonhomogeneous spherical particle model should be capable of calculating the DEP force exerted on the bioparticles. The concentric multi-shell model is widely used for calculation of the DEP force that acts on biological particles. In the simplest case, a cell is considered to be a spherical single-layer model. In this case, as shown in Figure S1 (See Supplementary Online Information at www.celljournal.org), the layered particle model is substituted as a homogenous particle with an equivalent radius and permittivity.

According to the description provided, the complex permittivity of particle $\tilde{\varepsilon}_p$ is replaced with equivalent complex permittivity $\tilde{\varepsilon}_p'$. Thus, the effective complex permittivity of $\tilde{\varepsilon}_p'$ is substituted in the Clausius-Mossotti factor, which is defined as (24):

$$f_{cm}(\tilde{\varepsilon}_m, \tilde{\varepsilon}_p') = (\tilde{\varepsilon}_p' - \tilde{\varepsilon}_m)/(\tilde{\varepsilon}_p' + 2\tilde{\varepsilon}_m) \quad [10]$$

Where (24):

$$\tilde{\varepsilon}_p' = \tilde{\varepsilon}_1 [(a^3 + 2(\tilde{\varepsilon}_2 - \tilde{\varepsilon}_1)/(\tilde{\varepsilon}_2 + 2\tilde{\varepsilon}_1))/(a^3 - (\tilde{\varepsilon}_2 - \tilde{\varepsilon}_1)/(\tilde{\varepsilon}_2 + 2\tilde{\varepsilon}_1))] \quad [11]$$

and 'a' is defined as R1/R2 .

Cellular interior conductivity and permittivity can be measured with the electrorotation method. In this method, the rotation of cells is measured under the influence of the torsional torque generated by the rotational electric field as a function of electric field frequency. In order to estimate the dielectric properties of cells, the measured spectral data is fitted to a curve using the optimization of single-shell model parameters (28). The Clausius-Mossotti factor can be calculated using the estimated dielectric properties of the cells. Table 1 lists the dielectric and physical properties of platelets, red blood cells, neutrophils, large lymphocytes and their suspension medium, including the cell diameter (d), membrane thickness (t), the specific membrane capacitance (C_{mem}), the internal electrical conductivity (σ_{int}), the internal relative permittivity (ε_{rint}), the membrane electrical conductivity (σ_{mem}), and the membrane relative permittivity (ε_{mem}).

Figure S2 (See Supplementary Online Information at www.celljournal.org) shows the DEP spectra of spherical particles with a single-shell model for dielectric properties of blood cells using the medium with a conductivity of 55 mS/m, where the Clausius-Mossotti factor is computed in the MATLAB software with a single-shell model. The real part of the Clausius-Mossotti factor ranges from -0.5 to 1 and can increase or decrease the DEP forces. If the Clausius-Mossotti factor takes a positive sign (P-DEP), the particles are attracted to the higher electric field zone; if the factor takes a negative sign, the particles are attracted to the lower electric field zone (N-DEP).

When the applied electric field frequency is less than 100 (KHz), the Clausius-Mossotti factor for platelets, red blood cells, neutrophils, and large lymphocytes will approach -0.5 and, consequently, the blood cells experience N-DEP forces. According to equation [4], the dielectrophoretic force is proportional to the cube of the radius, and this results in the separation of blood cells in the downstream branches of the microchannel.

Modelling and simulation

The medical importance of this study is to purify blood cells concentration at the microfluidic chip outlets to further biological investigations for diagnostic and therapeutic studies. The proposed separation method could be replaced by a fluorescence-activated cell sorter (FACS) for biomedical applications or differential cell counters in haematology analysis in medical laboratories. Furthermore, the designed chip can also be used as a home-use device for personalized medicine.

The schematic design of the microchip is shown in Figure S3 (See Supplementary Online Information at www.celljournal.org). There are two inlet branches and four exit branches in the design, which are connected to input and output reservoirs. The input reservoirs are for injection of buffer solution and samples into the microchannels "A" and "B", respectively. The length of the main microchannel is 1400 μm and the width of the microchannel is 300 μm. Microchannel "B" is 150 μm wide. The widths of the branch microchannels "C", "D", "E", and "F" are 120 μm, 100 μm, 120 μm and 100 μm, respectively. Each of the microchannels has a depth of 50 μm. The electrodes are placed on the right side of the microchannel. Electrodes 1 and 2 have a width of 170 μm and 40 μm, respectively. The electric fields can be calculated by the Laplace equation (equation [12]). In the mentioned schematic, the insulated microchannels are connected to the reservoirs and the electrodes that apply the AC electric fields on the passing fluid through the main microchannel.

$$\nabla^2 \overline{\emptyset} = 0 \qquad [12]$$

Table 1: The dielectric and physical properties of different blood cells and their suspension medium

Property	Platelets	Red blood cells	Neutrophils	Large lymphocytes	Suspension medium
Diameter (d, μm)	2.0 (18, 29)	6.2 (30)	10.0 (31, 32)	12.0 (32, 33)	-
Thickness (t, nm)	8 (34)	8 (35)	7 (36)	7 (36)	-
C_{mem} (mF/m^2)	7.9 (34)	8 (36)	11 (37)	16.2 (38)	-
σ_{int} (S/m)	0.16 (34)	0.31 (39)	0.6 (37)	0.83 (38)	0.055
ε_{rint}	50 (34)	59 (39)	150.9 (37)	73.2 (38)	78
σ_{mem} (S/m)	1e-7 (34)	1e-6 (39)	1.4e-7 (37)	1.4e-7 (38)	-
ε_{mem}	7.2 (34)	4.44 (39)	8.7 (37)	12.8 (38)	-

Where: $\overline{\emptyset}$ is defined as the phasor of the alternating electrical potential applied on the electrodes.

In the proposed design (Fig.S3) (See Supplementary Online Information at www.celljournal.org), the Reynolds number is extremely low; therefore, the inertial term in the Navier-Stokes equation can be omitted, resulting in:

$$\mu\nabla^2 u=\nabla p \qquad [13]$$

Where: u is the fluid velocity, ∇p is the pressure gradient, and μ is the dynamic viscosity. For the walls of the microchannels, we considered the no-slip boundary conditions. The flow velocities at the input "A" and "B" are fixed and the output flow at positions "C", "D", and "E" flows within the exited reservoirs with zero gauge pressure. We took into consideration the following assumptions for conducted simulation: i. The fluid flow has very low Reynolds number values ($Re \ll 1$) and the inertial term in the Stokes equations is dropped. Consequently, the fluid flow is considered a type of creeping flow, ii. The fluid flow is diluted to the extent that the effect of particle interaction is ignored and the particles do not exert any significant force on each other. In addition, the coupling between the fluid and particle phase is considered to be one-way. Thus, there is negligible particle force on the fluid, iii. The fluid flow is injected in the microchannel from branches "A" and "B" (Fig.S3) (See Supplementary Online Information at www.celljournal.org). The flow field is planar and thus the "z" component of the velocity is negligible compared with the two other components of the velocities, iv. The chip is installed horizontally. Consequently, the gravitational force can only cause particle deposition, v. The walls of the microchannels and the particles are not porous. Therefore, the effect of the particles and the walls are considered impermeable solids, and vi. The thermal gradient inside the microchannels is relatively low and does not affect the particles and fluid velocities.

The displacement changes of the particles can be calculated by time integrating the particles velocity, as:

$$x_p(\tau)=x_0+\int u_p(t)\,dt \qquad (0 \ll t \ll \tau) \qquad [14]$$

Where: $x_p(\tau)$ is the location of the microchannel liquid outlet at the discharge hoses, x_0 is the initial position of the particle, and $u_p(t)$ is the particle velocity.

According to Newton's law, the translational motion of a particle is explained by (24):

$$F_{ext}=m_p(du_p/dt) \qquad [15]$$

Where: F_{ext} is defined as the total of the superficial and volumetric forces applied to the particles and m_p is considered the particle mass.

The exerted drag force on a spherical particle is calculated at a very low Reynolds number ($Re \ll 1$) by the following relation according to Stokes low (40):

$$F_{drag}=3\pi\mu d(u-u_p) \qquad [16]$$

Where: μ is the dynamic viscosity, d is the particle diameter, u is the fluid velocity, and u_p is the particle velocity within the fluid.

In the conducted design, it is assumed that the particles move across the microchannels at a constant velocity. Substituting equations [16] and [4] into equation [15], we calculate the particle velocity as:

$$u_p=u-(\varepsilon_m Re[f_{cm}]R^2\nabla E_{rms}^2)/3\mu \qquad [17]$$

Results

The particle separation that resulted from the dielectrophoresis force

Separation of platelets, red blood cells, neutrophils, and large lymphocytes was simulated by the DEP field-flow-fractionation in COMSOL Multiphysics software (version 5.1; https://www.comsol.de/products). Both forces of the flow focusing and the DEP affected the particles' trajectories and resulted in separation of the cells according to size. The prepared sample and buffer solution are injected into the downstream branches. Using the applied hydrodynamic pressures on the inlet solutions, the cells focused on the right side of the microchannel and, at the same time, the dielectrophoretic voltage is applied to the electrodes, which resulted in separation of the particles.

Figure 1 shows the magnitude of the exerted dielectrophoretic forces on the blood cells and the resultant fluctuations of dielectrophoretic forces from the alternating electric field can be seen in this figure.

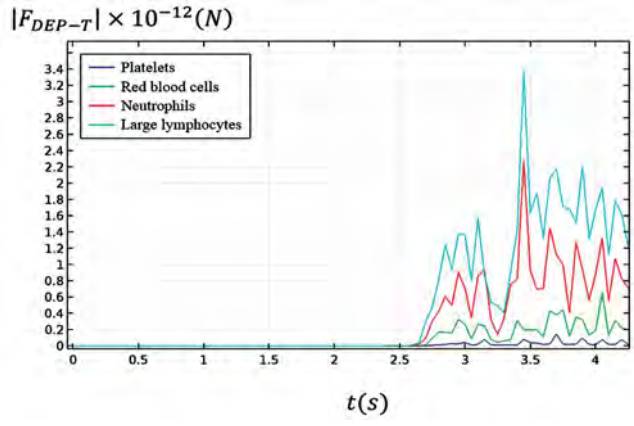

Fig.1: Comparison of the applied dielectrophoretic forces on platelets, red blood cells, neutrophils, and large lymphocytes.

The slope of the beginning of the graph is almost zero, whereas the slope of the end gradually decreased because in these areas the effect of the electric field decreased compared with surrounding areas and in a time decreasing

nature. The maximum slope of the diagram occurred during the time interval of 3.4 to 3.5 seconds because, in this interval, the particles experienced the maximum electric field gradient.

We used the proposed design for continuous separation of the cells, where the localized AC-DEP forces were applied to cells located around the electrode blocks. Figure 2 shows the electric field streamlines, exerted forces diagram on the cell, and velocity magnitude distribution near the electrodes for a cell that passed through the microchannels. The particles were followed by the fluid flow streamlines because the electrodes did not apply the alternating electric field to the microchannels. In contrast, since an electric potential was imposed on the electrodes, the electric field gradient was created by the electrodes around the corners of the electrode blocks, which resulted in the generation of the DEP forces. In this design, the nDEP forces were exerted on the cells, which caused them to be repelled from the corners of the electrodes. Among the leaded cells, the white blood cells had the largest size and experienced the greatest nDEP force magnitude, and were conducted to outlet channels "E" and "F". The red blood cells and the platelets moved through the outlet channels "D" and "C" respectively, and experienced the nDEP forces proportional to their volumes.

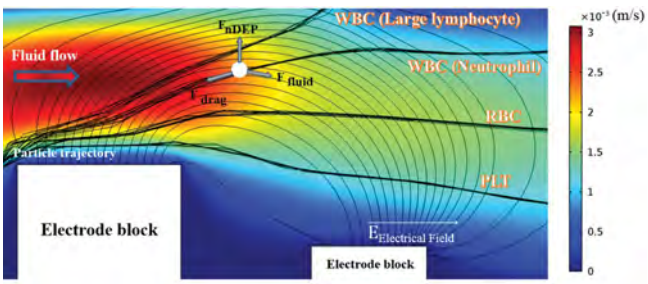

Fig.2: Electric field streamlines, force diagram, and fluid velocity distribution near the electrode blocks, where the blood cells are repelled of zone with higher electric field and are carried by the hydrodynamic force exerted by fluid.

Figure S4 (See Supplementary Online Information at www.celljournal.org) shows the convergence plot of the absolute error versus iteration number. The validation process is performed for the steady-state condition of the fluid flow. The Newton-Raphson method is used to correct the absolute error terms of the momentum equations. To solve the equations, the Newton-Raphson method starts with an initial guess and continues to converge the obtained answer to the exact answer with the desired precision. In Figure S4 (See Supplementary Online Information at www.celljournal.org), we show the absolute error plot of the fluid flow equation solutions with an absolute error of 0.85, which continued until it converged to an absolute error less than 10^{-13}.

In Table S2 (See Supplementary Online Information at www.celljournal.org), the applied drag force on the neutrophils is calculated in the middle zone of the microchannel (t=2.85 seconds after injection of the particles). The results showed that magnitude of the applied drag force on the neutrophils was independent of mesh size for the normal to the fine grid sizes with an uncertainty of 1 e -11 N. The magnitude of the drag force was equal to 1.758 e -10 on average.

We used the geometrical model applied by Ye et al. (21) to validate the simulation. The simulation showed that latex particles (polystyrene microspheres) with diameters of 3 μm, 10 μm, and 25 μm were conducted into different outlet channels. The path lines of the particles were compared with the experimental path lines presented in the reference article. Figure 3 shows a comparison of the two mentioned models, where the applied frequency to the electrodes equalled 1 MHz and flow velocity ratio between branch "A" and branch "B" (inlets) equalled 4.2. Of note, the applied alternating voltage on the electrodes could affect the magnitude of the applied dielectrophoretic force on the particles (Fig.3A-D).

The relative error with respect to the experimental data is expressed as:

$$\alpha=|(P_A - P_B)/P_A|\times 100 \quad [18]$$

Where: P_A is the measured distance of the particles from the upper wall of the microchannel branches and P_B is the calculated distance.

Considering that in Figure 3A, the 25 μm particles did not cross through just one branch. Thus, in order to measure P_A in Figure 3A and P_B in Figure 3B, we took into consideration the upper walls of both outlets "E" and "D". According to our image processing, we assumed that in Figure 3A, 80% of particles with a diameter of 25 μm passed through outlet "D".

Table 2 shows the magnitude of α for different sizes of polystyrene microspheres with diameters of 25 μm, 10 μm, and 3 μm for the 112.5 V and 150 V voltages applied to the electrodes.

The results showed that the particle trajectory of the present work was similar to that reported by Ye et al. (21), with an acceptable deviation of 22.5%. This indicated that the presented model could be used in the separation applications. Therefore, we developed the model for 4 different size channels in order to separate the 4 blood cell types.

It is important that the particle separation be independent of the initial position of the released particles. We have taken this into consideration in the design and it could affect the separation precision. The released particles of the initial various locations were separated successfully (Fig.S5) (See Supplementary Online Information at www.celljournal.org). The density and viscosity values of the buffer solution are ρ_f=1000 Kg/m^3 and μ_f=10^{-3} Pa.s, respectively. According to Figure S2 (See Supplementary Online Information at www.celljournal.org), the electric field frequency is considered to be 100 KHz. For this reason, the Clausius-Mossotti factor of the cells approached -0.5.

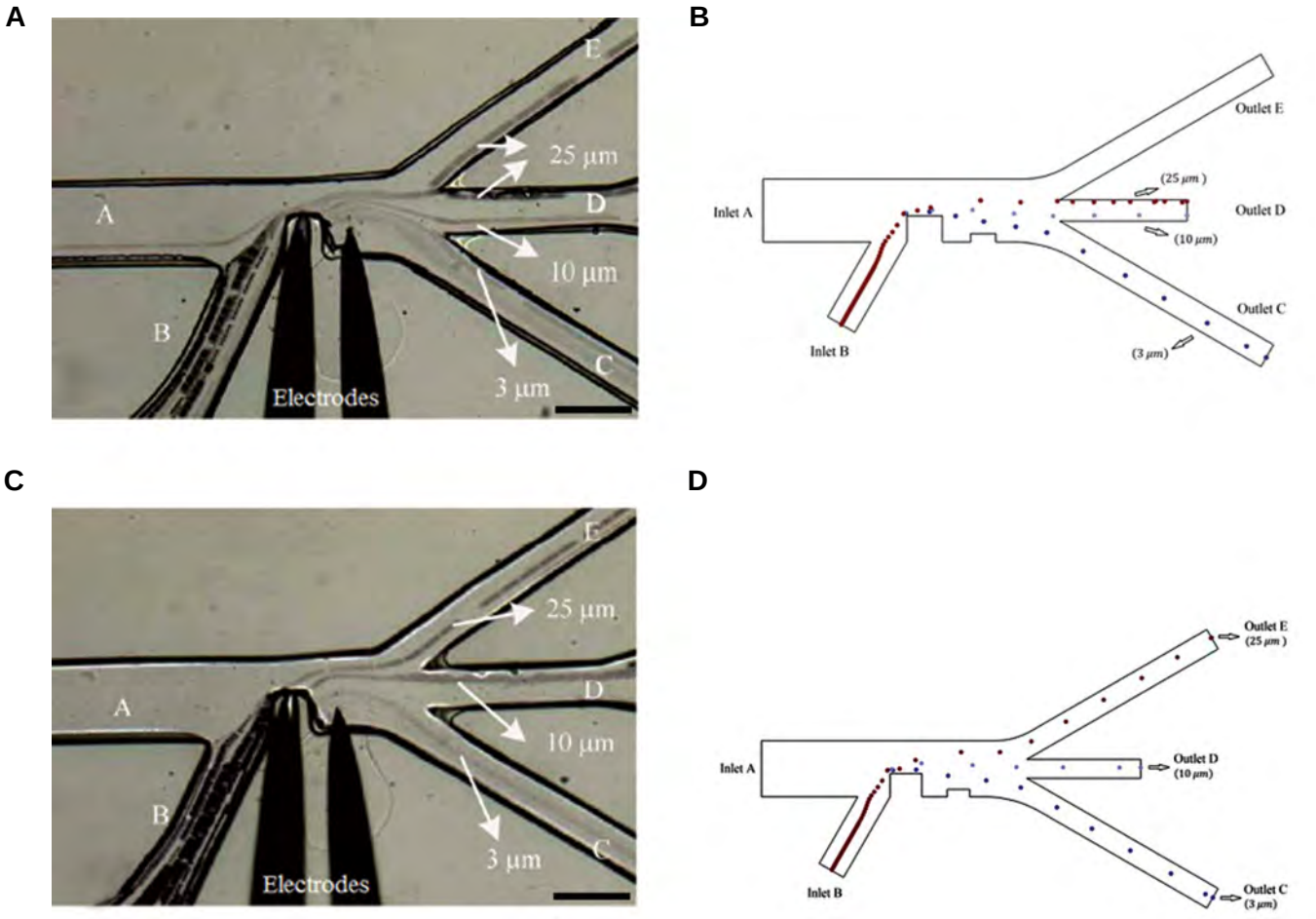

Fig.3: A comparison of the presentation model in this manuscript with the presentation model by Ye et al. (21). **A.** The path lines of three size particles for voltage of 112.5 V (experimental data reported by Ye et al. (21)), **B.** Prediction of the path lines of three size particles for voltage of 112.5 V (simulated data is reported in this article), **C.** The path lines of three size particles for voltage of 150 V (experimental data reported by Ye et al. (21)), and **D.** Prediction of the path lines of three size particles for voltage of 150 V (simulated data is reported in this manuscript).

Table 2: The magnitude of α for the polystyrene microspheres with different diameters and the voltages of 112.5 V and 150 V (21)

Voltage applied to the electrodes	Polystyrene microsphere diameters (µm)	Measured distance of the particles from the upper wall (µm)	Calculated distance of the particles from the upper wall (µm)	Corresponding relative errors (%)	Average of the relative errors (%)	Overall average of the relative errors (%)
	25	13.0	9.5	26.9		
112.5 V	10	82.2	74.0	10.0	24.0	
	3	49.6	67.1	35.3		
						22.5
	25	57.8	41.6	28.0		
150.0 V	10	36.1	43.2	19.6	21.1	
	3	55.4	46.6	15.8		

We used the applied voltage to the electrodes to generate the gradient of the electric field intensity (∇E^2) in the microchannel. The DEP forces were created by the gradient of the electric field intensity. Thus, in order to continuously separate the cells that had high purity, it was necessary to check the effect of the applied voltage on the cell separation process (Fig.4A-C). The electric field gradient in the corners of the electrodes was higher than at other places in the microchannels. Therefore, the particles experienced more DEP forces in the corners of electrodes, which resulted in cells that repelled from the corners. According to equation [4], the DEP force is a function of the gradient of the electric field intensity, the particle volume, and the real part of the Clausius-Mossotti factor.

Thus, as the diameter and the applied voltage become higher, repelling will increase.

Figure 4A-C shows separation of the blood cells. As depicted in Figure 4A, by applying voltage and pressure differences, the lymphocytes and the neutrophils were simultaneously removed from outlet "E", the red blood cells were removed from outlet "D", and the platelets were removed from outlet "C". This indicated that the particles did not experience successful separation from outlet "E" because the applied voltage was not enough to shift the larger particles further. Therefore, in this case, the performed separation was not successful.

In the next mode (Fig.4B), we applied a higher voltage to the electrodes. This applied voltage to the electrodes was 120 V_{pp} (peak-peak voltage). When the voltage was applied, the lymphocytes were shifted and removed from outlet "F" and the red blood cells were drawn toward the upper wall of the microchannel branch (branch "D"). This event increased the likelihood of the separation error.

Finally in the last mode, the applied voltage to the electrodes was 100 V_{pp}. Figure 4C shows successful separation of the blood cells. The simulation results show that the proposed design has the ability to separate the blood cells based on cell size with high accuracy. For a successful separation, it is necessary for the DEP and drag forces to be properly employed.

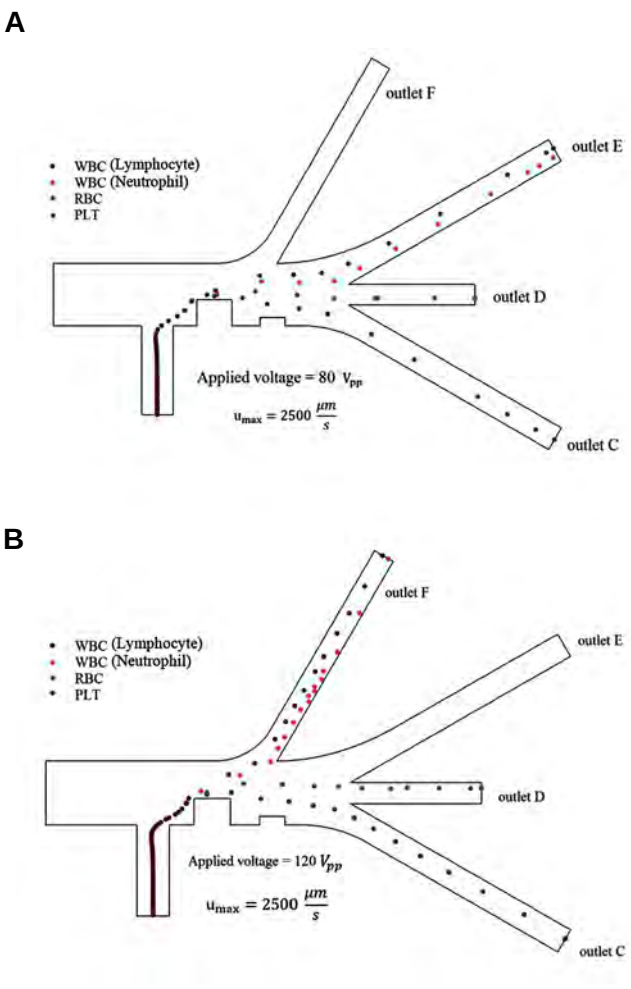

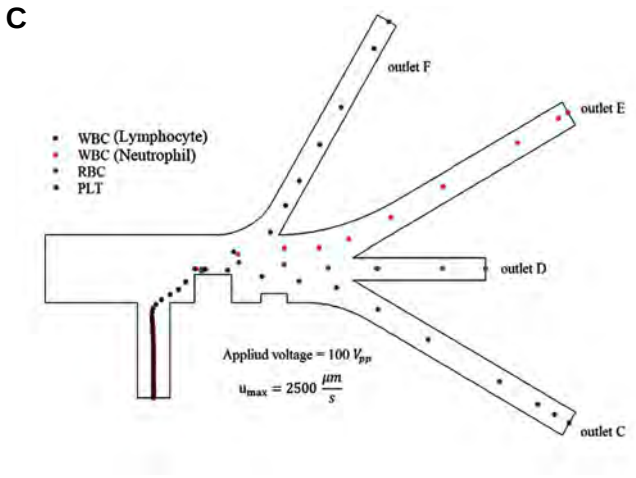

Fig.4: The blood cell trajectory when the applied voltage to the electrodes was: **A.** 80 V_{pp}, **B.** 120 V_{pp}, and **C.** 100 V_{pp}.

Discussion

We evaluated this design by simulating trajectories of large lymphocytes (diameter=12.0 µm) (32, 33), neutrophils (diameter=10.0 µm) (31, 32), red blood cells (d=6.2 µm) (30), and platelets (d=2.0 µm) (18, 29) in COMSOL Multiphysics software (version 5.1.) The COMSOL software is based on the finite element method for discretization of partial differential equations on the computational domain. In order to analyse the model, the finite element divide the model into small geometric zones. As the next step, polynomial functions were used to calculate the velocity and pressure components. At first, the alternating electric field and the fluid flow velocities were computed by considering the creeping flow and previously mentioned conditions, where the fluid flow has very low Reynolds number value ($Re \ll 1$). The suspending medium (the buffer solution) was diluted to the extent that, it was considered as water (ρ=997 kg/m^3, $\mu = 0.9\times10^{-3}$ kg/ms). The chip was installed horizontally. The flow field was planar and thus the "z" component of the velocity was negligible compared with the two other components of velocities. The walls of the microchannels and the particles were not porous and there was a negligible thermal gradient inside the microchannels. Finally, we simulated the particles' trajectories in the microchannels. In the simulation, the samples were released from different positions in inlet "B".

Conclusion

In this manuscript, we propose the four-branch model of the DEP method, taking into consideration the inherent properties of particles such as size, electrical conductivity, and permittivity coefficient. The presented design suggests a relatively simple setup to effectively separate 4 different blood cell types of 2.0 µm, 6.2 µm, 10.0 µm, and greater than 12.0 µm sizes. Therefore, it can be used to separate blood cells in different applications, including microfluidic separation devices and medical diagnostic processes. This device can separate blood

cells using the single-stage system. The applied voltages to the electrodes can be adjusted such that shear stresses and joule heating effect are neglected. In the future, we suggest that the proposed device be extended for use in biomedical and diagnostic applications, with the goal of separating all blood components.

Acknowledgements

There is no financial support and conflict of interests in this study.

Authors' Contributions

O.Z.S., M.S., M.Z.T., M.M.; Contributed extensively to data interpretation and the conclusion. All authors edited, finalised, and approved the final version of this manuscript for submission.

References

1. Whitesides GM. The origins and the future of microfluidics. Nature. 2006; 442(7101): 368-373.
2. Manz A, Graber N, Widmer HM. Miniaturized total chemical analysis systems: a novel concept for chemical sensing. Sensors and actuators B: Chemical. 1990; 1(1-6): 244-248.
3. Lopez GA, Estevez MC, Solera M, Lechuga LM. Recent advances in nanoplasmonic biosensors: applications and lab-on-a-chip integration. Nanophotonics; 2017; 6(1): 123-136.
4. Suresh S, Spatz J, Mills JP, Micoulet A, Dao M, Lim CT, et al. Reprint of: connections between single-cell biomechanics and human disease states: gastrointestinal cancer and malaria. Acta Biomater. 2015; 23 Suppl: S3-S15.
5. Zhang Y, Huang C, Kim S, Golkaram M, Dixon MW, Tilley L, et al. Multiple stiffening effects of nanoscale knobs on human red blood cells infected with Plasmodium falciparum malaria parasite. Proc Natl Acad Sci USA. 2015; 112(19): 6068-6073.
6. Takagi J, Yamada M, Yasuda M, Seki M. Continuous particle separation in a microchannel having asymmetrically arranged multiple branches. Lab Chip. 2005; 5(7): 778-784.
7. Wu Z, Chen Y, Wang M, Chung AJ. Continuous inertial microparticle and blood cell separation in straight channels with local microstructures. Lab Chip. 2016; 16(3): 532-542.
8. Hsu CH, Di Carlo D, Chen C, Irimia D, Toner M. Microvortex for focusing, guiding and sorting of particles. Lab Chip. 2008; 8(12): 2128-2134.
9. Davis JA, Inglis DW, Morton KJ, Lawrence DA, Huang LR, Chou SY, et al. Deterministic hydrodynamics: taking blood apart. Proc Natl Acad Sci USA. 2006; 103(40): 14779-14784.
10. Yamada M, Seki M. Microfluidic particle sorter employing flow splitting and recombining. Anal Chem. 2006; 78(4): 1357-1362.
11. Bagdi P, Bhardwaj P, Sen AK. Analysis and simulation of a micro hydrocyclone device for particle liquid separation. J Fluids Eng. 2012; 134(2): 021105.
12. Huang C, Smith JP, Saha TN, Rhim AD, Kirby BJ. Characterization of microfluidic shear-dependent epithelial cell adhesion molecule immunocapture and enrichment of pancreatic cancer cells from blood cells with dielectrophoresis. Biomicrofluidics. 2014; 8(4): 044107.
13. Inglis DW, Riehn R, Austin RH, Stum JC. Continuous microfluidic immunomagnetic cell separation. Appl Phys Lett. 2004; 85(21): 5093-5095.
14. Huang SB, Chen J, Wang J, Yang CL, Wu MH. A new optically-induced dielectrophoretic (ODEP) force-based scheme for effective cell sorting. Int J Electrochem Sci. 2012; 7: 12656-12667.
15. Ma Z, Collins DJ, Ai Y. Detachable Acoustofluidic System for Particle Separation via a Traveling Surface Acoustic Wave. Anal Chem. 2016; 88(10): 5316-5323.
16. Pohl HA. Dielectrophoresis: the behavior of neutral matter in nonuniform electric fields. New York: Cambridge University Press; 1978.
17. Kim U, Qian J, Kenrick SA, Daugherty PS, Soh HT. Multitarget dielectrophoresis activated cell sorter. Anal Chem. 2008; 80(22): 8656-8661.
18. Piacentini N, Mernier G, Tornay R, Renaud P. Separation of platelets from other blood cells in continuous-flow by dielectrophoresis field-flow-fractionation. Biomicrofluidics. 2011; 5(3): 34122-341228.
19. Li M, Li Sh, Li W, Wen W, Alici G. Continuous particle manipulation and separation in a hurdle-combined curved microchannel using DC dielectrophoresis. In: Yu A, Dong K, Yang R, Luding S, editors. Proceedings of the 7th International Conference on Micromechanics of Granular Media; Australia: AIP Publishing; 2013; 1150-1153.
20. Lewpiriyawong N, Yang C. Continuous separation of multiple particles by negative and positive dielectrophoresis in a modified H-filter. Electrophoresis. 2014; 35(5): 714-720.
21. Ye T, Yukun R, Hui Y, Hongyuan J. Continuous separation of multiple size microparticles using alternating current dielectrophoresis in microfluidic device with acupuncture needle electrodes. Chinese Journal of Mechanical Engineering. 2016; 29(2): 325-331.
22. Kale A, Patel S, Xuan X. Three-dimensional reservoir-based dielectrophoresis (rDEP) for enhanced particle enrichment. Micromachines (Basel). 2018; 9(3): 123.
23. Bain BJ. A beginner's guide to blood cells. 2nd ed. London: John Wiley & Sons: 2017.
24. Jones TB. Electromechanics of particles. England: Cambridge University Press; 2005.
25. Liao SH, Chang CY, Chang HC. A capillary dielectrophoretic chip for real-time blood cell separation from a drop of whole blood. Biomicrofluidics. 2013; 7(2): 24110.
26. Li, M, Qu Y, Dong Z, Wang Y. Limitations of Au particle nanoassembly using dielectrophoretic force-a parametric experimental and theoretical study. IEEE Transactions on Nanotechnology. 2008; 7(4): 477-479.
27. Pethig, R. Review-Where is dielectrophoresis (DEP) going? J Electrochem Soc. 2017; 164(5): B3049-B3055.
28. Huang Y, Wang XB, Hölzel R, Becker FF, Gascoyne PR. Electrorotational studies of the cytoplasmic dielectric properties of Friend murine erythroleukaemia cells. Phys Med Biol. 1995; 40(11): 1789-1806.
29. Pommer MS, Zhang Y, Keerthi N, Chen D, Thomson JA, Meinhart CD, et al. Dielectrophoretic separation of platelets from diluted whole blood in microfluidic channels. Electrophoresis. 2008; 29(6): 1213-1218.
30. Turgeon ML. Clinical hematology: theory and procedures. 4th ed. London: Lippincott Williams & Wilkins; 2005.
31. Conover MR, Vail RM. Human diseases from wildlife. 1st ed. Boca Raton: CRC Press; 2014.
32. Downey GP1, Doherty DE, Schwab B 3rd, Elson EL, Henson PM, Worthen GS. Retention of leukocytes in capillaries: role of cell size and deformability. J Appl Physiol (1985). 1990; 69(5): 1767-1778.
33. Rozenberg G. Microscopic haematology: a practical guide for the laboratory. Elsevier Australia: Churchill Livingstone; 2011.
34. Eggera M, Donath E, Spangenberg P, Bimmler M, Glaser R, Till U. Human platelet electrorotation changed induced by activation: inducer specificity and correlation to serotonin release. Biochimica et Biophysica Acta (BBA)-Molecular Cell Research. 1988; 972(3): 265-276.
35. Gagnon ZR. Cellular dielectrophoresis: applications to the characterization, manipulation, separation and patterning of cells. Electrophoresis. 2011; 32(18): 2466-2487.
36. Pethig RR. Dielectrophoresis: theory, methodology and biological applications. Hoboken: John Wiley & Sons; 2017; 213-244.
37. Morgan H, Holmes D. Multi-frequency impedance method and apparatus for discriminating and counting particles expressing a specific marker. 2012, Google Patents.
38. Huang Y, Wang XB, Gascoyne PRC, Becker FF. Membrane dielectric responses of human T-lymphocytes following mitogenic stimulation. Biochimica et Biophysica Acta (BBA)-Biomembranes. 1999; 1417(1): 1-62.
39. Adekanmbi EO, Srivastava SK. Dielectrophoretic applications for disease diagnostics using lab-on-a-chip platforms. Lab Chip. 2016; 16(12): 2148-2167.
40. Leal LG. Advanced transport phenomena: fluid mechanics and convective transport processes. Cambridge University Press; 2007.

Original Article

Optimizing The Cell Seeding Protocol to Human Decellularized Ovarian Scaffold: Application of Dynamic System for Bio-Engineering

Leila Mirzaeian, M.Sc.[1, 2], Farideh Eivazkhani, M.Sc.[2], Maryam Hezavehei, Ph.D.[2], Ashraf Moini, M.D.[3, 4, 5], Fereshteh Esfandiari, Ph.D.[6], Mojtaba Rezazadeh Valojerdi, Ph.D.[2, 7], Rouhollah Fathi, Ph.D.[2]*

1. Department of Developmental Biology, University of Science and Culture, Tehran, Iran
2. Department of Embryology, Reproductive Biomedicine Research Center, Royan Institute for Reproductive Biomedicine, ACECR, Tehran, Iran
3. Department of Endocrinology and Female Infertility, Reproductive Biomedicine Research Center, Royan Institute for Reproductive Biomedicine, ACECR, Tehran, Iran
4. Department of Gynecology and Obstetrics, Arash Women's Hospital, Tehran University of Medical Sciences, Tehran, Iran
5. Vali-e-Asr Reproductive Health Research Center, Tehran University of Medical Sciences, Tehran, Iran
6. Department of Stem Cells and Developmental Biology, Cell Science Research Center, Royan Institute for Stem Cell Biology and Technology, ACECR, Tehran, Iran
7. Department of Anatomy, Faculty of Medical Science, Tarbiat Modares University, Tehran, Iran

**Corresponding Address: P.O.Box: 16635-148, Department of Embryology, Reproductive Biomedicine Research Center, Royan Institute for Reproductive Biomedicine, ACECR, Tehran, Iran*
Email: rfathi79@royaninstitute.org

Received: 11/November/2018, Accepted: 26/February/2019

Abstract

Objective: Decellularized tissue scaffolds provide an extracellular matrix to control stem cells differentiation toward specific lineages. The application of mesenchymal stem cells for artificial ovary production may enhance *ex vivo* functions of the ovary. On the other hand, the scaffold needs interaction and integration with cells. Thus, the development of ovarian engineered constructs (OVECs) requires the use of efficient methods for seeding of the cells into the ovarian and other types of scaffolds. The main goal of the present study was to develop an optimized culture system for efficient seeding of peritoneum mesenchymal stem cells (PMSCs) into human decellularized ovarian scaffold.

Materials and Methods: In this experimental study, three methods were used for cellular seeding including rotational (spinner flask) and static (conventional and injection) seeding cultures. OVECs were evaluated with Hematoxylin and Eosin staining and viability analyses for the seeded PMSCs. Then, immunohistochemistry analysis was performed using the best method of cellular seeding for primordial germ cell-like cells, mesenchymal stem cells and proliferation markers. Stereology analysis was also performed for the number of penetrated cells into the OVECs.

Results: Our results showed that rotational seeding increases the permeability of PMSCs into the scaffold and survival rate of the seeded PMSCs, comparing to the other methods. On the other hand, rotationally seeded PMSCs had a more favorable capability of proliferation with Ki67 expression and differentiation to ovarian specific cells with expression of primordial germ cell line markers without mesenchymal stem cells markers production. Furthermore, stereology showed a more favorable distribution of PMSCs along the outer surfaces of the OVEC with further distribution at the central part of the scaffold. The average total cell values were determined 2142187 cells/mm^3 on each OVEC.

Conclusion: The rotational seeding method is a more favorable approach to cell seeding into ovarian decellularized tissue than static seeding.

Keywords: Mesenchymal Stem Cells, Ovary, Peritoneum, Seeding, Tissue Engineering

Cell Journal(Yakhteh), Vol 22, No 2, July-September (Summer) 2020, Pages: 227-235

Citation: Mirzaeian L, Eivazkhani F, Hezavehei M, Moini A, Esfandiari F, Valojerdi MR, Fathi R. Optimizing the cell seeding protocol to human decellularized ovarian scaffold: application of dynamic system for bio-engineering. Cell J. 2020; 22(2): 227-235. doi: 10.22074/cellj.2020.6604.

Introduction

Tissue engineering techniques provide a suitable decellularized extra cellular matrix (ECM) for renewal of functions of impaired tissues. It has been assumed that low levels of unfavorable immune response due to lack of cells leads to use decellularized ECMs as a practical technique especial in the case of allo and xeno-transplantation (1). ECM, consists of complex enclosed compositional and architectural elements, depending on the tissue source, and directly determines the cellular fate map (2, 3). ECM ultrastructure facilitates penetration of selected cell types (4), and modulates the migration of cells into the scaffold and influences tissue specification, cell morphology and differentiation potential (5, 6). Mesenchymal stem cells (MSCs) are favorable candidates to be used in tissue engineering and regenerative medicine for secretion of paracrine factors, ovarian damage treatment and no immunogenicity (7-11). Among the sources of mesenchymal cells, the peritoneal mesothelium has specific properties such as plastic adherence, self-renewal, appearance of MSCs surface markers and differentiation potential to mesoderm and non-mesoderm cell lines called peritoneum mesenchymal stem cells (PMSCs) (12-14).

Regenerative medicine is increasingly gaining importance in the treatment of female infertility. The production of ovarian engineered constructs (OVECs)

can potentially restore fertility in women with ovarian dysfunctions like premature ovarian failure (POF) and ovarian cancer or postmenopausal re-fertility. Scientists believe that decellularized tissue scaffolds have a microenvironment for MSCs, which allows them to differentiate into tissue specified cells. Thus, it seems promising to introduce cells into the decellularized ovarian ECM in women for restoration of female fertility. This is challenging and requires development of optimized methods for seeding MSCs into ovarian scaffolds and making an organoid.

The use of static culture systems such as tissue culture petri dishes for MSCs seeding is simple, rapid and well established, but has serious limitations such as variability and user dependence. Furthermore, seeding efficiency under this environment is as low as 10-25%. Thus, it is important to extend and develop alternative systems like stirred vessels or rotational seeding to minimize cell death and increase cell penetration. This particular seeding technique has been reported to increase the seeding efficiency to approximately over 90% (15). The rotational seeding method holds promise for the development of artificial ovaries.

In the current study, human decellularized ovarian scaffold was used as a natural bed for cell attachment, penetration, expansion and differentiation to tissue specific cells. Rotational and static seeding methods were used to compare migration and distribution of the PMSCs within the human decellularized ovarian scaffold, to evaluate their survival rate and differentiation potential into ovarian cell-like cells.

Materials and Methods

Human ovarian tissue decellularization

In this experimental study, all the steps were designed to abide by the rules of research Ethics Committee of Royan Institute (IR.ACECR.ROYAN.REC.1396.67). Ovarian tissue was collected from trans-sexual humans. Ovarian tissue was trimmed into 2 mm-thick sections of cortex and medulla. In order to decellularize human ovarian tissue slices, the samples were stored at -80˚C overnight and then placed and agitated in 0.5 M NaOH solution at room temperature, overnight. Tissue slices were finally treated with a nuclease supplemented solution (RNase/DNase, Thermo fisher, USA) and washed in sterile phosphate buffered saline (PBS, Invitrogen, USA) for 48 hours with 6 times exchange.

Scanning electron microscopy study

For scanning electron microscopy (SEM) analyses, some of the samples were fixed with a fresh prepared 2.5% glutaraldehyde solution (Sigma, USA) at 4˚C for 24 hours. The samples were immersed into PBS overnight and fixed in 1% osmium tetroxide (Sigma, USA) at 25˚C for 2 hours. Dehydration was performed with ethanol at ascending concentrations of 30, 70, 80, 90, and 100%. After mounting on aluminum foil, the samples were covered with a gold layer. Then the structures of samples were investigated using a SEM (VEGA\TESCAN, Czech Republic).

Seeding of peritoneum mesenchymal stem cells into human decellularized ovarian scaffold

In our previous study, we isolated and characterized PMSCs and demonstrated their differentiation abilities into ovarian cell-like cells (14). Briefly, Peritoneum mesothelial was separated from mouse anterior abdominal walls and washed with PBS. Tissue fragments were split into smaller pieces and cultured in Dulbecco's modified Eagle's medium/F12 (DMEM/F12, Gibco, USA) supplemented with 15% fetal bovine serum (FBS, Gibco, USA), 1% non-essential amino acids 100× (Gibco, USA), 1% insulin transferrin selenium (ITS, Gibco, USA), 1% Glutamax (Gibco, USA), 1% (5000 U/ml) penicillin/streptomycin (Thermo fisher, USA) under 21% O_2, 5% CO_2, 97% humidified atmosphere at 37˚C. PMSCs were expanded on the basis of plastic adherence in cell culture T25 flasks for 8 passages. Two separate approaches were applied for PMSCs seeding into human decellularized ovarian scaffold. To compare the influence of rotational or static seeding on the tissue-engineered ovarian construct, the decellularized ovarian scaffolds were divided into three groups as follows: 1) Rotational culture by spinner flask, 2) Static culture by conventional protocol, and 3). Static culture post cell injection (Fig.1). For this purpose, human ovarian decellularized ECM pieces ($5\times5\times1$ mm^3) stored at -20˚C, were washed three times in PBS, then sterilized using 70% ethanol (2 hours) and ultraviolet (20 minutes) and soaked in the culture medium for 1 hour at 37˚C under a 5% CO_2, humidified atmosphere. In group 1, PMSCs expansion was performed using of 100 ml spinner flask with stirring speed of 20 rpm to support cellular adhesion and distribution into exterior and interior surfaces of the scaffolds. In each repetition, six scaffolds were placed in each spinner flask plunged in 2×10^6 cells per scaffold (2×10^6 cells/scaffold). The volume of culture medium was 100 ml (Fig.1A). In group 2, the same number of PMSCs suspended in a solution, were injected with an insulin syringe (G-27) into different parts of the scaffold and in group 3, PMSCs were placed on sample surfaces with the same culture medium, in 12 well tissue culture plates covered with 1% agarose gel (Fig.1B). All samples were cultured at 37˚C in 5% CO_2 for 1 week and 50% of the medium was replaced every 3 days. In each group, three tissue constructs were fabricated and used for histological characterizations and cell viability analyses. Finally, after finding the optimum seeding protocol, immunohistochemistry staining and stereology tests were carried out to the most appropriate group to assess proliferation and penetration ability of the seeded PMSCs.

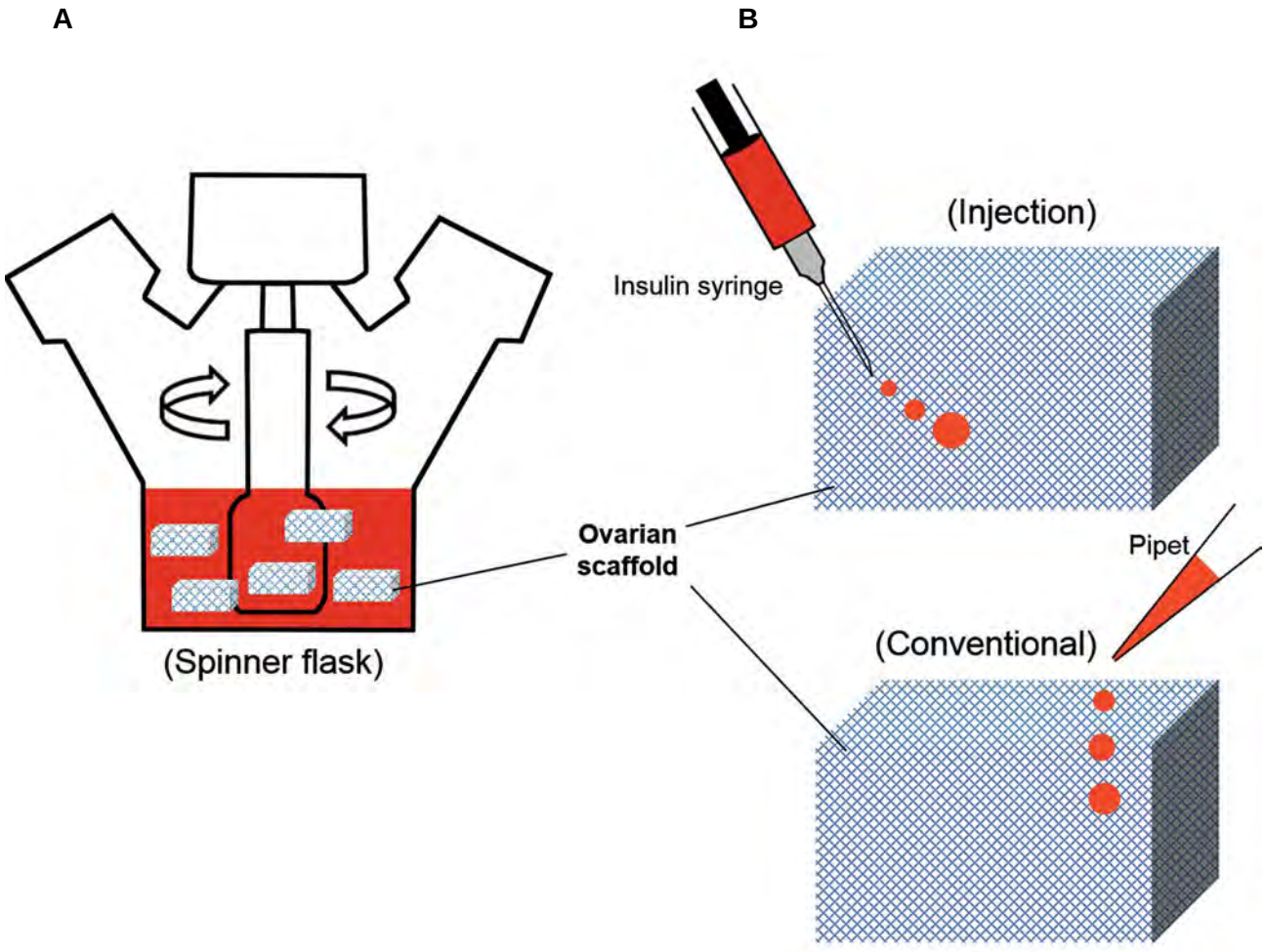

Fig.1: Cell seeding protocols. **A.** Rotational seeding: scaffolds are located in a spinner flask with 100ml volume of cell suspension and **B.** Static seeding: cell suspension is transferred directly into the human ovarian scaffold with insulin syringe (G-27) or onto the outer surfaces of the scaffold with pipet.

Cellular viability

OVECs were observed under light microscope (Olympus CKX41, Japan). Analyses of the viable or metabolic activated cells seeded into exterior and interior surfaces of the OVECs were made using 3-(4,5-dimethylthiazol-2-yl)-5-(3-carboxymethoxyphenyl)-2-(4-ulfophenyl)-2H-tetrazolium (MTS) assay. For this purpose, the OVECs were transferred to a new well after being washed in PBS for 3-4 hours. Then, the constructs were incubated with 100 µl of the DMEM/F12 free medium supplemented with 20 µl of MTS/PMS, which produced a color response in the presence of viable cells. To avoid the effect of the matrix on spectrophotometry, 100 µl of the reaction medium from each well was relocated to another well. Cell viability was recorded as absorbance at 490 nm by microplate reader (thermo scientific, America).

Histology assessments

OVECs derived from three seeding protocols were fixed for Hematoxylin and Eosin (H&E) staining, in Bouin's (24 hours), and then they were transferred to 10% buffered formalin (24-72 hours). The OVECs were then washed, processed and embedded in paraffin wax. The blocks were serial sectioned to 6 µm thickness using a microprocessor machine (Thermofisher, USA). The sections were labeled on glasses and stained with H&E. All images of OVECs cross sections were captured on an upright microscope (Olympus IX51, Japan) and cellular distribution and migration of seeded PMSCs were evaluated.

Immunohistochemistry for Stella, Prdm14, Blimp1, CD90 and Ki67

In order to assess PMSCs differentiation into primordial germ cell-like cells in cultured OVECs in spinner flask, developmental proteins were detected by immunohistochemistry. For this purpose, sections (with 6 µm thickness) were placed on charged slides, in 60˚C for 30-40 minutes. After deparaffinization and hydration, sodium citrate buffer (PH=6) was applied for 30 minutes at 90˚C to retrieve masked antigens. Then sections were immersed into PBS-tween (0.05%). For peroxidase-linked immunostaining, endogenous peroxidase was removed by 10% hydrogen peroxide (H_2O_2) for 30 minutes and rinsed twice in PBS-tween. Then, Triton X-100 (0.5%) was used for 15 minutes for membrane permeability. Non-specificities were blocked with 10% secondary host serum at 37˚C for 1 hour and rinsed twice in PBS-tween. Primary antibodies were diluted in 10%

secondary host serum and PBS (one to one ratio) and incubated overnight at 4˚C. Purchased primary antibodies were anti-Stella (1:100, Santa Cruz, USA), anti-Prdm14 (1:100, Abcam, USA), anti-Blimp1 (1:100, Cell signaling, USA) anti-CD90 (1:100, BD, USA) and anti-Ki67 (1:100, Biolegend, USA). Subsequently, the sections were washed thrice with PBS-Tween, and incubated for 1 hour with one secondary antibody. Peroxidase-conjugated goat anti-rabbit (1:500, Invitrogen, USA) and rabbit anti-goat (1:500, Abcam, USA) IgG antibodies were used and washed thrice with PBS-Tween and treated with the diaminobenzidine (DAB) reagent (ABC, detection IHC kit) in the dark at room temperature for 5-20 minutes. In the presence of peroxidase enzyme, DAB produces a brown precipitate. Negative control was made by incubating the sections only with secondary antibodies. Washing was repeated and sections were counterstained with hematoxylin. Sections were mounted under coverslips, dried overnight, dehydrated, cleared and observed under light microscopy (Olympus IX51, Japan). The percentage of positive cells was calculated by counting the number of brown-stained cells versus the number of hematoxylin-positive nucleus, representing the total cell numbers.

Estimating cell number and migration by stereology

Stereological methods produced 3D results from 2D images of OVECs. To calculate the number of PMSCs, an optical dissector was used. In this method, fixed OVECs cultured in rotational seeding were embedded in paraffin block. The technique was used to achieve isotropic uniform random (IUR) sections. The paraffinized scaffolds were serially sectioned to 20 µm thickness (H&E staining) for cell number estimation. The selected sections were studied using an upright microscope (×100 magnification) and a microcator (ND 221 B, Heidenhain, Germany) connected to a computer for measuring the Z-axis travel. The nuclei of PMSCs were observed using an unbiased counting frame covered on the monitor. Any nucleolus derived from maximal focus was selected if it was placed in the counting edge or touched the inclusion edge and did not touch the exclusion boundaries (Fig.2). Finally, the following formula was used to calculate the numerical density of the cells: $Nv\ (cells)=[\Sigma Q/(a/f\times\Sigma P\times h)]\times V$, in which "$\sum Q$" is the total number of the counted cells, "$\sum p$" is the total number of the points superimposed on the selected fields, "h" represents the tissue thickness and "a/f" stands for the frame area in the tissue actual scale. To obtain the total cell number, the results were multiplied by the total volume (V) of the scaffold (16).

Statistical analysis

The results were reported as the mean ± SEM and was conducted by using three technical and biological replicates. Statistical analyses were performed using SPSS software (version 21, IBM, USA). Analysis of variance was carried out and data were subjected to one-way ANOVA test, followed by the Tukey test. $P<0.05$ was considered as significant.

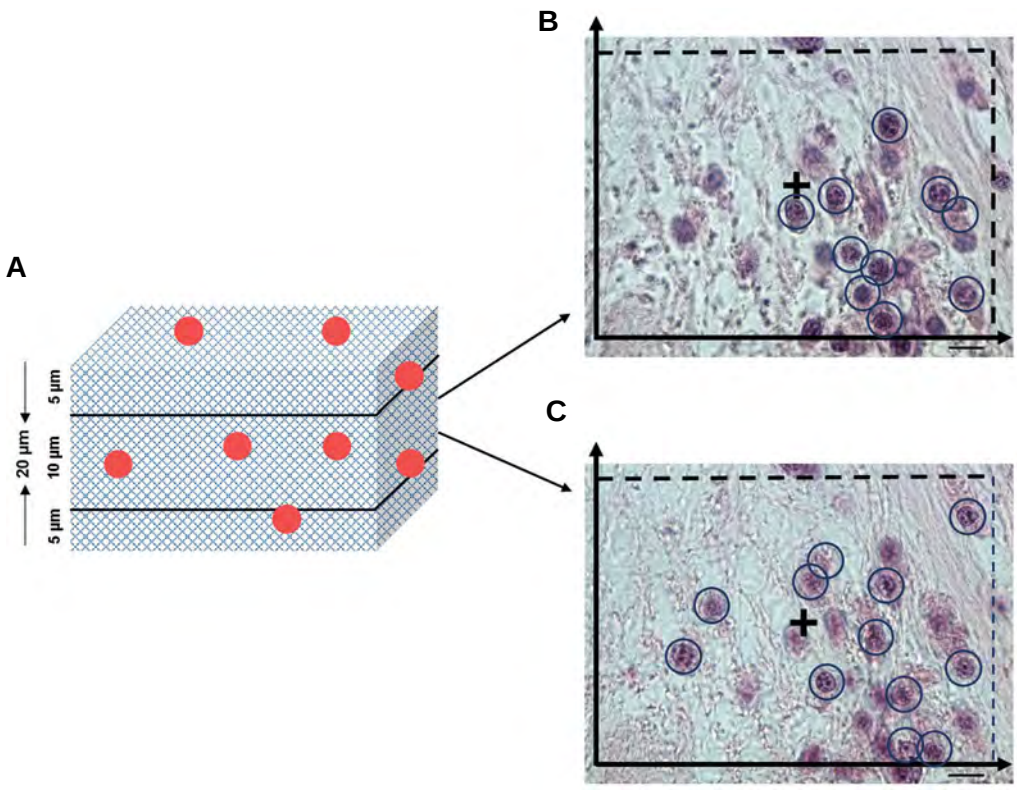

Fig.2: Cell number estimation in OVECs by using the optical dissector. **A.** Two regions of the gourd zone with 5 µm from the up and down areas of the sections are not counted, **B,** and **C.** Two different depths of 10 µm in which the count is performed. An unbiased counting frame of area superimposed on each sampling field used to sample the cell nucleoli (scale bars: 10 µm).

Results

Morphology characterization of ovarian engineered constructs

OVECs produced by rotational seeding were red in color, but in static seeding, they were paled (Fig.3A). Also, SEM shows that the pore size without and with ovarian cells was approximately 50 µm and this allowed the cells to penetrate into the scaffold (Fig.3B). In order to evaluate and compare the attachment and infiltration of PMSCs into human decellularized ovarian ECM, H&E staining was carried out for serial sections obtained from OVECs. In rotational seeding, PMSCs penetrated not only into the exterior surfaces also to the depth of the scaffolds and mitosis divisions were seen as well. Active division increased the cell number on tissue periphery and PMSCs expanded in the scaffold. On the other hand, the cells and nuclei exhibited appropriate morphology and alignment (Fig.3C). But in static (injection) seeding, few cells were evident via H&E staining in marginal parts of the tissue and morphology of PMSCs seeded into decellularized ECM did not represent well condition. In conventional seeding, PMSCs not only did not penetrate to decellularized scaffold, also they could not migrate into the ECM clefts. In addition, in static seeding, the presence of many grooves in decellularized scaffold may indicate the separation of the components. Generally, rotational seeding increased cell seeding penetration and uniformity of the decellularized scaffold more than the other methods (Fig.3C).

Viability of seeded peritoneum mesenchymal stem cells

Mean viability rate of PMSCs seeded into the scaffolds measured by mitochondrial activity, in rotational seeding were significantly ($P<0.05$) more than both static seeding methods. In addition, the expression of ki67 as a proliferative marker confirmed that rotational seeding method retains proliferation ability of PMSCs in addition to increasing their survival rate (Fig.3D). Cell division after applying this technique verified the previous observation (Fig.3C). Therefore, it could be concluded that the rotational seeding technique resulted in more suited recellularized construct.

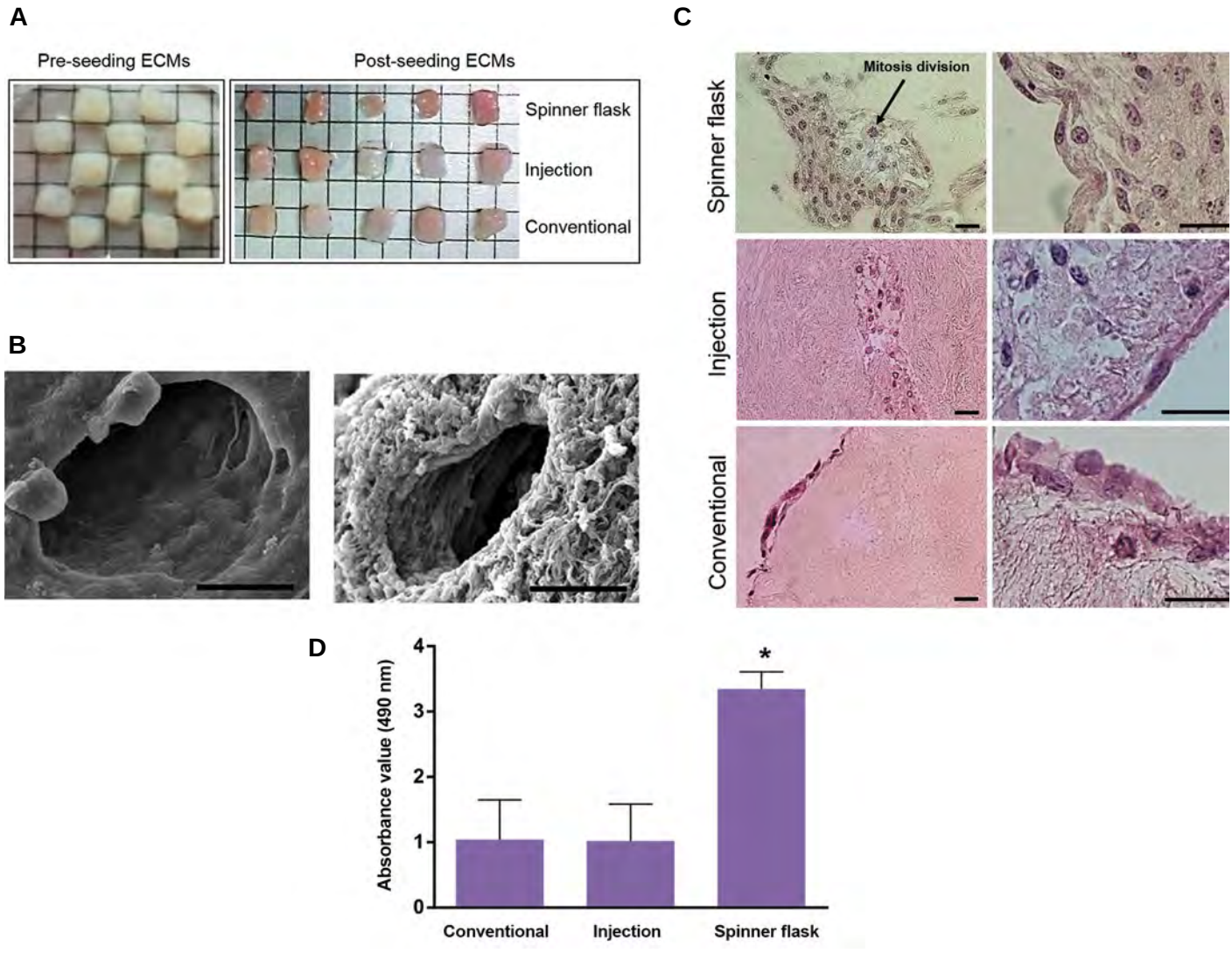

Fig.3: Comparison of seeding protocols. **A.** Morphological, **B.** SEM, **C.** H&E staining, and **D.** MTS analyses. Comparison of recellularized human ovarian ECM with PMSCs through 3 seeding protocols (scale bars: 25 µm). ECM; Extra cellular matrix, MTS; 3-(4,5-dimethylthiazol-2-yl)-5-(3-carboxymethoxyphenyl)-2-(4-ulfophenyl)-2H-tetrazolium, SEM; Scanning electron microscopy and *; $P<0.05$.

Immunohistochemistry and cell differentiation

The results of H&E staining and viability analysis showed that the spinner flask generated the best results of cell seeding more than static methods. Thus, the OVECs derived from rotational technique were processed for cell phenotype characterization using immunohistochemistry staining. Figure 4 shows that the seeded cultured cells displayed a primordial germ cell-like cells properties by expressing Stella, Prdm14, and Blimp1 (Fig.4A-C). The low expression of mesenchymal stem cell marker (CD90) in PMSCs seeded into OVECs indicates a decrease in mesenchymal features in these cells (Fig.4D). On the other hand, production of proliferation protein (Ki67) shows self-renewal in seeded cultured PMSCs (Fig.4E). There was no positive staining in the negative controls (Fig.4F, J), showing that the secondary antibodies labeled to specific antigens.

3D cell distribution in scaffolds cultured under rotational condition

The cellular distribution and density were evaluated within the OVEC produced by rotational seeding method after 7 days of incubation. This method led to PMSCs distribution throughout the ovarian decellularized ECM. The seeding efficiency of rotational method (spinner flask) was 53.5%. Total cell values on the OVEC were determined to be 2142187 cells/mm^3. The images showed more favorable distribution of PMSCs throughout the peripheral parts of the tissue sections. Vertical delivery of the cells in the cross-section showed low density of cells (1133 cells/mm^2) on the upper part of the scaffold. The interior part of the scaffold showed improved cell penetration, with cell density of 3960 cells/mm^2 for the central zones. The cell density diminished slightly at the lowest surface of the scaffold, at 1762 cells/mm^2 density (Fig.5).

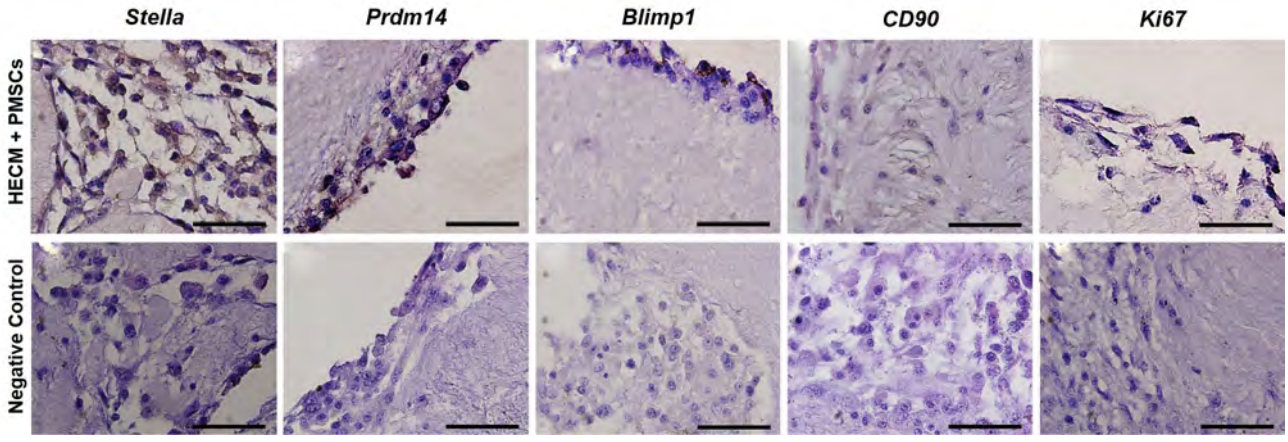

Fig.4: Immunohistochemical analysis of recellularized human ovarian matrix with PMSCs through spinner flask for antibodies against germ cell markers (Stella, Prdm14 and Blimp1) mesenchymal stem cell (CD90) and proliferation markers (Ki67) (scale bars: 20 µm).

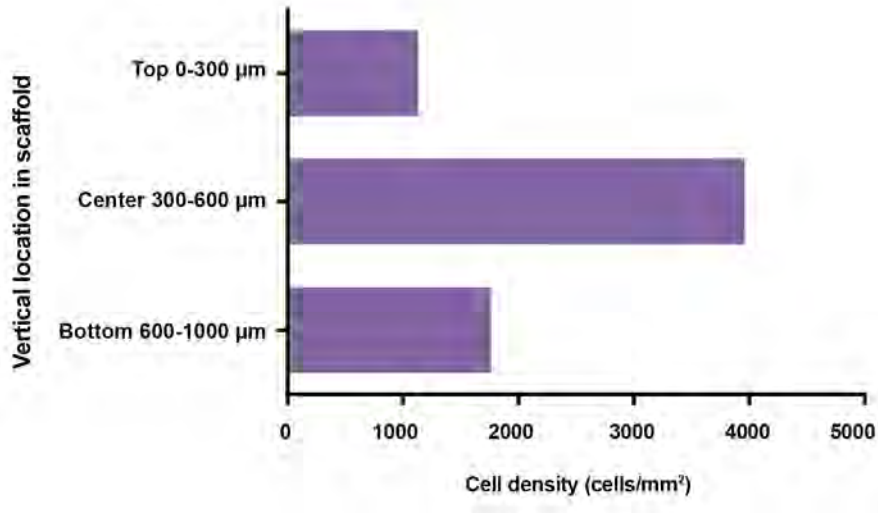

Fig.5: Cross-sectioned counted cell density in OVEC (n=1). OVEC was divided into three equal zones representing the exterior outer surfaces, the center of the section and the bottom zone. From the seeded surface, the cell density increased with increasing depth to the center and decreased below to the lower exterior surface.

Discussion

Ovarian tissue cryopreservation is one of the strategies to fertility preservation of cancer affected women. Tissue engineered ovaries from decellularized ovarian scaffolds can prevent reintroduction of malignant cells and lead to development of a transplantable scaffold. Decellularized ovarian scaffolds could be recellularized with MSCs and implanted after appropriate *ex vivo* regeneration steps. This technology also can apply to women with POF. In the present study, tissue engineering was used for primarily recellularization of human decellularized ovarian scaffold with mouse PMSCs. We obtained ovarian decellularized scaffolds from trans-sexual human ovaries that preserved their natural properties and showed retention of main ECM structure in SEM.

Many techniques are used for cellular seeding into whole organ or tissue segment scaffolds but the best protocol for PMSCs seeding into 5×5×1 mm segments of ovarian scaffold must be chosen. The effects of rotational and static seeding protocols on cell repopulation and arrangement beside of cell permeability level, morphology and viability were evaluated and compared after 1 week of *in vitro* culture. H&E staining showed penetration of fewer PMSCs in the static seeding method without cellular arrangement but the rotational seeding promoted cell repopulation deep into the ovarian scaffold. Therefore, static culture protocols (conventional and injection) have serious limitations for cellular seeding. On the other hand, the porous structure of the decellularized ovarian scaffold as shown by SEM causes cell leakage during injection and the lack of medium flow leads to the absence of cellular entrance into scaffold in the conventional method.

Our results showed that the rotational culture system using a spinner flask has many advantages. It supports cell alignment and stimulates OVECs formation. The first recellularization attempts of decellularized ovaries by Laronda et al. (17) were made using mouse conventional ovarian cells seeding into bovine decellularized ovary for 2 days. Low-speed rotational seeding plays an important role to increase the efficiency of early cell seeding, stimulate cell adhesion, differentiation and construct development. In the present study, spinner flask operating at a speed of 20 rpm was able to preserve cell viability, proliferation and differentiation. However, the efficiency of cellular proliferation and differentiation rates are still low. Rotational seeding homogenizes culture medium and may induce transient oxygen and supplements and this, in turn, can increase the quantity and distribution of cells in the decellularized ovary. Wang et al, indicated that rotational MSCs seeding was more effective than static tissue culture in oxygenation of the recellularized myocardial scaffolds (18). Moreover, immunohistochemistry staining for the OVECs confirmed that rotational seeding generated positive tissue remodeling.

It seems that the attachment of PMSCs to ovarian ECM leads to cell and tissue interaction signals. It is believed that peritoneum mesothelial cells have a common embryonic origin with ovarian surface epithelium (OSE) cells (19). Bukovsky et al. (20) displayed that OSE cells can be a bipotent source for granulosa and germ cells. Therefore, PMSCs, both in terms of location and origin are more likely to differentiate into ovarian cell-like cells than other MSCs. As in our previous study, we have displayed the differentiation potential of PMSCs in human follicular fluid and cumulus cell conditioned media into ovarian cell-like cells *in vitro* (14). Our results in this study showed that the differentiated cells have primordial germ cell-like cells phenotypes through expression of Stella, Prdm14, and Blimp1 proteins. These markers cause proliferation and migration induction in primordial germ cells (21). Stella plays a significant role in maturing oocytes and preimplantation embryos (22). This protein may be involved in germ line determination in ovarian ECM. Furthermore, Ki67 as a proliferation protein was observed in one-week cultured OVECs.

Cortiella et al. (23) compared the influence of decellularized lung, gelfoam, Matrigel, and collagen I hydrogel matrices on mouse embryonic stem cells attachment, differentiation and formation in a tissue complex. A rotational approach was used for cellular seeding and the results showed that decellularized lung scaffold had improved cell preservation with more differentiation rate of embryonic stem cells into epithelial and endothelial cells than those of others. It is believed that rotational seeding culture decreases stress and maintains a steady flow of nutrients to the developing constructs. Collectively, rotational seeding data showed that ovarian scaffolds are likely to have the necessary signals to support initial attachment, proliferation and differentiation. Ji et al. (24) also showed that a dynamic culture system was more favorable than static culture in improving seeding of mouse bone marrow mesenchymal stem cells into rat liver scaffold by creating optimal stream rate and led to significantly advanced proliferation. Scaffold induced lineage-specific differentiation hepatocyte-like cells from MSCs. Moreover, Vermeulen et al. (25) showed that pig immature decellularized testicular scaffold is able to support human sertoli cells attachment, proliferation and functionality. Extremely low expression or even lack of expression of CD90 as a MSCs surface marker in our study confirmed that rotational seeded and attached PMSCs into ovarian ECM, lost mesenchymal properties. However, the nature of mesenchymal stem cells were confirmed in the cells by immunoflorosent assay before cell injection into the ECM.

Santos et al. (26) believed that microcarrier-based stirred culture system subjected to an agitation, affects the cell surface antigens and reduces CD90 expression in human adipose tissue stem cells. It seems that prolonged agitation time to 2 weeks in the mentioned study led to alteration in surface markers expression. Therefore, our suggestion is that mesenchymal properties of PMSCs may change belong to their attachment to ovarian ECM and their differentiation. Woloszyk et al. (27) showed that mineralized matrix formation potential in human dental

pulp stem cells seeded and grown on porous 3D silk fibrin scaffolds, is enhanced in the rotational culture system. Furthermore, Xue et al. (28) showed that rat adipose tissue derived stem cells can attach, grow and differentiate to vascular endothelial and tubular cells in rat decellularized kidney scaffold.

There is a need to develop a simple, effective and inexpensive method for evaluation of cell distribution and penetration rates into scaffolds. We calculated the total number and density of distributed PMSCs into OVECs by the stereological method. There have, hitherto been few studies on the measurement of seeded cell density and distribution in tissue-engineered constructs. Thevenot et al. (29) investigated the permeability and distribution rate of fibroblasts in a variety of seeding protocols. They concluded that dynamic seeding technique facilitates moving a cell solution along the scaffold and leads to cell penetration into the scaffold pores, as well as on the outer surfaces. In comparison, the efficiency of rotational seeding in our study was 53.5%, which is almost equal to centrifuge seeding efficiency (52%) as reported by Thevenot et al. (29). Finally, in the current study, the use of stereology helped find actual and accurate cell seeding ability data and showed that rotational seeding technique leads to a wide distribution of PMSCs on ovarian exterior surface as well as deep penetration into the center of OVEC.

Conclusion

The use of spinner flask causes PMSCs movement around the ovarian scaffolds and enhances contact between the cells and the scaffold. This makes it a more favorable technique for cell seeding into decellularized ovarian tissue than conventional and injection methods.

Acknowledgements

This research study was supported by Royan Institute, the Iranian Council of Reproductive Biomedicine Research Center (Tehran, Iran), and Royan-Lotus Charity Fund for financial support. We would like to thank from Dr. Alireza Yousefzadeh as editor of this manuscript. The authors declare no conflict of interest.

Authors' Contributions

L.M.; Collected and analyzed of data, and drafted the manuscript. F.E.; Collaborated in ovarian tissue decellularization. M.H.; Collaborated in stereological study. A.M.; Collaborated in human ovarian tissue preparation. F.E., M.R.V.; Advisor in project. R.F.; Concepted and designed of the study, contributed in interpretation of the data and the conclusion. All authors read and approved the final manuscript.

References

1. Liu WY, Lin SG, Zhuo RY, Xie YY, Pan W, Lin XF, et al. Xenogeneic decellularized scaffold: a novel platform for ovary regeneration. Tissue Eng Part C Methods. 2017; 23(2): 61-71.
2. Badylak SF, Freytes DO, Gilbert TW. Extracellular matrix as a biological scaffold material: structure and function. Acta Biomater. 2009; 5(1): 1-13.
3. Smith LR, Cho S, Discher DE. Stem cell differentiation is regulated by extracellular matrix mechanics. Physiology (Bethesda). 2018; 33(1): 16-25.
4. Grauss RW, Hazekamp MG, Oppenhuizen F, van Munsteren CJ, Gittenberger-de Groot AC, DeRuiter MC. Histological evaluation of decellularised porcine aortic valves: matrix changes due to different decellularisation methods. Eur J Cardiothorac Surg. 2005; 27(4): 566-571.
5. Gong J, Sagiv O, Cai H, Tsang SH, Del Priore LV. Effects of extracellular matrix and neighboring cells on induction of human embryonic stem cells into retinal or retinal pigment epithelial progenitors. Exp Eye Res. 2008; 86(6): 957-965.
6. Brown B, Lindberg K, Reing J, Stolz DB, Badylak SF. The basement membrane component of biologic scaffolds derived from extracellular matrix. Tissue Eng. 2006; 12(3): 519-526.
7. Ankrum JA, Ong JF, Karp JM. Mesenchymal stem cells: immune evasive, not immune privileged. Nat Biotechnol. 2014; 32(3): 252-260.
8. Zhou L, Tu J, Fang G, Deng L, Gao X, Guo K, et al. Combining PLGA scaffold and MSCs for brain tissue engineering: a potential tool for treatment of brain injury. Stem Cells Int. 2018; 2018: 5024175.
9. Aggarwal S, Pittenger MF. Human mesenchymal stem cells modulate allogeneic immune cell responses. Blood. 2005; 105(4): 1815-1822.
10. Li N, Sanyour H, Remund T, Kelly P, Hong Z. Vascular extracellular matrix and fibroblasts-coculture directed differentiation of human mesenchymal stem cells toward smooth muscle-like cells for vascular tissue engineering. Mater Sci Eng C Mater Biol Appl. 2018; 93: 61-69.
11. Ibsirlioglu T, Elçin AE, Elçin YM. Decellularized biological scaffold and stem cells from autologous human adipose tissue for cartilage tissue engineering. Methods. 2019. pii: S1046-2023(18)30435-3.
12. Rezanejad Keshteli FZ, Parivar K, Joghatayi MT, Ali Beik H. Study of the differentiation of rat omentum stem cells to nerve cells using brain tissue extract of Wistar rats. International Journal of Cellular and Molecular Biotechnology. 2013; 2014(2014): 1-13.
13. Sarvandi SS, Joghataei MT, Parivar K, Khosravi M, Sarveazad A, Sanadgol N. In vitro differentiation of rat mesenchymal stem cells to hepatocyte lineage. Iran J Basic Med Sci. 2015; 18(1): 89-97.
14. Mirzaeian L, Eftekhari-Yazdi P, Esfandiari F, Eivazkhani F, Rezazadeh Valojerdi M, Moini A, et al. Induction of mouse peritoneum mesenchymal stem cells into germ cell-like cells using follicular fluid and cumulus cells conditioned media. Stem Cells Dev. 2019; 28(8): 554-564.
15. Villalona GA, Udelsman B, Duncan DR, McGillicuddy E, Sawh-Martinez RF, Hibino N, et al. Cell-seeding techniques in vascular tissue engineering. Tissue Eng Part B Rev. 2010; 16(3): 341-350.
16. Noorafshan A, Ahmadi M, Mesbah SF, Karbalay-Doust S. Stereological study of the effects of letrozole and estradiol valerate treatment on the ovary of rats. Clin Exp Reprod Med. 2013; 40(3): 115-121.
17. Laronda MM, Jakus AE, Whelan KA, Wertheim JA, Shah RN, Woodruff TK. Initiation of puberty in mice following decellularized ovary transplant. Biomaterials. 2015; 50: 20-29.
18. Wang B, Borazjani A, Tahai M, Curry AL, Simionescu DT, Guan J, et al. Fabrication of cardiac patch with decellularized porcine myocardial scaffold and bone marrow mononuclear cells. J Biomed Mater Res A. 2010; 94(4): 1100-1110.
19. Auersperg N, Wong AS, Choi KC, Kang SK, Leung PC. Ovarian surface epithelium: biology, endocrinology, and pathology. Endocr Rev. 2001; 22(2): 255-288.
20. Bukovsky A, Caudle MR, Svetlikova M, Upadhyaya NB. Origin of germ cells and formation of new primary follicles in adult human ovaries. Reprod Biol Endocrinol. 2004; 2: 20.
21. Strauss JF, Barbieri RL. Yen & Jaffe's reproductive endocrinology. Physiology, pathophysiology, and clinical management. 6th ed. Elsevier Health Sciences; 2009; 3-33.
22. Sato M, Kimura T, Kurokawa K, Fujita Y, Abe K, Masuhara M, et al. Identification of PGC7, a new gene expressed specifically in preimplantation embryos and germ cells. Mech Dev. 2002; 113(1):

91-94.
23. Cortiella J, Niles J, Cantu A, Brettler A, Pham A, Vargas G, et al. Influence of acellular natural lung matrix on murine embryonic stem cell differentiation and tissue formation. Tissue Eng Part A. 2010; 16(8): 2565-2680.
24. Ji R, Zhang N, You N, Li Q, Liu W, Jiang N, et al. The differentiation of MSCs into functional hepatocyte-like cells in a liver biomatrix scaffold and their transplantation into liver-fibrotic mice. Biomaterials. 2012; 33(35): 8995-9008.
25. Vermeulen M, Del Vento F, de Michele F, Poels J, Wyns C. Development of a cytocompatible scaffold from pig immature testicular tissue allowing human sertoli cell attachment, proliferation and functionality. Int J Mol Sci. 2018; 19(1). pii: E227.
26. Santos Fd, Andrade PZ, Abecasis MM, Gimble JM, Chase LG, Campbell AM, et al. Toward a clinical-grade expansion of mesenchymal stem cells from human sources: a microcarrier-based culture system under xeno-free conditions. Tissue Eng Part C Methods. 2011; 17(12): 1201-1210.
27. Woloszyk A, Holsten Dircksen S, Bostanci N, Müller R, Hofmann S, Mitsiadis TA. Influence of the mechanical environment on the engineering of mineralised tissues using human dental pulp stem cells and silk fibroin scaffolds. PLoS One. 2014; 9(10): e111010.
28. Xue A, Niu G, Chen Y, Li K, Xiao Z, Luan Y, et al. Recellularization of well-preserved decellularized kidney scaffold using adipose tissue-derived stem cells. J Biomed Mater Res A. 2018; 106(3): 805-814.
29. Thevenot P, Nair A, Dey J, Yang J, Tang L. Method to analyze three-dimensional cell distribution and infiltration in degradable scaffolds. Tissue Eng Part C Methods. 2008; 14(4): 319-331.

Original Article

Helios, CD73 and CD39 Induction in Regulatory T Cells Exposed to Adipose Derived Mesenchymal Stem Cells

Maryam Fakhimi, M.Sc.[1, 2], Abdol-Rasoul Talei, M.D.[3], Abbas Ghaderi, Ph.D.[1, 2], Mojtaba Habibagahi, Ph.D.[2], Mahboobeh Razmkhah, Ph.D.[1*]

1. Shiraz Institute for Cancer Research, School of Medicine, Shiraz University of Medical Sciences, Shiraz, Iran
2. Department of Immunology, School of Medicine, Shiraz University of Medical Sciences, Shiraz, Iran
3. Breast Diseases Research Center (BDRC), Shiraz University of Medical Sciences, Shiraz, Iran

**Corresponding Address: P.O.BOX: 71345-1798, Shiraz Institute for Cancer Research, School of Medicine, Shiraz University of Medical Sciences, Shiraz, Iran*
Email: razmkhahm@sums.ac.ir

Received: 23/August/2018, Accepted: 25/February/2019

Abstract

Objective: Mesenchymal stem cells (MSCs) have prominent immunomodulatory roles in the tumor microenvironment. The current study intended to elucidate Treg subsets and their cytokines after exposing naïve T lymphocytes to adipose-derived MSCs (ASCs).

Materials and Methods: In this experimental study, to obtain ASCs, breast adipose tissues of a breast cancer patient and a normal individual were used. Magnetic cell sorting (MACS) was employed for purifying naïve $CD4^+$ T cells from peripheral blood of five healthy donors. Naïve $CD4^+$ T cells were then co-cultured with ASCs for five days. The phenotype of regulatory T cells (Tregs) and production of interleukine-10 (IL-10), transforming growth factor beta (TGF-β) and IL-17 were assessed using flow cytometry and ELISPOT assays, respectively.

Results: $CD4^+CD25^-FOXP3^+CD45RA^+$ Tregs were expanded in the presence of cancer ASCs but $CD4^+CD25^+Foxp3^+CD45RA^+$ regulatory T cells were up-regulated in the presence of both cancer- and normal-ASCs. This up-regulation was statistically significant in breast cancer-ASCs compared to the cells cultured without ASCs ($P=0.002$). $CD4^+CD25^+$ $FOXP3^+Helios^+$, $CD4^+CD25^-$ $FOXP3^+Helios^+$ and $CD25^+$ $FOXP3^+CD73^+CD39^+$ Tregs were expanded after co-culturing of T cells with both cancer-ASCs and normal-ASCs, while they were statistically significant only in the presence of cancer-ASCs ($P<0.05$). Production of IL-10, IL-17 and TGF-β by T cells was increased in the presence of either normal- or cancer-ASCs; however, significant effect was only observed in the IL-10 and TGF-β of cancer-ASCs ($P<0.05$).

Conclusion: The results further confirm the immunosuppressive impacts of ASCs on T lymphocytes and direct them to specific regulatory phenotypes which may support immune evasion and tumor growth.

Keywords: Adipose-Derived Mesenchymal Stem Cell, Breast Cancer, Immunomodulatory Effects, Regulatory T Cells

Cell Journal(Yakhteh), Vol 22, No 2, July-September (Summer) 2020, Pages: 236-244

Citation: Fakhimi M, Talei AR, Ghaderi A, Habibagahi M, Razmkhah M. Helios, CD73 and CD39 induction in regulatory T cells exposed to adipose derived mesenchymal stem cells. Cell J. 2020; 22(2): 236-244. doi: 10.22074/cellj.2020.6313.

Introduction

Mesenchymal stem cells (MSCs) are multipotent adult stem cells and their primitive origin is mesoderm. They possess self-renewal ability and are capable of differentiating into not only mesodermal cell lineage, but also ectodermic and endodermic cell lineages (1, 2). MSCs have the ability to home and engraft at sites of injury in the pathological conditions such as inflammation, neoplasia and tissue repair. These cells are recruited into tumor microenvironment in response to cytokines and chemokines produced by tumor cells. Within the tumor mass, MSCs can differentiate into fibroblasts, myofibroblasts, pericytes and carcinoma-associated fibroblast and cooperate with endothelial and inflammatory cells exacerbating tumor status (3, 4).

The anti-inflammatory and immune-modulating properties of MSCs have been shown in many studies. For instance, prohibiting effector T-cells activation along with increase in regulatory T cells (Tregs) population (5, 6) are known as important immune-modulating mechanisms. The suppression mechanism of T-cells by MSCs could be direct (cell-cell contact) or may occur indirectly by secreting soluble factors such as nitric oxide (NO), indoleamine 2,3-dioxygenase (IDO), prostaglandin E2 (PGE2), interleukine-10 (IL-10) and transforming growth factor beta (TGF-β) (7, 8). They inhibit activation and function of T-cells by down-regulating major histocompatibility complex (MHC) class II molecules and IL-12, decreasing interferon-γ (IFN-γ) and inducing generation of Tregs through IL-10 production, besides of releasing human leukocyte antigen-G (HLA-G) (9, 10). Tregs are generally characterized by the expression of forkhead box transcription factor (FOXP3) and play prominent roles in peripheral tolerance and controlling immune responses, towards the autoimmune diseases, allergies, infection-induced organ pathology and tumors (11, 12).

Soluble mediators such as TGF-β, IL-10 and IL-35 in addition to immunosuppressive metabolites, including adenosine production, are responsible for the suppressive mechanisms of Tregs (13-15). Naturally occurring Treg cells and antigen-induced $CD4^+CD25^+FOXP3^+$ Tregs have been widely studied. However, other additional subsets and markers of Treg cells have received less

attention in identification and characterization of these cells (16). CD45RA, CD25, CD73, CD39 and Helios are among the most important markers of Treg cells, whose roles have recently been identified (17). CD39 and CD73 are recognized as markers of Tregs with the capability of circular adenosine monophosphate (cAMP) or adenosine mediated suppression (18). Recent studies confirmed that MSC-exposed Tregs carry more immunosuppressive properties than Tregs co-cultured without MSCs (19). Here, we further clarified Treg subsets through assessment of CD45RA, CD73, CD39 and Helios expression after adipose derived mesenchymal stem cell (ASC)-T cell crosstalk. Then, expression level of IL-10, TGF-β and IL-17 were determined in T cells co-cultured in the presence of ASCs.

Materials and Methods

This experimental study was approved by the Ethics Committee of Shiraz University of Medical Sciences (Shiraz, Iran, Code No. 9113). All donors were provided written and signed informed consent to take part in this study.

Isolation, culture and characterization of human adipose-derived mesenchymal stem cells

ASCs were provided from breast adipose tissues of one breast cancer patient and one normal individual undergoing mammoplasty surgery as previously explained (15, 20, 21). Briefly, fragments of adipose tissue were washed with phosphate buffered saline (PBS), minced and digested using 0.2% collagenase type I (Gibco, USA) at 37˚C for about 45 minutes. The digested materials were centrifuged at 400 g for 10 minutes. The stromal vascular fraction (SVF) was separated using Ficoll gradient (Biosera, UK) through centrifugation at 400 g for 20 minutes. The cells were washed with PBS and plated into T-25 plastic cell culture flasks in Dulbecco's Modified Eagle's Medium (DMEM, Biosera, UK) containing 10% fetal bovine serum (FBS, Gibco, USA) and 1% penicillin/streptomycin (Gibco, USA). The cultured cells were incubated at 37˚C and 5% CO_2 with 95% humidity. Following 24 hours incubation, non-adherent cells were discarded. The medium was exchanged every 72 hours. The harvested cells were sub-cultured and used for further experiments. To characterize the cells with flow-cytometer, ASCs were stained with fluorescein isothiocyanate (FITC)-conjugated mouse anti-human CD45, CD34 and CD14 (BD Biosciences, USA) as well as phycoerythrin (PE)-conjugated mouse anti-human CD90, CD105, CD44, CD73 (BD Biosciences). To evaluate differentiation capacity of the cells, they were treated with conditioned medium for osteocyte, chondrocyte and adipocyte differentiation, as previously described (15, 20, 21). ASCs isolated from the breast cancer patient and normal subject are hereafter called cancer-ASCs and normal-ASCs in this article.

Isolation of naïve CD4$^+$ T cells from human peripheral blood mononuclear cells

Peripheral blood mononuclear cells (PBMCs) were isolated by density gradient centrifugation using Ficoll gradient (Biosera, USA) from six healthy donors with respectively the mean ± standard deviation (SD) and median age of 33.8 ± 2.7 and 35 years old. To exclude monocytes from mononuclear cells, isolated PBMCs were cultured at 37˚C for 45 minutes. After incubation time, the remaining flout cells were collected as peripheral blood lymphocytes (PBLs). Separation of naïve CD4$^+$ T cells was performed using the Human Naive CD4$^+$ T cell Isolation Kit II (Miltenyi Biotec, Germany). In brief, highly pure naïve CD4$^+$ T cells were achieved by depletion of magnetically labeled non-CD4$^+$ T cells and CD45RO$^+$ memory T cells using a cocktail of biotin-conjugated antibodies against CD8, CD14, CD15, CD16, CD19, CD25, CD34, CD36, CD45RO, CD56, CD123, T cell receptor (TCR) γ/γ, HLA-DR, CD235a and anti-Biotin micro-beads (Miltenyi Biotec, Germany). The cell subset purity was regularly tested using flow cytometer, for the expression of CD4 and CD45RA.

Co-culture of adipose-derived mesenchymal stem cells and naïve CD4$^+$ T cells

Naïve CD4$^+$ T cells (25×10^4) were directly cultured with ASCs (25×10^3) at a ratio of 10 to 1 in RPMI 1640 (Biosera, UK) containing 10% FBS, 1% penicillin/streptomycin, 20 ng/ml phytohemagglutinin (PHA, Roche, Germany) and 7% autologous serum of healthy donors. The culture was incubated at 37˚C and 5% CO_2 with 95% humidity for five days.

Flow cytometry analysis

T cells were removed from culture and subjected to flow cytometer for characterization. To blockade Fc receptors, all cells were incubated for 10 minutes at 4˚C with 10 µl/ml human serum before staining with fluorescent antibodies. Fluorescent antibodies and the respective isotype controls were then added. Flow cytometry analysis was performed with a FACSCalibur (BD Biosciences) using directly labeled monoclonal Abs (mAbs), PerCP mouse anti-human CD4, FITC mouse anti-human CD25, APC mouse anti-human CD45RA, PerCP-CY™5.5 mouse anti-human CD73, APC mouse anti-human CD39, PE mouse anti-human FOXP3 (BD Biosciences), APC anti-mouse/human Helios (Biolegend, Germany) and isotype control antibodies, all according to the manufacturers' protocol. The collected data were analyzed using FlowJo 7.6 software.

Measurement of cytokine production by enzyme linked immunosorbent spot assay

ASCs (25×10^3) were directly co-cultured with isolated naïve CD4$^+$ T cells (25×10^4) in RPMI 1640 containing 10% FBS, 1% penicillin/streptomycin, 20 ng/ml PHA and

7% autologous serum of healthy donors. After five days, T cells were extracted from the culture and the production of cytokines including IL-10 (U-CyTech Biosciences, Netherland), TGF-β (R&D, USA) and IL-17 (U-CyTech Biosciences, Netherland) was measured. The ELISPOT assays were performed according to the manufacturers' instruction.

Statistical analysis

The data are represented as mean ± standard error mean (SEM). All statistical analyses were performed using statistical package for the social sciences (SPSS, Chicago, IL, USA) software version 16.0, nonparametric Mann-Whitney U test, Friedman and Dunn's and Kruskal-Wallis H tests. All graphs were plotted and evaluated by means of FlowJo 7.6.2 and GraphPad Prism 5 software. The $P<0.05$ were considered statistically significant.

Results

Adipose-derived mesenchymal stem cells isolation and characterization

ASCs had adhesion properties to the bottom of culture flasks and they were appeared as a homogenously spindle shaped population (Fig.1A). The flow cytometry analysis of ASCs revealed that more than 90% of all cancer and normal ASCs were positive for the stem cell specific markers, including CD90, CD105, CD44 and CD73, but they were negative for the expression of hematopoietic specific markers, such as CD45, CD34 and CD14 (Fig.1B).

Purity of the isolated naïve $CD4^+$ T cells

After isolating naïve $CD4^+$ T cells from peripheral blood of healthy donors, their purity were verified by CD4 and CD45RA expression analyses using flow cytometry. Results showed more than 96% purity for $CD4^+CD45RA^+$ cells (Fig.2).

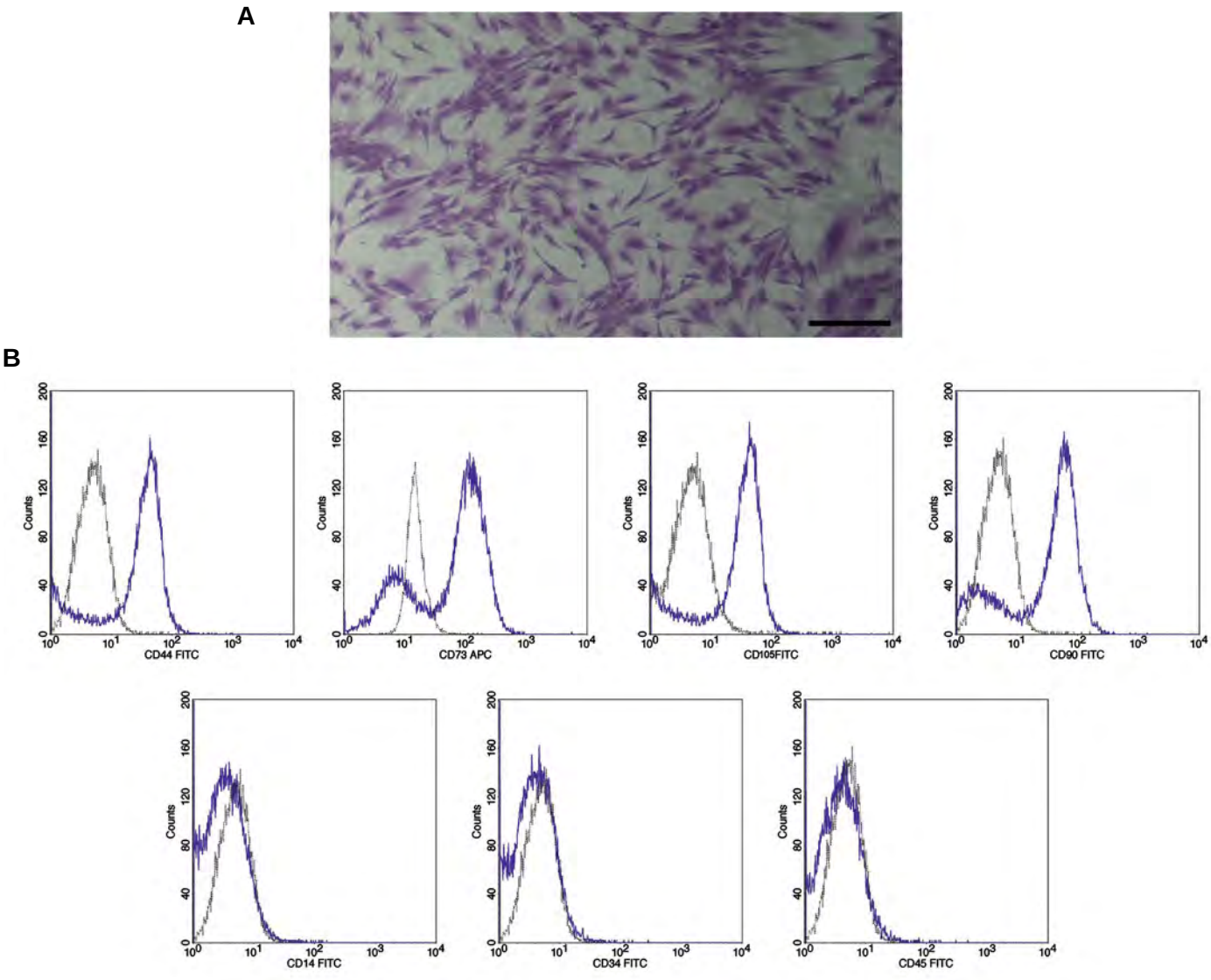

Fig.1: Morphological characterization of adipose-derived mesenchymal stem cells (ASCs) as well as flow cytometry analysis. **A.** ASCs were appeared with spindle shape in culture (scale bar: 100 µm) and **B.** The flow cytometry analysis of ASCs illustrate that more than 90% of all cancer and normal ASCs were positive for stem cell specific markers including CD44, CD105, CD73 and CD90, but they were negative for the expression of hematopoietic specific markers such as CD14, CD45 and CD34.

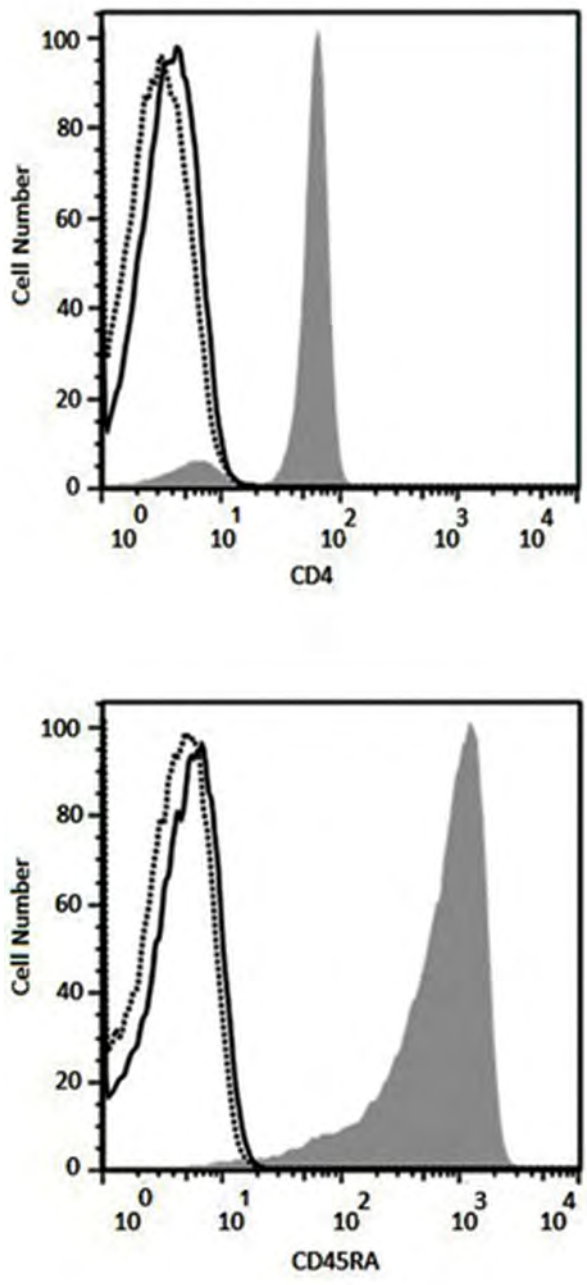

Fig.2: Purity of the isolated naïve $CD4^+$ T cells was evaluated using flow cytometry for the expression of CD4 and CD45RA (solid histograms). Results illustrate more than 96% purity for $CD4^+$ and $CD45RA^+$ cells. Solid and lined histograms represent isotype control and unstained cells, respectively.

Phenotypic analysis of harvested regulatory T cells

Phenotype of the harvested Tregs was studied more in detail, as $CD45RA^+$ and $Helios^+$ T cells were determined in the population of $CD4^+CD25^+FOXP3^+$ and $CD4^+CD25^-FOXP3^+$ T lymphocytes. $CD73^+CD39^+$ T lymphocytes were also assessed in the population of $CD25^+$ $FOXP3^+$ and $CD25^-$ $FOXP3^+$ cells.

$CD45RA^+$ T cells in the population of $CD4^+CD25^+FOXP3^+$ and $CD4^+CD25^-FOXP3^+$ cells

After five days co-culturing naïve T cells with normal- and cancer-ASCs, $CD45RA^+$ T cells were investigated in the population of $CD4^+CD25^+FOXP3^+$ and $CD4^+CD25^-FOXP3^+$ cells. Results showed that the effect of cancer-ASCs was more significant than normal-ASCs on augmenting $CD45RA^+$ cells, compared to the control group (P=0.002). Mean ± SEM percentage of $CD4^+CD25^+FOXP3^+CD45RA^+$ phenotype was 24.05 ± 5.5%, 21.36 ± 4.7%, and 9.51 ± 3.6% respectively after co-culturing with cancer-ASCs and normal-ASCs and in the control group (Fig.3A). Although naïve T cells co-culture with cancer-ASCs resulted in approximately two-fold expansion of $CD45RA^+$ T cells in the population of $CD4^+CD25^-FOXP3^+$ cells compared to the control group, this expansion was not statistically significant (P>0.05, Fig.3B).

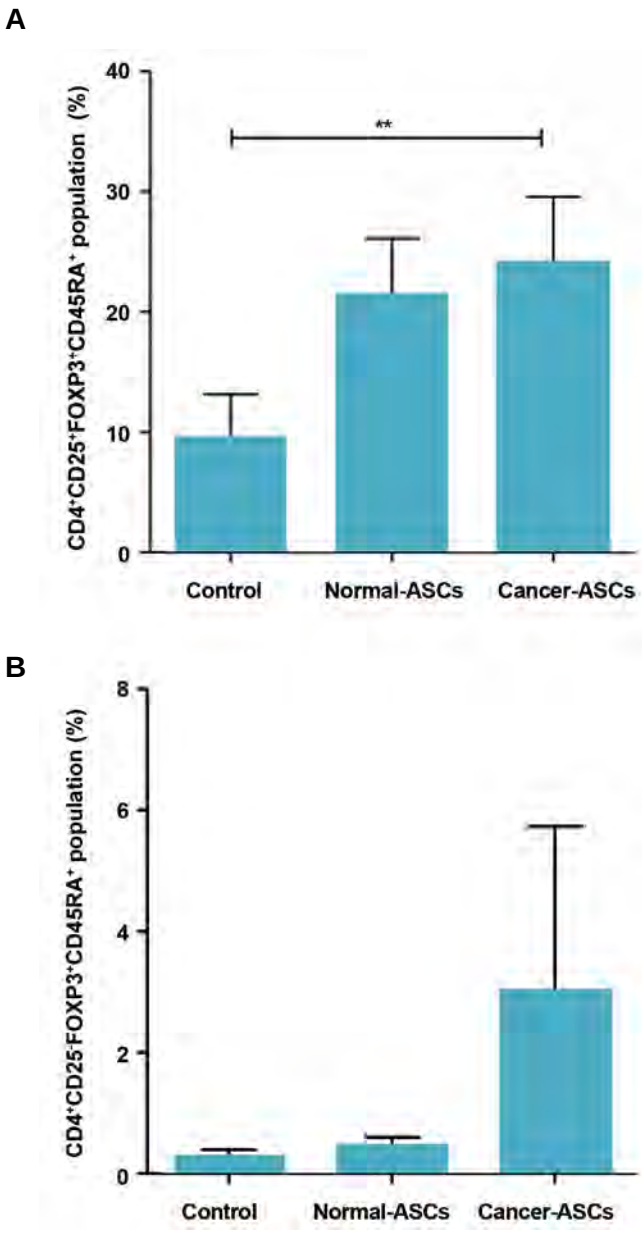

Fig.3: The percentage of $CD45RA^+CD4^+CD25^+FOXP3^+$ and $CD45RA^+CD4^+CD25^-FOXP3^+$ Tregs population. After five days culturing of naïve $CD4^+$ T cells with adipose-derived mesenchymal stem cells (ASCs), the percentage of **A.** $CD45RA^+CD4^+CD25^+FOXP3^+$ T cells and **B.** $CD45RA^+CD4^+CD25^-Foxp3^+$ T cells was evaluated by flow cytometry method. The results illustrate mean ± SEM of cell percentages. **; P<0.01 compared to the control group.

Helios$^+$ T cells in the population of CD4$^+$CD25$^+$FOXP3$^+$ and CD4$^+$CD25$^-$FOXP3$^+$ cells

Presence of normal-ASCs and cancer-ASCs in the culture increased Helios$^+$ T cells in the population of CD4$^+$CD25$^+$FOXP3$^+$ cells. The results showed that effect of cancer-ASCs was more significant than normal-ASCs on augmenting Helios$^+$ cells compared to the control group (P=0.005). Mean ± SEM percentage of T cells with CD4$^+$CD25$^+$FOXP3$^+$Helios$^+$ phenotype were 15.59 ± 4.6%, 12.63 ± 3.6%, and 5.90 ± 2.6% in the presence of cancer-ASCs and normal-ASCs and in the control group, respectively. (Fig.4A).

Helios$^+$ T cells, in the population of CD4$^+$CD25$^-$FOXP3$^+$, were increased in the presence of normal-ASCs and cancer-ASCs. Additionally, the effect of cancer-ASCs on augmentation of Helios$^+$ T cells was significant, compared to the control group (P=0.005, Fig.4B).

CD4$^+$CD25$^+$FOXP3$^-$Helios$^+$ and CD4$^+$CD25$^+$FOXP3$^+$Helios$^-$ T lymphocytes were also investigated in this study. The results showed that co-culturing naïve CD4$^+$ T cells with cancer-ASCs and normal-ASCs caused decreased population of CD4$^+$CD25$^+$FOXP3$^-$Helios$^+$ in comparison with the control group (P=0.028 and 0.028, respectively). Mean ± SEM percentage of CD4$^+$CD25$^+$FOXP3$^-$Helios$^+$ phenotype was 11.15 ± 0.6%, 12.47 ± 0.9% and 31.02 ± 4.2% after co-culturing with cancer-ASCs, normal-ASCs and control group, respectively. Changes in the phenotype of CD4$^+$CD25$^+$FOXP3$^+$Helios$^-$ T lymphocytes were not statistically significant (P>0.05).

CD73$^+$CD39$^+$ T cells in the population of CD25$^+$FOXP3$^+$ and CD25$^-$FOXP3$^+$ cells

When we compared presence of the normal-ASCs and cancer-ASCs to the control group, the percentage of CD25$^+$FOXP3$^+$CD73$^+$CD39$^+$ phenotype was increased in both normal and cancer-ASCs. Although, this was only significant in the presence of cancer-ASCs (P=0.005). Mean ± SEM percentage of CD73$^+$CD39$^+$CD25$^+$FOXP3$^+$ T cells cultured with cancer-ASCs, normal-ASCs and control group were respectively 4.00 ± 0.84, 2.41 ± 0.47, and 0.93 ± 0.08. Phenotypic changes of CD39$^+$CD73$^+$ T cells in the population of CD25$^-$FOXP3$^+$ was not significant (P> 0.05, Fig.5A, B).

The populations of CD39$^+$CD73$^+$CD25$^+$FOXP3$^+$ and CD39$^+$CD73$^+$CD25$^-$FOXP3$^+$ T lymphocytes were phenotypically compared when naïve CD4$^+$ T cells cultured with cancer-ASCs, normal-ASCs and control group. Results showed significant phenotypic changes between these two populations when naïve CD4$^+$ T cells were cultured with normal-ASCs and cancer-ASCs (P=0.017 and 0.008, respectively).

Mean ± SEM percentage of CD73$^+$CD39$^+$CD25$^+$FOXP3$^+$ and CD73$^+$CD39$^+$CD25$^-$FOXP3$^+$ T cells, cultured with cancer-ASCs, were 4 ± 0.8 and 0.88 ± 0.2, respectively. Mean ± SEM percentage of CD73$^+$CD39$^+$CD25$^+$FOXP3$^+$ and CD73$^+$CD39$^+$CD25$^-$FOXP3$^+$ T cells, cultured with normal-ASCs, were respectively 2.4 ± 0.4 and 0.67 ± 0.2. Phenotypic changes of these two populations, when naïve CD4$^+$ T cells cultured as control group, was not statistically significant (P >0.05).

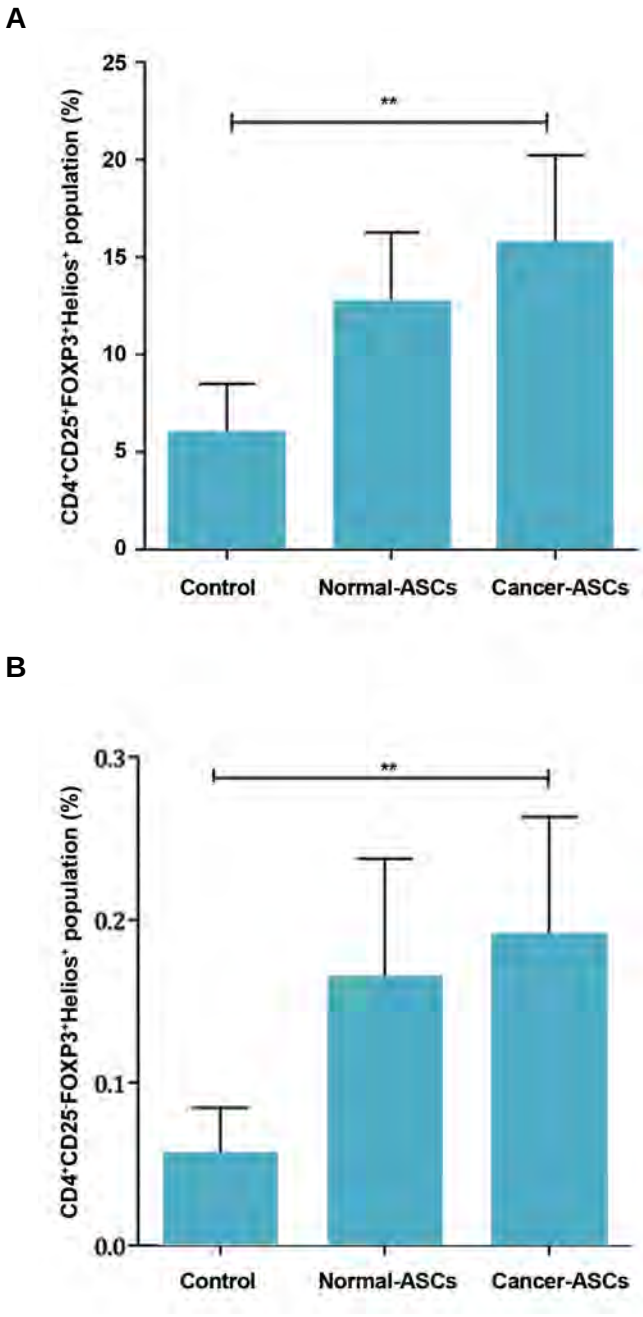

Fig.4: Percentage of the Helios$^+$ Tregs population. After five days culturing of naïve CD4$^+$ T cells with adipose-derived mesenchymal stem cells (ASCs). Percentage of **A.** The CD4$^+$CD25$^+$FOXP3$^+$Helios$^+$ T cells was evaluated by flow cytometry method and **B.** Percentage of the CD4$^+$CD25$^-$FOXP3$^+$Helios$^+$ T cells population was also determined. The results illustrate mean ± SEM of cell percentages. **; P<0.01 compared to the control group.

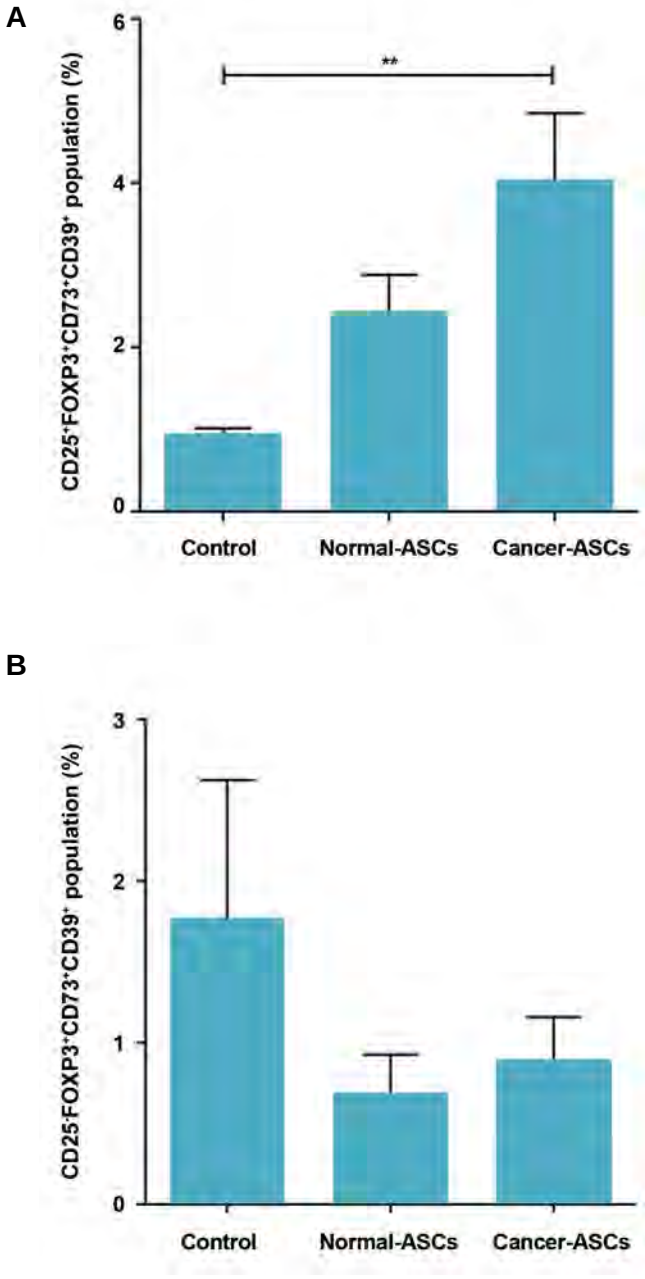

Fig.5: Percentage of the $CD39^+CD73^+$ in $CD25^+FOXP3^+$ and $CD25^-FOXP3^+$ T cells population subsequent to co-culturing with adipose-derived mesenchymal stem cells (ASCs). After five days culturing of naïve $CD4^+$ T cells with ASCs, percentage of $CD39^+CD73^+$ T cells in **A.** $CD25^+FOXP3^+$ population and **B.** $CD25^-FOXP3^+$ population was evaluated by flow cytometry method. The results illustrate mean ± SEM. **; P<0.01 compared to the control group.

Measurement of cytokine production by ELISPOT assay

Production of IL-10, TGF-β and IL-17 by T cells was evaluated in the presence and absence of ASCs, employing ELISPOT technique. The results showed that production of the cytokines was increased in the presence of ASCs. IL-10 production was increased by T cells, after exposure of naïve $CD4^+$ T cells to either normal- or cancer-ASCs. This effect was statistically significant for the cancer-ASCs compared to the control group (P=0.038). Mean ± SEM number of IL-10 spots by T cells cultured with cancer-ASCs, normal-ASCs and control group were 47.17 ± 15.1, 23.17 ± 7.5, and 3.167 ± 0.72, respectively. TGF-β production of the T cells was increased in the presence of cancer-ASCs compared to normal-ASCs and absence of the ASCs (P=0.0006 and 0.003, respectively). Mean ± SEM number of TGF-β spots by T cells, cultured with cancer-ASCs, normal-ASCs and control group were respectively 36.08 ± 4.7, 15.96 ± 2.8, and 10 ± 1.4. IL-17 production of T cells was increased while they were co-cultured with ASCs and the effect of normal-ASCs on IL-17 production was significant compared to the naïve T cells which were not cultured with ASCs (P=0.015). Mean ± SEM of IL-17 spots by T cells, cultured with cancer-ASCs, normal-ASCs and control group were respectively 41.5 ± 1.8, 64.33 ± 17.2, and 3.7 ± 1.9 (Fig.6).

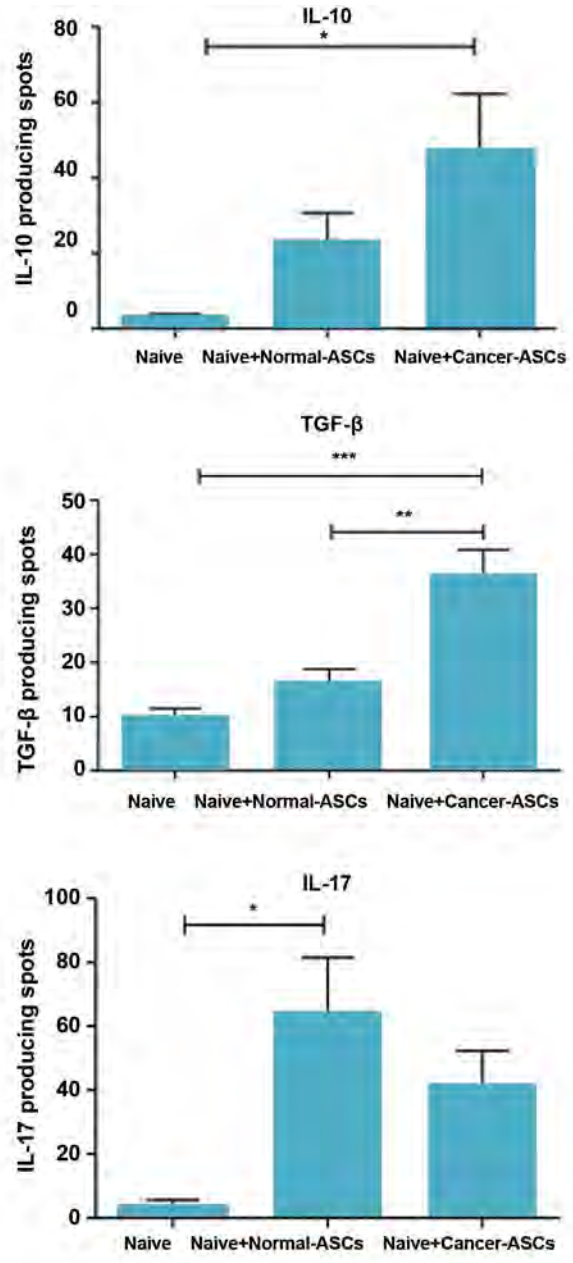

Fig.6: Producing interleukine-10 (IL-10), transforming growth factor beta (TGF-β) and IL-17 by T cell after co-culturing with adipose-derived mesenchymal stem cells (ASCs). After five days culturing of naïve $CD4^+$ T cells with ASCs, IL-10, TGF-β and IL-17 produced by T cells were evaluated using ELISPOT method. The results illustrate mean ± SEM. *; P<0.05, **; P<0.01 and ***; P< 0.001 compared to naïve T cells which were not co-cultured with ASCs (control group).

Discussion

Previous studies have indicated that high infiltration of tumors by regulatory $CD4^+FOXP3^+$ T cells associate with poor prognosis in different types of solid tumors, through limiting antitumor immune responses (22). Low numbers of tumor infiltrating $FOXP3^+$ T cells and high numbers of infiltrating $CD8^+$ lymphocytes have been suggested as favorable prognostic markers for invasive ductal carcinoma of the breast (23). It is proposed that tumor promoting effects of Tregs is mostly mediated through their recruitment to the tumor microenvironment or local expansion rather than increased suppressive properties in the tumor sites (5, 22).

Among several cell types in the vicinity of tumor cells, MSCs are known as important players with immunomodulatory effects on both innate and adaptive immunity through direct cell to cell contact or secretion of soluble factors (5). Herein, ASC-naïve $CD4^+$ T cell crosstalk was assessed and Treg subsets were subsequently further clarified in detail. The initial results disclosed that normal and cancer ASCs induced both $CD25^+$ and $CD25^-$ Tregs, but cancer ASCs showed stronger effect for inducing $CD25^-$ phenotype compared to the normal ASCs. The observed expansion of $CD25^-FOXP3^+$ Tregs in this study has been reported in previous researches (15, 21). $CD25^-$ T cells are a subset of Tregs induced by tumor and involved in tumor-induced immunosuppression (24). Yang et al. (25) realized that a specific proportion of intratumoral $CD4^+$ T cells in non-Hodgkin lymphoma patients was $CD4^+CD25^-FOXP3^+$ Tregs with the ability of suppressing T cells proliferation. In another study, both conventional and $CD4^+CD25^-FOXP3^+$ Tregs were detected in tumor draining lymph nodes of colorectal cancer patients but $CD25^-$ T cells were characterized with lower suppressive properties (26). Thus according to the results of this part of our study, ASCs from breast cancer tissues may suppress immune responses through increasing population of $CD4^+CD25^-FOXP3^+CD45RA^+$ Tregs, beside the conventional Tregs in the tumor microenvironment.

It was thought that majority of Tregs have memory phenotype, while they were defined by high expression of CD45RO and low expression of CD45RA. Memory Tregs survive longer than naïve Tregs and they have specialized subsets in different tissues (27). $CD45RA^+$ Tregs showed increased level of FOXP3 and strong suppressive ability as well as memory Tregs (28). Herein, there was no reduction of $CD45RA^+$ lymphocytes after co-culturing with neither cancer nor normal ASCs and the likelihood of increased memory population ($CD45RO^+$ Tregs). It seems that the balance between naive and memory Tregs is reversed in some autoimmune diseases, such as multiple sclerosis (MS) showing reduced number and function of $CD45RA^+$ Tregs, while expansion of memory Tregs has been reported in these patients (29, 30). Anyway, for achieving more reliable conclusions from our results, it was better to check $CD45RO^+$ Tregs or co-culture the cells for a longer period of time.

Helios, is an Ikaros transcription factor family member known as a marker of natural Treg (nTregs). Although recently, several reports have also shown that inducible Tregs (iTregs) express Helios *in vitro* and *in vivo* (31, 32). Other studies on mixed populations of naïve and memory $Helios^+$ or $Helios^-$ Tregs showed higher expression of IFN-γ, IL-17 and IL-2 by $Helios^-$ Tregs compared to $Helios^+$ Tregs (33). In contrast, Himmel et al. (34) revealed that $Helios^+$ and $Helios^-$ nTregs are not different in their functional properties for suppressing T cell proliferation. In the present study, we investigated the expression of Helios in the population of both $CD4^+CD25^+FOXP3^+$ and $CD4^+CD25^-FOXP3^+$ Tregs and the results revealed expansion of this subset in both population after exposing the cells to ASCs, specially to cancer ASCs. Consequently, ASCs not only increase the population of $FOXP3^+$ Tregs, but also induce the expression of Helios in these cells. This transcription factor, along with FOXP3, can increase suppressive activity of Tregs and since $Helios^+$ cells produce less inflammatory cytokines than $Helios^-$ cells (33), the former cells probably show more suppressive activity in the tumor site. The significance of this role of ASCs for inducing Helios is more pronounced when we refer to Yates et al. (35) study. They reported that under the chronic inflammation, Tregs may lose their Helios expression which can result in differentiating to effector T helper cells and consequently suppressing tumor growth.

Tregs mediate their immunosuppressive functions through various mechanisms including cell to cell contact, secretion of IL-35, IL-10 and TGF-β as well as the conversion of adenosine triphosphate (ATP) to adenosine through expression of CD39 and CD73 (36). CD39 and CD73 are two ectonucleotidases that collaborate in the production of extracellular adenosine through ATP hydrolysis. Indeed, CD39 generates adenosine monophosphate (AMP), which is in turn used by the CD73 ectonucleotidase to synthesize adenosine. Consequently, co-expression of CD73 and CD39 on Tregs surface is necessary for the maximum suppressor function (37, 38). In the present study, expressions of CD73 and CD39 were studied when naïve $CD4^+$ T cells were co-cultured with ASCs. The results revealed that co-culturing of naïve T cells with ASCs increased $CD73^+CD39^+$, but not $CD73^-CD39^+$ and $CD73^+CD39^-$ subsets of T cells, which was statistically significant in the presence of cancer-ASCs. Interestingly, $CD25^-$ $FOXP3^+CD73^+CD39^+$ cells were reduced after exposing to both cancer- and normal-ASCs compared to the control group. The results suggest that induced $CD25^+$ Tregs in the presence of ASCs, especially cancer-ASCs, may have stronger immunosuppressive effects compared to the $CD25^-$ counterparts due to co-expression of CD73 and CD39. This can result in inducing metabolic disruption of the recruited effector T cells to the tumor site. The current results are further confirmed by Saldanha-Araujo et al. (39) who showed that the amount of adenosine and $CD73^+$ T lymphocytes augmented significantly after exposing to bone marrow

MSCs. Collectively, it can be proposed that adenosine signaling would be important for immunomodulatory properties of ASCs.

According to the results of functional assay obtained from co-cultured naïve T cells, all three cytokines, IL-10, TGF-β and IL-17 were increased upon co-culturing of naïve T-cells with ASCs. Although cancer-ASCs had more significant effects on developing IL-10- and TGF-β-producing Tregs, normal-ASCs induced IL-17-producing Tregs. Despite most studies indicate secretion of anti-inflammatory cytokines by Tregs, it is well demonstrated that specific subgroups of these cells are capable of producing pro-inflammatory cytokines, such as IL-17 with immunosuppressive functions (40).

Conclusion

Both cancer and normal ASCs create immunomodulatory effects, but it seems that tumor cells educate ASCs for inducing immunosuppressive Tregs. Herein, the obtained results may represent a better understanding of how immune cells and stromal components of tumor site, in particular MSCs, communicate with each other. This can help us predict more successful therapeutic approaches for treatment of breast cancer.

Acknowledgements

We are grateful of normal individuals and breast cancer patients participating in this project. This study was conducted as a requirement for the Immunological M.Sc. thesis defended by Ms. Maryam Fakhimi and supported by funding from Shiraz University of Medical Sciences, Grant No. 94-01-01-9113 and Shiraz Institute for Cancer Research [ICR-100-504]. The authors declared no conflict of interest regarding this study.

Authors' Contributions

M.R.; Designing the project, supervising lab experiments, data analysis and preparing the manuscript. M.F.; Doing lab experiments, analyzing the data and preparing manuscript draft. A-R.T.; Helping us to choose the patients, preparing the samples, and reading the manuscript. A.Gh.; Designing and supervising the project and preparing the manuscript. M.H.; Providing the IL-10 ELISPOT Kit and reading the manuscript. All authors read and approved the final manuscript.

References

1. Yang X, Hou J, Han Z, Wang Y, Hao C, Wei L, et al. One cell, multiple roles: contribution of mesenchymal stem cells to tumor development in tumor microenvironment. Cell Biosci. 2013; 3(1): 5.
2. Zhang T, Lee YW, Rui YF, Cheng TY, Jiang XH, Li G. Bone marrow-derived mesenchymal stem cells promote growth and angiogenesis of breast and prostate tumors. Stem Cell Res Ther. 2013; 4(3): 70.
3. Whiteside TL. The tumor microenvironment and its role in promoting tumor growth. Oncogene. 2008; 27(45): 5904-5912.
4. Yi T, Song SU. Immunomodulatory properties of mesenchymal stem cells and their therapeutic applications. Arch Pharm Res. 2012; 35(2): 213-221.
5. Di Nicola M, Carlo-Stella C, Magni M, Milanesi M, Longoni PD, Matteucci P, et al. Human bone marrow stromal cells suppress T-lymphocyte proliferation induced by cellular or nonspecific mitogenic stimuli. Blood. 2002; 99(10): 3838-3843.
6. Duffy MM, Ritter T, Ceredig R, Griffin MD. Mesenchymal stem cell effects on T-cell effector pathways. Stem Cell Res Ther. 2011; 2(4): 34.
7. Al-Nbaheen M, Vishnubalaji R, Ali D, Bouslimi A, Al-Jassir F, Megges M, et al. Human stromal (mesenchymal) stem cells from bone marrow, adipose tissue and skin exhibit differences in molecular phenotype and differentiation potential. Stem Cell Rev. 2013; 9(1): 32-43.
8. Bajenoff M, Egen JG, Koo LY, Laugier JP, Brau F, Glaichenhaus N, et al. Stromal cell networks regulate lymphocyte entry, migration, and territoriality in lymph nodes. Immunity. 2006; 25(6): 989-1001.
9. Abumaree M, Al Jumah M, Pace RA, Kalionis B. Immunosuppressive properties of mesenchymal stem cells. Stem Cell Rev. 2012; 8(2): 375-392.
10. Baer PC, Geiger H. Adipose-derived mesenchymal stromal/stem cells: tissue localization, characterization, and heterogeneity. Stem Cells Int. 2012; 2012: 812693.
11. Bonelli M, Savitskaya A, Steiner CW, Rath E, Smolen JS, Scheinecker C. Phenotypic and functional analysis of CD4+ CD25- Foxp3+ T cells in patients with systemic lupus erythematosus. J Immunol. 2009; 182(3): 1689-1695.
12. Li Z, Li D, Tsun A, Li B. FOXP3+ regulatory T cells and their functional regulation. Cell Mol Immunol. 2015; 12(5): 558-565.
13. Peterson RA. Regulatory T-cells: diverse phenotypes integral to immune homeostasis and suppression. Toxicol Pathol. 2012; 40(2): 186-204.
14. Ray A, Khare A, Krishnamoorthy N, Qi Z, Ray P. Regulatory T cells in many flavors control asthma. Mucosal Immunol. 2010; 3(3): 216-229.
15. Razmkhah M, Abedi N, Hosseini A, Imani MT, Talei AR, Ghaderi A. Induction of T regulatory subsets from naive CD4+ T cells after exposure to breast cancer adipose derived stem cells. Iran J Immunol. 2015; 12(1): 1-15.
16. Wang RF. CD8+ regulatory T cells ,their suppressive mechanisms, and regulation in cancer. Hum Immunol. 2008; 69(11): 811-814.
17. Miyara M, Yoshioka Y, Kitoh A, Shima T, Wing K, Niwa A, et al. Functional delineation and differentiation dynamics of human CD4+ T cells expressing the FoxP3 transcription factor. Immunity. 2009; 30(6): 899-911.
18. Borsellino G, Kleinewietfeld M, Di Mitri D, Sternjak A, Diamantini A, Giometto R, et al. Expression of ectonucleotidase CD39 by Foxp3+ Treg cells: hydrolysis of extracellular ATP and immune suppression. Blood. 2007;110(4): 1225–1232.
19. Yan Z, Zhuansun Y, Chen R, Li J, Ran P. Immunomodulation of mesenchymal stromal cells on regulatory T cells and its possible mechanism. Exp Cell Res. 2014; 324(1): 65-74.
20. Razmkhah M, Jaberipour M, Hosseini A, Safaei A, Khalatbari B, Ghaderi A. Expression profile of IL-8 and growth factors in breast cancer cells and adipose-derived stem cells (ASCs) isolated from breast carcinoma. Cell Immunol. 2010; 265(1): 80-85.
21. Razmkhah M, Jaberipour M, Erfani N ,Habibagahi M, Talei AR, Ghaderi A. Adipose derived stem cells (ASCs) isolated from breast cancer tissue express IL-4, IL-10 and TGF-beta1 and upregulate expression of regulatory molecules on T cells: do they protect breast cancer cells from the immune response? Cell Immunol. 2011; 266(2): 116-122.
22. Facciabene A, Motz GT, Coukos G. T-regulatory cells: key players in tumor immune escape and angiogenesis. Cancer Res. 2012; 72(9): 2162-2171.
23. Xu Y, Lan S, Zheng Q. Prognostic significance of infiltrating immune cell subtypes in invasive ductal carcinoma of the breast. Tumori. 2018; 104(3): 196-201.
24. Han Y, Guo Q, Zhang M, Chen Z, Cao X. CD69+ CD4+ CD25- T cells, a new subset of regulatory T cells, suppress T cell proliferation through membrane-bound TGF-beta 1. J Immunol. 2009; 182(1): 111-120.
25. Yang ZZ, Novak AJ, Ziesmer SC, Witzig TE, Ansell SM. CD70+ non-Hodgkin lymphoma B cells induce Foxp3 expression and regulatory function in intratumoral CD4+CD25 T cells. Blood. 2007; 110(7): 2537-2544.
26. Jafarinia M, Mehdipour F, Hosseini SV, Ghahramani L, Hosseinzadeh M, Ghaderi A. Determination of a CD4+CD25- FoxP3+ T cells subset in tumor draining lymph nodesof colorectal cancer secreting IL-2 and IFN-γ. Tumour Biol. 2016; 37(11): 14659-14666.

27. Rosenblum MD, Way SS, Abbas AK. Regulatory T cell memory. Nat Rev Immunol. 2016; 16(2): 90-101.
28. Seddiki N, Santner-Nanan B, Tangye SG, Alexander SI, Solomon M, Lee S, et al. Persistence of naive CD45RA+ regulatory T cells in adult life. Blood. 2006; 107(7): 2830-2838.
29. Haas J, Fritzsching B, Trubswetter P, Korporal M, Milkova L, Fritz B, et al. Prevalence of newly generated naive regulatory T cells (Treg) is critical for Treg suppressive function and determines Treg dysfunction in multiple sclerosis. J Immunol. 2007; 179(2): 1322-1330.
30. Venken K, Hellings N, Broekmans T, Hensen K, Rummens JL, Stinissen P. Natural naive CD4+CD25+CD127low regulatory T cell (Treg) development and function are disturbed in multiple sclerosis patients: recovery of memory Treg homeostasis during disease progression. J Immunol. 2008; 180(9): 6411-6420.
31. Muto S, Owada Y, Inoue T, Watanabe Y, Yamaura T, Fukuhara M, et al. Clinical significance of expanded Foxp3(+) Helios(-) regulatory T cells in patients with non-small cell lung cancer. Int J Oncol. 2015; 47(6): 2082-2090.
32. Ross EM, Bourges D, Hogan TV, Gleeson PA ,van Driel IR. Helios defines T cells being driven to tolerance in the periphery and thymus. Eur J Immunol. 2014; 44(7): 2048-2058.
33. Thornton AM, Shevach EM. CD4+CD25+ immunoregulatory T cells suppress polyclonal T cell activation in vitro by inhibiting interleukin 2 production. J Exp Med. 1998; 188(2): 287-296.
34. Himmel ME, MacDonald KG, Garcia RV, Steiner TS, Levings MK. Helios+ and Helios- cells coexist within the natural FOXP3+ T regulatory cell subset in humans. J Immunol. 2013; 190(5): 2001-2008.
35. Yates K, Bi K, Haining WN, Cantor H, Kim HJ. Comparative transcriptome analysis reveals distinct genetic modules associated with Helios expression in intratumoral regulatory T cells. Proc Natl Acad Sci USA. 2018; 115(9): 2162-2167.
36. Vignali DA, Collison LW, Workman CJ. How regulatory T cells work. Nat Rev Immunol. 2008; 8(7): 523-532.
37. Bono MR, Fernandez D, Flores-Santibanez F, Rosemblatt M, Sauma D. CD73 and CD39 ectonucleotidases in T cell differentiation: beyond immunosuppression. FEBS Lett. 2015; 589(22): 3454-3460.
38. Deaglio S, Dwyer KM, Gao W, Friedman D, Usheva A, Erat A, et al. Adenosine generation catalyzed by CD39 and CD73 expressed on regulatory T cells mediates immune suppression. J Exp Med. 2007; 204(6): 1257-1265.
39. Saldanha-Araujo F, Ferreira FI, Palma PV, Araujo AG, Queiroz RH, Covas DT, et al. Mesenchymal stromal cells up-regulate CD39 and increase adenosine production to suppress activated T-lymphocytes. Stem Cell Res. 2011; 7(1): 66-74.
40. Beriou G, Costantino CM, Ashley CW, Yang L, Kuchroo VK, Baecher-Allan C, et al. IL-17-producing human peripheral regulatory T cells retain suppressive function. Blood. 2009; 113(18): 4240-4249.

Original Article

The Effects of Embryonic Cerebrospinal Fluid on The Viability and Neuronal Differentiation of Adipose Tissue-Derived Stem Cells in Wistar Rats

Mohammad-Hossein Mohammadi-Mahdiabadi-Hasani, M.Sc.[1], Mohammad Nabiuni, Ph.D.[1]*, Kazem Parivar, Ph.D.[2], Siamak Yari, Ph.D.[3], Alireza Sahebi, M.Sc.[1], Jaleel Miyan, Ph.D.[4]

1. Department of Cell and Molecular Biology, Faculty of Biological Sciences, Kharazmi University, Tehran, Iran
2. Department of Biology, Sciences and Research Branch, Islamic Azad University, Tehran, Iran
3. Department of Biology, Faculty of Sciences, Bu-Ali Sina University, Hamedan, Iran
4. Faculty of Biology, Medicine and Health Division of Neuroscience and Experimental Psychology, The University of Manchester, Manchester, UK

Corresponding Address: P.O.Box: 31979-37551, Department of Cell and Molecular Biology, Faculty of Biological Sciences, Kharazmi University, Tehran, Iran
Email: devbiokharazmi@gmail.com

Received: 25/December/2018, Accepted: 8/April/2019

Abstract

Objective: The embryonic cerebrospinal fluid (e-CSF) contains various growth factors and morphogens. Recent studies showed that e-CSF plays significant roles in embryonic brain development. Adipose tissue-derived stem cells (ADSCs) have a mesodermal origin that can be differentiated into mesodermal and ectodermal lineages. This study aimed to evaluate the effects of e-CSF on the proliferation, viability, and neural differentiation of ADSCs in rats.

Materials and Methods: In this experimental study, adipose tissue was dissected out from the inguinal region of adult male rats. Then, ADSCs were isolated by enzymatic digestion from adipose tissues and mesenchymal cells were confirmed using the flow cytometry analysis that measured the cell surface markers including CD90, CD44, CD73, CD105, CD34, CD45, and CD11b. The multi-potential characteristics of ADSCs were assessed by osteogenic and adipogenic potentials of these cells. Under suitable *in vitro* conditions, ADSCs were cultured in DMEM supplemented with and without additional 10% e-CSF. These fluids were collected from Wistar rats at the E17, E18, and E19 gestational ages. Cellular proliferation and viability were determined using the MTT assay. Immunocytochemistry was used to study the expression of β-III tubulin in ADSCs. The neurite outgrowth of cultured cells was assessed using the ImageJ software.

Results: The results of the present study demonstrated that the viability of ADSCs in cell culture conditioned with E17 and E18 e-CSF were significantly increased in comparison with controls. Cultured cells treated with e-CSF from E18 and E19 established neuronal-like cells bearing long process, whereas no process was observed in the control groups or cultured cells treated with E17 e-CSF.

Conclusion: This study showed that e-CSF has the ability to induce neuronal differentiation and viability in ADSCs. Our data support a significant role of e-CSF as a therapeutic strategy for the treatment of neurodegenerative diseases.

Keywords: Adipose Tissue, Cerebrospinal Fluid, Neuronal Differentiation, Stem Cells

Cell Journal(Yakhteh), Vol 22, No 2, July-September (Summer) 2020, Pages: 245-252

Citation: **Mohammadi-Mahdiabadi-Hasani MH, Nabiuni M, Parivar K, Yari S, Sahebi AR, Miyan J. The effects of embryonic cerebrospinal fluid on the viability and neuronal differentiation of adipose tissue-derived stem cells in wistar rats. Cell J. 2020; 22(2): 245-252. doi: 10.22074/cellj.2020.6560.**

Introduction

Cerebrospinal fluid (CSF) is a clear and colorless fluid, secreted mainly (about two-third of its volume) from the epithelial structure in the choroid plexus, and it could also be released from other regions in the brain such as capillaries surrounded by astrocytes, ependymal epithelium of the ventricles, and subarachnoid plexus (1). The CSF secretion starts at the early stages of the neural tube development. It contains many morphogenic and growth factors such as neurotrophin-3 (NT-3), hepatocyte growth factor (HGF), transforming growth factor-β (TGF-β), insulin-like growth factor (IGF), nerve growth factor (NGF-3), basic fibroblast growth factor (b-FGF), and brain-derived neurotrophic factor (BDNF), involved in the proliferation, differentiation, and survival of neural cells (2, 3).

Previous studies have shown that embryonic cerebrospinal fluid (e-CSF) is a rich source of proteins, which are involved in the proliferation, differentiation, and migration of neural progenitor cells during brain development. E-CSF affects the neuroepithelial cells by regulating the proliferation, differentiation, and survival of these types of cells. Similar to CSF, e-CSF is a cocktail of various growth and morphogenesis factors (4, 5).

Adult stem cells are characterized by self-renewal ability, long-time survival, and multipotency (6). Compared with the embryonic stem cells, adult stem cells are immune-

compatible, non-tumorigenic, and working with them has no ethical issues (7).

Due to easy accessibility, mesenchymal stem cells (MSCs)-commonly obtained from the bone marrow - are a new cell resource for clinical practice and research (8). However, the clinical use of bone marrow-derived stem cells is restricted due to its highly invasive nature required for cell extraction and low proliferative capacity of the isolated cells (9). In a search for an alternative MSCs source, recently MSCs has been isolated from adipose tissues (10).

Adipose tissue-derived stem cells (ADSCs) have high proliferation potential that can be differentiated into a variety of mesenchymal cell lineages such as osteoblasts and adipocytes. They also have regenerative properties and potency to differentiate into nerve and Schwann cells (11, 12). As they could be obtained using minimally invasive methods and have high proliferation capacity, ADSCs are a promising tool for regenerative medicine (13). Thus, the current study aimed to evaluate whether e-CSF can induce neural proliferation and differentiation in ADSCs, as well as assessing the impact of e-CSF on the viability of ADSCs.

Materials and Methods

Animals

In this experimental study, 22 male and 56 pregnant female Wistar rats were used. The animals were kept in an animal house located in the Department of Biology at the Kharazmi University. They were kept in large rat boxes with free access to food and water under a 12:12 light/dark cycle. All animals were treated according to the guidelines set by the Kharazmi University based on the National Institutes of Health (NIH) Guidelines for the Care and Use of Laboratory Animals (C: 616/919). Individual male and female rats were mated and checked daily for the vaginal plug presence, designated as embryonic day 0 (E0). The embryonic age was calculated from E0. At specific times, pregnant rats were euthanized with urethane (1.5 g/kg urethane i.p., Sigma, UK), and the uterus was quickly evacuated into an icebox. Then, litters were immediately separated from pregnant Wistar rats. Each pregnant rat delivered separated from litters in each delivery.

Collection of embryonic cerebrospinal fluid samples

To evaluate e-CSF effects on ADSCs cultures, e-CSF was collected from cisterna magna of rat embryos on day 17 (E17), 18 (E18), and 19 (E19) using a glass micropipette. Because of large fluid space, the cisterna magna is an ideal site for extracting uncontaminated e-CSF. Besides, the cisterna magna is exposed upon dissecting the skin and the removal of the overlying muscles. Due to the lack of bone formation in this area and its flexibility, the risk of blood contamination in CSF would be decreased. All samples were collected in sterile microtubes and centrifuged immediately at 4000 rpm for 5 minutes to separate the fluid from cellular debris. Afterward, the supernatant was transferred and preserved in a new sterile tube. The samples were stored at -40˚C until the subsequent use. About 10 to 50 µl of e-CSF was collected from each litter. All steps mentioned above were carried out on an ice box to avoid denaturation of e-CSF proteins (14).

Isolation and culture of adipose tissue-derived stem cells

Adult male rats (180-220 g) were anesthetized with urethane (1.5 g/kg i.p.). Under sterile conditions, all parts of white adipose tissue samples were isolated from the abdominal inguinal region and transferred into phosphate-buffered saline (PBS, Gibco, UK). Adipose tissues were minced to pieces in sizes between 1 and 2 mm^3 using scissors and then washed repeatedly with equal volumes of PBS to remove blood cells. Next, each piece was transferred into a falcon tube containing 0.075% collagenase type I enzyme (Sigma Aldrich, USA). Tubes were placed on a shaker incubator at 37˚C for 30 minutes. After that, samples were centrifuged at 2000 rpm for 5 minutes. Undigested pieces were removed, and the remaining suspension containing stem cells were collected. Extracted ADSCs were cultured in Dulbecco's Modified Eagle Medium (DMEM, Gibco, Invitrogen, USA) containing 10% fetal bovine serum (FBS, Gibco, UK) and 1% penicillin/streptomycin. The cultures were kept in a humidified atmosphere incubator at 37˚C with 5% CO_2. The culture media were renewed every three days (15). In this study, cell cultures were divided into five groups: I. Control: without e-CSF treatment, II. E17: treatment with e-CSF from E17 (10% v/v), III. E18: treatment with e-CSF from E18 (10% v/v), IV. E19: treatment with e-CSF from E19 (10% v/v), and V. β-Mercaptoethanol (β-ME): treatment with β-ME (10 ng/ml) as the positive control.

Cell viability assay

In the present study, the harvested ADSCs were rinsed with PBS, transferred into 24-well plates (7×10^4 cells/well), treated with e-CSF (E17, E18, and E19) (10% v/v), and β-ME (10 ng/ml, Sigma Aldrich, USA) for six days. The wells without any treatment were considered as controls. Cell survival and viability were measured by the MTT assay. MTT (3-(4,5-Dimethylthiazol-2 thiazolyl)-2,5- diphenyl 2 tetrazolium bromide) is a yellow tetrazolium dye that responds to activated mitochondrial dehydrogenases and changes the yellow color of samples to dark blue formazan crystals. The cells were incubated with MTT (5 mg/mL in PBS, Merck, Germany) at 37˚C for 3 hours. Finally, the absorbance was recorded at 570 nm using a plate reader (ELx808™, BioTek® instruments, USA). Each experiment was repeated in triplicate (16).

Adipose tissue-derived stem cells multi-lineage differentiation potential

Another feature of mesenchymal cells is their ability to differentiate into osteocytes and adipocytes. Therefore, in the present study, the differentiation of MSCs into adipose and bone cells was evaluated. For this purpose, ADSCs were harvested at three passages and cultured in the osteogenic and adipogenic inducing medium for 21 days. Osteogenic differentiation culture media consisted of DMEM-LG (low glucose) supplemented with 10% FBS, 0.1 μM dexamethasone, 10 μM β-glycerophosphate, and 50 μM ascorbate. To assess mineralization, cultures were stained with 2% Alizarin Red (Sigma-Aldrich, USA). Adipogenic inducing culture media contained DMEM-LG, supplemented with 10% FBS, 0.5 mM IBMX (3-isobutyl-1-methylxanthine), 10 mg/ml insulin, 1 mM dexamethasone, and 100 mM indomethacin. Cells were stained with Oil Red (Sigma-Aldrich, USA) for the detection of adipocytes (17).

Flow cytometry analysis

After second consecutive passages, to measure the cell surface markers of MSCs and to confirm their development, we used the following conjugated antibodies: PE Mouse Anti-Rat CD44, PE Mouse Anti-Rat CD73, PE Mouse Anti-Rat CD105, FITC Mouse Anti-Rat CD90, PE Mouse Anti-Rat CD34, PE Mouse Anti-Rat CD45, PE Mouse Anti-Rat CD11b, and isotype control antibody. After trypsinization of the cells with 0.25% trypsin/ ethylenediaminetetraacetic acid (EDTA) solution, they were re-suspended in PBS and counted using hemocytometer. A number of 1×10^6 cells were incubated in fluorochrome-conjugated antibody at a dilution ratio of 1:10 at room temperature for 20 minutes in the dark place. The stained ADSCs were analyzed using a BD FACSCaliber™ flow cytometer (BD Biosciences, USA) and the FlowJo software (version 10.4). A total of 200,000 cells were assessed in each sample.

Morphological properties and neurite-like processes assessment

In order to evaluate the morphology and growth rate of ADSCs, cells were imaged using an inverted microscope (Olympus, Japan) and the obtained images were analyzed by the ImageJ software (NIH). The morphological properties of the cells, as well as the length of neurite-like processes, were compared among cell treatments.

Immunocytochemistry

In this study, β-III tubulin was considered a neural differentiation marker. After three times washing with PBS, cells were fixed with cold 4% paraformaldehyde for 15 minutes. Then, 0.1% Triton X-100 (Merck, Germany) was employed for the increase of cell permeability at room temperature for 30 minutes. The cells were blocked with 1% BSA (Sigma-Aldrich, USA) in T-PBS (Tween 20 in PBS) (T-PBS, Gibco, UK) at room temperature for 1 hour. After that, the cells were incubated at 4˚C overnight in the presence of anti-β III tubulin (1:100 Dilution, Abcam, UK) as a primary antibody. The next day, cells were rinsed three times with T-PBS and incubated with a Cy3-conjugated secondary antibody (1:300 Dilution, Abcam, UK) at room temperature for 1 hour. Finally, cells were washed with PBS, and nuclear staining was carried out with 4',6-Diamidino-2-Phenylindole (DAPI, Sigma-Aldrich, USA). Photomicrography was done under a fluorescent microscope (Olympus, Japan).

Statistical analyses

Ordinary one-way analysis of variance (one-way ANOVA) was applied for the statistical analysis, followed by Tukey's post hoc test to compare multiple groups. Data are expressed as the mean and standard error of the mean (mean ± SEM). The $P<0.05$ was considered statistically significant. Data were analyzed using the the IBM SPSS Statistics for Windows, Version 24.0. Armonk, NY: IBM Corp. (Released 2016).

Results

Morphological characteristics and pluripotency of adipose tissue-derived stem cells

Cultured cells were adherent and had spindle-shaped morphology. Besides, cultured ADSCs were pluripotent and differentiated into osteoblasts and adipocytes in specific conditioned media. Alizarin red and Oil Red staining were carried out for the confirmation of ADSCs differentiation into osteoblasts and adipocytes (Fig.1A-C).

Flow cytometry analysis of the expression of stem cells markers in adipose tissue-derived stem cells population

Cell surface markers were utilized on the second passage to characterize ADSCs population. The flow cytometry analysis of cell surface markers showed that these cells expressed CD90, CD44, CD73, and CD105 as MSCs markers, whereas they did not express CD34, CD45, and CD11b markers (Fig.1D).

Effects of embryonic cerebrospinal fluid on adipose tissue-derived stem cells viability

After six days of treatment, viability assessment was implemented in all cultured groups. As shown in Figure 2, the MTT absorbance was increased significantly in cultured cells conditioned with CSF (10% v/v) from E17, E18, and E19. However, the MTT absorbance was decreased after the cells were treated with β-ME (positive control) compared with the control group. The highest viability was observed at E17 and E18 in e-CSF treatment (Fig.2).

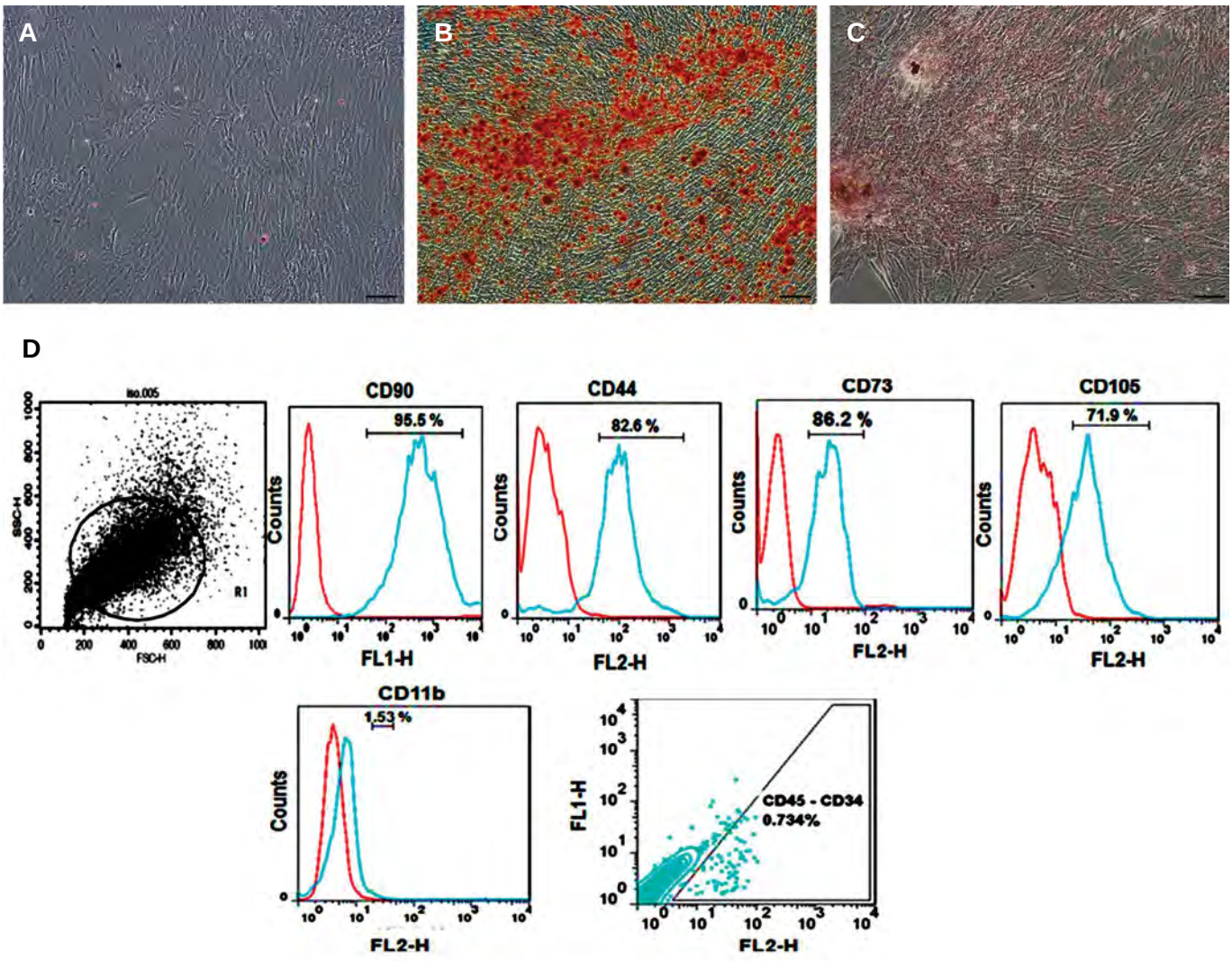

Fig.1: Morphological characteristics and pluripotency of adipose tissue-derived stem cells (ADSCs). Photomicrographs of ADSCs show typical spindle-shaped morphology. **A.** Cultured ADSCs in complete growth medium (control group), **B.** Adipogenic differentiation of ADSCs (Oil Red staining), **C.** Osteogenic differentiation of ADSCs (Alizarin Red staining), (scale bars: 100 µm), and **D.** Flow cytometry histograms indicating immunophenotype of mesenchymal stem cells isolated from rat's adipose tissue. The cells expressed the cell surface markers namely CD90, CD44, CD73, and CD105, but not CD34, CD45, and CD11b.

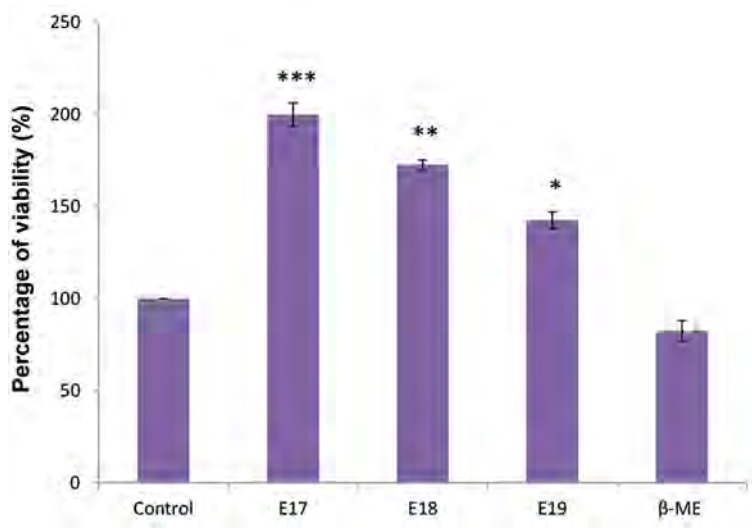

Fig.2: Survival rates of adipose tissue-derived stem cells (ADSCs) in cell culture treated with embryonic cerebrospinal fluid (e-CSF, 10% v/v) and β-Mercaptoethanol (β-ME, 10 ng/ml) using the MTT assay (n=5). All cultured ADSCs indicated an increase in viability after treatment with e-CSF. The increase was significant in treatment with CSF from embryonic days 17, 18 and 19 (E17, E18, and E19). Data are expressed as the percentage of control levels (cell culture without the addition of CSF). *; P<0.05, **; P<0.01, and ***; P<0.001 as compared with the control group.

The Effects of embryonic erebrospinal fluid on neurite outgrowth of adipose tissue-derived stem cells

Photomicrographs of the cultured cells are shown in Figure 3. Neurite outgrowth and morphological differentiation were observed in treatment groups with β-M (Fig.3B) and e-CSF at E17 (Fig.3C), E18 (Fig.3D), and E19 (Fig.3E), whereas no morphological differentiation was evident in the control group (Fig.3A). The diameter of ADSCs was measured by the ImageJ software. ADSCs treatment with e-CSF at E18 and E19 significantly increased neurite outgrowth compared with the control samples, but the increase in the experimental group treated with e-CSF at E17 was not statistically significant (Fig.3F).

Immunocytochemistry characteristics of differentiated adipose tissue-derived stem cells

For neural induction, ADSCs were incubated whit β-ME (traditional neural inducer) as the positive control. As shown in Figure 4, the majority of ADSCs in this condition have a high level of β III-tubulin expression. Moreover, the number of cells were positive for β III-tubulin were significantly increased in cultured cells conditioned with CSF at E17, E18, and E19. However, no changes were observed in the expression of β III-tubulin in ADSCs of the control group (Fig.4).

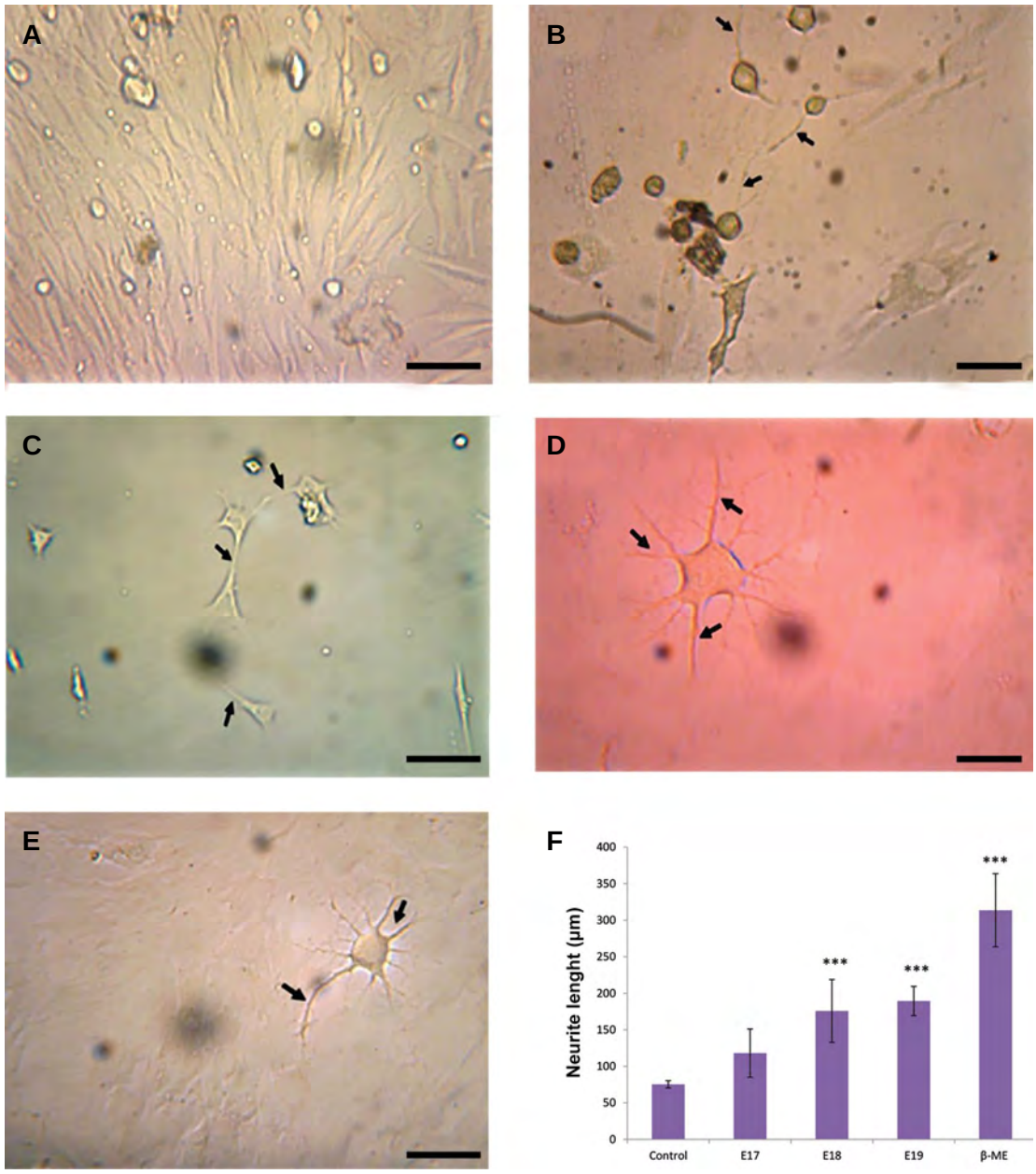

Fig.3: Morphological differentiation and neurite outgrowth length of adipose tissue-derived stem cells (ADSCs) after a 6-days period treatment with embryonic cerebrospinal fluid (e-CSF, 10%v/v) and β-Mercaptoethanol (β-ME, 10 ng/ml). **A.** Control without treatment, **B.** Treatment with β-ME, **C.** Treatment with e-CSF at E17, **D.** Treatment with e-CSF at E18, **E.** Treatment with e-CSF at E19. Treatment of ADSCs with β-ME and e-CSF at E17, E18, and E19 showed neurite outgrowth (arrows) and morphological differentiation as compared to the control group. No morphological changes were observed in the control group (scale bar: 10 µm), and **F.** The length of neurites in ADSCs treated with e-CSF at E18 and E19 and β-ME (positive control) was significantly increased compared to the control sample. Data are presented as the mean ± S.E.M. ***; P<0.001.

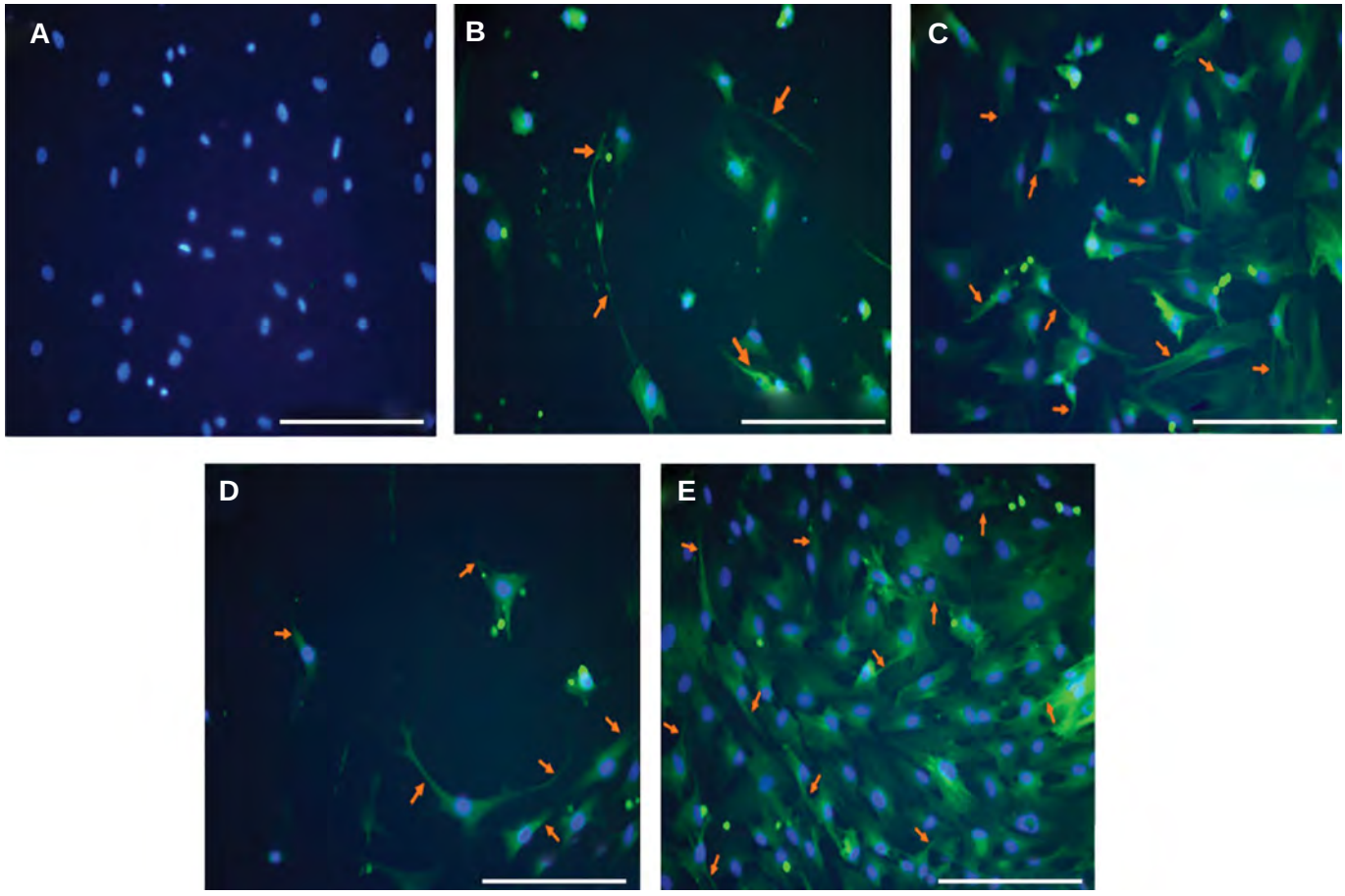

Fig.4: Immunofluorescence localization of β III-tubulin (orange arrow) in adipose tissue-derived stem cells (ADSCs) (green) treated with embryonic cerebrospinal fluid (e-CSF) at E17, E18, and E19 (10% v/v) and β-Mercaptoethanol (β-ME, 10 ng/ml). **A.** ADSCs in the control group without e-CSF expressed no β III-tubulin, **B.** ADSCs treated with β-ME, **C.** ADSCs treated with e-CSF at E17, **D.** E18, and **E.** E19. Cell nuclei are stained with DAPI (blue) (scale bars: 100 μm).

Discussion

Considering the benefits of the ADSCs in comparison with other sources of MSCs, e.g. being less invasive compared to lipo-aspiration, having less ethical issues (10, 18), providing more homogenous stem cells with less variations in morphological features, and being ideal for the assessment of environmental changes (19); in the present study, ADSCs were taken into account as an appropriate model for our investigation.

Our flow cytometry data showed that CD90, CD44, CD73, and CD105 as MSCs-specific markers were expressed by ADSCs, whereas CD34, CD45, and CD11b were not, demonstrating the mesenchymal origin of ADSCs. ADSCs also share some morphological characteristics with MSCs, such as being spindle-shaped and possessing fibroblast-like properties (10, 20). MSCs are highly multipotent and can differentiate into mesodermal lineage such as adipogenic, chondrogenic, and osteogenic cells (17). Our findings confirmed that ADSCs could differentiate into bone and adipose tissues. There are several studies that applied different approaches for the neural induction of MSCs, such as β-Mercaptoethanol, valproic acid, butylated hydroxyanisole, hydrocortisone, azacytidine, isobutylmethylxanthine, indomethacin, insulin (17, 19, 21), glial growth factors, as well as a mixture of bFGF, platelet-derived growth factor, BDNF, and retinoic acid (22). Briefly, the protocols mentioned earlier could be divided into two main groups: i. Chemical and ii. Growth factor-based methods. It has been demonstrated that chemical-based induction methods lead to the production of nonfunctional neuron-like cells and induce an increment in the rate of apoptosis (23).

The CSF contains various biological factors such as neuropeptides and neurotransmitter, possessing different concentrations during various gestational ages. Several studies also showed that adult CSF isolated from human and rat could stimulate the proliferation and viability of neural stem cells.

Additionally, e-CSF comprises of several growth factors including TGF-β, NGF, BDNF, NT-3, and IGF (24, 25). In recent years, several studies demonstrated that the changes in the levels of CSF factors have multiple impacts on the proliferation and differentiation of brain cells in different animal models under various conditions (24). In the present study, we observed that the application of e-CSF, as a growth factor-based method, induced morphological changes in the neural phenotype of MSCs and increased cell viability. Yari et al. (26) also indicated that e-CSF enhanced the proliferation of neural progenitor cells and increased neurosphere size in culture

media. Mercaptoethanol, as a chemical inducer, could also cause ADSCs differentiation in culture media, but significantly reduced cell viability (27).

Dual effects of e-CSF on ADSCs proliferation and differentiation are probably caused by various growth factors, their concentration changes in different embryonic stages, and their interaction in each step. Several reports demonstrated that e-CSF collected from different embryonic days of the rat brain (E16, E17, E18, E19, and E20) has different effects on neuronal progenitors derived from the embryonic brain of rats. By E16 and E18, these effects have stimulatory roles on the proliferation and survival of neuronal progenitors. It has been implicated that e-CSF extracted at E20 and E19 has a significant impact on the differentiation (26, 28, 29). Nabiuni et al. (28) evaluated the effect of rat embryonic CSF on PC12 cells. They observed that the proliferation and viability of PC12 cells that underwent exposure to CSF at E18 are significantly elevated, but PC12 cells cultured in media supplemented with b-FGF (neural inducer) and CSF at E20, represented neural-like morphology. In another study, Yari et al. (26) investigated the effect of embryonic CSF on neural progenitors cells. In this study, e-CSF extracted at E18 induced the proliferative impact on neural progenitors cells and significantly increased cell viability. In the presence of e-CSF at E18 and E19, the neuronal process growth in cultured ADSCs was also markedly increased compared with the control samples.

Previous studies indicated that e-CSF isolated at E18 and E19 might differentiate cells into neuronal cells (26, 28). The results of the neuronal process growth confirmed the differentiation of these cells towards neurons. In fact, the effects of e-CSF extracted from different gestational days (E17, E18, and E19) on cultured ADSCs are age-dependent and probably due to the changes in the concentration of various growth factors in a time-dependent manner.

The mechanisms by which the e-CSF contents are altered in different time points is probably related to the developmental changes in the CSF-brain barrier. It has been reported that the permeability of CSF-brain barrier changes in an age-dependent manner during embryonic and adult life. The changes in permeability are due to the differential distribution of junctional proteins in the CSF-brain barrier. Therefore, alterations in permeability could be a source of e-CSF composition changes in different gestational periods (30).

In this study, there were limitations on e-CSF extraction from the cisterna magna region of rats' embryo. Due to the low volume of e-CSF obtained from this area, we suggest the extraction of e-CSF could be performed on animal models since they provide a high amount of e-CSF for the experiment. Also, we propose the application of other techniques such as real-time PCR for the precise evaluation of the expression of genes involved in differentiation and proliferation of ADSCs exposed to e-CSF.

Conclusion

Previous studies have shown that various factors with different concentrations are presented in embryonic CSF and their level varies on different embryonic days. The results of this study indicated the changes in the e-CSF compositions in a time-dependent manner, which had a positive impact on ADSCs survival and differentiation. Considering specific properties of ADSCs, their differentiation in response to exposure to e-CSF may be regarded as a novel therapeutic strategy for the treatment of neurodegenerative disorders.

Acknowledgements

This research was financially supported by the Department of Biology, Faculty of Science, Kharazmi University, Tehran, Iran. The authors declare no conflict of interest.

Authors' Contributions

M.N., K.P., J.M.; Conceived and designed the study. M.N.; Revised the manuscript. M.-H.M.-M.-H.; Contributed to all experimental work, data analysis, interpretation of data, and preliminary writing of the manuscript. S.Y.; Contributed to the literature research, data collection, data analysis and manuscript preparation. A.S.; Contributed to the e-CSF collection and cell viability assay. All authors read and approved the final manuscript.

References

1. Tumani H, Huss A, Bachhuber F. The cerebrospinal fluid and barriers–anatomic and physiologic considerations. Handb Clin Neurol. 2017; 146: 21-32.
2. Mashayekhi F, Azari M, Moghadam LM, Yazdankhah M, Naji M, Salehi Z. Changes in cerebrospinal fluid nerve growth factor levels during chick embryonic development. J Clin Neurosci. 2009; 16(10): 1334-1337.
3. Johanson CE, Duncan JA 3rd, Klinge PM, Brinker T, Stopa EG, Silverberg GD. Multiplicity of cerebrospinal fluid functions: new challenges in health and disease. Cerebrospinal Fluid Res. 2008; 5: 10.
4. Alonso MI, Lamus F, Carnicero E, Moro JA, de la Mano A, Fernández JM, et al. Embryonic cerebrospinal fluid increases neurogenic activity in the brain ventricular-subventricular zone of adult mice. Front Neuroanat. 2017; 11: 124.
5. Ren C, Yin P, Ren N, Wang Z, Wang J, Zhang C, et al. Cerebrospinal fluid-stem cell interactions may pave the path for cell-based therapy in neurological diseases. Stem Cell Res Ther. 2018; 9(1): 66.
6. Heo JS, Choi Y, Kim HS, Kim HO. Comparison of molecular profiles of human mesenchymal stem cells derived from bone marrow, umbilical cord blood, placenta and adipose tissue. Int J Mol Med. 2016; 37(1): 115-125.
7. Hyun I. The bioethics of stem cell research and therapy. J Clin Invest. 2010; 120(1): 71-75.
8. Stoltz JF, de Isla N, Li YP, Bensoussan D, Zhang L, Huselstein C, et al. Stem cells and regenerative medicine: myth or reality of the 21th century. Stem Cells Int. 2015; 2015: 734731.
9. Koobatian MT, Liang MS, Swartz DD, Andreadis ST. Differential effects of culture senescence and mechanical stimulation on the proliferation and leiomyogenic differentiation of MSC from different sources: implications for engineering vascular grafts. Tissue Eng Part A. 2015; 21(7-8): 1364-1375.
10. Bajek A, Gurtowska N, Olkowska J, Kazmierski L, Maj M, Drewa T. Adipose-derived stem cells as a tool in cell-based therapies. Arch Immunol Ther Exp (Warsz). 2016; 64(6): 443-454.
11. Almalki SG, Agrawal DK. Key transcription factors in the differen-

tiation of mesenchymal stem cells. Differentiation. 2016; 92(1-2): 41-51.
12. Georgiou M, Golding JP, Loughlin AJ, Kingham PJ, Phillips JB. Engineered neural tissue with aligned, differentiated adipose-derived stem cells promotes peripheral nerve regeneration across a critical sized defect in rat sciatic nerve. Biomaterials. 2015; 37: 242-251.
13. Andreas K, Haupl T, Lubke C, Ringe J, Morawietz L, Wachtel A, et al. Antirheumatic drug response signatures in human chondrocytes: potential molecular targets to stimulate cartilage regeneration. Arthritis Res Ther. 2009; 11(1): R15.
14. Shokohi R, Nabiuni M, Moghaddam P, Irian S, Miyan JA. Fetal cerebrospinal fluid promotes proliferation and neural differentiation of stromal mesenchymal stem cells derived from bone marrow. Braz Arch Biol Technol. 2017; 60: e17160221.
15. Liu SY, He YB, Deng SY, Zhu WT, Xu SY, Ni GX. Exercise affects biological characteristics of mesenchymal stromal cells derived from bone marrow and adipose tissue. Int Orthop. 2017; 41(6): 1199-1209.
16. Iser IC, Ceschini SM, Onzi GR, Bertoni AP, Lenz G, Wink MR. Conditioned medium from adipose-derived stem cells (ADSCs) promotes epithelial-to-mesenchymal-like transition (EMT-like) in glioma cells in vitro. Mol Neurobiol. 2016; 53(10): 7184-7199.
17. Lo Furno D, Mannino G, Cardile V, Parenti R, Giuffrida R. Potential therapeutic applications of adipose-derived mesenchymal stem cells. Stem Cells Dev. 2016; 25(21): 1615-1628.
18. Gao F, Chiu SM, Motan DA, Zhang Z, Chen L, Ji HL, et al. Mesenchymal stem cells and immunomodulation: current status and future prospects. Cell Death Dis. 2016; 7: e2062.
19. Salehi H, Amirpour N, Niapour A, Razavi S. An overview of neural differentiation potential of human adipose derived stem cells. Stem Cell Rev. 2016; 12(1): 26-41.
20. Mo M, Wang S, Zhou Y, Li H, Wu Y. Mesenchymal stem cell subpopulations: phenotype, property and therapeutic potential. Cell Mol Life Sci. 2016; 73(17): 3311-3321.
21. Talwadekar M, Fernandes S, Kale V, Limaye L. Valproic acid enhances the neural differentiation of human placenta derived-mesenchymal stem cells in vitro. J Tissue Eng Regen Med. 2017; 11(11): 3111-3123.
22. Zhang J, Lu X, Feng G, Gu Z, Sun Y, Bao G, et al. Chitosan scaffolds induce human dental pulp stem cells to neural differentiation: potential roles for spinal cord injury therapy. Cell Tissue Res. 2016; 366(1): 129-142.
23. Fu X, Tong Z, Li Q, Niu Q, Zhang Z, Tong X, et al. Induction of adipose-derived stem cells into Schwann-like cells and observation of Schwann-like cell proliferation. Mol Med Rep. 2016; 14(2): 1187-1193.
24. Salehi Z, Mashayekhi F. The role of cerebrospinal fluid on neural cell survival in the developing chick cerebral cortex: an in vivo study. Eur J Neurol. 2006; 13(7): 760-764.
25. Zappaterra MD, Lisgo SN, Lindsay S, Gygi SP, Walsh CA, Ballif BA. A comparative proteomic analysis of human and rat embryonic cerebrospinal fluid. J Proteome Res. 2007; 6(9): 3537-3548.
26. Yari S, Parivar K, Nabiuni M, Keramatipour M. Effect of embryonic cerebrospinal fluid on proliferation and differentiation of neuroprogenitor cells. Cell J. 2013; 15(1): 29-36.
27. Sun W, Incitti T, Migliaresi C, Quattrone A, Casarosa S, Motta A. Viability and neuronal differentiation of neural stem cells encapsulated in silk fibroin hydrogel functionalized with an IKVAV peptide. J Tissue Eng Regen Med. 2017; 11(5): 1532-1541.
28. Nabiuni M, Rasouli J, Parivar K, Kochesfehani HM, Irian S, Miyan JA. In-vitro effects of fetal rat cerebrospinal fluid on viability and neuronal differentiation of PC12 cells. Fluids Barriers CNS. 2012; 9(1): 8.
29. Shokohi R, Nabiuni M, Irian S, Miyan JA. In-vitro effects of wistar rat prenatal and postnatal cerebrospinal fluid on neural differentiation and proliferation of mesenchymal stromal cells derived from bone marrow. Cell J. 2018; 19(4): 537-544.
30. Whish S, Dziegielewska KM, Møllgård K, Noor NM, Liddelow SA, Habgood MD, et al. The inner CSF-brain barrier: developmentally controlled access to the brain via intercellular junctions. Front Neurosci. 2015; 9: 16.